UNIVERSITY OF BURGOS

HIGHER POLYTECHNIC SCHOOL

DEPARTMENT OF ARCHITECTURAL BUILDING, CONSTRUCTION AND GROUND ENGINEERING

DOCTORAL THESIS

IMPROVED ENGINEERING SOLUTIONS FOR THERMAL DESIGN OF ARTIFICIAL GROUND FREEZING

Diego Sancho Calderón

Directors:

Dr. Civil Engineer Sergio Ibáñez García,

Dr. Civil Engineer Santiago Ortiz Palacio

Dr. Mining Engineer Sven Bock

Burgos, July 2022

Foreword

Artificial ground freezing is a safe, proven and reliable method for various construction projects in water-bearing, unstable soils and rock, from special civil engineering (e.g. for excavations), to tunnel construction and mine shafts. Essential for the design and control of the freezing process are the thermal calculations. Historically, these have been performed by using analytical methods. However, the project-specific geometrical and geological conditions and the construction sequence have a significant influence on the design, which is difficult to consider using analytical and empirical methods only. A partial solution to more complex design challenges is currently the use of numerical models. An important advantage of numerical modelling, among others, is the use of 3D models, which becomes practically necessary in many present challenges of engineering and allows a suitable representation of the geological structure. Numerical models also make possible the proper combined simulation of the excavation sequence, the ground support and the coupling thermo-hydro-geomechanical approach.

It must be stated, however, that the results of numerical calculations are known to be mesh-dependent, which means that for too “coarse” meshes a correct interpretation of the analysed physical phenomena is not possible. Unfortunately, there are also other factors which significantly influence the accuracy of numerical calculations.

The research work of Diego Sancho Calderón starts at this point, reviewing the analytical and numerical approaches. He selected different freezing problems, which he investigated and analysed. Based on the performed verification, he was able to define the limitations and applicability of both analytical and numerical methods. In my opinion, the presented results are a step forward in the scientific research of artificial ground freezing. Furthermore, the presented adjustment of the Sanger & Sayles formula and the code of good practice for thermal numerical modelling are of great practical importance for construction projects using the artificial ground freezing technique.

It was a great pleasure for me to assist and support Diego in his work and I would like to thank him for the opportunity to be a part of this very important research.

Kamen, June 2022

Dr. Sven Bock

Acknowledgements

Writing this doctoral thesis has been a long and amazing journey of over three years, which would not have been possible without the backing of extraordinary mentors.

First, I would like to express my gratitude to my thesis directors: Dr. Sergio Ibáñez, Dr. Santiago Ortiz and Dr. Sven Bock, who, with their continuous support, have enlightened the path to creating this dissertation. Sergio has been essential in getting the thesis into its final form, orienting me into polishing the draft and making it more readable. Santi has provided great insights and original ideas to explore. Sven has been instrumental in my learning FLAC3D and has been of continuous help in focusing the investigation. Not only have my three directors given me the technical and academic orientation, but most importantly, have been great friends along the way.

I would also like to acknowledge my former and current managers and mentors, Dr. Jürgen Franz and Dr. Christof Gehle, for teaching me how to write technical and academic documents, and for insisting on them being of the highest quality.

Special thanks go to my friend Nikolai Hentrich, who taught me the workings of ground freezing engineering and thermal modelling, among many other things.

Naturally, I also want to thank my closest ally in this adventure: my wife Alba, who has provided support in the hardest days and made it possible for me to find the time for the thesis, through a generous allocation of her time.

Finally, my family has provided the foundation for me to become a civil engineer and to write this thesis. In this process, they have always been there for me, providing “outsider” counsel, moral support and an open mind to listen to the issues of the thesis. To you, Dad, Mum and Mario, goes my most profound gratitude.

Table of Contents

List of Figures

List of Tables

List of Symbols

Latin symbols

Symbol	Name
a	Exponent of T_{II} in the adjustment for a_r
a_r	Ratio between the radius of the zone affected by the temperature drop due to the influence of the freeze pipe (temperature penetration depth) and the freeze radius.
$a_{r,adjusted}$	Adjusted a_r based on the interpolation of the results of the numerical model for the different problems studied.
$a_{r,calculated}$	Calculated a_r based on the numerical model.
$a_{r0.05}$	Ratio of the radius in which the temperature has changed by 0.05ºC to the freeze radius.
$a_{r0.1}$	Ratio of the radius in which the temperature has changed by 0.1ºC to the freeze radius.
$a_{r0.2}$	Ratio of the radius in which the temperature has changed by 0.2ºC to the freeze radius.
$a_{r0.5}$	Ratio of the radius in which the temperature has changed by 0.5ºC to the freeze radius.
A_f	Parameter defined by Bakholdin: $\frac{1}{2}\ln\left[2\left(\cosh\frac{2\pi y}{s}-\cos\frac{2\pi x}{s}\right)\right]$
b	Exponent of T_I in the adjustment for a_r
c	Exponent of c_{av} in the adjustment for a_r
C	Courant number
c_{av}	Average of frozen and unfrozen specific heat capacities
c_s	Specific heat capacity
c_1	Specific heat capacity of the frozen phase
c_2	Specific heat capacity of the unfrozen phase
c_3	Specific heat capacity of the mushy phase
d	Exponent of k_{av} in the adjustment for a_r
d_{zone}	Length of the zone / element in the direction of the energy transmission
e	Exponent of l_s in the adjustment for a_r

$\mathbf{erf}\,(\mathbf{z})$	Error function
$\mathbf{erfc}\,(\mathbf{z})$	Complementary error function
$\boldsymbol{E'}$	Average rate of energy absorption
$\boldsymbol{E_i(z)}$	Exponential integral function
$\boldsymbol{f}$	Exponent of r_0 in the adjustment for a_r
$\boldsymbol{g}$	Exponent of the variable n_1, number of elements in the model in the adjustment for the computing time
$\boldsymbol{h}$	Exponent of the variable m_1, number of time steps simulated in the adjustment for the computing time
$\boldsymbol{H}$ **or** $\boldsymbol{H(T)}$	Enthalpy function
$\boldsymbol{i}$	Exponent of the variable u, number of time steps after which the freeze status is updated in the adjustment for the computing time
$\boldsymbol{k}$	Thermal conductivity
$\boldsymbol{k_{av}}$	Average thermal conductivity (between frozen and unfrozen)
$\boldsymbol{k_{ij}}$	Ratio of thermal conductivities between phases: k_i/k_j
$\boldsymbol{k_j^n}$	Thermal conductivity of element j at time n.
$\boldsymbol{k_x}$	Thermal conductivity (x-direction)
$\boldsymbol{k_y}$	Thermal conductivity (y-direction)
$\boldsymbol{k_z}$	Thermal conductivity (z-direction)
$\boldsymbol{k_1}$	Thermal conductivity of phase 1 (frozen phase)
$\boldsymbol{k_2}$	Thermal conductivity of phase 2 (unfrozen phase)
$\boldsymbol{k_3}$	Thermal conductivity of phase 3 (mushy phase)
$\boldsymbol{l}$	Latent heat per unit mass
$\boldsymbol{l_s}$	$\frac{l_{water}\,\omega\,\rho_d}{\rho}$: crystallisation heat of the groundwater, per unit mass of ground
$\boldsymbol{l_v}$	$l_{water}\,\omega\,\rho_d$: crystallisation heat of the groundwater, per unit volume of ground
$\boldsymbol{l_{water}}$	Latent heat of water

L_c	$\frac{volume\ of\ solid\ of\ one\ element}{surface\ area\ \text{of one element}\ exchanging\ heat}$: smallest characteristic length of any zone
L_F	$l_v - \frac{1}{2}c_1T_I + c_2T_{II}\left(\frac{a_r-1}{\ln(a_r)}\right)$: volumetric latent heat of the unfrozen area, freeze wall case (used in Sanger & Sayles' solution)
L_I	$l_v + \frac{(a_r^2-1)}{2\ln a_r}\ c_2T_{II}$: volumetric latent heat of the unfrozen area, single freeze pipe case (used in Sanger & Sayles' solution)
L_{IIe}	$l_v + 2.5c_2T_{II} - 0.5c_1T_I$: volumetric latent heat of the unfrozen area, outer boundary of freeze circle (according to Sanger & Sayles)
L_{IIi}	$l_v + 2.0c_2T_{II} - 0.5c_1T_I$: volumetric latent heat of the unfrozen area, inner boundary of freeze circle (according to Sanger & Sayles)
L_{zone}	Amount of latent heat in the zone
m	Constant, larger than one, which depends on the geometrical discretisation
m_1	Number of time steps simulated
n	Number of data points
n_1	Number of elements in the model
p	Calibrated parameter for the correlation of a_r
$P(x,t)$	Flux per unit surface
q	Calibrated parameter for the correlation of the computing time
q_g	Energy released per unit volume and per unit time
q_s	Constant heat flux extracted at the origin
q_x	Flux or heat transfer rate in the direction of the "x" axis
q_1	Constant heat flux applied at boundary 1
r	Radial coordinate
r_0	Freeze pipe radius
r_1	Radius of source in annular problem
r_2	Radius of external boundary in annular problem
$R(t)$ or R	For the single freeze pipe problem: Freeze radius

	For the freeze wall problem: Half-width of the freeze wall (freeze radius in the direction perpendicular to the freeze wall)
R^2	Coefficient of determination
R_e	External radius of the freeze annulus (in the freeze circle problem)
R_i	Internal radius of the freeze annulus (in the freeze circle problem)
s	Separation between pipes
S_T	Stefan number
$S_\perp$	Surface of the zone perpendicular to the direction of the energy transmission
t	Temporal coordinate (time)
t_I	Freeze time up to a freeze radius R
t_{IIe}	Time to reach the external freeze radius (in a freeze circle problem)
t_{IIi}	Time to reach the internal freeze radius (in a freeze circle problem)
T	Temperature
$T(x)$	Temperature distribution in the direction of the "x" coordinate
T_f	Phase-change temperature or upper limit of freeze temperature range
T_m	Lower limit of freeze temperature range
T_s	Source (freeze-pipe) temperature
T_I	$T_s - T_f$: freeze-pipe temperature minus phase-change temperature
T_{II}	$T_0 - T_f$: initial temperature minus phase-change temperature
T_0	Initial temperature
$T_1(x,t)$	Temperature distribution in the frozen phase
$T_2(x,t)$	Temperature distribution in the unfrozen phase
T_2	Temperature at the boundary 2.
u	Update period (every how many time steps) with which the "freeze block" routine is executed
v	$v^2 = \frac{R^2 - {r_0}^2}{4\alpha_1 \cdot t}$: variable defined in Ständer's solution for the single freeze pipe
v_g	Groundwater velocity
V	Zone / element volume

W	Freeze wall width
W_I	Average freeze wall width at closure
X	$-\frac{k_1 \cdot T_I}{k_2 \cdot T_{II}}$: parameter in Ständer's solution for the single freeze pipe
x	Linear spatial coordinate in the x-direction
x_i^{exact}	value of the variable x, from the exact analytical solution
x_i^{num}	value of the variable x, from the numerical method
x_2	Thickness of slab
$X(t)$	Distance from the phase-change interface to the source (freeze front position)
y	Linear spatial coordinate in the y-direction
Y	$-\frac{k_1 \cdot T_I}{\alpha_1 \cdot \rho \cdot q_s}$: parameter in Ständer's solution for the single freeze pipe
z	Linear Spatial coordinate in the z-direction
Z	$\frac{R}{r_0}$: parameter in Ständer's solution for the single freeze pipe

Greek symbols

Symbol	Name
α	$\alpha = k/\rho c$: thermal diffusivity
α_1	Thermal diffusivity of phase 1 (frozen phase)
α_2	Thermal diffusivity of phase 2 (unfrozen phase)
α_{12}	α_1/α_2 : ratio of thermal diffusivities
β	Constant coefficient in the condition of stability of the FTCS scheme
γ	Dimensionless parameter
δ	Half-width of the freeze annulus or freeze wall at closure time
$\delta(t)$	Temperature penetration depth
Δt_{cr}	Critical time step
$\Delta \mathbf{T}$	Temperature difference between phases
Δt	Time step
Δx	Discrete interval of length in the coordinate x

$\boldsymbol{\varepsilon}$	Phase-change temperature range
$\boldsymbol{\eta}$	$x/(2\sqrt{\alpha_1 t})$, similarity variable
$\boldsymbol{\eta_1}$	$\frac{r^2}{4\alpha_1 t}$, first similarity variable
$\boldsymbol{\eta_2}$	$\frac{r^2}{4\alpha_2 t}$, second similarity variable
$\boldsymbol{\lambda}$	Dimensionless parameter
$\boldsymbol{\mu}$	Average
$\boldsymbol{\xi}$	Unfrozen water function
$\boldsymbol{\xi_j^n}$	Unfrozen water content of element j at time n
$\boldsymbol{\rho}$	Density of the medium
$\boldsymbol{\rho_1}$	Density of the frozen phase
$\boldsymbol{\rho_2}$	Density of the unfrozen phase
$\boldsymbol{\sigma}$	Standard deviation
$\boldsymbol{\varphi(z)}$	$\int_0^z \frac{e^z-1}{z} dz = \sum_{n=1}^{\infty} \frac{z^n}{n\, n!}$ with $z = 2\, ln \frac{R}{r_0}$ (in Leibenson's solution)
$\boldsymbol{\phi(x,t)}$	Exact, continuous solution
$\boldsymbol{\phi(x_i,t_m)}$	Exact solution evaluated at the mesh point i at time instant t_m
$\boldsymbol{\phi_i}$	Approximate numerical solution evaluated at the mesh point i
$\boldsymbol{\phi_{i+1}}$	Approximate numerical solution evaluated at the mesh point i +1
$\boldsymbol{\phi_i^m}$	Approximate numerical solution evaluated at the mesh point i at time instant t_m
$\boldsymbol{\omega}$	Water content

Other symbols

Symbol	Name
$\boldsymbol{\mathcal{O}(\Delta x)}$	Notation used to indicate that the truncation error is proportional (linearly) to Δx
$\boldsymbol{\frac{\partial T}{\partial x}}$	Temperature gradient in the direction of the "x" axis
$\boldsymbol{\frac{\partial T}{\partial y}}$	Temperature gradient in the direction of the "y" axis

$\frac{\partial T}{\partial z}$	Temperature gradient in the direction of the “z” axis
∇^2	Laplacian operator

List of Abbreviations

AGF: Artificial Ground Freezing

BC: Boundary Conditions

BTCS: Backward Time, Centred Space method

$CaCl_2$: Calcium Chloride

FD: Finite Difference

FDM: Finite Difference Method

FEM: Finite Element Method

FLAC3D: Fast Lagrangian Analysis of Continua (3D)

FTCS: Forward Time, Centred Space method

HBIM: Heat Balance Integral Method

LNG: Liquefied Natural Gas

ODE: Ordinary Differential Equation

PDE: Partial Differential Equation

RMSE: Root-Mean-Square Error

THM: Thermal-Hydraulic-Mechanical

2D: Two Dimensions

3D: Three Dimensions

Glossary and naming convention for numerical models

Glossary

Average of absolute values of errors: The average of the absolute (positive) values of the errors.

Artificial ground freezing: A method used in geotechnical engineering for stabilising the ground and / or preventing groundwater from entering an excavation.

Boundary conditions: Conditions imposed at the boundaries (limits) of a problem which is described by differential equations inside those boundaries.

Closure time: Time required to close the freeze body.

Computing time: Time required by a computer to perform a certain numerical calculation.

Critical time step: Largest time step for which the explicit method is stable for a certain model.

Freeze block / Freeze routine: Block of numerical code used in FLAC3D to simulate the phase change effects.

Freeze body: Frozen body of ground, usually used for structural improvement and/or groundwater cut-off. The freeze body may present different shapes (wall, cylinder, annulus…).

Freeze circle: An annular or cylindrical freeze body, engendered by a set of freeze pipes disposed at regular intervals in a circle, usually in order to provide protection for a circular excavation. It is also applicable to refer to the circular-shaped freeze pipe disposition itself.

Freeze front: Time-dependent phase-change interface.

Freeze pipe: A pipe inserted into a borehole into which a coolant circulates with the purpose of freezing the ground around it.

Freeze pipe temperature: Temperature of the freeze pipe.

Freeze radius: Radius of the freeze front (used in problems with radial symmetry).

Freeze status: Status of the zones / elements in the numerical model (unfrozen, freezing or already frozen).

Freeze wall: A straight or linear freeze body, generated by a set of freeze pipes disposed at regular intervals in a row. It may be used to protect a side of a rectangular excavation.

Freeze temperature: Phase-change temperature or phase-change point of the groundwater.

Initial temperature: Initial temperature of the ground before the start of the ground freezing process.

Plateau: Horizontal area in the temperature-time graph produced by numerical simulation of a ground freezing problem, generated due to the typical oscillations occurring in the enthalpy method.

Root-Mean-Square Error (RMSE): A measure of the error which is defined as the square root of the sum of the squares of the errors of the different points.

Single freeze pipe: Problem with one singular freeze pipe. This problem has one of the simpler geometries and has been extensively studied.

Source temperature: Temperature of the cooling or heating source.

Steady state: A state of a system in which it does not change in time, e.g. for a thermal system, a state in which the temperature of all its points does not change in time.

Temperature penetration depth / radius: Distance from the thermal source to the farthest point of the material whose temperature has been affected by the source.

Thermal time: Simulated time considered in a thermal calculation.

Time step: Discretisation of time in a numerical model. The numerical calculations are performed at the intervals defined by the time step.

Verified numerical model: Numerical model for ground freezing which uses appropriate numerical parameters according to the conclusions of the evaluations from chapter 5.

Zone / element (mesh zone / mesh element): Portion into which the space is discretised for numerical calculations using the Finite Element or Finite Difference Methods.

Naming convention for numerical models

The following naming convention for numerical models has been used in the dissertation:

MH*a*-TS*b*-UF*c*-TE*d*-SO*e*-SC*f*-ST*g*-TP*h*-AG*i*-*j*_*k*

The meanings of the variables (the lower-case letters in italics) are as follows:

- MH*a*: variable *a* is the mesh size, in cm.
- TS*b*: variable *b* is the time step, in seconds.
- UF*c*: variable *c* is the update period (every how many time steps) with which the "freeze block" routine is executed.
- TE*d*: variable *d* is the type of elements ("h" for rectangular prisms and "t" for triangular prisms).
- SO*e*: variable *e* stands for the source type ("s" for surface, "p" for punctual).
- SC*f*: variable *f* is the type of phase change ("a" for abrupt, "g" for gradual).
- ST*g*: variable *g* represents the presence or not of phase change ("p" for problems with phase change, "n" for problems without phase change).
- TP*h*: variable *h* is the maximum temperature difference (initial temperature of the ground minus temperature of the "cold boundary").
- AG*i*: variable *i* stands for the solving algorithm, ("E" for explicit, "I" for implicit).
- *j*: variable *j* represents the geometry of the model ("NE" for Neumann, "CY" for single freeze pipe, "fw" for freeze wall and "fc" for freeze circle).
- *k*: variable *k* is used for additional parameters changed in the models, e.g. larger models, models with a longer computed thermal time or models without any latent heat (shown as LHT=0).

An example of a model name following this convention is presented below:

MH1-TS1-UF1-TEh-SOs-SCa-STp-TP250-AGE-NE_LHT=0

Abstract

Artificial ground freezing is a method widely used for improvement of the ground stability and water cut-off for excavation in water-bearing ground. The engineering design of these ground improvement measures requires thermal calculations in order to prognose the time necessary for sufficient freeze wall thickness and thus the power of the freezing machines and the energy consumption. Nowadays, there are two main methods to perform such calculations: analytical and numerical.

Thermal problems with phase change are described mathematically by means of partial differential equations with a moving (time-dependent) boundary, which are usually known as Stefan problems. Due to the intricacy of these problems, despite intensive research, only a small number of exact solutions are known. Furthermore, these solutions are usually applicable for problems with very specific conditions only, such as the well-known Neumann solution for the semi-infinite slab. Therefore, the designer of artificial ground freezing projects has to recur to numerical or approximate analytical solutions for thermal design.

Numerical methods, because of their very nature, need to be verified and calibrated in order to limit and control the errors in the results. In the present thesis, several numerical models for thermal calculations with phase change were verified against the exact Neumann solution. This was performed by an in-depth analysis of the effects of several numerical parameters, such as the mesh size and type, the time step, the frequency of updating the freeze status of the mesh elements and the type of solving method (implicit or explicit). Additionally, a sensitivity analysis was performed to investigate the effect of the initial and boundary conditions of the problems, such as the initial temperature gradient, the amount of latent heat, the graduality of the phase change and the thermal characteristics of the ground. In this way, the applicability limits of the numerical model were sought and the conditions for an accurate, verified model were found. It was concluded that the mesh size has the most significant impact on the accuracy of the results. A code of good practice for numerical modelling of thermal problems with phase change was created based on the results of these investigations.

In addition to the numerical methods, approximate analytical solutions for engineering design were studied. These solutions are applicable to three usual practical configurations: single freeze pipe, freeze wall and freeze circle. The accuracy of the approximate analytical solutions from Leibenson, Khakimov, Ständer, Sanger & Sayles and Lunardini was investigated by comparing them with the results from the previously verified numerical model for several problems with several initial and boundary conditions, similarly to the sensitivity analysis for the verification of the numerical model. The values of these parameters were chosen to cover usual and potential cases in engineering projects. It was concluded that Ständer's solution was the one with the highest accuracy for most of the problems, especially for the single freeze pipe and freeze wall geometries, although it does not appear to be widely known in the literature. One drawback of Ständer's solution is that it is not in a closed form, so it is more complex to use than other formulae. Thus, it was

attempted to create a solution which is easy to use and accurate at the same time. With this intent, Sanger & Sayles' formula was adjusted by benchmarking it with the verified numerical model, with positive results.

Finally, experimental and project data from several literature sources were used to further confirm the usability of the numerical and analytical solutions. The empirical data and the calculated results could be reconciled, providing further evidence of the usefulness of the approach employed and reinforcing the conclusions of the thesis.

Resumen

La congelación artificial del terreno es un método que se utiliza habitualmente en excavaciones en terrenos acuíferos con el fin de estabilizarlos y evitar la entrada de agua subterránea. Para diseñar esta medida de mejora del terreno es necesario realizar cálculos térmicos, de los cuales se derivan el tiempo necesario hasta alcanzar el espesor de pared congelada, la requerida potencia de las máquinas de congelación y el consumo energético. Actualmente existen dos métodos principales para estos cálculos: analítico y numérico.

Los problemas térmicos con cambio de fase pueden describirse matemáticamente mediante ecuaciones diferenciales en derivadas parciales con frontera móvil, que representan los llamados problemas de Stefan. La complejidad de estos problemas es tal que, a pesar de la intensiva investigación en este campo, solamente se conocen soluciones exactas para unos pocos de estos problemas. Estas soluciones son aplicables normalmente sólo para problemas con condiciones muy específicas, como el conocido problema de Neumann. Así, el ingeniero de diseño de proyectos de congelación artificial tiene que recurrir a soluciones aproximadas para el diseño térmico, ya sean analíticas o numéricas.

Cuando se utilizan métodos numéricos, debido a su propia naturaleza, es necesario verificarlos y calibrarlos para limitar y controlar los errores en los resultados. En esta tesis, se han verificado varios modelos numéricos para el cálculo térmico comparándolos con la solución exacta de Neumann. Este proceso se ha realizado mediante un análisis en profundidad de los efectos de diferentes parámetros numéricos, como el tamaño y tipo de malla, la duración de los pasos de tiempo, la frecuencia de actualización del estado de congelación de los elementos y el tipo de método de resolución (implícito o explícito). Adicionalmente, se ha realizado un análisis de sensibilidad sobre las condiciones iniciales y de contorno del problema, como el gradiente de temperatura inicial, la cantidad de calor latente, el tipo de cambio de fase (abrupto o suave) y las características térmicas del terreno. De este modo, se ha tratado de hallar los límites de aplicabilidad del modelo numérico, encontrando las condiciones que hacen que el modelo sea preciso. Con el fin de condensar los resultados de estas investigaciones, se ha creado un código de buenas prácticas para la modelación numérica de problemas térmicos con cambio de fase.

Además de los modelos numéricos, se han estudiado algunas soluciones aproximadas para el diseño ingenieril. Estas soluciones son aplicables a tres configuraciones habituales de tuberías de congelación: tubería aislada, tuberías en fila (pared congelada) y tuberías en círculo (círculo de congelación). La precisión de las soluciones analíticas aproximadas de Leibenson Khakimov, Ständer, Sanger & Sayles y Lunardini ha sido investigada comparando sus resultados con los del modelo numérico previamente verificado. Esta comparación se ha realizado para varios problemas con diferentes condiciones iniciales y de contorno, de forma similar a los análisis de sensibilidad para la verificación del modelo numérico. Los valores de estos parámetros han sido elegidos para cubrir casos habituales y potenciales en proyectos de ingeniería. Se ha concluido que la solución de Ständer es la más precisa para la mayoría de los problemas, especialmente para la tubería aislada y tuberías en fila, aunque sin embargo, según la bibliografía, esta solución no parece ser

ampliamente conocida. Una desventaja de la solución de Ständer es que no se presenta en forma de fórmula cerrada, de manera que su uso es más complicado que otras fórmulas. Por ello, se ha tratado de crear una solución que sea a la vez fácil de usar y precisa. A tal fin, se ha ajustado la fórmula de Sanger & Sayles basándose en los resultados del modelo numérico verificado, con resultados positivos.

Finalmente, datos experimentales y de proyectos de diferentes fuentes bibliográficas se han utilizado para confirmar la utilidad de las soluciones numéricas y analíticas. Los datos empíricos y los resultados de los cálculos concuerdan suficientemente, aportando evidencia adicional sobre la utilidad de los métodos empleados y reforzando las conclusiones de la tesis.

1. Introduction

Underground openings and excavations often require stabilisation and groundwater control methods to prevent failure of the excavation face and water inflow into the excavation. One of the ground improvement methods which may be used in those situations is artificial ground freezing (AGF). AGF is based on freezing the ground prior to excavation by means of circulation of a cooled fluid in boreholes, which improves the ground stability and watertightness. It has been widely used in mining (especially for shaft sinking) and civil engineering. AGF is often considered as providing more certainty and less geotechnical and hydrogeological risk than other ground-treatment methods, such as grouting, as reported e.g. in Leung et al. (2012) for tunnel construction in Hong Kong and in Sturk and Stille (2008) for the Hallandsås railway tunnel in Sweden. In the same lines, Bock (2018) stated: "Today, the ground freezing method is still unrivalled in terms of providing safe and predictable work conditions during mine shaft sinking".

The method of artificial ground freezing for groundwater control originated during the second half of the 19th century for the execution of mine shafts in granular soils and water-bearing rock. This application in shaft sinking has continued throughout the time in numerous shafts (see e.g. Harris (1995), Franz (2015) and Czaja et al. (2020)). In the last decades, it has been increasingly applied to projects in civil engineering (Chang and Lacy, 2008) (Vitel et al., 2015), such as cross-passages between parallel tunnels (Wenke and Willner, 2008) (Roberti, 2012) (Mueller et al., 2015) (Filippo Mira-Catto, 2018) (Phillips et al., 2021) or between the tunnel and an escape shaft (Zhou et al., 2021), tunnelling under freeze body roof protection (Aerni, 1979) (Hu et al., 2018c), launching starting shafts for TBMs and excavations in soils in urban environments (Klösges and Müller, 2021), e.g. shallow tunnels near sensitive structures (Jones and Brown, 1979) (Zhou, 2013). It has also been used for temporary soil improvement under foundations or in order to seal leakages (Haß and Schäfers, 2013). An interesting example of its use in foundations is the rehabilitation of the historical building of the 15th century *Casa del Cordón* in Burgos, Spain (Muzás, 1985). Artificial ground freezing is also used at times as an emergency solution, e.g. after other methods such as grouting, micropiling, etc. have failed (Schmall and Braun, 2006) (Chang and Lacy, 2008) (Orth and Müller, 2013) (Arroyo, 2017) (Nikolaev and Shuplik, 2019). A more exceptional but highly interesting application is the long-term ground freezing of a large area to avoid groundwater inflow. Examples of this application are found in the Cigar Lake mine in Canada (see Newman et al. (2011) and Roworth (2013)) and in the Banji coal mine in China (Zueter et al., 2021). In cases of very complex geological or geometrical conditions, artificial ground freezing may be the only solution with high success chances (Arroyo, 2017).

As already indicated, the main aim of the design of the ground freezing process is to ensure the stability and/or watertightness of the freeze wall and the safety of the excavation. To achieve that, it is required to perform geotechnical and thermal calculations for the ground freezing project (Zhou, 2013). "The theory and application of ground freezing appear deceptively simple" (Powers et al., 2007): there are many factors which may influence the

ground freezing process, such as the geological and hydrogeological conditions, the performance of the freezing station or the freeze pipe deviations. Naturally, these factors have to be assessed and controlled for a successful project delivery.

The prediction of the effects of ground freezing (freezing progress, strength improvement, etc.) is critically required to ensure the safety of the excavation, evaluate the construction costs and schedule (Sopko, 2017a), as well as to optimize the design (Casini et al., 2016). The ground strength and creep properties are highly dependent on its temperature (the strength improves dramatically in the temperature range around the phase-change temperature and generally increases with decreasing temperatures below the phase-change temperature, see e.g. Harris (1995) and Roberti (2012)). Hence, the temperature field, derived from thermal calculations, is an essential input for the geotechnical calculations (P.E.Frivik, 1981) (Hu et al., 2016b). This means that thermal calculations are essential for the design of the ground freezing project (Müller, 2014) (Bosch, 2017), for instance, for the optimization of the freeze pipe arrangement, the estimation of the time of use and required power of the freezing machines, the total energy consumption, the time to achieve the required freeze wall thickness and the control of the freezing progress and freeze wall stability during the excavation works. Additionally, thermal simulations may be compared to the results of a monitoring programme or used to back-analyse the thermal properties of the ground, as in Pimentel et al. (2011).

Thermal design for artificial ground freezing has the main goal of predicting the temperature field in the ground given certain initial and boundary conditions, such as the initial ground temperature, the thermal properties of the ground and the freeze pipe temperature. In order to perform the design, a moving boundary problem in partial derivatives, a so-called Stefan problem, must be solved. For this type of problems, only a few exact analytical solutions have been found for very specific, simple geometries and conditions. However, several approximate analytical formulations for the prediction of the freezing time were developed as early as 40-60 years ago (see also Sopko Jr. (1990)), e.g. by Ständer (1967) and Sanger and Sayles (1979), and have been extensively used for thermal design of AGF in the past. Up to the present day, design engineers commonly make use of these formulae, at least in the first stages of the design process, due to the lower effort involved than with numerical methods. Thus, the search for accurate and reliable analytical methods is still of interest (Xu et al., 2020). In the past years, commercial codes for thermal numerical modelling have been developed and have increasingly popularized for the design of ground freezing engineering projects. Therefore, it is becoming increasingly common nowadays to make use of numerical software for thermal modelling of AGF, especially for the detail design stage, as a result of its better accuracy and versatility in the consideration of the specific conditions of the project (e.g. time-dependent brine temperature, inhomogeneous ground or freeze pipe deviations with respect to the idealised design geometry, see Hentrich and Franz (2015) and Bock (2018)).

Oftentimes, using the ground freezing method has been economically challenging due to the high costs, uncertainties in the estimation of the required energy (Schüller, 2015) or installation time (Powers et al., 2007). This may be one of the reasons why AGF is

considered a very specific technology, which is not extensively used in construction (Roberti, 2012). One of the sources of uncertainty and thus need for overconservative designs is the insufficient knowledge of the thermal behaviour of the system (Ziegler et al., 2010). Therefore, it is critical for the economical application of ground freezing that the thermal distribution forecasted by the calculations is realistic and that the freeze pipe arrangement is optimized in the design phase and tailored for the prevailing conditions. For instance, researchers have studied the optimization of the freeze pipe distribution under groundwater flow and found that it can significantly shorten the freezing time (Ziegler et al., 2010). Also in other neighbouring technical fields, such as permafrost calculations (Hwang et al., 1972) (Osterkamp, 1987) (Dagher et al., 2014), LNG underground storage (Neaupane et al., 1999), the effect of glacial periods on geological nuclear repositories (Nasir et al., 2013) and thermal storage of latent heat for solar systems (Lunardini, 1986), air heat exchangers and underground buildings, thermal calculations to simulate the phase change of the ground have to be performed and suitable design tools are required (Rees et al., 2000). With the aim of improving the design tools for ground freezing, the existing analytical solutions should be reviewed and updated with the currently available means. Regarding numerical methods, their accuracy and sensitivity to numerical parameters should also be investigated.

1.1. Problem discussion and formulation

As a result of the complexity of the phase-change problem, the natural inhomogeneity and the different components of the ground (air, water, grains) and potential groundwater flows, analytical formulae are only available for simple, specific cases (Lunardini, 1986) (Paynter and Life, 1999) (Ziegler et al., 2010). A few exact analytical formulae have been developed, e.g. for the one-dimensional semi-infinite slab with constant imposed and initial temperatures (the Neumann problem), but they possess only limited applicability to the practice, due to the very different geometrical and boundary conditions in real projects. In the last years, several steady-state solutions have also been developed, however, it is essential to solve the transient problem for AGF projects (Alzoubi et al., 2020). There are also a few approximate solutions for practical transient problems in ground freezing for the commonly used geometries: single freeze pipe, freeze circle and freeze wall. As already stated in the previous section, two solutions frequently used for the estimation of the freezing time and power in current engineering practice are the ones from Ständer (1967) and Sanger and Sayles (1979), both dating from the 1960-70s. Their results differ widely between them and also compared to numerical simulations (see e.g. Hentrich and Franz (2015) and Sancho-Calderón et al. (2021)), because they make different simplifications or assumptions and / or differ in the calculation method. Also the rules of thumb for estimation of the freeze power produce results varying in a large range (Schüller, 2015). Thus, it is worth investigating the source of these differences and their accuracy. Furthermore, improving these solutions or developing additional analytical solutions would be very helpful for engineering design, especially for estimating purposes in the first project phases, as analytical solutions are usually easier and faster to use than numerical models. The

solution should be sufficiently precise to be of practical utility to forecast the freezing process in most of the cases, while being relatively simple to use in practice (e.g. in the form of an explicit mathematical expression).

As the practical applicability of analytical formulations is limited by the complexity of real projects, the solutions to the phase change problems and the design of AGF frequently require the use of numerical calculations (Li et al., 2018), which are predictive and useful for the design, being able to model complex geometries and conditions (Colombo, 2010). Therefore, the analysis of the accuracy and sensitivity of numerical methods is also very relevant. Already in the 1980s, Furzeland (1980) concluded that although research had been directed towards finding numerical methods for special or general phase-change or Stefan problems, more investigation was required to find out which type of methods were more suitable for which problems and to compare their relative computational effort and accuracy. Nowadays, similarly, there is on one hand a vast amount of literature on improvements to the numerical methods from the mathematical side, frequently verified under theoretical conditions which are not directly applicable to engineering practice, e.g. applicable only to idealized, simplified geometries, to materials of uniform thermal properties or verified for just a very small timeframe of a few minutes or several hours. On the other hand, engineers tend to use analytical or numerical methods for the design of the ground freezing process in real projects and have only limited time to prepare the design, which makes it necessary to optimise the computing time. In these projects, the spatial scale is larger (of the order of several meters), the duration ranges from several weeks (e.g. for a cross-passage (Sopko, 2017c)) to months or even more than a year (Alzoubi et al., 2019), there exist many uncertainties regarding the initial and boundary conditions and the geometry is usually not ideal. Due to the limited time and resources for the design of the project, it is often challenging to perform calibrations and sensitivity analyses of the model during the course of the project.

The main difficulty in the thermal simulation of AGF is the non-linearity introduced by the phase change, and the associated challenge of tracking the interface position (Alzoubi et al., 2020). The problem is usually simulated via the enthalpy method, which is known to produce oscillations and temperature plateaux (Voller and Cross, 1981), and therefore has a certain degree of inaccuracy. Also, it has been noticed in the literature and in preliminary calculations that the results vary significantly when the numerical parameters are changed (see also e.g. Alekseev et al. (2018) for examples of errors in numerical models for ground freezing). For instance, regarding the time and space discretisation, Zhang et al. (2008) notes that finer mesh and time step theoretically lead to higher accuracy, but it comes at the cost of a higher computing time and modelling effort: “A balance must be achieved between simulation accuracy and computational efficiency”. Tounsi et al. (2019) also found that the results vary with the mesh and the type of source representing the freeze pipes (surface or punctual/linear sources). These variations may be unacceptable for practical purposes, even using meshes that would be accepted *a priori* as "sufficiently fine". In fact, not only the fineness of the mesh, but also many other numerical parameters may influence the accuracy and correctness of numerical calculations, such as the size of the time steps, the

convergence criteria, the type of mesh (structured or unstructured) and elements/zones (triangular / quadrilateral, first / second order...), the way of modelling the phase change of the ground (abrupt change of the thermal properties at the phase-change temperature or gradual change over a small range of temperature), the type of heat / cold sources that represent the freeze pipes (point or line sources, surface or volume sources, etc.). Furthermore, some of these factors are interrelated, such as the mesh size and time step (see Recktenwald (2004) for the theoretical bases and GEO-SLOPE International Ltd. (2014) for a more practical approach). There is only very limited literature focused on evaluating the effect of the numerical parameters on the accuracy of the model for AGF numerical models. However, these effects and especially the response of the numerical code in the phase change zone (freezing range) are critical for the accuracy of the simulation and need to be investigated further.

1.2. Objectives

The overall aim of the present thesis is to review and improve the practicability and accuracy of the analytical and numerical thermal calculation methods for predicting and monitoring the advance of the freeze front in ground freezing projects. The time-dependent temperature field and the interface between the frozen and unfrozen ground are derived from the solution to the mathematical moving boundary problem and are the inputs for the structural design of the freeze body and the assessment of its closure and stability. Thus, their accurate determination is of utmost importance for ground freezing design.

The first objective of this thesis is to study in detail the potential, limitations and errors of thermal numerical calculations with phase change. This has been done using a custom code to simulate phase change developed for the commercial program FLAC3D. As explained in chapter 1.1, there are significant differences between the results of the commercial numerical programs when calculating using different numerical parameters, e.g. with different spatial (mesh) and time discretisations. Therefore, this first objective involves establishing the conditions under which these numerical codes provide results with reasonable accuracy and within a practical computing time. To verify the code and determine these conditions, the numerical results have been compared to known exact analytical solutions, so that the accuracy of the numerical method could be measured. A code of good practice for thermal numerical calculations has been created on the basis of these results. This should assist design engineers in minimizing the errors when using the numerical codes and provide them with more confidence in the accuracy of their models.

It is well-known that numerical methods usually require a considerable amount of time and may not be practicable for the early stages of the engineering project, when only limited budget and information are available. In those cases, as already stated previously, analytical methods are still nowadays very useful (Colombo, 2010) for easy estimations or quick sensitivity analyses of ground thermal parameters, which are often not known accurately. The second goal of this thesis is therefore to analyse and improve the existing analytical methods for the estimation of the freezing time, in particular for the cases of one freeze pipe, freeze wall and freeze circle.

As the results of some of the currently available analytical solutions differ significantly from one another (see chapter 1.1), it was necessary to review them and propose adjustments or new solutions. Ideally, an analytical solution should be both sufficiently precise and practical for engineering applications. Such a solution would be useful even if it were more complex mathematically than past solutions, since more advanced means of calculation are currently available to solve the mathematical problem than in the past. This solution has been sought for the single freeze pipe problem and created based on an adjustment of Sanger & Sayles' solution and the verified numerical model.

All in all, the present thesis should support practitioners in two main ways. First, it poses the basis for new, practical and accurate analytical methods for thermal calculations during the early project phases. Second, it supplies guidelines for choosing suitable numerical parameters in order to achieve a sufficiently accurate and efficient numerical model in more advanced project stages.

1.3. Extent and limitations

Freezing of a porous inhomogeneous medium such as natural ground is a very complex physical phenomenon involving thermal, mechanical and hydraulic processes which is influenced by numerous factors (Schüller, 2015). Thus, the most realistic and comprehensive modelling method for ground freezing problems is ideally a calibrated fully coupled Thermal-Hydraulic-Mechanical (THM) simulation (see examples in Nasir et al. (2013), Huang et al. (2018) and Spiridonov et al. (2022)). However, simplifying the simulation is often required in engineering projects due to time and resource limitations during the design phase. For these reasons, it is frequent practice in engineering design to first perform a thermal analysis and then to introduce its results as part of the input for a geomechanical simulation, sometimes also neglecting the groundwater movement. The present thesis is focused exclusively on the time-dependent (transient) thermal problem of heat conduction in ground freezing, the hydraulic and mechanical components of the problem being out of its scope. The accuracy of the geometry of the problem and other boundary and initial conditions has not been investigated either but will be taken as known data from design assumptions, in-situ or laboratory tests. For instance, the evaluation of the thermal properties of the ground and the design of the freeze pipe pattern deserve studies on their own and have not been handled in this thesis. The thermal properties of the ground have been extensively studied; a review of this subject can be found e.g. in Rees et al. (2000) and Baier (2008). A sensitivity analysis regarding the effect of the thermal properties of the ground on thermal calculations was already done in Schüller (2015).

As frequently considered in engineering design, it is assumed that the groundwater velocity is sufficiently low so as not to affect the freezing process. Besides, the effects of convection are usually smaller than those of heat conduction (see chapter 2.3.2 and Hu et al. (2016b)). Thus, in the present thesis, heat transfer is assumed to happen only due to conduction. The geomechanical stability of the ground is assumed as given and not taken into further consideration. Therefore, no seepage or geotechnical calculations were performed. Furthermore, the study of the effects of volume changes as a result of freezing or thawing

(as e.g. in Hirai and Komori (1971)), which may create surface heaves or settlements, is also out the scope of this thesis. The migration of water during the freezing process, which plays a crucial role in the creation of ice lenses, especially in silty soils (Kellner, 2007), as well as the diffusion of solutes (e.g. salt, see Vasilyev (2009)) were not considered. For instance, the complexity of coupled problems is such that further assumptions would be required to obtain analytical solutions for them (Neaupane et al., 1999).

Following a typical simplification in practical engineering design, the freeze pipes were considered in a simplified manner, as a cylinder or a line at a constant temperature, i.e. the detailed heat transfer processes inside the pipe system and towards the ground as for example done in Ziegler et al. (2013), Vitel et al. (2016) or Kazemi et al. (2022) were not simulated, as they are not the main focus of this thesis.

Finally, it is the usual approach in ground freezing design and in most commercial software to consider the ground as a homogenous and fully saturated medium, i.e. it is studied from the macroscopic point of view. Research regarding the heat and mass transport at the mesoscopic scale of the ground has been performed, e.g. by Wang et al. (2017). These effects, e.g. nucleation, supercooling, capillary and absorption forces, which are due to interactions between the components of the ground (solid grains, water, voids, etc.) are not in the scope of the present thesis.

1.4. Methodology and structure of the thesis

After the introduction of the problem, objectives and methodology of the thesis in the present chapter, the ground freezing method is presented in chapter 2, presenting an overview of the current challenges in the thermal design of ground freezing projects. Afterwards, the state of the art of analytical and numerical calculations for phase-change problems is reviewed in chapters 3 and 0, respectively, in order to create a solid basis from which to build up the investigations.

In chapter 5, the exact analytical solution from Neumann is used to measure the accuracy of the numerical model and to find out the conditions under which it provides reasonably accurate results within a practicable computing time. In this way, a verified numerical model is obtained.

Once the verified numerical model has been attained, it is extrapolated to different geometries and used as a benchmark to measure the accuracy of the approximate analytical solutions in chapter 6. Based on these results, the analytical solution from Sanger & Sayles is adjusted and improved in chapter 7.

The numerical and analytical solutions are checked against experimental results and real engineering projects in chapters 8 and 9, respectively. The results of the previous chapters are discussed in chapter 10 and the limitations of the thesis are drafted in chapter 11. Finally, the conclusions of the thesis are drawn in chapter 12.

2. The artificial ground freezing method

The most common aims of artificial ground freezing are the stabilisation of the ground and the achievement of watertightness, e.g. in mine shafts, tunnelling or excavations. The ground freezing process allows the construction of underground structures with a low environmental impact, because it does not introduce external materials into the ground (Jessberger, 1979a) (Zhou, 2013) (Arroyo, 2017) and the ground is less altered than with the grouting method, i.e. it generally reverses to its original state after thawing (Alzoubi et al., 2020). In addition to these applications, it is also used for containment of contaminants or waste in the ground (Hu et al., 2018a), e.g. at the Fukushima Daiichi nuclear plant (Gallardo and Marui, 2016) (Alzoubi et al., 2019) or combined with a heat pump (Hu et al., 2018b). In some cases, ground freezing is used as an emergency measure or after other methods have failed in sealing and stabilising the excavation, as reported for example in Sopko (2017b).

The artificial ground freezing method is considered a versatile and safe method, which can be designed and monitored reliably. It can be applied to nearly any kind of water-bearing ground (Jessberger, 1979a) (Arroyo, 2017) (Sopko, 2017b): in ground from highly permeable coarse soils to clays and fractured rock (Schmall and Braun, 2006). Thus, it is more flexible than grouting in that respect (Harris, 1995) (Leung et al., 2012). The freeze body can embed any obstacles, and its geometry can be adapted to the requirements of the subsequent excavation (Schüller, 2015). In addition to preventing groundwater inflows into the excavation, the freeze body can serve as a temporary support (Zhelnin et al., 2020).

Among the drawbacks of artificial ground freezing, its typically higher costs compared to alternative methods (such as grouting) is one of the most important (see e.g. Braun et al. (1979), Chang and Lacy (2008) and Orth and Müller (2013)). However, it tends to be a cost-effective option to ensure structural stability and groundwater control especially at high depths or in difficult ground (Schmall and Braun, 2006) (Powers et al., 2007) (Filippo Mira-Catto, 2018). An additional downside of AGF is that the microstructure of the ground changes when it freezes and it does not completely recover its initial state after thawing (see Harris (1995) and An et al. (2021)). It has been demonstrated by means of experiments that this leads to a decrease of its strength, more markedly after several freeze-thaw cycles (Chen et al., 2021). This effect can also be observed for seasonal freezing in natural slopes (Chen et al., 2017). Another consequence of the changes in the ground after freeze-thaw cycles, reported by Dalla Santa (2022), is the increase in permeability and pore size. Another potential negative consequence of artificial ground freezing is frost heave (Kellner, 2007) (Zhao, 2019) (Zhou et al., 2021), which is produced by the formation of ice lenses and, to a lesser extent, the increase of volume of water turning into ice (Zhang, 2014). This may generate issues in structures above the frozen ground area and lead to heave after freezing and settlements after thawing, which are especially problematic if uneven. A detailed study of freeze-thaw cycles and a mathematical model for numerical simulations of these effects can be found in Zhang (2014). Another effect which needs to be considered

in the geomechanical design of the freeze body is that frozen ground creeps under stress (Harris, 1995).

All in all, artificial ground freezing is deemed to be a proven and reliable method (Sopko, n.d.-a) (Müller, 2014) provided that proper design and monitoring programmes are put in place (insufficient design and monitoring, among other reasons, have led to major issues in the past, e.g. flooding (Czaja et al., 2020) and breaches of the freeze wall (Cleasby et al., 1975) (Sopko and Braun, 2000). AGF is considered "one [of] the most reliable techniques for very complex projects" (Filippo Mira-Catto, 2018), see also Roberti (2012) for a comparison of its risks with other methods, such as piling, diaphragm walls, low-pressure injections and jet-grouting. In addition, it may be used in small spaces (Roberti, 2012), which is advantageous for urban environments. Due to these advantages and the strong urbanization trend, the relevance of the ground freezing technique will tend to increase in the future in underground engineering projects (Haß and Schäfers, 2013).

2.1. History of artificial ground freezing

In the winter of 1852, French engineers found out that it was advantageous to construct a mine shaft under frozen conditions, as it was in otherwise unstable water-bearing ground (Harris, 1995). The first application of artificial ground freezing is recorded by Siebe Gorman & Co on a coal mine shaft in Swansea, South Wales, UK, around the year 1862 (Hu et al., 2018b) (Alzoubi et al., 2020). The ground freezing technique was then patented by Friedrich Hermann Poetsch in Germany in 1883 (Poetsch, 1883) (Vitel et al., 2015). A detailed account of the history of this invention, Poetch's achievements and the development of the ground freezing technique in Germany until the 1960s can be found in Hoffmann (1962). The first ground freezing application in the United States was done in 1888 at the Chapin Mine Co. in Montana (Schmall and Maishman, 2007).

Originally, AGF was developed to sink mine shafts through water-bearing layers down to coal seams (Haß and Schäfers, 2013). It was later on internationalised and has been used repeatedly in numerous countries around the world. Khakimov (1966) estimates that, just for subway construction, more than 1 million m^3 of soil were frozen between 1947 and 1957 in the Soviet Union. Also in China, ground freezing has been used for more than 55 years (Li et al., 2006). It has also been used for underground construction in New York, Beijing, Shanghai, Nanjing, Guangzhou, Shenzhen, Napoli or Moscow, among others (Nikolaev and Shuplik, 2019) (Yan et al., 2019). Ground freezing has been used extensively for shaft sinking for gold mines in mining regions such as Siberia (Russia) too. For instance, all copper mine shafts and most hard-coal mine shafts in Poland have been sunk using the ground freezing method, with water-bearing layers up to depths of 700 m (Czaja et al., 2020) (Kamiński, 2021). In the coal-mining Ruhr area in Germany, the ground freezing method has also been used extensively, for example for shaft Rheinberg (Arbeitsgemeinschaft Schacht Rheinberg, n.d.). Deep shafts have also been built by means of AGF for purposes of underground nuclear waste repositories, for example in Mol (Belgium) (Ramaeckers et al., 2000) and in Gorleben (Germany) (Jessberger, 1994).

A further advance was made in 1962, when freezing with liquid nitrogen was first used in France (Ritter, 1962) (from Sanger and Sayles (1979)). In the past, simple, conservative models were used to estimate the ground freezing requirements, whereas more intensive investigations in the ground freezing field were first performed in the 1970s (Schüller, 2015). Afterwards, AGF has been widely used in mining and civil engineering. In the last 20-30 years, its application has increased in tunnelling and urban areas (Zhou, 2013) (Schüller, 2015), see e.g. Haß and Schäfers (2013) for examples of such projects.

As artificial ground freezing has been widely used since the early 20th century for underground construction, it is a mature technology which has been applied to numerous engineering projects (Hu et al., 2018a). Indeed, Harris (1995) compiled about 400 of them from the period 1862-1990.

2.2. The principles of the artificial ground freezing technique

The ground freezing method is used to improve the stability and watertightness of the ground prior to excavation by freezing the groundwater, as already presented in chapter 1.

The usual ways to freeze the groundwater are either to circulate a cooled fluid, usually brine (a solution of calcium chloride, $CaCl_2$, in water), at about –20 to -38ºC (see e.g. Kellner (2007), Haß and Schäfers (2013) and Hentrich and Franz (2015)), or liquid nitrogen, at about -196ºC (Harris, 1995), through pipes installed in the ground (freeze pipes). In that way, the groundwater in the soil or rock starts freezing from the neighbourhood of the pipes towards the regions further from the pipe. As a consequence, the water in the ground pores turns into ice, improving the mechanical properties of the soil or rock. The ground becomes practically watertight (provided it is saturated) and its strength increases to a variable extent, which depends on its characteristics. In the case that it is desired to apply the ground freezing method to non-saturated ground, it is possible to inject water into the ground in order to increase its water content, as e.g. done for the construction of cross-passages for the Westerschelde tunnel in the Netherlands (Haß and Schäfers, 2013). Figure 2.1 shows a picture of the application of AGF for a tunnel in Naples (Italy), which shows the freeze pipe heads and manifold.

Figure 2.1: Freeze pipes around a platform tunnel in Naples (Viggiani and De Sanctis, 2009)

For ground freezing with brine, a freezing station is required, which cools the brine. Additionally, connecting pipes are installed, which carry the brine from the station to the freeze pipes. The freeze pipes typically consist of an outer pipe and a supply inner pipe (or downpipe), which are installed in boreholes. The inner pipe is opened at its further end and carries the brine from the freeze head towards the end of the borehole. It is surrounded by an outer closed pipe, in which the cooling fluid circulates in the reverse direction and cools the surrounding ground, before finally returning to the freezing station. A schematic illustration of a freeze pipe is shown in Figure 2.2.

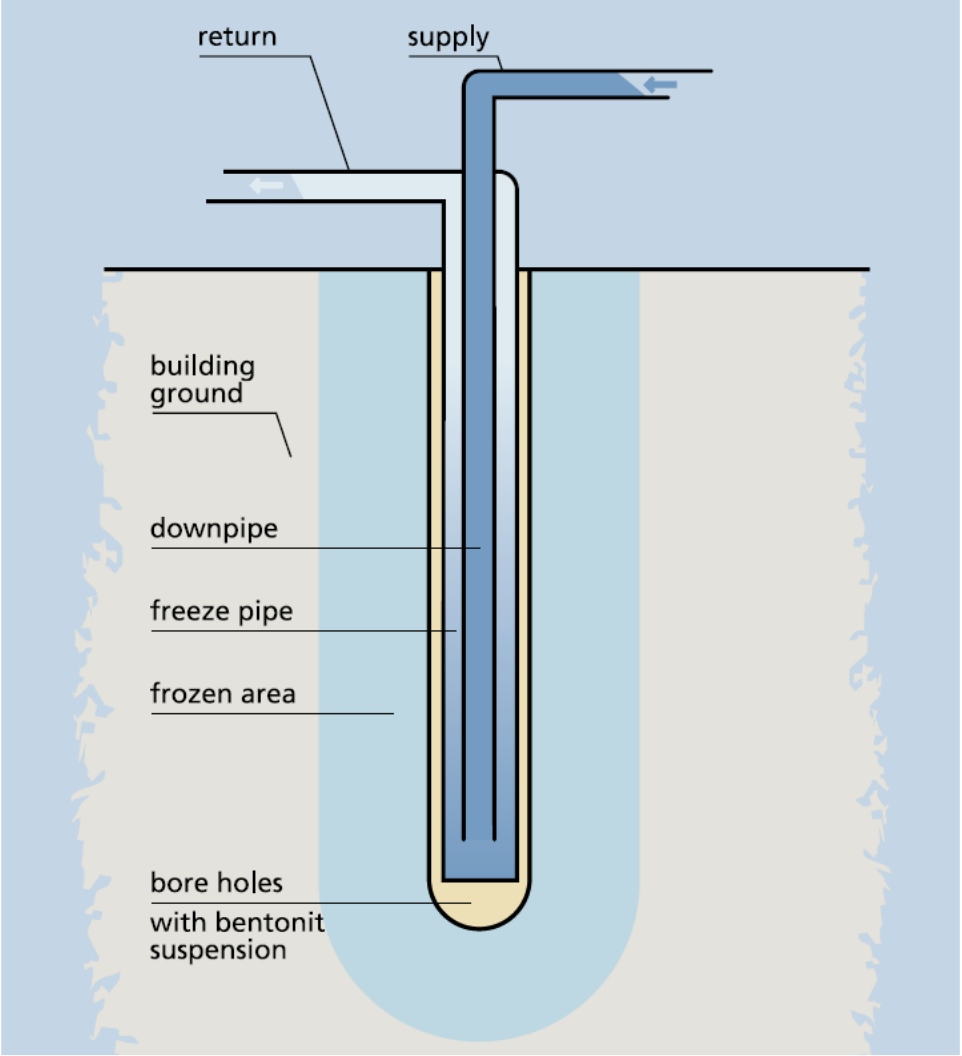

Figure 2.2: Schematic view of a freeze pipe (Müller, 2014)

The freezing station cools down the brine with a refrigeration cycle with e.g. ammonia or CO_2 and dissipates the heat produced by using water or air. An exemplary overview of the ground freezing setup is presented in Figure 2.3.

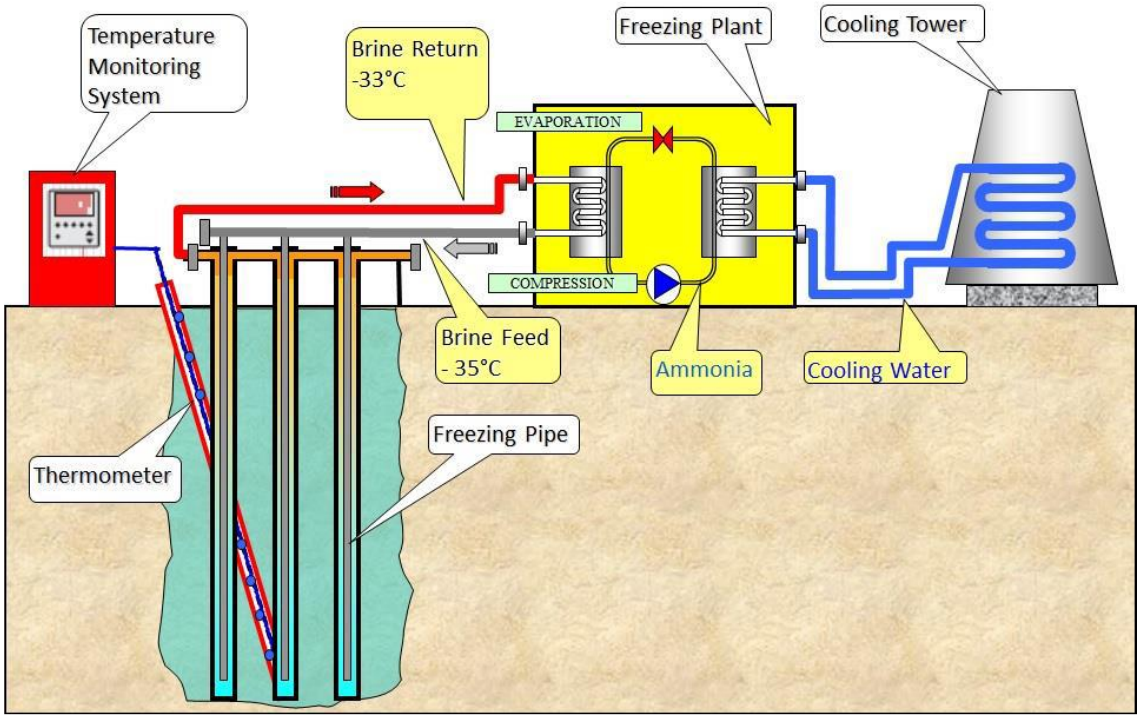

Figure 2.3: Exemplary ground freezing setup with brine (Filippo Mira-Cattò, 2016)

If ground freezing with nitrogen is chosen, liquid nitrogen is delivered by tank trucks to the site and injected into the pipes at a temperature of approx. -196ºC. After having cooled the ground, it exhausts towards the exterior as a gas (Pimentel et al., 2011). A scheme of a ground freezing arrangement with nitrogen is shown in Figure 2.4.

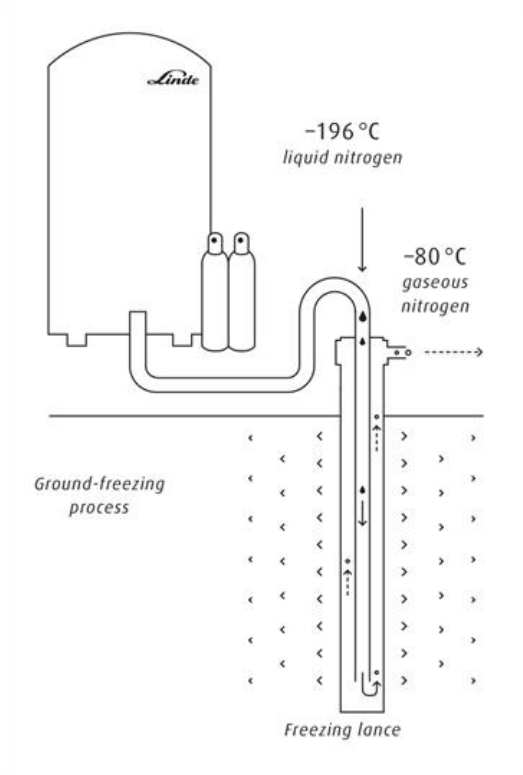

Figure 2.4: Scheme of ground freezing method with nitrogen (Linde plc, 2021)

In general, ground freezing with brine requires a larger site setup than nitrogen freezing, which does not require either a freezing station or electrical power. Another drawback of brine freezing is that it does not achieve as quick a freezing progress as nitrogen freezing does, which may be an issue in certain projects. For instance, nitrogen freezing was applied for this reason in the metro from Valencia after attempting to use the brine freezing method (Muzás, 1989). Thus, nitrogen freezing may be the preferred method for emergency cases. However, the daily costs are much lower with brine freezing than with nitrogen freezing (Sopko, 2017a), which is why the former is typically used for projects running for a longer time (from several weeks to years), while nitrogen freezing tends to be applied for short periods of time or emergency situations. A practical comparison of these methods, including economic considerations, can be found in Roberti (2012). It is also possible to combine both methods, using nitrogen freezing at the start of the project, to generate the freeze body quickly and to switch afterwards to brine freezing to maintain the freeze wall during a longer time (e.g. for the metro of Naples, in the Piazza Municipio station (Manassero et al., 2008) (Viggiani and De Sanctis, 2009) and for metro tunnels in Warsaw (Arroyo, 2017)). Another technique, though less commonly used, is to use liquid or solid carbon dioxide (CO_2) (Nikolaev and Shuplik, 2019) (Shuplik and Nikolaev, 2019). Ground freezing may also be combined with other ground improvement methods, such as jet grouting and injections (see e.g. Muzás (1989)).

Several phases can be differentiated in the freezing process. The first one (pre-freezing) starts when the freeze pipes are put into operation and frozen cylinders grow from the pipes outwards. The second phase (maintenance) begins when these cylinders have merged with each other, generating a continuous, watertight freeze body. At some point in time, the freeze body will reach the minimum thickness required for stability reasons (in the case that the freeze body is required to stabilize the ground) and the excavation may begin. Afterwards, the so-called maintenance phase starts, in which the size of the freeze body just needs to be maintained and the freezing station is typically run intermittently and/or using less power. The phases are shown in Figure 2.5 for a freeze circle. As the temperature gradient between the freeze pipe and the ground is steadily reduced, the power consumed by the freezing station typically decreases continuously during the whole freezing process (Schüller, 2015). Finally, when the excavation has been finalised and the permanent lining installed, the freezing plant can be disconnected, the freeze pipes are usually backfilled, and the freeze body left to thaw. In most cases, the thawing process is natural, but in some projects the ground is heated from the freeze pipes to accelerate the process, as e.g. in the *Fernbahntunnel Lot 3* in Berlin (Haß and Schäfers, 2013).

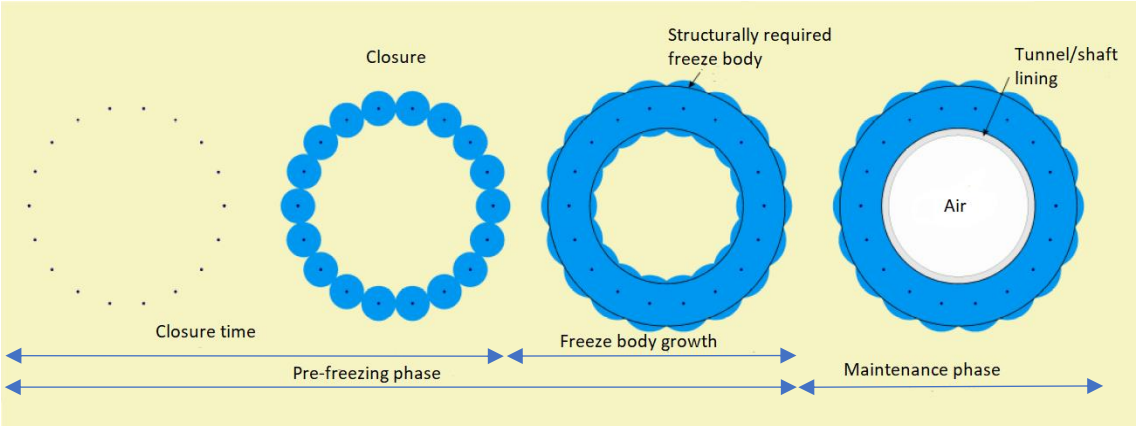

Figure 2.5: Evolution and phases of the freezing process in a freeze circle, adapted from Baier (2008)

2.3. Design and monitoring of ground freezing engineering projects

The aim of ground freezing engineering design is to achieve a safe excavation by controlling the groundwater and stabilising the ground, while at the same time minimizing the costs and the overall schedule of the works (Filippo Mira-Catto, 2018). It needs to be highlighted that a suitable design and monitoring programme is key to the safety of the works and avoidance of accidents, as can be learned from the cases presented in Sopko and Braun (2000), Shawn et al. (2016) and Levin et al. (2017). In fact, the success of ground freezing projects rests largely on a suitable design (an overview of the design components is given in Figure 2.6), which requires "appropriate modelling and understanding of the ground freezing problem" (Zueter et al., 2021).

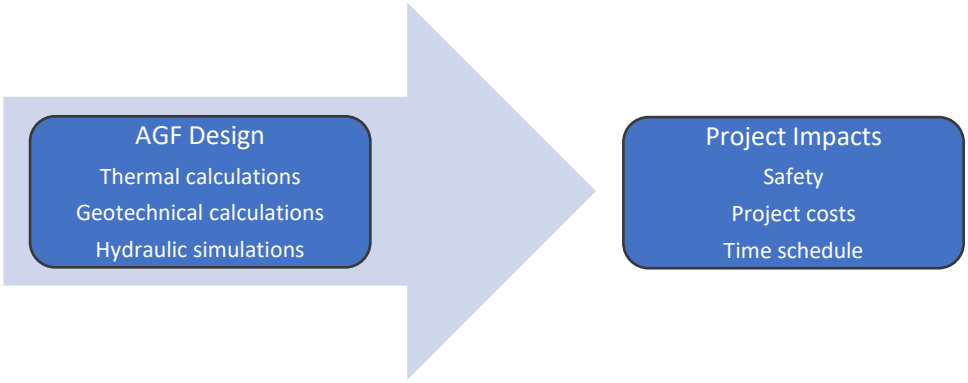

Figure 2.6: AGF design process and project impacts

As no norms or standards for ground freezing design exist to the author's knowledge, a brief description of the design process is presented below.

Ground freezing design typically starts with the evaluation of the geometrical requirements of the project and a preliminary determination of the freeze pipe pattern. For instance, a cylindrical shaft will usually imply the use of a circular pattern of freeze pipes around the future excavation, while a row of pipes may be required to support a plane wall of a straight excavation. Aside from the geometry, the thermal and mechanical characteristics of the ground are considered for the design, as they may affect the freeze pipe spacing and disposition. In order to collect these data, a suitable ground investigation programme

focused on the future ground freezing application needs to be performed prior to the design, otherwise assumptions may be taken based on the available ground data and literature values. Suitable input data to the design is required for an adequate and cost-effective design and efficiency of the calculations (Frivik, 1981).

Once the geometry of the excavation and freeze pipe pattern and the ground properties for design are determined, it is possible to start the thermal and geomechanical calculations. In the case that the freeze body is required for stability reasons, geomechanical calculations are performed to determine the shape and thickness of the freeze body required for the stability of the excavation. Then, a transient thermal analysis is performed in order to predict the required time until the targeted freeze body geometry is achieved and the required power of the freezing station for the project. This analysis may be performed with analytical tools in the early design stages and is nowadays usually refined with numerical methods for final design (Powers et al., 2007). Nomograms like the one in Figure 2.7, which are based on analytical methods, also represent an alternative to the calculations and may be useful in early stages. A historical review of the thermal design of AGF can be found in Frivik (1981).

Ground freezing design is usually an iterative process, for instance, the design (brine temperature, number of pipes, pipe pattern) may be adapted according to the results of the first geomechanical and thermal analyses, e.g. the number of pipes may need to be increased in order to reduce the freezing time or may need to be reduced to optimize the number of boreholes to be drilled and decrease the project costs. In the end, there is often a trade-off between the schedule improvement for the works and the costs of the ground freezing measure.

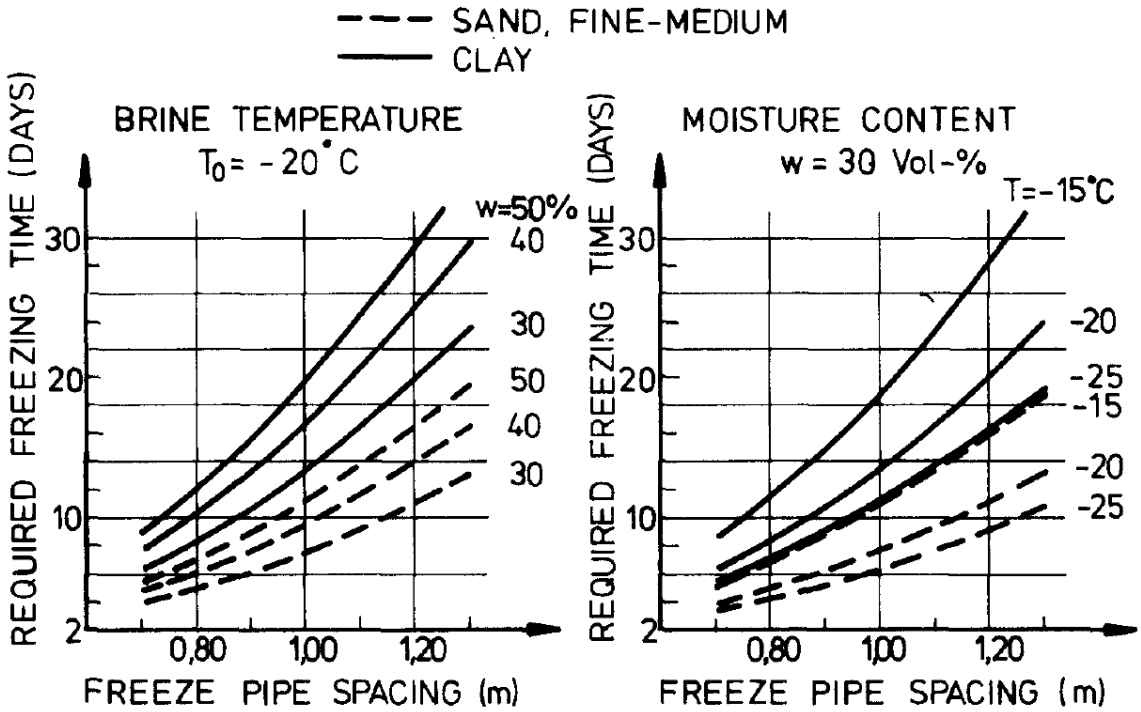

Figure 2.7: Exemplary nomograms for ground freezing thermal design (Jessberger, 1979b)

In addition to a suitable freeze design, a full quality control and monitoring program during execution are essential to achieve a successful ground freezing project (Max Bögl, n.d.) (Chris K W Leung, 2012). A sample of such a program can be found in Powers et al. (2007). For instance, the position of the pipes has to be surveyed to measure their deviations and the tightness of the piping system needs to be controlled. Additionally, several temperature monitoring boreholes and piezometer boreholes are required and a relief borehole in the centre of the shaft or tunnel is often installed. The data from the monitoring system can be used in order to control the freezing progress as well as to refine or verify the design model (Chang and Lacy, 2008), such as done in Colombo (2010).

2.3.1. The ground as thermodynamic system

In thermodynamic analysis, materials are usually considered as a continuum at a macroscopic scale, i.e. it assumed that it is possible to analyse a reference volume with average properties (Lunardini, 1986). The ground is an inhomogeneous, porous medium composed mainly by mineral particles, water and air (in case it is saturated, it can be considered to contain no air). If it is frozen, it will normally contain a mixture of water and ice. Figure 2.8 presents a conceptual model for saturated ground, showing its different phases.

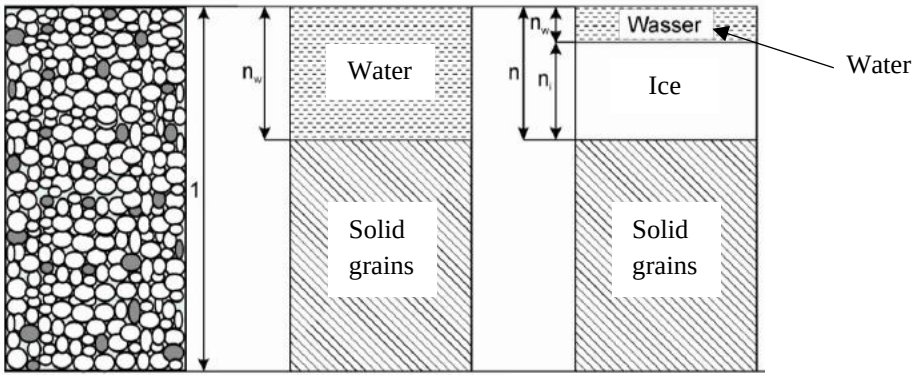

Figure 2.8: Phase model for saturated ground, modified from Ziegler et al. (2010)

Unlike pure substances, which change phase at a constant temperature, the ground presents a gradual phase change (Osterkamp, 1987) (Ramos, 1996). In ground systems, it is known that water does not freeze at a constant temperature due to adsorption forces (Baier, 2008), see also Sres (2009). Even at very low temperatures, a certain amount of unfrozen water remains, especially in fine soils (clays and silts), because of their higher specific surface (Baier, 2008). Extensive investigations have been performed to find out the relationship between temperature and unfrozen water content in soils. An overview of the unfrozen water content for different types of soil is presented in Figure 2.9.

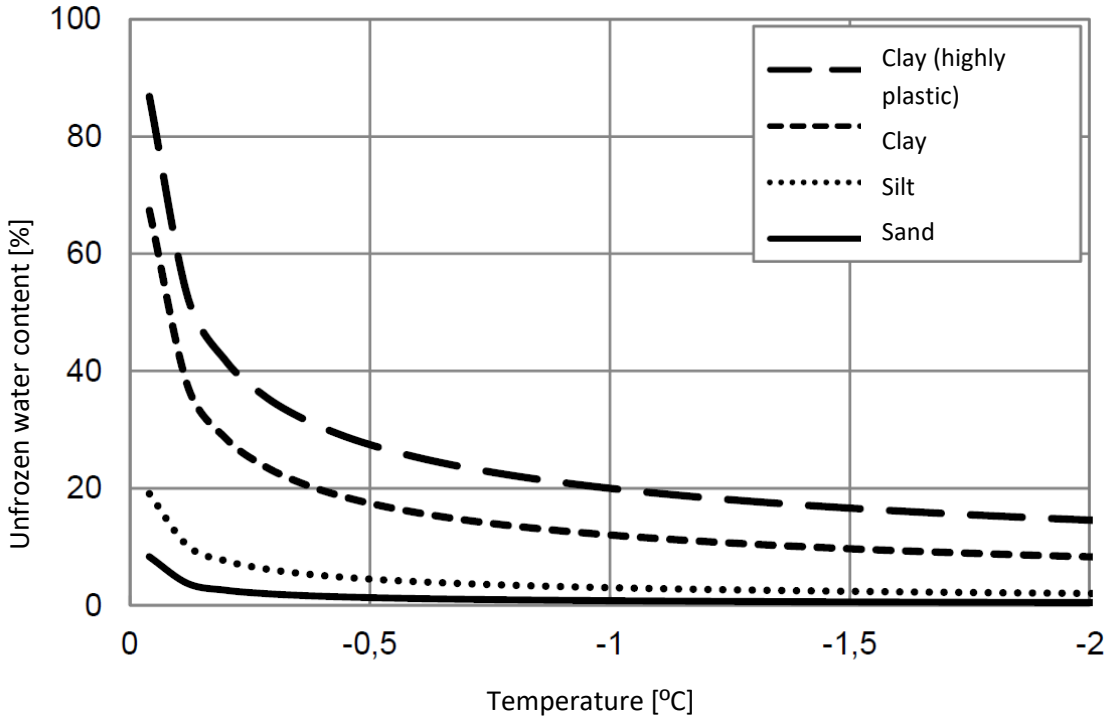

Figure 2.9: Typical unfrozen water content functions for different soils, adapted from Jessberger (1990) and Schüller (2015)

The unfrozen water content discussed above has the effect that, unlike pure substances, water-bearing soils and rocks change phase at a temperature range (Lunardini, 1988) and therefore an abrupt simulation of the phase change in analytical and numerical models may not accurately represent the reality of the process. From a mathematical point of view, phase change problems in porous materials, such as soil, are governed by similar differential equations as the solidification of metals or semiconductor crystals (Rodrigues and Urbano, 1999).

As natural ground is inhomogeneous (at a micro- as well as at a macroscopic scale), it is usually challenging to determine the thermal properties of the soils and rocks in engineering projects. The thermal properties are typically determined at the macroscopic scale, i.e. considering the soil as a homogeneous mixture at the microscopic scale. The determination of the thermal characteristics of soils is usually performed in the laboratory on relatively small samples, which may or may not be representative of the in-situ conditions. Another factor is that water migrates during the process (Jame and Norum, 1980), complicating the thermal calculations (Berggren, 1943) and causing ice lenses, frost heave or high frost pressures, especially in finely grained soils (Kellner, 2007). Additionally, the volumetric expansion of water during the freezing process also produces frost heave or pressure (Jessberger, 1979a), which may damage nearby structures.

The thermal properties of the ground depend heavily on the mineralogy, grain size and water content. For instance, coarser soils (gravels and sands) typically have a higher thermal conductivity and a lower specific heat capacity than clays; furthermore, the latter exhibit molecular bonds between their minerals and water (see e.g. Arroyo (2017)).

Therefore, coarser soils typically display a faster freezing progress. Figure 2.10 and Figure 2.11 present typical values of thermal conductivity and specific heat capacity for different types of soils.

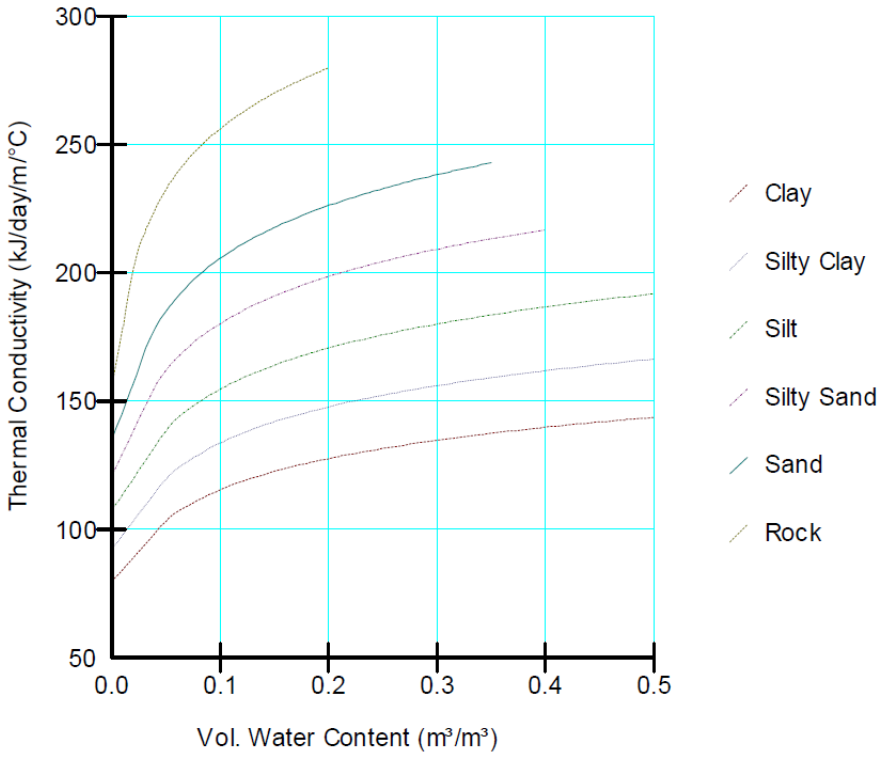

Figure 2.10: Typical thermal conductivity of different types of soils (GEO-SLOPE International Ltd., 2014)

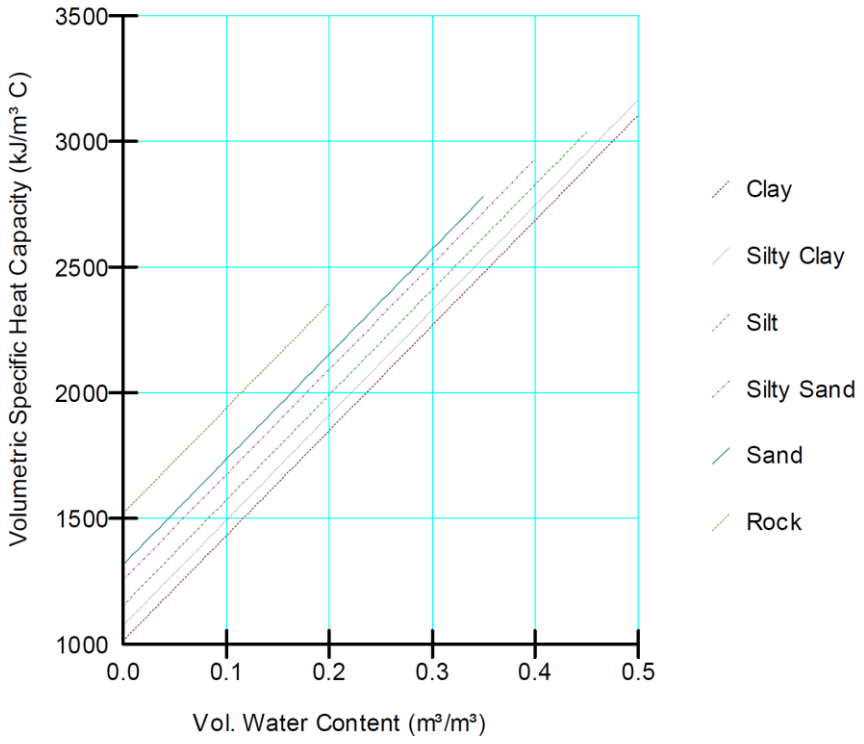

Figure 2.11: Typical specific heat capacity of different types of soils (GEO-SLOPE International Ltd., 2014)

2.3.2. Typical assumptions & simplifications in AGF design

It is usual in engineering design of ground freezing projects to make certain assumptions in order to achieve a sufficiently accurate design while limiting the costs and time required for the design.

One possible assumption is to model the freeze pipe as a punctual/linear cooling source of constant temperature (as done e.g. in Hentrich and Franz (2015)). This simplifies the real three-dimensional geometry of the pipe and the detailed heat transfer mechanisms. For instance, in reality the fluid travels down the internal pipe and goes up through the exterior ring, so the fluid temperature is usually non-uniform over the depth, an effect which is typically not considered in the design. A detailed study of the heat transfer between the pipe and the ground can be found in Vitel et al. (2016). Their model aims to optimize the design of the freezing system.

Regarding the thermal properties of the ground, it is usual to assume the specific heat capacity and thermal conductivity of each phase as constant (see e.g. Hentrich and Franz (2015) and Colombo (2010)), even though they are variable with temperature (Ziegler et al., 2010). However, the variation of these properties with the temperature, within each of the phases, is relatively minor for the temperature ranges relevant in civil or mining engineering (see e.g. GEO-SLOPE International Ltd. (n.d.), Lunardini (1987), Robertson (1988) and Misra et al. (1995)).

The thermal properties are often considered as independent of stress and strain state, i.e. in this case, the thermal and mechanical fields are simulated separately, as not coupled. To further simplify the problem, the hydraulic field is also often uncoupled from the thermal field: convection is ignored and the migration of water to the freeze front is neglected in the thermal simulation. These assumptions are used for example in G. Gioda (1994), Hentrich and Franz (2015) and Colombo (2010).

The necessity to consider the effects of the groundwater flow on the freeze body has been studied in several papers and doctoral theses. Jame and Norum (1980), Baier (2008), Sres (2009), Ziegler et al. (2010), Zhou (2013) and Vitel et al. (2016) conclude that water movement may affect the freezing process and has to be considered under certain conditions. With respect to specific values of groundwater flow, it is said in Stuizalec (1989) that a flow velocity of more than 1 m/day is normally taken as affecting the ground freezing process. Andersland and Ladanyi (2004) point out a velocity of 1 m/day to 2 m/day as impeding the closure of the freeze wall. Harris (1995), Arroyo (2017), Chang and Lacy (2008), Zhou (2013) (from Schultz et al. (2008)) and Filippo Mira-Catto (2018) provide an approximate limit of approx. 2 m/day for brine freezing (also cited by Powers et al. (2007), based on several sources) and 4-6 m/day for liquid nitrogen freezing. Haß and Schäfers (2013) report that for the *Fernbahntunnel Lot 3* in Berlin the groundwater velocity of 1.5 m/day was considered as uncritical for ground freezing. The actual groundwater velocity depends on the gradient and also on the permeability of the soil, according to Darcy's law: in highly permeable soils, such as gravels, critical velocities may be reached even under relatively low gradients (Roberti, 2012). For ground freezing with nitrogen, a

groundwater flow of more than 10 m/day was reported to have a significant effect (Wang et al., 2020).

As shown above, there are several studies which have proved that groundwater flow may have a significant influence on the ground freezing process and should be considered in ground freezing design, at least in certain cases, see e.g. Baier (2008), Sres (2009) and Schüller (2015). Naturally, the critical groundwater velocity also depends on several factors, such as the freeze pipe temperature and freeze pipe separation (Roberti, 2012), the phase-change temperature of the groundwater and the thermal properties and water content of the ground. Nevertheless, the effects of convection and radiation are usually low relative to the conduction in ordinary ground freezing projects (Lunardini, 1998) (Hu and Zhang, 2013). The relative importance of the heat transfer mechanisms in the ground with respect to its saturation and grain size is presented in Farouki (1981) and summarised in Figure 2.12. Therefore, in the present thesis, only conduction has been considered, as defined in chapter 1.3 above, which is a valid approach for many cases (Lunardini, 1987), although its applicability needs to be evaluated under the particular circumstances of the problem.

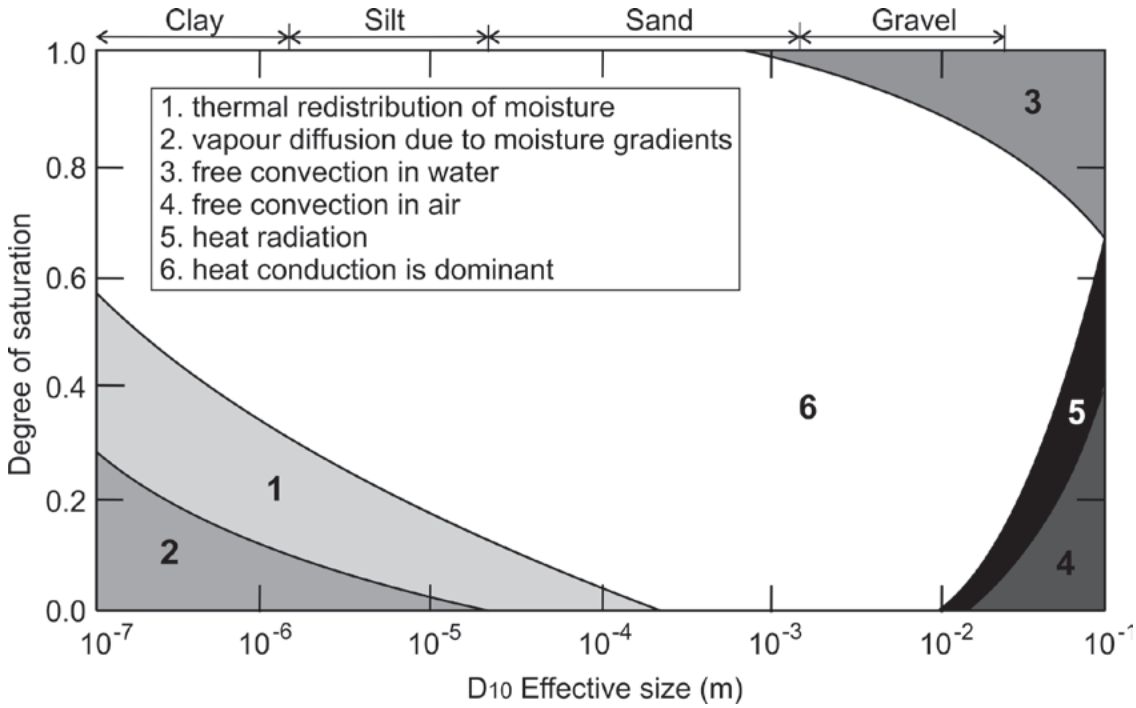

Figure 2.12: Relative importance of various heat transfer mechanisms in different soils (Farouki, 1981), redrawn by Loveridge (2012)

3. Review of the state of the art in analytical thermal calculations for ground freezing design

The physical phenomenon underlying the ground freezing technique is the phase change of groundwater. Phase change of matter is a process which plays a crucial role in nearly every aspect of everyday life, science and engineering. When a material turns from liquid to solid, it is said to be freezing, which is, naturally, the relevant phase change process for the present thesis. During that process, latent heat is released at the interface between the two phases. Latent heat for pure water is high compared to other materials and to its own specific heat capacity, amounting to 333,600 J/kg.

In thermodynamics, a phase-change problem consists of predicting the temperature field and physical state of the material which is undergoing phase change, given certain boundary and initial conditions. The phase change problem can be classified mathematically as a free boundary problem, specifically, it is a moving boundary problem. A free boundary problem is a problem described by differential equations which includes a boundary condition whose position is not known *a priori*, but which has to comply with certain constraints (Friedman, 2000) (Chen et al., 2015), in the case of phase-change problems, among others, energy conservation and constant temperature. As the determination of this moving boundary is part of the solution to the problem, these problems are non-linear (Furzeland, 1980). With respect to the regularity of the solution, it has been proved that in general one-dimensional Stefan problems are well-posed, i.e. a unique and classical continuous solution exists (Ayasoufi, 2004).

A further distinction typically made in the literature is between one- and two-phase problems. In one-phase problems, it is assumed that one of the two phases can be neglected in the problem. One representative case is that the material is at the phase-change temperature at the beginning of the problem, gradually melting due to a heat source located at the boundary. The classical Stefan problem is an example of a one-phase moving boundary problem which can be applied to ground freezing. Stefan (1891) performed investigations on the depth of the frozen zone in the polar seas and solved the mathematical one-phase problem, which is why moving boundary problems are named after him. However, the first recorded contribution regarding the heat transfer problem with phase change is by the French mathematician Lamé and Clapeyron (1831) (Jonsson, 2013). Franz Ernst Neumann (c.1860) found the solution for the corresponding two-phase problem, which is a one-dimensional case of a semi-infinite space with a plane source (Lunardini, 1986). In artificial ground freezing for engineering projects, the typical situation requires solving two-phase 2D or 3D problems, because the initial ground temperature rarely coincides with the phase-change temperature of the groundwater.

Interestingly, free boundary problems appear in various fields of science and technology: apart from the phase change problem in thermodynamics (with applications in artificial ground freezing, permafrost depth prediction, solidification of volcanic lava, food preservation, melting of alloys, welding or compact energy storage), they govern processes

in other areas of physics, chemistry, engineering, finance and biology, among others (Basu and Date, 1988) (Chen et al., 2015) (Zhou et al., 2018) (Bollati, 2019). Among the specific problems they govern are the determination of the pricing and optimal exercise value of American options in Black-Scholes models in economics, the prediction of the movement of tumours in mathematical biology (Chen et al., 2015) or the sediment mass transport (Kumar and Singh, 2020). More examples of applications of free boundary problems can be found in the areas of geophysics, semiconductor design and cryosurgery (Mackenzie and Robertson, 2000) (see also Friedman (2000)). Stefan problems have been extensively studied (Roscani and Tarzia, 2018) and are nowadays the subject of intense research, from the experimental, numerical and analytical viewpoints (Chen et al., 2015).

The occurrence of the phase change implies a change of the thermal, mechanical and hydraulic properties of the material and the release or absorption of latent heat during the phase change process. Thus, it introduces a non-linearity in the boundary conditions (BCs) of the differential equations governing the heat exchange. This non-linearity considerably increases the difficulty of solving the system of equations. For instance, the superposition principle cannot be used due to the non-linearity (Özişik, 1993). As a consequence, only a limited number of exact closed analytical solutions for specific phase-change problems with practical applicability have been found to date (Lunardini, 1986) (Paynter and Life, 1999). Still, exact solutions have several practical applications, even if only a few of them are available, typically for idealized problems. First, they may be used to check the accuracy of approximate analytical or numerical solutions (Gottlieb, 2002) (Zhou et al., 2018) (Kumar and Singh, 2020). Moreover, analytical solutions often present explicit formulae, which are convenient and relatively fast to use for sensitivity analysis and simplified engineering calculations in early stages of the design.

A widely used parameter in Stefan problems is the Stefan number S_T, a dimensionless parameter which intends to characterise the ratio of sensible heat to latent heat, as defined in Equation (3.1). For large Stefan numbers, heat conduction governs the heat transfer process, while for small Stefan numbers, the phase change has a dominant effect (Alexiades, 2017).

$$S_T = \frac{c_s \cdot \Delta T}{l} \tag{3.1}$$

where:

c_s: specific heat capacity

l: latent heat per unit mass

S_T: Stefan number, [-]

ΔT: temperature difference between phases

3.1. Theory of thermal conduction without phase change

Before studying the heat transfer in systems with phase change, the equations for conductive heat transfer without phase change are presented shortly. The energy transfer by conduction follows Fourier's law (Fourier, 1955) (from Lunardini (1986)), which is based on the first law of thermodynamics (conservation of energy). Fourier's law in one dimension can be written, exemplarily for heat transfer in the x-direction, as:

$$q_x = -k_x \cdot S_\perp \cdot \frac{\partial T}{\partial x} \tag{3.2}$$

where:

k_x: thermal conductivity in the direction of the "x" axis

q_x: flux or heat transfer rate in the direction of the "x" axis

$S_\perp$: surface of the zone perpendicular to the direction of the energy transmission

$\frac{\partial T}{\partial x}$: temperature gradient in the direction of the "x" axis

According to this equation, the flux q_x in the direction of the temperature gradient is proportional to the surface $S_\perp$ and the gradient $\partial T/\partial x$, being the thermal conductivity k_x the proportionality constant (Lunardini, 1986).

This equation can be completed with the consideration of energy sources (due to chemical reactions, electricity current, latent heat, etc.). This is done by adding a generation term q_g to the equation, which represents the energy released or absorbed per unit volume and time (Lunardini, 1986).

Furthermore, materials store energy when they change temperature and possess a certain specific heat capacity, c_s. For a material at rest and neglecting the effect of radiation, the conduction is governed by the following parabolic partial differential equation (PDE) (Lunardini, 1986):

$$\frac{\partial}{\partial x}\left(k_x \cdot \frac{\partial T}{\partial x}\right) + \frac{\partial}{\partial y}\left(k_y \cdot \frac{\partial T}{\partial y}\right) + \frac{\partial}{\partial z}\left(k_z \cdot \frac{\partial T}{\partial z}\right) + q_g = \rho c_s \frac{\partial T}{\partial t} \tag{3.3}$$

where:

k_x, k_y, k_z: thermal conductivities in the directions of the "x", "y" and "z" axes, respectively

q_g: energy released by the source per unit volume and per unit time

$\frac{\partial T}{\partial x}, \frac{\partial T}{\partial y}, \frac{\partial T}{\partial z}$: temperature gradient in the direction of the "x", "y" and "z" axes, respectively

ρ: density of the material

If the material is thermally isotropic, the equation can be presented in a more compact form using the Laplacian operator $\nabla^2 T$ (Lunardini, 1986), as:

$$\nabla^2 T + \frac{q_g}{k} = \frac{1}{\alpha}\frac{\partial T}{\partial t} \tag{3.4}$$

where k is the thermal conductivity and $\alpha = k/\rho c$ is the thermal diffusivity.

The heat transfer problem requires setting initial and boundary conditions. These conditions are set at certain regions of time and space, for example at $t = 0$, $x = 0$ and $x = s$. These boundary conditions may be a fixed temperature (Dirichlet condition), a fixed flux (Neumann condition) or mixed conditions. The solution to this PDE is the temperature distribution, a function $T(x, y, z, t)$, which fulfils the PDE and the boundary conditions at all points in space (x, y, z) in the region considered, at all times, and additionally satisfies the initial conditions (Causon and Mingham, 2010).

The previous equation can be written in cylindrical coordinates, which is very useful for problems with cylindrical symmetry. If the only relevant coordinate is the radius and there are no flux sources, the equation can be simplified as follows (Lunardini, 1986):

$$\frac{1}{r} \cdot \frac{\partial}{\partial r}\left(r \cdot \frac{\partial T}{\partial r}\right) = \frac{1}{\alpha}\frac{\partial T}{\partial t} \tag{3.5}$$

where r is the radial coordinate.

3.1.1. **Steady-state solutions to heat transfer problems**

Steady-state analysis evaluates the heat-transfer problem without transient effects, which is analogous to considering the state reached after a sufficiently long time. Solutions to one-dimensional steady-state problems can be obtained more easily than to transient problems with phase change (unknown, n.d.-b).

3.1.1.1. <u>One-dimensional conduction between two surfaces at constant temperature</u>

The solution for an infinitely high and long slab of finite thickness x_2, with known heat flux at one side q_1 and known temperature T_2 at the other, can be obtained by integrating the general differential heat equation (unknown, n.d.-b), resulting in:

$$T(x) = \frac{q_1}{k}\,(x_2 - x) + T_2 \tag{3.6}$$

where $T(x)$ is the temperature distribution in the direction of the coordinate "x".

3.1.1.2. <u>Single cylindrical sink with constant flux</u>

In analogue manner to the previous chapter, a few exact solutions for problems in cylindrical coordinates have been found (unknown, n.d.-c) (unknown, n.d.-b). For example, the temperature distribution for the problem with a constant given heat flux q_1 at $r = r_1$ and a constant temperature T_2 at $r = r_2$, is given by (unknown, n.d.-b):

$$T(r) = \frac{q_1 r_1}{k} \ln\left(\frac{r_2}{r_1}\right) + T_2 \tag{3.7}$$

3.1.2. Transient solutions to heat transfer problems

Transient solutions for thermodynamic systems without phase change may be obtained by integrating the time-dependent heat equation. Transient analysis is required, among other reasons, due to the effect of the sensible heat, which may be large and needs to be considered (Rees et al., 2000) (sensible heat does not affect the results of steady-state analyses). These solutions are the basis to build upon and simulate ground freezing problems appropriately. Exemplarily, a solution for a 1-dimensional problem is presented below. A review containing further solutions to problems without phase change can be found in Rees et al. (2000).

3.1.2.1. One-Dimensional semi-infinite slab

The solution to the one-dimensional transient problem without phase change in a semi-infinite solid (domain $x = 0$ to $x = \infty$) is presented here. This may be compared to the same problem with phase change: the Neumann problem presented in chapter 3.2.1.

Let the whole solid be at an initial constant temperature T_0 at $t = 0$ and be suddenly exposed to a fixed temperature $T = 0$ at the boundary $x = 0$. The problem is defined by the following PDE and BCs:

$$\frac{1}{\alpha} \cdot \frac{\partial T}{\partial t} = \frac{\partial^2 T}{\partial x^2} \tag{3.8}$$

$$T(x, 0) = T_0 \tag{3.9}$$

$$T(0, t) = 0 \tag{3.10}$$

Unknown (n.d.-b) obtains the solution making use of the Laplace transform, leading to:

$$T(x, t) = T_0 \cdot \mathrm{erf}\frac{x}{2\sqrt{\alpha t}} \tag{3.11}$$

where erf (z) is the error function.

Solutions to more problems in cartesian and cylindrical coordinates with relatively simple geometry and boundary conditions have been obtained, e.g. by use of the method of separation of variables (unknown, n.d.-b). Further solutions for multisource problems have been proposed by means of superposition techniques, although they are semi-analytical and therefore not exact (Fossa and Rolando, 2014).

3.2. Exact analytical solutions for Stefan problems

A review of the most relevant of the few known exact analytical solutions to Stefan problems is performed in this chapter. These solutions are derived by applying the mathematical and physical principles, to problems with a certain geometry, material characteristics and boundary conditions. In the case of exact solutions, no approximations or empirical parameters are incorporated in the formulas. This makes them principally distinct from the approximate solutions, also analytical, presented in chapters 3.3 and 3.4.

As already exposed in previous chapters, only a small number of exact solutions for Stefan problems have been found (Lunardini, 1986). Reviews of the analytical and numerical methods to solve them are frequent in literature: compilations of these have been published by Carslaw and Jaeger (1959), Wilson (1978), Lunardini (1986) and Tarzia (2011). Most of these problems deal with relatively simple conditions (see for example Neumann's or Carslaw's solutions), such as a constant initial temperature and isotropic thermal properties, or with very specific conditions, such as a power-type latent heat (see Zhou et al. (2018)).

3.2.1. Neumann Problem: one-dimensional semi-infinite slab

This is the classical and well-known problem solved by Neumann (c.1860). The one-phase variant of this problem, in which the initial temperature is the phase-change temperature, was solved by Stefan (1891). A semi-infinite region initially in liquid phase and at a constant temperature is considered, in which a temperature below the phase-change point is applied to the boundary of the region and remains constant. An overview of the problem is presented in Figure 3.1. This problem is equivalent to one with the heat flux condition proportional to $t^{-1/2}$ posed at the boundary, as shown in Boucíguez et al. (2007). The detailed mathematical development of this solution can be found, among others, in Lunardini (1986) or Jonsson (2013). A summarized description of the procedure to obtain this solution is presented below.

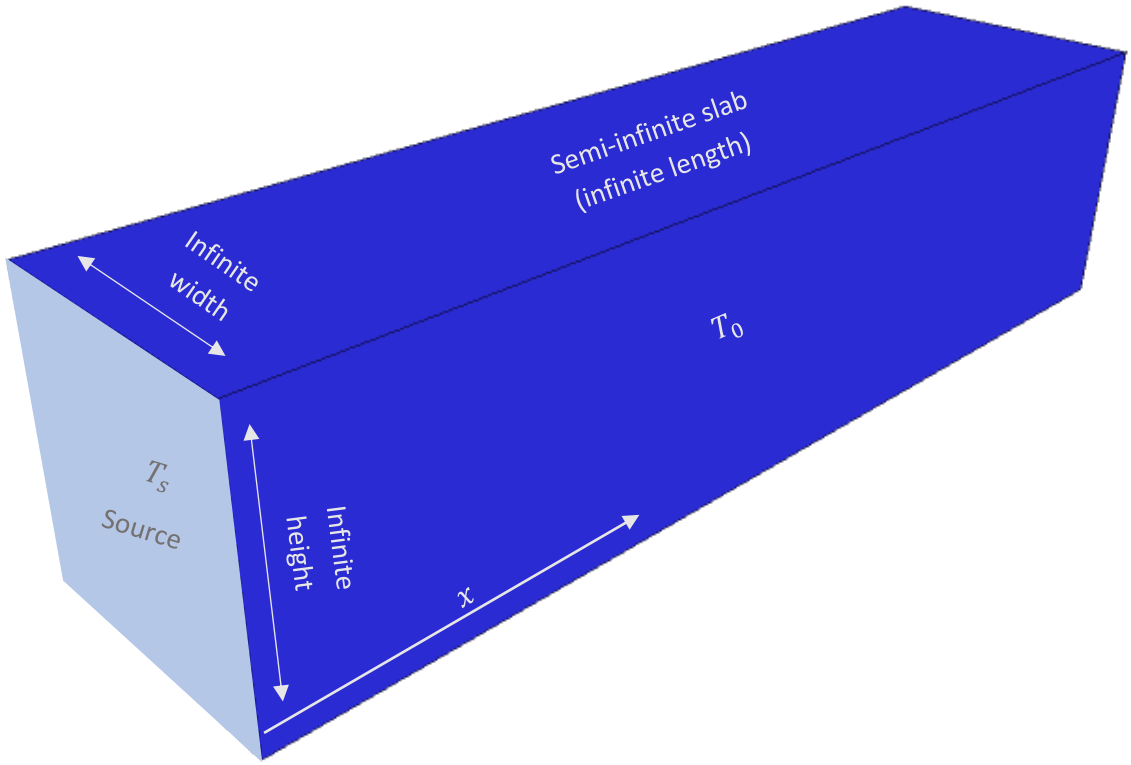

Figure 3.1: Overview of the Neumann problem

The Neumann problem is described by a system of two heat transfer PDEs, one for each phase, with two independent variables (the time t and space x coordinates), together with the initial and boundary conditions. This system is presented below (from Lunardini (1986), see also Sancho-Calderón et al. (2021)):

System of partial differential equations:

$$\frac{\partial^2 T_1(x,t)}{\partial x^2} = \frac{1}{\alpha_1}\frac{\partial T_1(x,t)}{\partial t} \tag{3.12}$$

$$\frac{\partial^2 T_2(x,t)}{\partial x^2} = \frac{1}{\alpha_2}\frac{\partial T_2(x,t)}{\partial t} \tag{3.13}$$

Initial condition and boundary condition at the freezing source:

$$\lim_{x\to\infty} T_2(x,t) = T_0 \tag{3.14}$$

$$T_1(0,t) = T_s \tag{3.15}$$

Boundary conditions at the moving interface $X(t)$:

$$T_1(X(t),t) = T_2(X(t),t) = T_f \tag{3.16}$$

$$k_1 \frac{\partial T_1(x,t)}{\partial x} - k_2 \frac{\partial T_2(x,t)}{\partial x} = \rho\, l\, \frac{dX}{dt}\ ;\ x = X(t) \tag{3.17}$$

where:

c_1: specific heat capacity of the frozen phase (used to define α_1 below)

c_2: specific heat capacity of the unfrozen phase (used to define α_2 below)

k_1: thermal conductivity of phase 1 (frozen phase)

k_2: thermal conductivity of phase 2 (unfrozen phase)

l: latent heat per unit mass

T_f: phase-change temperature

T_0: initial temperature

T_s: source temperature

$T_1(x,t)$: temperature distribution in the frozen phase

$T_2(x,t)$: temperature distribution in the unfrozen phase

$X(t)$: distance from the phase-change interface to the source

$\alpha_1 = k_1/\rho c_1$: thermal diffusivity of phase 1 (frozen phase)

$\alpha_2 = k_2/\rho c_2$: thermal diffusivity of phase 2 (unfrozen phase)

ρ: density of the medium (assumed the same for both phases)

It is possible to find an exact solution to this problem by means of the similarity method, which consists of substituting the variables *x* and *t* by a so-called similarity variable, which is a function of the two. This method solves the problem if all the PDEs as well as the initial and boundary conditions can be expressed exclusively in terms of this variable, which is useful for the Neumann problem but unfortunately not the case for many other problems with e.g. non-uniform initial temperature, time-dependent boundary temperatures, finite domains, etc. (Lunardini, 1986) (Lunardini, 1987). Nevertheless, this is the case for the Neumann problem, in which the similarity transformation $\eta = x/(2\sqrt{\alpha_1 t})$ transforms the system of PDEs into a system of two ODEs (Ordinary Differential Equations) in the variable η, which can be solved. In this case, the solution to the system of ODEs is given by:

$$T_1(x,t) = T_s + \frac{T_f - T_s}{\mathrm{erf}(\gamma)} \cdot \mathrm{erf}\frac{x}{2\sqrt{\alpha_1 t}} \tag{3.18}$$

$$T_2(x,t) = T_0 + \frac{T_0 - T_s}{\text{erf}(\gamma\sqrt{\alpha_{12}})} \cdot \text{erfc}\frac{x}{2\sqrt{\alpha_2 t}} \tag{3.19}$$

where:

erfc(z): complementary error function

$\alpha_{12} = {}^{\alpha_1}/_{\alpha_2}$: ratio of thermal diffusivities

γ: dimensionless parameter

The parameter γ needs to be solved for from the transcendental equation below (Lunardini, 1986):

$$\frac{\exp(-\gamma^2)}{\text{erf}(\gamma)} - k_{21} \cdot \sqrt{\alpha_{12}} \frac{(T_0 - T_f)e^{-\alpha_{12}\gamma^2}}{(T_f - T_s)\,\text{erfc}\,(\gamma\sqrt{\alpha_{12}})} = \frac{l\,\gamma\,\sqrt{\pi}}{c_1(T_f - T_s)} \tag{3.20}$$

The position of the phase-change interface is given by:

$$X(t) = 2\gamma\sqrt{\alpha_1 t} \tag{3.21}$$

The uniqueness of the root γ implies that there is only one similarity solution; this problem is well-posed in the mathematical sense (Alexiades, 2017). The equations can be easily adapted for the thawing case, in which the material is initially frozen and starts melting as it is exposed to a temperature at the boundary which is higher than the phase-change temperature. It can be proven that the solution exists, is unique and is a continuous function of the initial and boundary conditions, conditions which are required for the numerical analysis (Jonsson, 2013).

With respect to experimental verification, Ständer (1967) performed several laboratory experiments with results which match the predictions from Neumann's equation.

As the Neumann formula is implicit and relatively complex, it has not been frequently used (Kurylyk, 2016). In this regard, Kurylyk (2016) gave simplified polynomial correction factors for the Stefan equation, which aim to provide a higher accuracy with a more practical formula than the Neumann one.

Several solutions for additional variants of this problem under specific conditions or assumptions have been published. For instance, solutions for specific boundary or initial conditions, small volumetric heat relatively to the latent heat or frozen and unfrozen material with the same characteristics can be found in Lunardini (1986), Paynter and Life (1999) or Tarzia (2011). An exact solution of a variant of this problem with consideration of temperature-dependent thermal conductivity in the two phases is reported in Cho and Sunderland (1974). Another specific solution to the problem in which the specific heat capacity and thermal conductivity of the material follow Storm's condition (used for simple monoatomic metals), can be found in Briozzo and Natale (2014). Voller et al. (2004) found an exact solution for the one-phase, one-dimensional problem with latent heat varying linearly with the distance to the origin, which could be applicable to shoreline movement in a sedimentary basin.

3.2.2. One-dimensional semi-infinite slab with gradual phase change

As already presented in chapter 2.3.1, phase change in highly porous materials, such as soil or rock, is not abrupt like in pure substances, but it occurs over a temperature range. In this case, at least two moving boundaries will exist in the moving boundary problem, which may be called a "moving zone" problem (Kellner, 2007). Between those boundaries, there is a partially frozen zone which is usually named the "mushy zone". An approximation to the behaviour of the soil is to assume that the unfrozen water content function ξ in the mushy zone varies linearly in the temperature range during the freezing process. For this case, Lunardini (1985) (also published in Lunardini (1988)) obtained an exact solution. Although this is not completely realistic for the soil material (as the unfrozen water function typically follows a curve, see Figure 2.9), this exact formula can be used to check approximate solutions.

It is further assumed by Lunardini for this problem that the thermal properties are constant for each phase. The latent heat is gradually released (in accordance with the unfrozen water content function ξ) in the mushy zone. The solution is obtained in a similar way to the Neumann problem, but it requires solving a system of two transcendental equations for two parameters.

Figure 3.2 shows the temperature profile with gradual phase change compared to the Neumann solution (sharp phase change).

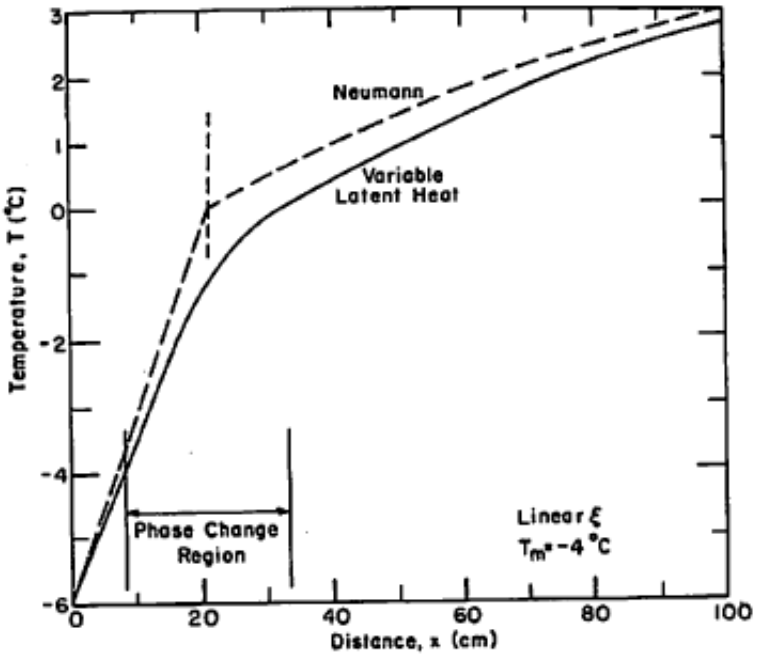

Figure 3.2: Temperature distributions for a semi-infinite slab with sharp and gradual phase change according to Lunardini (1985)

Weiner (1955) solved a similar problem: a semi-infinite slab with a multiphase material (a material which changes phase an arbitrary number of times) at a constant temperature,

whose border is initially at a different temperature. This solution may be applied for example to the phase change of carbon steel.

3.2.3. Linear constant-flux heat source with phase change in an infinite medium

In cylindrical coordinates, the main exact solution with potential practical applications in ground freezing is the one given by Carslaw and Jaeger (1959) for an infinite medium with a line source extracting a constant heat flux q_s at the origin r = 0. They arrive to the following solution by means of the similarity method using the similarity variables η_1 and η_2:

$$T_1 = T_f + \frac{q_s}{4\pi k_1}\left(E_i(-\eta_1) - E_i(-\lambda^2)\right) \qquad \text{for } 0<r<R \tag{3.22}$$

$$T_2 = T_0 - \frac{T_0 - T_f}{E_i(-\alpha_{12}\lambda^2)}\, E_i(-\eta_2) \qquad \text{for } r>R \tag{3.23}$$

The dimensionless parameter λ is found by solving the following transcendental equation:

$$\frac{q_s}{4\pi}\, e^{-\lambda^2} + \frac{k_2(T_0 - T_f)}{E_i\left(-\frac{\lambda^2\alpha_1}{\alpha_2}\right)} e^{\left(-\frac{\lambda^2\alpha_1}{\alpha_2}\right)} = \lambda^2\, \alpha_1\, l\, \rho \tag{3.24}$$

where:

$E_i(x)$ is the exponential integral function

$\eta_1 = \frac{r^2}{4\alpha_1 t}$, first similarity variable

$\eta_2 = \frac{r^2}{4\alpha_2 t}$, second similarity variable

Finally, the phase-change interface R(t) is calculated as $R(t) = 2\lambda\sqrt{\alpha_1\, t}$ (Lunardini, 1986).

3.2.4. Linear constant-flux heat source with gradual phase change

Li et al. (2018) found a solution to the steady-state Stefan problem with constant initial temperature and a line heat sink with constant flux considering gradual phase change of the soil material. They simulated the continuous phase change of the soil by considering a polymorphous material, i.e. with a step-by-step phase change. They arrived at an explicit solution whose coefficients are determined by a set of non-linear equations. The solution has a certain parallelism to that one found by Carslaw and Jaeger (1959) for the same problem with abrupt phase change. However, the consideration of a polymorphous material causes the temperature to be a piecewise function with several steps (the number of which depends on the discretisation of the phase change) and increases the number of equations

for the parameters. A solution to the linear constant-flux heat source with gradual phase change was also found by Özişik and Uzzell Jr (1979).

3.2.5. Further solutions to Stefan problems

Researchers have continuously tried to find further exact solutions for moving boundary problems. Several solutions have been found for very specific conditions, which tend to limit their applicability to engineering problems (Zhou et al., 2018). Furthermore, these solutions are usually more complex than the solutions presented in the chapters above, a fact which also makes it difficult to use them in engineering practice. The disadvantages of solutions requiring a high mathematical effort were already noticed by Kurylyk (2016) for the comparatively handy Neumann equation. However, even if having limited practical application for engineering projects, exact solutions are useful as a benchmark to compare approximate solutions against (Gottlieb, 2002). Compendia of solutions can be found in Carslaw and Jaeger (1959), Lunardini (1986), Crank (1987), Özişik (1993) and Tarzia (2011). Tarzia (2000) also produced an extensive bibliography of moving and free boundary problems. In this chapter only a sample of the available solutions are presented exemplarily below.

Kumar and Singh (2020) were able to find a solution for a one-phase Stefan problem with variable thermal conductivity, assuming that the conductivity follows a certain function of time and temperature. Their solution uses a similarity variable and the “tau method based on shifted Chebyshev operational matrix of differentiation”. Salva (2011) found the solution to the two-phase Stefan problem of a semi-infinite material with variable (linear) latent heat of fusion and constant heat flux boundary conditions.

Another exact solution for a particular one-phase, unidimensional, Stefan problem was given by Layeni and Johnson (2016). A differential-difference formulation of the problem was used to find the solution for cylinders with thermal properties which depend on the inverse-square of the radius. Also for cylindrical coordinates, a solution for inwards freezing of a cylinder with specific and latent heat proportional to the inverse square of the radial distance was found by Gottlieb (2002).

Zhou et al. (2018) investigated a two-phase Stefan problem with latent heat following a power function of the position, which could be applicable to the consolidation process of soils. They used the similarity transformation and Kummer functions. Following a similar approach, Voller et al. (2004) provided a solution for a one-phase, one-dimensional Stefan problem with latent heat linearly dependent on the position. Bollati (2019) found further solutions to problems with latent heat variable with the position.

Ramos (1996) found exact solutions for Stefan problems with thermal conductivity and specific heat capacity dependent on temperature following a power law. They used the enthalpy formulation to find solutions for flat, cylindrical and spherical shapes.

Cherniha and Kovalenko (2009) studied the one-dimensional problem of melting and evaporation of metals by means of the classical Lie symmetry.

Fractional space and time derivatives were used in Voller (2014) to solve the Stefan problem with heterogeneity, which can cause anomalous diffusion.

3.2.6. Inverse Stefan problems

Scholars have also sought solutions for the inverse Stefan problem, in which, starting from a known temperature field, some of the characteristics of the material are determined. This could also be potentially applied in ground freezing engineering, e.g. for the case that in-situ temperature measurements are available from a past ground freezing project, but the thermal characteristics of the soil are unknown and required to design another ground freezing project. However, these problems usually imply an even more complex mathematical framework than usual Stefan problems. Examples are the solution found by Tarzia (2015) for the one-phase fractional Lamé-Clapeyron-Stefan problem, the artificial intelligence algorithms used in Hetmaniok et al. (2014) or the iterative approach described in Levin et al. (2017), which minimises the errors of the solution by applying the gradient descent method.

3.3. Analytical methods to find approximate solutions

As only a few exact solutions to Stefan problems have been found, scholars have also sought approximate solutions. Two groups of analytical methods have commonly been used to find approximate analytical solutions. They are the Heat Balance Integral Method (HBIM) and the quasi-stationary and quasi-steady-state approximations. Other approximate techniques are the power series expansion, the isotherm migration method (which takes temperature as the independent variable (Savovic and Caldwell, 2009)) and source and sink methods (Yigit, 2008).

3.3.1. The heat balance integral method

The Heat Balance Integral Method (HBIM) was introduced by Goodman (1958) for Stefan problems and aims to reduce the PDE problem to an ODE problem, which can be more easily solved. The HBIM has also been applied to model other processes, such as the temperature in a thermistor or the ignition time of wood (Myers, 2010).

The HBIM is an approximate method which assumes that the temperature penetration depth (the distance from the thermal source to the farthest point of the material whose temperature has been affected by the source) is given by a function $\delta(t)$ (Lunardini, 1986). In this case, the temperature profile from the source to the affected material is assumed to follow a certain approximating function. Finally, the heat equation is integrated in the interval whose temperature has changed, between 0 and $\delta(t)$ (Myers, 2010). A representation of the temperature penetration depth is shown in Figure 3.3.

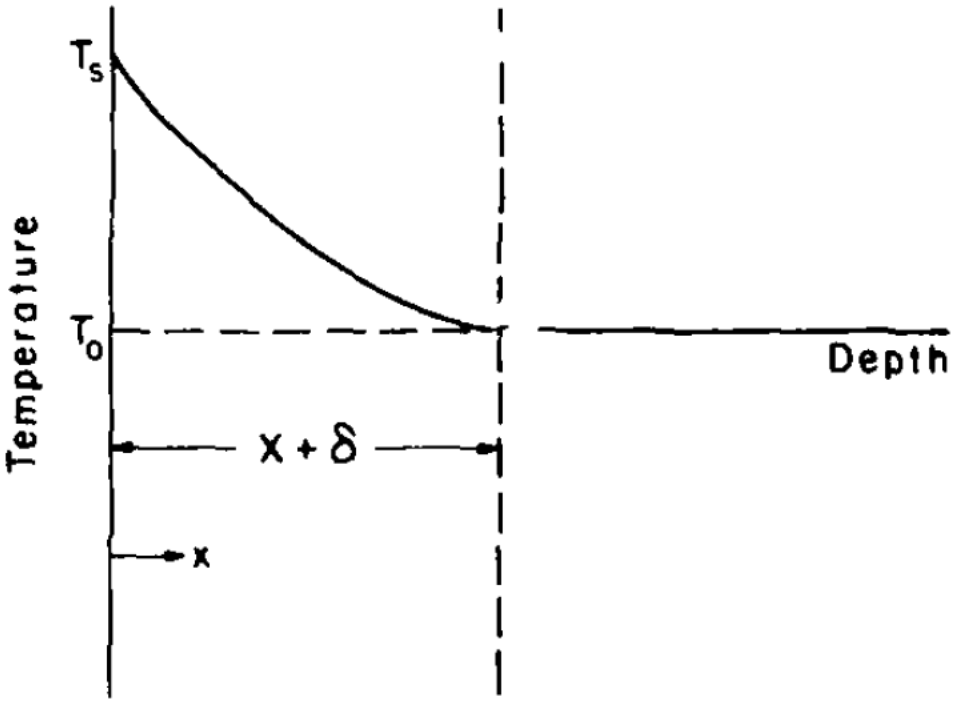

Figure 3.3: Temperature penetration depth for HBIM, adapted from Lunardini (1986)

The approximating coefficients of the function are determined by the initial and boundary conditions (Layeni and Adegoke, 2011). Polynomial temperature profiles are commonly chosen for their simplicity, being the most usual the quadratic and linear ones (Lunardini, 1986). A caveat of this procedure is that, even if in general the accuracy improves with increasing degree of the polynomial, it may decrease (Lunardini, 1986), so choosing the most accurate function is not straightforward. Another possibility is to use piecewise linear or polynomial approximations, which tend to increase the accuracy of the method, are generally applicable, and imply a low computational effort (Mosally et al., 2002).

Therefore, the determination of the optimal temperature profile has been the object of intensive research, e.g. Hristov (2010) studied the optimization of a parabolic profile with unspecified exponent. The optimization of the polynomial degree has been studied by minimising an error function in Myers (2010). The optimal polynomial degree "*n*" seems to depend on the boundary conditions: for a fixed-temperature condition, *n* close to 2 (1.8) was found to be accurate; if the condition is a constant-flux one, it was found that *n* should be chosen as 3.6 (Myers, 2010).

Variants of the HBIM method are often proposed and their accuracy is measured against the known exact solutions, e.g. as in Bollati (2018). Non-polynomial profiles have also been evaluated, for instance, the Gaussian profile is considered one of the most accurate (Layeni and Adegoke, 2011). Exponential profiles have been discussed too, although they seem to achieve a better accuracy only at the cost of increasing the difficulty of choosing the appropriate function (Mosally et al., 2002).

There is evidence that the accuracy of the HBIM depends on the boundary conditions of the problem (Myers, 2010). Two further drawbacks of this method are the facts that the assumed temperature profile may not be adequate or valid for the problem and that the order of accuracy of the solution obtained is unknown (Mitchell and Vynnycky, 2014).

3.3.2. The quasi-stationary and quasi-steady state approximations

The quasi-stationary assumption is mainly based on neglecting the moving interface and the diffusive flux (Lunardini, 1986). It is possible to consider initial conditions with this approximation, but it may not be valid if the temperature is affected by the movement of the phase interphase. A further simplification is the quasi-steady state approximation, which neglects the transient term of the equation, so it cannot satisfy the initial conditions of the problem. However, it has been used widely for freezing problems because it simplifies the problem to a significant extent (Lunardini, 1986).

Solutions following these approaches may be useful after a certain time has elapsed since the start of the freezing process, when the temperature field becomes similar to the one given by the steady-state approximation (Hu and Han, 2013). Furthermore, they could be used in practical projects to obtain the thickness of the freeze wall from punctual temperature measurements.

Some solutions by Hu and others (see e.g. Hong and Hu (2019) and Wang et al. (2020)) using the quasi-steady state approximation have been directly applied to find temperature distributions in the framework of the ground freezing technique for different geometries (freeze circle, freeze wall, etc.). A few of them are presented below.

3.3.2.1. Single pipe with phase change

Trupak (1954) found the solution to the temperature field of the single-pipe problem with the steady-state approximation (Hu et al., 2016b):

$$T(r) = T_{\mathrm{f}} + \frac{\ln\left({}^{r}/_{R}\right)}{\ln\left({}^{r_0}/_{R}\right)}\left(T_s - T_{\mathrm{f}}\right) \tag{3.25}$$

where:

r_0: freeze pipe radius

R: freeze radius

Building up on this solution, a solution for several pipes in a random disposition based on the potential superposition theory was found by Hu et al. (2016b).

3.3.2.2. Single row of pipes with phase change

A solution to this problem based on the steady-state approximation was given by Bakholdin (1963) (Hu and Han, 2013). His solution gives a temperature field as follows:

$$T(r) = \frac{T_s - T_\mathrm{f}}{\ln(2\pi\, r_0/s) - \pi R/s}\left(A_f - \frac{\pi R}{s}\right) + T_\mathrm{f} \tag{3.26}$$

where:

$A_f = \frac{1}{2}\ln\left[2\left(\cosh\frac{2\pi y}{s} - \cos\frac{2\pi x}{s}\right)\right]$

R: half-width of the freeze wall (freeze radius in the direction perpendicular to the freeze wall)

s: separation between pipes

Hu and Han (2013) produced a further solution for the variant in which the freezing process is asymmetric, e.g. due to an existing boundary in one of the sides of the pipe row. In another paper, Hu and Zhang (2013) studied the temperature distribution between pipes at different temperatures based on the thermal potential superposition. Further investigations in this direction with the undetermined coefficient method were performed in Zhang et al. (2021).

3.3.2.3. Circle of pipes with phase change

Hu et al. (2018b) found a solution for the steady-state temperature field of the freeze circle pipe configuration using conformal mapping and the boundary separation method for harmonic equations. The particularity of their solution is that it considers the waviness of the freeze body, which is usually neglected in order to simplify the problem (i.e. the freeze body of a freeze circle is typically simplified as a cylindrical annulus). The solution is expressed as:

$$T(x,y) = (T_s - T_\mathrm{f}) \cdot \frac{\frac{1}{2}\ln\left(2\left(\cosh\frac{2\pi y}{s} - \cos\frac{2\pi x}{s}\right)\right) - \frac{\pi R}{s}}{\ln\frac{2\pi r_0}{s} - \frac{\pi R}{s}} + T_\mathrm{f} \tag{3.27}$$

where the symbols represent the same variables as in the previous equations.

3.4. Approximate semi-empirical solutions applied to thermal design of artificial ground freezing

In chapter 3.2 it has been shown that, although there exist several exact solutions for Stefan problems, most of them are restricted to simple geometries, uniform thermal properties and very specific boundary and initial conditions, such as uniform initial temperature (Ayasoufi, 2004) (Alexiades, 2017). Also, there are no explicitly solvable Stefan problems in 2 or 3 dimensions (Alexiades, 2017).

Furthermore, the solutions and mathematical techniques presented in chapter 3.3, even if approximate, tend to be limited to one-dimensional analysis and/or produce complicated mathematical solutions (Yigit, 2008), which are not easy to apply to problems in engineering practice.

With respect to analytical solutions for artificial ground freezing, distinguished scholars already expressed the associated challenges during the First International Symposium on Ground Freezing in Bochum (Braun et al., 1979), from Frivik (1981), as follows:

> "The thermal analysis for a ground freezing system is fundamentally crude. Complex, three-dimensional, transient heat transfer in a heterogeneous porous medium including phase change, is essentially indeterminate. Furthermore, the specific refrigeration system and procedures utilized by the contractor frequently determine the actual field performance of the system and the in-situ thermal regime that will exist. Because of these factors, refined thermal analysis is pointless, preconstruction determination of refrigeration requirements is largely an art tinged with science, much the same as the selection and sizing of dewatering system or the determination of grouting requirements."

This is also condensed in the statement from Sanger and Sayles (1979), in Frivik (1981): "A rigorous treatment of the design and construction of structures of artificially frozen ground is impossible. It is an art in which *'experimentia docet'*". The assertion from Jumikis (1979) that "In practice, all heat-transfer solutions in thermal soil mechanics are approximative ones" still holds today (see also Lunardini (1987)).

Therefore, approximate analytical solutions based on further simplifications and/or assumptions and on empiric experience, however less accurate than the ones presented above, have been developed and are very useful for practical use in engineering design (Colombo, 2010). They have been commonly used for design during the 20th century and the beginning of the 21st century (Bock, 2018). Some relevant approximate solutions are presented in this chapter.

Although they are not exact, these solutions are informative and may be good enough for the early stages of many engineering projects, as they are fast and efficient tools for calculating under certain circumstances (Rees et al., 2000). Moreover, in engineering projects there are usually other additional sources of uncertainty, which may have an even larger effect than the inaccuracies due to approximations in the analytical formula itself. Some examples of these practical uncertainties are the errors in the determination of the initial temperature, thermal parameters, water content and phase-change temperature of the ground. Furthermore, applying the more complex exact mathematical solutions to practical projects would probably require additional simplifications, such as simplifying the real geometry of the problem. Finally, approximate solutions are often easier and quicker to use than the more complex numerical solutions (which are handled in chapter 0), so they are more practical for early stages in the project.

The solutions presented in this chapter originated between 50-90 years ago. Trupak's solution, presented in chapter 3.3.2.1, can also be cited as an early attempt on this problem. It was proposed already in 1954 for one freeze pipe and also for several pipes, using a simple superposition of the thermal fields of the single pipes (Hu et al., 2018b). One of the first rough simplifications for the transient problem neglected the specific heat capacity of the ground, proposing solutions valid only for small Stefan numbers. However, these solutions tend to largely overestimate the freezing rate and consequently to be of limited use (Khakimov, 1966).

Another rather obvious simplification would be to neglect the latent heat of the ground, which largely simplifies the mathematics of the process. However, this does not yield accurate results (Vitel et al., 2015).

All the solutions presented below do not consider the effect of groundwater flow. Furthermore, they assume homogeneous and isotropic ground, a uniform initial ground temperature, a constant freeze pipe temperature and constant thermal properties within each of the two phases. Regarding the solutions for patterns with several freeze pipes (freeze circle and freeze wall), they assume an ideal geometry and uniform pipe spacing. Finally, they generally provide the user with a formula for the determination of the freeze radius with respect to time, instead of the time-dependent temperature distribution.

Their results differ greatly, as shown e.g. in Hentrich and Franz (2015) and Sancho-Calderón et al. (2021), which stems from the fact that they make diverse simplifications and assumptions and apply different calculation methods.

As heat-transfer equations are in general reversible (Jumikis, 1979), the solutions may also be used for thawing problems. An example of an approximate solution for a thawing problem can be found in Zhang et al. (2012).

3.4.1. **Single freeze pipe**

As already stated by Lunardini (1981): "No exact, general, solution exists for phase change in a cylindrical geometry. In fact, even approximate solutions are rare and limited in applicability." This summarizes quite well the difficulties that are found by the design engineer, who would favour having a closed analytical solution which is easy to use and sufficiently accurate. Five solutions from the literature are presented in this chapter and considered in more detail in the subsequent ones. Another solution which has been created recently is the one by Cai et al. (2018). However, it has not been yet used in many engineering projects, and it seems comparatively difficult to use, requiring mathematical software, such as Maple (from Maple Inc., *https://www.maplesoft.com/*), which may not be typically available to the design engineer.

3.4.1.1. Leibenson's solution

Leibenson (1931), in the 1930s, similarly to Trupak, assumes a quasi-stationary state temperature distribution and neglects the sensible heat for the unfrozen region. This assumption introduces an error unless the initial temperature of the ground is the

phase-change temperature. Indeed, Sanger and Sayles (1979) estimate the sensible heat for the unfrozen region at about 30% of the total heat, which is significant. Leibenson arrived at a relatively simple formula (Ständer, 1967):

$$t_I = -\frac{\rho \cdot l_s \left(R^2 \cdot \ln\frac{R}{r_0} - \frac{R^2 - r_0^2}{2}\right) - c_1 \rho_1 T_I \left(\frac{R^2 - r_0^2}{2} - \frac{r_0^2}{2}\,\varphi(z)\right)}{2k_1 T_I} \qquad (3.28)$$

where:

c_1: specific heat of the frozen phase

$l_s = \frac{l_{water}\,\omega\,\rho_d}{\rho}$: crystallisation heat of the groundwater, per unit mass of ground

t_I: freezing time up to a freeze radius r

$T_I = T_s - T_f$: freeze-pipe temperature minus phase-change temperature

ρ_1: density of the frozen phase

$\varphi(z) = \int_0^z \frac{e^z - 1}{z} dz = \sum_{n=1}^{\infty} \frac{z^n}{n\,n!}$ with $z = 2\,ln\frac{R}{r_0}$ (this definition of z is only meant for this equation, as z generally represents the coordinate z)

3.4.1.2. Khakimov's solution

Khakimov (1966), building up on Leibenson's solution, makes use of the quasi-stationary approximation and assumes that the temperature penetration depth is directly proportional to the freeze radius, similarly to Sanger and Sayles (1979), see chapter 3.4.1.4. Furthermore, according to experimental data, he assumes that the temperature penetration depth is about 4.5 to 5.5 times the freeze radius. This parameter is assumed as 5 for the analyses performed in the following chapters of the present thesis. Another assumption made is that the temperature is assumed to follow a logarithmic distribution up to a finite distance from the source. He uses the specific heat capacity of the frozen ground to account for the sensible heat also in the unfrozen area. As the specific heat capacity of ice is smaller than that of water, his solution predicts a faster freezing progress than it should (Ständer, 1967). His solution can be expressed as:

$$t_I = -\frac{\rho \cdot l_s + c_2 \rho_2 T_{II} \frac{{a_r}^2 - 1}{2\ln(a_r)} \left(R^2 \cdot \ln\frac{R}{r_0} - \frac{R^2 - r_0^2}{2}\right) + c_1 \rho_1 T_I \left(\frac{R^2 - r_0^2}{2} - \frac{r_0^2}{2}\,\varphi(z)\right)}{2k_1 T_I} \qquad (3.29)$$

where:

$T_{II} = T_0 - T_f$: initial temperature minus phase-change temperature

c_2: specific heat of the unfrozen phase

ρ_2: density of the unfrozen phase

a_r: ratio of the radius of the zone affected by the temperature descent due to the influence of the freeze pipe (temperature penetration depth) and the freeze radius

3.4.1.3. Ständer's solution

Ständer (1967) proposed practical solutions for some cases relevant to artificial ground freezing: single freeze pipe, freeze wall and freeze circle, and tested those solutions against laboratory experiments. These solutions have since been used in several engineering projects, see e.g. Hentrich and Franz (2015) and Bosch (2017).

For the single freeze pipe, he starts discussing the approximate solutions known at his time, starting with a very rough approximation consisting of neglecting the sensible heat of the ground. Then, as presented in chapter 3.4.1.1, in the 1930s, Leibenson found an approximate solution which considers the sensible heat of the freeze body, but neglects the sensible heat of the non-frozen region (Ständer, 1967). Furthermore, he also discusses Khakimov's solution (see chapter 3.4.1.2). He questions Khakimov's assumption (which is also made by Sanger and Sayles (1979)) that the temperature penetration depth is a constant multiple, which is determined only empirically, of the freeze radius. In fact, that multiple is dependent on the thermal characteristics of the ground and is therefore not constant; the error of this simplification being unknown (Ständer, 1967).

The solution by Ständer (1967) takes as a starting point the exact solution for the punctual source with constant heat flux by Carslaw and Jaeger (1959), which was presented in chapter 3.2.3. He then takes the average over time of the temperature on the freeze pipe from that exact solution and equates it to the freeze pipe temperature of the problem considered.

Ständer (1967) performed experiments to check his solutions. However, the experiments were conducted during a relatively short time of a few hours.

Ständer's solution is comparatively more difficult to use in practice than the other formulae in this chapter, because it involves solving equations which are relatively complex. Indeed, he provided numerous nomograms to solve them. With the current available means, his solution for the single freeze pipe, which is shown in Equation (3.30) can, however, be solved entirely analytically, e.g. with the commercial software Maple 2018.

$$\frac{1}{X}=\frac{e^{\alpha_{12}v^2}E_i(-\alpha_{12}v^2)}{e^{v^2}\frac{Z^2}{Z^2-1}\left(e^{-v^2/Z^2}-\frac{1}{Z^2}e^{-v^2}+\left(1+v^2/Z^2\right)\left(E_i\left(-v^2/Z^2\right)-E_i(-v^2)\right)\right)}+\frac{k^2E_i(-\alpha_{12}v^2)e^{\alpha_{12}v^2}}{Y} \tag{3.30}$$

where:

v is related to the freeze radius as follows:

$$v^2=\frac{R^2-{r_0}^2}{4\alpha_1\cdot t}$$

$X=-\frac{k_1\cdot T_I}{k_2\cdot T_{II}}$

$$Y = -\frac{k_1 \cdot T_I}{\alpha_1 \cdot \rho \cdot l_s}$$

$$Z = \frac{R}{r_0}$$

3.4.1.4. Sanger & Sayles' solution

Sanger and Sayles (1979) created a widely used solution for the calculation of the freezing progress from a single freeze pipe. It has been applied in numerous practical engineering projects (Holden, 1997) (Sopko, 2017a), e.g. in Manassero et al. (2008), Colombo (2010), Pigorini et al. (2012), Hentrich and Franz (2015) or Filippo Mira-Cattò (2016).

They aim to provide a solution for freeze walls with multiple pipes by dividing the process in two stages. The first stage, which is described in the present chapter, describes the growth of the freeze front growing from a single freeze pipe, without consideration of the potential influence of any neighbouring pipes.

Three basic assumptions are taken in Sanger and Sayles (1979):

1. "Isotherms move so slowly they resemble those for steady-state conditions. […]" This corresponds to the quasi-stationary approximation.
2. "The radius of the unfrozen soil affected by the temperature of the freeze pipe [temperature penetration depth] can be expressed as a [constant] multiple of the frozen soil radius prevailing at the same time." For the single-pipe case, this multiple is assumed as $a_r = 3$. (This assumes that this multiple is constant with time, for all types of ground and for different freeze-pipe, phase-change and initial temperatures).
3. "The total latent and sensible heat can be expressed as a specific energy which when multiplied by the frozen volume gives the same total as the two elements computed separately."

The relatively simple and practically applicable expressions of Sanger and Sayles (1979) for estimating the freeze time around a single pipe are presented below.

The formula to find the time t_I to achieve a certain freeze radius R is:

$$t_\mathrm{I} = \frac{R^2 L_I}{4\, k_1 v_s}\left(2 \ln\left(\frac{R}{r_0}\right) - 1 - \frac{c_1 T_I}{L_I}\right) \tag{3.31}$$

The required power per unit length of freeze pipe is given by Sanger and Sayles (1979) as:

$$P_I = -2\,\pi \frac{k_1 T_I}{\ln \frac{R}{r_0}} \tag{3.32}$$

where:

a_r: Ratio of the radius of the zone affected by the temperature drop due to the influence of the freeze pipe (temperature penetration depth) and the freeze radius

c_1: specific heat capacity of frozen ground

c_2: specific heat capacity of unfrozen ground

k_1: thermal conductivity of frozen ground

k_2: thermal conductivity of unfrozen ground

$l_v = l_{water}\ \omega\ \rho_d$: crystallisation heat of the groundwater, per unit volume of ground

$L_I = l_v + \frac{(a_r^2-1)}{2\ln a_r}\ c_2 T_{II}$: volumetric latent heat of the unfrozen area

r_0: freeze pipe radius

R: freeze radius

3.4.1.5. Lunardini's solution

Lunardini (1981) developed an approximate solution for the single pipe problem by using the effective thermal diffusivity method and the heat balance integral method with a polynomic approximation having a degree of 20. The effective thermal diffusivity is defined as a fictitious diffusivity, which introduced in the solution to the analogue problem with zero latent heat, gives the same results as the problem with latent heat. The solution reached by Lunardini (1981) requires the sequential use of several formulae, some of which are transcendental equations, and is therefore not as straightforward as the one from Sanger and Sayles (1979).

3.4.2. **Flat freeze wall**

Flat freeze walls may be used to protect rectangular excavation pits in water-bearing ground. For instance, artificial ground freezing was applied at the excavation pit for the Berlin opera (*Staatsoper*) (BAUER Spezialtiefbau GmbH, 2018). Ständer (1967) and Sanger and Sayles (1979) provided approximate solutions for the flat freeze wall which are used in engineering projects.

3.4.2.1. Sanger & Sayles' solution

Sanger and Sayles (1979) provide a closed-form solution for the freeze wall problem which is easy to use in engineering practice. Based on experimental data from Khakimov (1966), they assume a value of $a_r = 5$ for the flat freeze wall.

The freezing process for a freeze wall is divided by Sanger and Sayles (1979) into two stages (see the representation in Figure 2.5). The first stage encompasses the time from the beginning of the freezing process until the single frozen cylinders around the pipes merge (freeze body closure). This first stage is described by the equation for the single freeze pipe in chapter 3.4.1.4. Thus, Sanger and Sayles (1979) do not consider either the cooling effect of the neighbouring pipes before the freeze wall closure or the temperature descent in the remaining unfrozen ground. The solution for the second stage has a form which is analogous, (although more complex) to the one for the first stage. A linear temperature

distribution in the frozen zone and a logarithmic one in the unfrozen zone are assumed. The freeze pipe pattern of the freeze wall is shown in Figure 3.4.

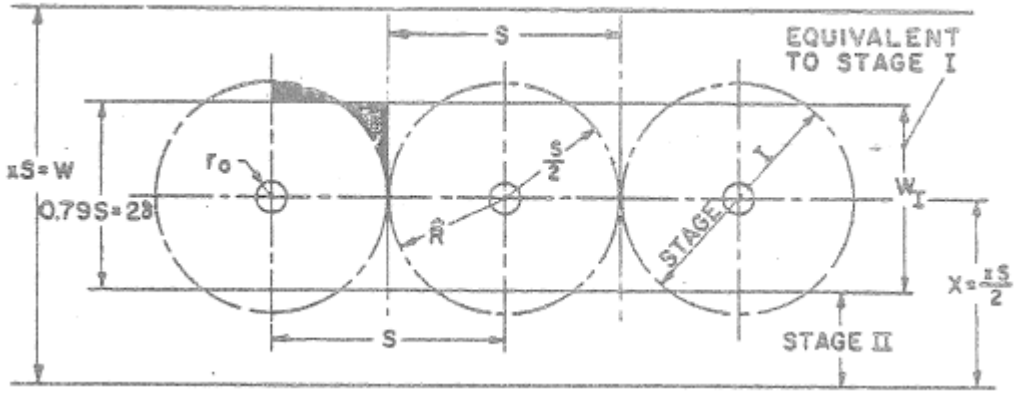

Figure 3.4: Schematic drawing of a freeze wall (Sanger and Sayles, 1979)

The solution from Sanger and Sayles (1979) for the freeze wall is presented below:

$$t_{\mathrm{II}} = -\frac{L_F}{2\,k_1 T_I}\left(\frac{\mathrm{W}^2}{4} - \frac{{W_I}^2}{4}\right) \tag{3.33}$$

where:

$L_F = l_v - \frac{1}{2}c_1 T_I + c_2 T_{II}\left(\frac{a_r - 1}{\ln(a_r)}\right)$

W: freeze wall width

W_I: average freeze wall width at closure

3.4.2.2. Ständer's solution

For the freeze wall calculation, Ständer (1967) uses similar assumptions as for the single pipe problem presented in chapter 3.4.1.3. He divides the freezing process for the freeze wall into two phases, before and after the closure of the freeze wall. In contrast to Sanger and Sayles (1979), he does consider, based on empirical values, the influence of the neighbouring freeze pipes on the freezing process before closure. Thus, the closing time decreases compared to the case in which they are considered independently. Moreover, for the second phase, he also takes into account the amount of cooling by the freeze pipes on the unfrozen ground until the closure. He determines experimentally an effective "starting ground temperature" for the second phase. For instance, he suggests using $t_{IIeffective} = t_{II} \cdot 0.270$ for the freeze wall. In this respect, he recognizes a probable error in the factor of about $\pm 15\%$.

For the second phase, Ständer (1967) calculates the spatial average of the temperature over the freeze line (row of pipes). Then, this temperature is averaged over the time passed between the start of the freezing process and the time corresponding to the sought freeze radius. Afterwards, he applies the exact Neumann solution for the semi-infinite-slab problem (presented in chapter 3.2.1), introducing the previously calculated average

temperature as the temperature of the plane source. The solution is more complex than his solution for the single freeze pipe, so it is relatively complicated to use in engineering projects.

3.4.3. **Freeze circle**

Artificial ground freezing with circular geometry is the oldest and most widely used freeze pipe pattern, very often applied to sink deep mine shafts (Hu et al., 2018b). There are two solutions for freeze circles often used in engineering projects: Ständer (1967) and Sanger and Sayles (1979), both dating from the 60-70s of the last century. These solutions stem from the solutions for the flat freeze wall and their formulations are therefore analogous to them.

3.4.3.1. Sanger & Sayles' solution

Sanger and Sayles (1979) proposed a relatively simple, explicit solution for the estimation of the freezing progress in a freeze circle. They proceeded based on the same assumptions as presented in chapter 3.4.1.4 for the single freeze pipe. The process to obtain the solution is analogous to the one for the freeze wall presented in chapter 3.4.2.1. Two equations are given for the second stage (after freeze body closure): one for the external freeze radius (outwards from the freeze pipes), see Equation (3.34), and another one for the internal freeze radius (see Equation (3.35)). Based on experimental data from Khakimov (1966), they assume a value of $a_r = 5$ for the external freeze wall and $a_r = 4$ for the internal freeze wall.

This solution has been widely used in engineering design, see e.g. Chang and Lacy (2008), Colombo (2010) and Hentrich and Franz (2015).

$$t_{\mathrm{IIe}} = \frac{1}{2\,k_1 v_s} L_{IIe} \left({R_e}^2 \ln \frac{R_e}{r_0 + \delta} - \frac{{R_e}^2 - (r_0 + \delta)^2}{2} \right) + \frac{c_1}{2\,k_1} \left(\frac{{R_e}^2 - (r_0 + \delta)^2}{2} \right) \tag{3.34}$$

$$t_{\mathrm{IIi}} = \frac{1}{2\,k_1 v_s} L_{IIi} \left((r_0 - \delta)^2 \ln \frac{r_0 - \delta}{R_i} - \frac{(r_0 - \delta)^2 - {R_i}^2}{2} \right) + \frac{c_1}{2\,k_1} \left(\frac{(r_0 - \delta)^2 - {R_i}^2}{2} \right) \tag{3.35}$$

where:

$L_{IIe} = l_v + 2.5 c_2 T_{II} - 0.5 c_1 T_I$ (for $a_r = 5$)

$L_{IIi} = l_v + 2.0 c_2 T_{II} - 0.5 c_1 T_I$ (for $a_r = 4$)

R_e: external radius of the freeze annulus

R_i: internal radius of the freeze annulus

t_{IIe}: time to reach the external freeze radius (R_e)

t_{IIi}: time to reach the external freeze radius (R_i)

δ: half-width of the freeze annulus at closure time (see Figure 3.4)

3.4.3.2. Ständer's solution

Ständer (1967) gives a solution for the freeze circle which is analogue to the one presented for the flat freeze wall in chapter 3.4.2.2. Ständer (1967) first calculates the average temperature in the freeze pipe circle, a similar approach to the one taken for the flat freeze wall. Then, he seeks the solution without consideration of the sensible heat and assuming the calculated average temperature over the freeze circle. He solves this problem using experimental data and analogies to the problems previously solved: flat freeze wall and single freeze pipe. After having arrived at a solution for the freeze circle without consideration of the sensible heat, he builds up a solution for the freeze circle under consideration of the latent and the sensible heat in the ground, using again the parallelism with the flat-freeze-wall problem. He uses two factors which adjust his solution from the plane problem without sensible heat. The first of the two considers the effect of the sensible heat and the second one the relationship between the plane and the cylindrical problems.

Ständer's solution for the freeze circle is relatively difficult to use in practice because it is not presented in the form of an explicit formula, but instead, several nomograms need to be used. However, this solution has sometimes been used for thermal design of freeze shafts by German-speaking authors (see e.g. Baier (2008), Pimentel (2012) or Hentrich and Franz (2015)). The nomograms contained in Ständer's paper are required to evaluate the solution (even with specialised mathematical software such as Maple 2018 it is difficult to automatize the formulae completely without the use of the nomograms). This complexity and the fact that the paper is written in German language (no English translation is known to the author) may be the reasons why this solution does not seem to be well-known outside of the German-speaking countries.

3.4.4. Summary of approximate semi-empirical solutions

Table 3.1 shows a summary of the main assumptions, limitations and other characteristics of the solutions presented in chapter 3.4.

Table 3.1: Summary of analytical solutions for ground freezing thermal design

Solution	Main Assumptions and limitations	Solution available for freeze wall and freeze circle	Easy-to-use closed Formula
Leibenson	• Quasi-stationary approximation • Neglection of sensible heat in the unfrozen region	No	Yes
Khakimov	• Quasi-stationary approximation • Temperature penetration depth directly proportional to freeze radius. Ratio according to experience. • Use of specific heat capacity of frozen ground also for unfrozen areas	No	Yes
Ständer	• Based on Carslaw and Jaeger's (1959) exact solution for a constant flux source • Several assumptions made to apply the parallelism with exact known solutions	Yes	No
Sanger & Sayles	• Quasi-stationary approximation • Temperature penetration depth directly proportional to freeze radius. Ratio according to experience. • The latent and sensible heat can be expressed as a total specific energy.	Yes	Yes
Lunardini	• Use of the Heat Balance Integral Method • Use of the effective thermal diffusivity method	No	No

4. Review of the state of the art in numerical thermal calculations with phase change

Already 40 years ago, Frivik (1981) reckoned that numerical methods would be required for thermal design of AGF, due to the limitations of analytical methods. Approximate analytical solutions for phase-change problems have limitations caused by the assumptions and simplifications used for their derivation, which is why the more flexible numerical solutions are sought (see also Sopko Jr. (1990) and Zueter et al. (2021)). Analytical solutions also tend to be limited to one-dimensional problems and its application becomes complex for multidimensional ones, among other limitations they have (Yigit, 2008). Therefore, the search for numerical solutions which can solve phase-change thermal problems with complex geometry and boundary conditions is the natural response to the limited number of available exact analytical solutions (Rees et al., 2000). Moreover, the flexibility of numerical methods is such that they can account, among other factors, for complex geometries, heterogeneous ground properties and time-dependent boundary conditions. Furthermore, it is possible to simulate 2D and 3D problems with numerical solutions, in contrast to most of the analytical solutions presented in chapter 3, which can be applied to 1D problems only.

Numerical methods for Partial Differential Equations (PDEs) use discrete approximations to find approximate solutions to the PDEs (Recktenwald, 2004). That is, instead of using differential elements (elements infinitely small) and infinitesimal time steps like in differential calculus, they use elements of finite size and time steps of finite duration. In numerical methods, the mathematical equations are proposed for every element instead of for the entire domain, and then they are combined to solve the whole problem (Babaei, 2016). The points in which the numerical solution is computed are called nodes, and the set of nodes makes up the mesh, which discretises the space domain (Recktenwald, 2004). The size of the elements of the mesh and of the time steps is defined by the user depending on several factors, such as the geometry of the problem and the available time for the computation. It is widely accepted that, in general, increasing the number of elements (i.e. decreasing their size) improves the resolution and accuracy of the numerical solution, see e.g. Recktenwald (2004).

The Finite Difference Method (FDM) was introduced in 1928 (Emery and Mortazavi, 1982), whereas the Finite Element Method (FEM) was introduced in the late 1960s to solve problems in geotechnics (Babaei, 2016). Already in the early 1960s 2D numerical methods capable of solving the heat transfer equations existed (P.E.Frivik, 1981). In Germany, (Ständer, 1967), a numerical method was applied to ground freezing, although probably only in a scientific way, as the calculations for practical engineering problems following that method would have been very time-consuming. In the 1970s, numerical methods capable of simulating the effect of latent heat were developed as tools to design several oil and gas pipelines in Northern Canada and Alaska (Pentland and Fredlund, 2001). Nowadays both FDM and FEM methods are commonly used for heat transfer problems

with phase change (see Table 4.3). A comparison of their principles, advantages and disadvantages can be found in Emery and Mortazavi (1982).

The computational methods have been significantly influenced in the last several decades by the improving computing capacity, the development of software for numerical calculations and the research of scholars (Paynter and Life, 1999). Nevertheless, numerical solutions have by its mere nature several limitations. For instance, they require much more computing power and time than analytical solutions (Fossa and Rolando, 2014) and may pose problems regarding their accuracy and stability, which need to be treated and limited to acceptable values which depend on the engineering problem they are applied to.

Another type of numerical schemes is based on semi-analytical methods. These schemes can usually be applied with larger time steps than those of conventional numerical schemes (Rizwan-uddin, 1998).

Choosing the most appropriate and efficient method for a given problem is not trivial, on the contrary, it is a complex issue. According to Voller (1996), the efficiency of a numerical scheme depends on "the implementation of the method, its accuracy, the problem to be modelled, the convergence criteria, the computer architecture and the choice of space and time steps". Furthermore, he claims that the solution scheme should be chosen considering its robustness, flexibility and accuracy, and the available computing resources. Gustafsson (2011) argues in a similar direction that the method chosen should be the one which results in the fastest solution for a given required accuracy.

4.1. Principles of the Finite Difference Method

As presented in the previous section, the two numerical methods most commonly used are the Finite Element and Finite Difference Methods. FLAC3D (commercialised by Itasca Consulting Group Inc., *https://www.itascacg.com/*) is the commercial software used for thermal numerical modelling in this thesis, which was chosen due to its flexibility and programmability (Bock, 2018). As FLAC3D is based on the Finite Difference (FD) Method, from here on the focus will be directed on this method. The Finite Difference Method is based on replacing the derivatives in the PDEs with finite-difference formulae, which are evaluated only in the nodes of the mesh, which discretises the region considered (Recktenwald, 2004), obtaining an approximate solution to the PDE at a finite set of nodes and time instants. Different approximations to the derivatives may have different characteristics in terms of being convergent or divergent, rate of convergence, maximum required time step (Δt) or mesh size ($\Delta x, \Delta y, \Delta z$), etc. The results of any unconditionally convergent method will tend towards the exact solution when Δx and Δt tend to zero (Recktenwald, 2004). However, some other schemes may not work properly for unfavourable conditions of Δx and Δt (Recktenwald, 2004). A finite difference scheme is convergent if its pointwise errors tend to zero when Δt and Δx tend to zero (Causon and Mingham, 2010). The scheme is stable if its pointwise errors do not grow without limit after a certain arbitrary time. For linear PDEs (like the heat conduction equation without

phase change), the Lax Equivalence Theorem states that stability and convergence are equivalent (Causon and Mingham, 2010).

An example of a discrete approximation which may be used in Finite Difference Methods is (Recktenwald, 2004):

$$\frac{\partial \phi(x,t)}{\partial x} \approx \frac{\phi_{i+1} - \phi_i}{\Delta x} \tag{4.1}$$

The notation in the equation above and in the rest of this chapter is as follows:

Δx: discrete interval of length in the coordinate x

$\phi(x,t)$: exact, continuous solution

$\phi(x_i, t_m)$: exact solution evaluated at the mesh point *i* at time instant t_m

ϕ_i: approximate numerical solution evaluated at the mesh point *i*

ϕ_{i+1}: approximate numerical solution evaluated at the mesh point *i* +1

ϕ_i^m: approximate numerical solution evaluated at the mesh point *i* at time instant t_m

A graphical representation of a mesh for a one-dimensional problem used in numerical methods is presented in Figure 4.1. The black squares represent the initial conditions, while the white ones show the boundary conditions. The solution is obtained with the numerical scheme at the positions and times represented by the circles (Recktenwald, 2004).

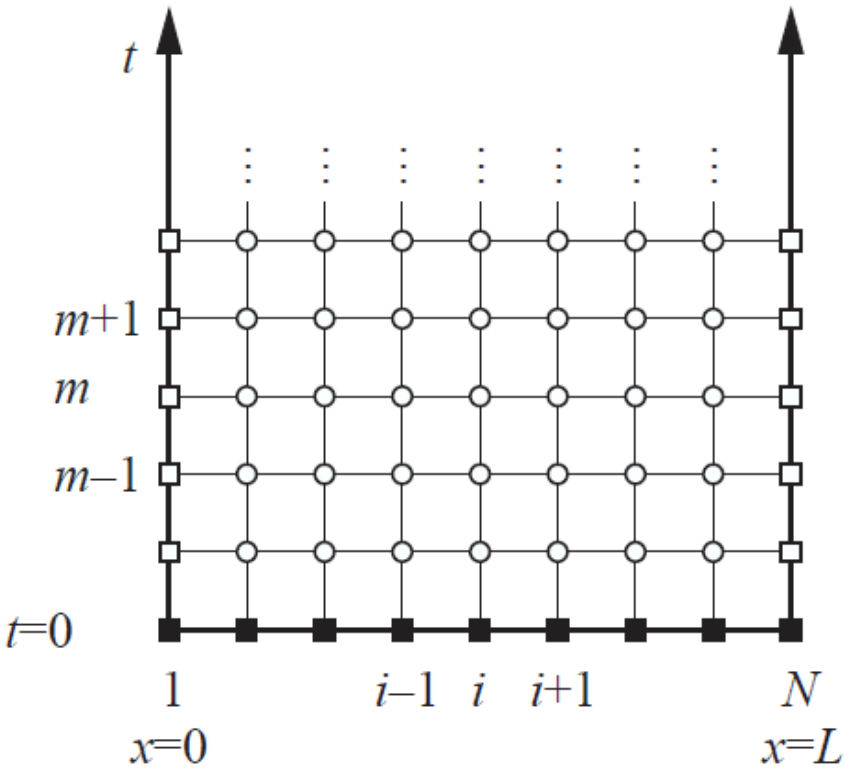

Figure 4.1: Mesh for a plane, semi-infinite heat conduction problem (Recktenwald, 2004)

4.2. Numerical schemes for thermal problems without phase change

The finite difference approximations may be computed following several schemes. To start with, they differ in their order of approximation. For instance, first-order schemes are based on truncating the Taylor series for $\phi(x)$ to the first term. Then, the scheme may be a forward or a backward scheme, which use the values of the solution ϕ in the next or in the previous node, respectively (Recktenwald, 2004). Another scheme is the central difference approximation. The truncation error is usually dependent on the mesh size. These usual schemes are presented below (formulae adapted from Recktenwald (2004)).

First order forward difference formula for $\frac{\partial \phi}{\partial x}$ at point $x = x_i$:

$$\frac{\partial \phi}{\partial x}\,(t = t_n, x = x_i) = \frac{\phi_{i+1}^n - \phi_i^n}{\Delta x} + \mathcal{O}(\Delta x) \tag{4.2}$$

where $\mathcal{O}(\Delta x)$ means that the truncation error is proportional (linear) to Δx.

First order backward difference formula for $\frac{\partial \phi}{\partial x}$ at point $x = x_i$ (for the next three equations, the time step is not explicitly shown in the formula; it is understood that the formula is applied to an arbitrary time step n):

$$\frac{\partial \phi}{\partial x}\,(x = x_i) = \frac{\phi_i - \phi_{i-1}}{\Delta x} + \mathcal{O}(\Delta x) \tag{4.3}$$

First order central difference formula for $\frac{\partial \phi}{\partial x}$ at point $x = x_i$:

$$\frac{\partial \phi}{\partial x}\,(x = x_i) = \frac{\phi_{i+1} - \phi_{i-1}}{2\Delta x} + \mathcal{O}(\Delta x^2) \tag{4.4}$$

$\mathcal{O}(\Delta x^2)$ means that the error is proportional to Δx^2.

From this central difference formula, it can be seen that the truncation error $\mathcal{O}$ approaches zero much faster than with the forward or backward formulae (Recktenwald, 2004), as it is proportional to the square of the mesh size instead of being linearly dependent of it. However, Equation (4.4) may cause problems when applied to a differential equation because ϕ_i does not enter into the formula (Recktenwald, 2004).

Approximate expressions for higher-order derivatives can be obtained analogously. As an example, the second order central difference approximation approximates the second derivative as follows:

$$\frac{\partial^2 \phi}{\partial x^2}\,(x = x_i) = \frac{\phi_{i+1} - 2\phi_i + \phi_{i-1}}{\Delta x^2} + \mathcal{O}(\Delta x^2) \tag{4.5}$$

Introducing this or other finite difference approximations into the PDE, a numerical solution may be obtained. The discretised equation is arranged as a time-marching scheme, so that it is possible to calculate the solution values for the following time step based on the solution values for the previous time step.

Applied to thermal problems, the finite difference approximations are used to find an approximate solution to the heat conduction equation (Equation (4.6), which is the one-dimensional form of Equation (3.4), without the energy release term):

$$\frac{\partial \phi}{\partial t} = \alpha \frac{\partial^2 \phi}{\partial x^2} \tag{4.6}$$

In transient problems, the time also needs to be discretised, analogously to the space discretisation shown above. One possible discretisation of Equation (4.6) is the Forward Time, Centred Space or FTCS approximation (Recktenwald, 2004):

$$\phi_i^{m+1} = \phi_i^m + \frac{\alpha \Delta t}{\Delta x^2} \left(\phi_{i+1}^m - 2\phi_i^m + \phi_{i-1}^m\right) \tag{4.7}$$

The error of this method is $\mathcal{O}(\Delta t) + \mathcal{O}(\Delta x^2)$, i.e. it is of order one in time and of order two in space.

It is essential to consider the stability of the numerical scheme, which depends on the physical properties of the material, as well as on the space and time discretisations, because if the solution is unstable, it may oscillate or diverge from the exact solution. The FTCS scheme can provide stable solutions (Recktenwald, 2004) only if the condition of Inequation (4.8) is fulfilled:

$$\frac{\beta \Delta t}{\Delta x^2} \leq \frac{1}{2} \tag{4.8}$$

where β is a constant coefficient.

That is, for a constant time step, if the mesh size is decreased and the previous condition is not met, the method will become unstable. Hence, the scheme will become unstable for time steps larger than the critical time step for given mesh size and material properties. Thus, Inequation (4.8) also implies that the choices of time step and mesh size need to be related (see also unknown (n.d.-d) and GEO-SLOPE International Ltd. (2014)).

Analogously to the FTCS method, there exists the Backward Time, Centred Space method (BTCS). This approximation can be represented by Equation (4.9):

$$\frac{\phi_i^m - \phi_i^{m-1}}{\Delta t} = \alpha \frac{\phi_{i-1}^m - 2\phi_i^m + \phi_{i+1}^m}{\Delta x^2} + \mathcal{O}(\Delta t) + \mathcal{O}(\Delta x^2) \tag{4.9}$$

The errors of the BTCS method have the same order of magnitude as the ones of the BTCS. There is, however, an important difference: Equation (4.9) cannot be rearranged as an explicit function of ϕ_i^m, which means that, unlike the former schemes, the BTCS scheme is implicit.

Explicit schemes may require a very small time step to stay stable. An alternative to them are implicit schemes, which have the significant advantage of being unconditionally stable (Recktenwald, 2004), i.e. they are stable and convergent for any time step. Thus, the time step can be chosen solely based on accuracy requirements (Causon and Mingham, 2010), as there is no stability restriction (Gustafsson, 2011). Consequently, a much larger time step

may be chosen than when using the explicit method. On the downside, as implicit methods require solving a non-linear system of equations every time step (Bonacina and Comini, 1973) (Voller, 1996), they require more computational effort per time step than explicit methods, such as the FTCS method. This is the reason why larger time steps are generally used for implicit methods (Voller, 1996). Typically, time steps used for implicit methods are in the range of fifty to a few hundred times of the maximum time step for the explicit method (unknown, n.d.-e).

Yet another frequently used method is the Crank-Nicholson scheme. This scheme has an additional advantage relative to the FTCS and BTCS schemes: it has a temporal error of second order, i.e. the error decreases faster with smaller time steps. It is implicit and also unconditionally stable (Recktenwald, 2004), which can be proven by means of the von Neumann stability analysis (Causon and Mingham, 2010). Although the von Neumann stability analysis is only applicable to linear schemes and thus cannot be used for schemes simulating phase change, applying it to the corresponding linearized scheme provides a necessary condition for the stability of the nonlinear scheme. In any case, the theory to establish convergence and stability of a method is frequently applicable to specific cases only, so it often needs to be combined with numerical experimentation (Causon and Mingham, 2010).

The Crank-Nicholson method approximates Equation (4.6) with the following implicit equation, with a truncation error of $\mathcal{O}(\Delta t^2) + \mathcal{O}(\Delta x^2)$.

$$\frac{\phi_i^m - \phi_i^{m-1}}{\Delta t} = \frac{1}{2}\left(\frac{\phi_{i-1}^m - 2\phi_i^m + \phi_{i+1}^m}{\Delta x^2} + \frac{\phi_{i-1}^{m-1} - 2\phi_i^{m-1} + \phi_{i+1}^{m-1}}{\Delta x^2}\right) \quad (4.10)$$

This expression can be extended to two space dimensions. For two dimensions, the PDE becomes more complicated, but it can be discretised and simplified with e.g. the operator splitting technique, splitting the PDE in different dimensions or terms (Causon and Mingham, 2010).

The values of the solution function ϕ for the time step m (the current time step which is being solved for) can be obtained from Equation (4.10), provided that the values of ϕ are known for the last time step $m-1$. For real problems with large meshes, this procedure originates a system of equations which may become very large. This system can be solved by direct methods, e.g. Gauss elimination, although for large sizes it is more efficient to use iterative solution methods, such as the Jacobi iteration (used by FLAC3D), the Gauss-Seidel iteration or the successive over-relaxation method (Causon and Mingham, 2010).

A representation of the FTCS, BTCS and Crank-Nicholson methods is found in Figure 4.2.

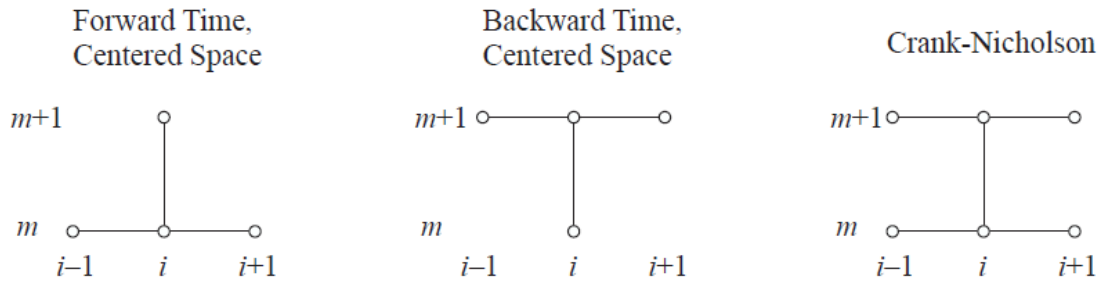

Figure 4.2: Graphical representation of different numerical schemes (Recktenwald, 2004)

4.3. Numerical methods for Stefan problems

The PDE that governs the heat conduction process without phase change is linear and, provided that the boundary conditions are constant, gives monotone, smooth and bounded solutions, which describe the transformation of the system from the initial state to a steady state (Recktenwald, 2004). On the contrary, the phase change process introduces a non-linearity, which causes the solution for the temperature field to have a discontinuous derivative (the temperature history is no longer smooth). For instance, if the thermal characteristics of the soil vary with temperature, for example due to the phase change process, the coefficients of the finite difference equation may need to be adjusted every time step in an iterative process (Bonacina and Comini, 1973).

There exist different numerical schemes to solve Stefan problems. Extensive reviews on these methods can be found, among others, in Crank (1987), Voller (1996), and Javierre et al. (2006). These numerical methods can be classified into "fixed grid" (the enthalpy method being the most extended among them) and "front tracking" methods (Voller, 1996) (Mackenzie and Robertson, 2000) (Savovic and Caldwell, 2009) (Ivanovic et al., 2017). A third type, similar to front tracking methods, is formed by front-fixing methods, such as the boundary immobilization method, which fixes the moving boundary (phase-change interface) via a coordinate transformation. Other methods, such as the perturbation method, require symbolic mathematics software or are only applicable under specific conditions, e.g. for small Stefan numbers (Caldwell and Kwan, 2004). A comparison of several of these methods applied to the one-dimensional Stefan problem can be found in Karabenli et al. (2016).

Fixed-grid methods are clearly more advantageous than front-tracking methods to solve problems in two or more dimensions (Voller, 1996). In general, problems in 2D and 3D are of high practical importance (Basu and Date, 1988), as most of the phenomena and real projects cannot be reduced to one-dimensional problems. Lastly, there are hybrid methods, like node jumping, local tracking and deforming enthalpy methods, which aim to profit of the advantages of both types of methods (Voller, 1996).

Finally, although there are well-established numerical solutions for Stefan problems, the field for future research is large, e.g. to simulate specific problems like the morphology of the mushy region or the coupling of thermal and other fields (Voller, 1996).

4.3.1. Front-tracking and front-fixing methods

In these methods, the phase change interface is continuously tracked (Savovic and Caldwell, 2009). The isotherm migration method, the variable grid method and the heat balance integral method are considered front-tracking schemes. The boundary immobilization method is a front-fixing method.

Front-tracking methods use an explicit representation of the interface (Javierre et al., 2006) and adjust the grid or the time steps to always locate nodes along the phase interface (Voller et al., 2004). The variable time step method adapts the time step so that the interface coincides with the grid lines at every time step (Basu and Date, 1988). Other methods are the boundary immobilization and the isotherm migration method. In these methods, which are common in finite-element literature (Voller, 1996), the Stefan condition (energy conservation) is explicitly imposed at the moving interface (Mackenzie and Robertson, 2000), thus an *a-priori* knowledge of the boundary geometry is usually required. The moving grid methods use an adaptable grid and have been shown to give the interphase position more accurately, while the former provide a more precise temperature distribution in the whole region. The applicability of the moving grid or moving mesh methods is however usually limited to relatively simple problems, with one-dimensional and uncomplex geometry (unknown, n.d.-a) (Stuizalec, 1989) (Ayasoufi, 2004).

Very low relative errors, of the order of 10^{-4} to 10^{-5}, have been documented in Karabenli et al. (2016) with the Finite Element Boundary Immobilization Method, the Finite Element Isotherm Migration Method and the Finite Element Variable Space Grid Method.

4.3.1.1. Variable grid and variable time step methods

In these methods, the spatial grid or the time step is adapted at every time step, so that the interphase is always located at the same nodes. For instance, the number of elements between a boundary and the phase interface is fixed to be N, so the interface will always be at the N^{th} line of the grid (Savovic and Caldwell, 2009). This method has advantages in the implementation and can be solved with symmetric matrices, which are easier to compute (Javierre et al., 2006). Furthermore, it gives smooth solutions for the phase interface and is more efficient than uniform mesh methods (Mackenzie and Robertson, 2002). The main drawback of this method for practical use is that the form of the phase change interface needs to be known *a priori*, so that it is currently applicable only for simple 1D geometries (see e.g. Savovic and Caldwell (2009) or Wu and Wang (2012)), or possibly for regular 2D geometries. Furthermore, it needs to be assumed that the moving boundary is moving smoothly and monotonically with time, which may not always be the case (Furzeland, 1980).

4.3.1.2. Isotherm migration method

The basic idea behind the isotherm migration method is that the temperature can be taken as the independent variable, whereas the spatial coordinates are considered as the dependent variables (Crank and Gupta, 1975). This approach is essentially tracking the movement of

the isotherms, one of which is the phase-change interface. This front-tracking method has been used to solve phase-change problems in one and two dimensions, however, its applicability is restricted to problems with symmetry (Crank and Gupta, 1975) or simple geometries.

4.3.1.3. Boundary immobilization method

The boundary immobilization method is a front-fixing method based on performing a coordinate transformation which practically fixes the phase change boundary. In exchange, however, a more complicated problem needs to be solved (Savovic and Caldwell, 2009). A representation of the methodology is shown in Figure 4.3. These kinds of methods are usually difficult to apply in problems with several phase interfaces, disappearing or merging interphases or gradual phase change. Additionally, this method does not seem to be easily applicable for 2D complex geometries, although it may be more accurate than the enthalpy method. Examples of application for typical geometries can be found in Kim and Kaviany (1990) and in Mitchell and Vynnycky (2009). Finally, this method requires a starting solution for small time (Caldwell and Kwan, 2004).

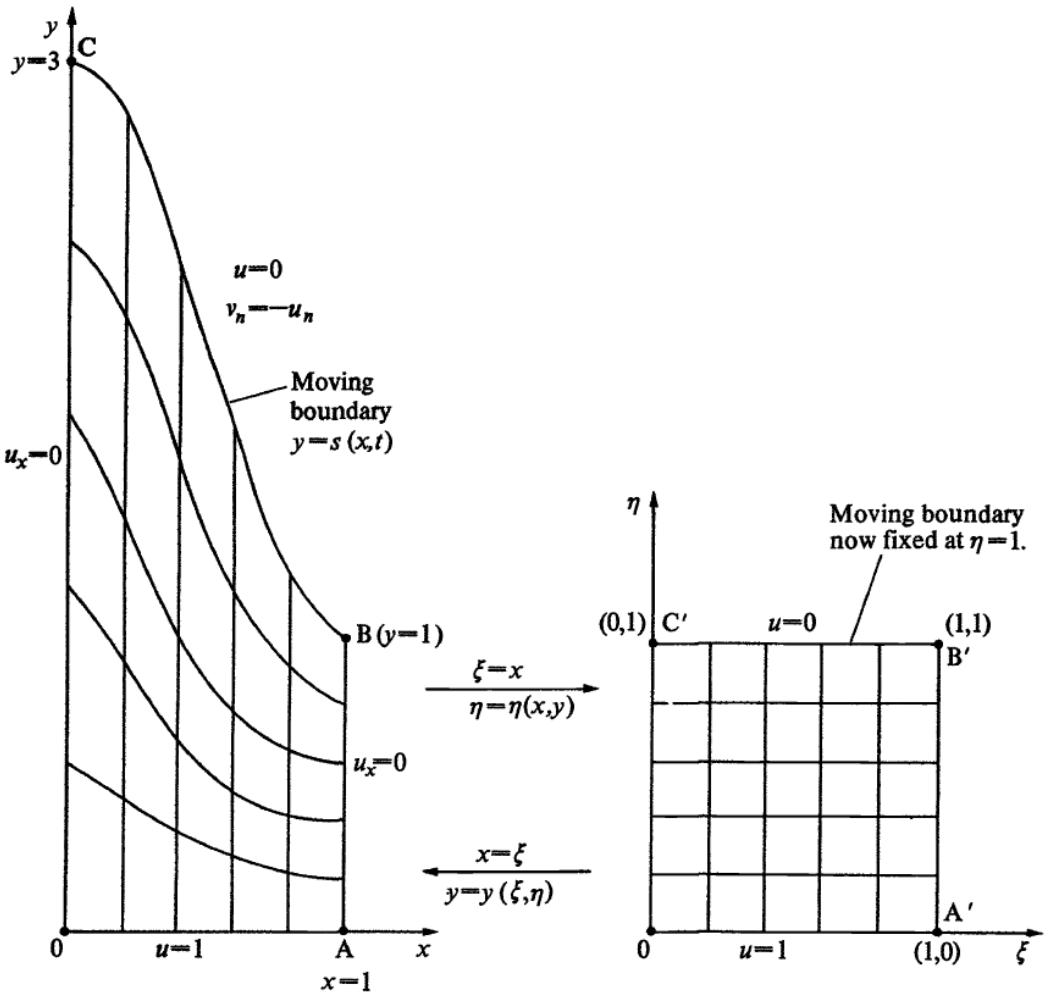

Figure 4.3: Real geometry and transformed geometry with fixed interphase (Crank, 1987)

4.3.2. **Fixed domain or fixed grid methods**

Fixed grid methods use a constant grid during the whole calculation. The most widely fixed grid method is the enthalpy method, which was first introduced by Eyres et al. (1946) to treat heat transfer problems with thermal conductivity varying with the temperature (Ayasoufi, 2004).

4.3.2.1. The enthalpy method

The enthalpy method is considered to be a "simple and flexible technique" to tackle phase-change problems (Esen and Kutluay, 2004). One of the early papers to discuss it was Rose (1960). It can be combined with finite element and finite difference schemes (Furzeland, 1980). In this method, the enthalpy function "H", which represents the total heat including specific and latent heat per unit mass, is defined by Equation (4.11) (Voller, 1996). As the defined enthalpy function is discontinuous, it is usual to use the weak (integral) formulation of the heat conduction PDEs (Crank, 1987).

$$H = \begin{cases} c_1 T & T < T_f \\ c_2 T + (c_1 - c_2)\, T_f + L & T \geq T_f \end{cases} \tag{4.11}$$

Where L is the absorbed latent heat per unit mass and c_1 and c_2 the respective frozen and unfrozen specific heat capacities.

This method does not track the phase interface directly (Furzeland, 1980) (Voller, 1996). It is said to be the only numerical method for phase-change simulation which can be applied to general problems (unknown, n.d.-a). Moreover, it is flexible, easy to program and provides a clear representation of the physical phenomena. It can be applied relatively easily to 2D and 3D problems (Scheerlinck et al., 1997), having the following advantages (Voller and Cross, 1981):

1. No additional conditions need to be imposed at the phase interface. The Stefan condition is not imposed at the interface, but it is obeyed automatically.
2. The phase interface does not need to be tracked and consequently it does not have to be assumed *a priori*, but can be extracted *a posteriori* if required.
3. The frozen and unfrozen areas do not need to be considered separately, but are treated together, using the enthalpy function instead of the temperature.
4. It is easy to simulate a "mushy" region.

These facts make it one of the most popular methods for solving Stefan problems (Caldwell and Kwan, 2004).

On the other hand, several disadvantages of the enthalpy method are presented below:

1. It may require a finer mesh than moving grid methods in order to reach the same level of accuracy (Furzeland, 1980).
2. For small Stefan numbers, it has accuracy and convergence issues (Ayasoufi, 2004).
3. The position of the interface has to be interpolated and is not directly calculated (Basu and Date, 1988).

Furthermore, another drawback is that for sharp interface problems, the enthalpy method tends to produce oscillations of the interface position and unrealistic plateaux followed by sharp drops in the temperature-time graph (see Figure 4.4) (Furzeland, 1980) (Voller and Cross, 1981) (Basu and Date, 1988) (Mackenzie and Robertson, 2000). These temporal oscillations of the temperature appear because when the interface is located at a certain node, the node is held at the phase-change temperature, which causes the neighbouring area to relax to a steady state (unknown, n.d.-a). When the interface progresses to the next node, the temperature adjusts to the new steady state. The extent of the oscillations depends, among other factors, on the properties of the material: with higher Stefan numbers, the plateaux in the temperature history tend to be less marked, but the phase interface history exhibits oscillations. The performance of the enthalpy method was also analysed by Voller (1996), who concluded that, at a low Stefan number of 0.1, it tracks quite accurately the phase-change interface. Oscillation issues are reduced in multidimensional problems and by applying Neumann instead of Dirichlet boundary conditions (Voller, 1996).

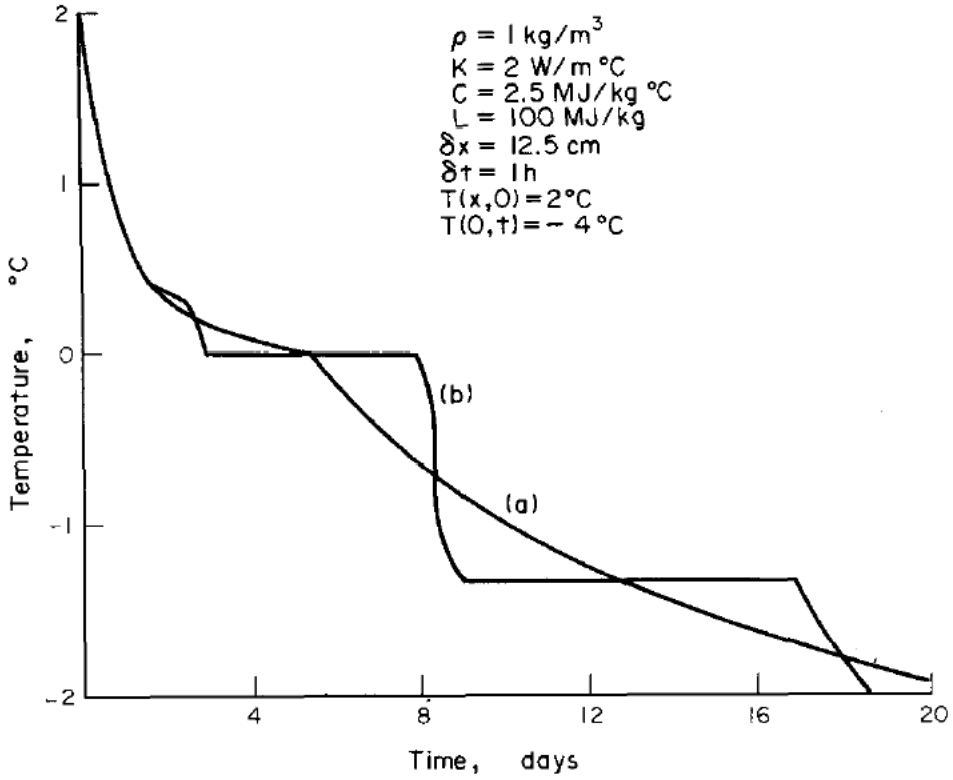

Figure 4.4: Comparison between the analytical solution (a) and the results from the enthalpy method (b) (Voller and Cross, 1981)

The enthalpy method with sharp phase change needs adjustments to achieve convergence and stability and to avoid oscillations (Ayasoufi, 2004). If the phase change is gradual and happens over a temperature range, instead of at a specific temperature, the enthalpy method delivers more stable results (Voller and Cross, 1981). Voller and Cross (1981) assessed the enthalpy method and concluded that smooth results can only be achieved if at every time step at least two elements (zones) are within the phase change range $(T_f - \varepsilon, T_f + \varepsilon)$. Thus, the size of the phase change range directly impacts the accuracy of the enthalpy method.

However, in the case that this range is just introduced for computational reasons (i.e. if it is not fixed to the real phase-change range of the material), the optimal or most suitable range has to be determined based on numerical experiments (Furzeland, 1980).

For gradual phase change with a range 2ε, the enthalpy function may be defined as in Equation (4.12) (Voller and Cross, 1981). This approach assumes that the latent heat is released uniformly over the phase change range, which corresponds to a linear unfrozen water function. A graphical representation of the enthalpy function versus the temperature is shown in Figure 4.5.

$$H = \begin{cases} c_1 T & T < T_f - \varepsilon \\ H(T_f - \varepsilon) + L\,(T - T_f + \varepsilon)/2\varepsilon & T_f - \varepsilon < T < T_f + \varepsilon \\ H(T_f + \varepsilon) + c_2(T - T_f - \varepsilon) & T_f + \varepsilon \leq T \end{cases} \tag{4.12}$$

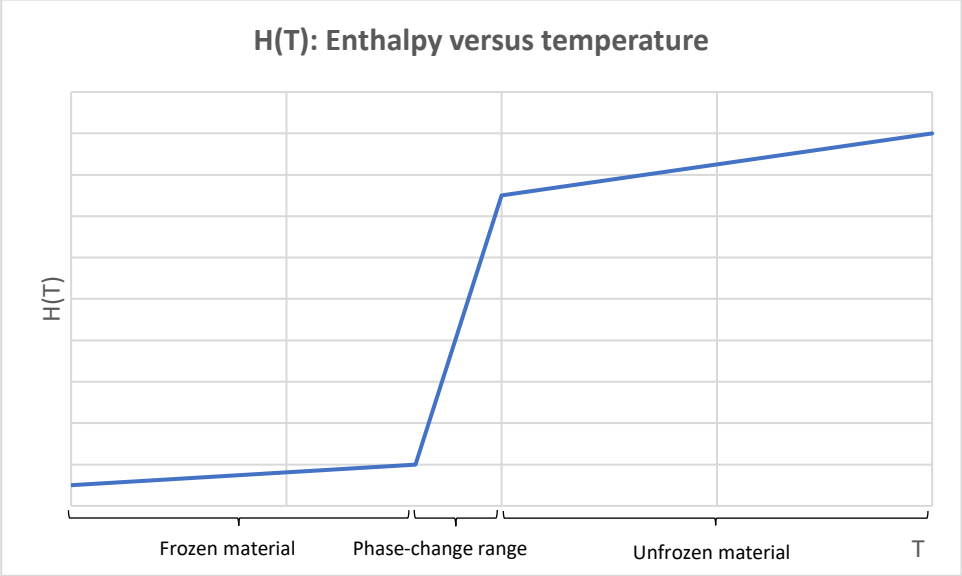

Figure 4.5: Enthalpy function versus temperature

The oscillations are less pronounced with decreasing mesh element (zone) size and may also be decreased by reducing the time step in relation to the mesh size. Therefore, it would be optimal to use a reduced mesh size in the area of the phase change interface (adaptive mesh). In this way, the small mesh size is applied only in the neighbourhood of the phase-change location, where it is required, but a larger mesh is used elsewhere, so that the model has a lower number of zones and is computationally efficient. An example of such an algorithm for 1D geometries can be found in Mackenzie and Robertson (2000).

In order to ensure the stability of the scheme, the time steps and grid size have to fulfil the following condition (Voller and Cross, 1981) (Voller, 1996):

$$\max\left|\frac{\Delta t\, k_1}{\rho\, c_1\, \Delta x^2}, \frac{\Delta t\, k_2}{\rho\, c_2\, \Delta x^2}\right| \leq \frac{1}{2} \tag{4.13}$$

Esen and Kutluay (2004) showed that the enthalpy method with finite differences using the hopscotch scheme, which combines explicit and implicit methods and is overall explicit and unconditionally stable, can produce good results compared to the exact solution.

Scheerlinck et al. (1997) published an improved finite element enthalpy method, combined with the Kirchhoff transform, which allows for larger time steps and a more stable system than the explicit finite element enthalpy method. The enthalpy method has also been applied to artificial ground freezing, e.g. in Vasilyeva et al. (2020).

An alternative fixed-grid method is the apparent heat capacity method. This commonly used method is based on reformulating the heat equation based on the apparent heat capacity (Voller, 1996), which is the derivative of the enthalpy with respect to the temperature. The so-called apparent or equivalent heat capacity is the specific heat capacity increased by a certain amount in the freezing range to account for the latent heat (Jame and Norum, 1980) (Ziegler et al., 2010). With this approach, the non-linearity is contained in the definition of the apparent heat capacity, so the Stefan problem can be solved by using a standard heat-transfer numerical scheme. The apparent heat capacity can be defined as follows:

$$c_{apparent} = \frac{\partial H}{\partial T} = \begin{cases} c_1 & T \leq T_f - \varepsilon \\ \dfrac{c_1 + c_2}{2} + \dfrac{L}{2\varepsilon} & T_f - \varepsilon < T < T_f + \varepsilon \\ c_2 & T \geq T_f + \varepsilon \end{cases} \tag{4.14}$$

Osterkamp (1987) found that this method is suitable for freezing problems even with small amounts of unfrozen water. Voller (1996) argues for the conserved enthalpy linearization (which needs a small additional computational effort) above the apparent heat capacity method because, unlike the latter, it conserves heat at every time step and point in space and does not have the oscillation problems of the apparent heat capacity method for early time steps. The apparent heat capacity method is commonly used in numerical modelling for artificial ground freezing projects, see for example Zhu and Michalowski (2005) or Zhao (2019).

Another possibility, which is said to be more stable and allow for larger time steps (while perhaps requiring more computational time), is to constrain the temperature of the nodes during the phase change (G. Gioda, 1994). An alternative but similar approach is to include the latent heat as a source term in the equations, as e.g. in Hwang et al. (1972) or Bock (2018). However, unknown (n.d.-a) reports that algorithms which model the latent heat by means of a source term tend to have more phase change missing problems.

Regarding the thermal properties of the material near the phase change interface, layers of solid and liquid material appear, so it may make sense to calculate the properties for the model zone containing the interface (and thus including solid and liquid material) according to a "serial" arrangement of the material (unknown, n.d.-a). For instance, the thermal conductivity of element "j" inside the zone considered could be calculated as follows:

$$\frac{1}{k_j^n} = \frac{\xi_j^n}{k_2(T_f)} + \frac{1-\xi_j^n}{k_1(T_f)} \tag{4.15}$$

where k_j^n and ξ_j^n are, respectively, the thermal conductivity and the unfrozen water content of element j at time n.

For simplicity, it is possible to take the arithmetic average of the conductivities of the solid and liquid phases, as done in Equation (4.14) for the specific heat capacities, (unknown, n.d.-a), especially if their values do not differ significantly. This is also applicable to the "mushy" zone in problems with gradual phase change. Nevertheless, as this zone is relatively thin, the exact distribution of the thermal properties in it is usually not of practical importance (Nakano and Brown, 1971).

4.3.2.2. Other fixed-grid schemes

There are other fixed-grid schemes, such as the phase field method. In this case, a phase field function is defined, which has different values for the two phases and intermediate values in the interface, which is considered as a region. This differs to other methods, in which a sharp interface is considered (Javierre et al., 2006). Numerical issues appear if the interface region is set very small in order to find the solution to the sharp-interface problem (Javierre et al., 2006). A difficulty presented by the phase field method is that obtaining the physical parameters required to apply the method may be complicated (Javierre et al., 2006).

Another fixed-grid method is the level-set method. It describes the position of the interface with a continuous function, which varies linearly in each phase and takes the value of zero at the interface. This method is useful to model merging interfaces. A fixed grid can be used, avoiding the effort of generating a new mesh at each time step (Javierre et al., 2006). Javierre et al. (2006) recommend the level-set method for 2D and 3D problems rather than the moving-grid method or the phase-field method.

4.4. Significant aspects in numerical modelling of Stefan problems

4.4.1. Meshing and time stepping for Stefan problems

The discretisation of the space and time continuum in numerical schemes can have a significant influence on the accuracy of the results and the efficiency of the computation. This is a very relevant area of study, even considering the improvements in computing capacity in the last years, because the increasing complexity of the models poses growing computing requirements. For instance, according to Akin (2009), a typical thermal mesh may have between 20,000 and 100,000 nodes and temperature equations. The computation time will depend on the required time per iteration and the rate of convergence of the iterative scheme (Causon and Mingham, 2010). Specially in non-linear schemes a good discretisation (mesh quality) is crucial to achieve sufficiently accurate results, stability and fast convergence (Itasca Consulting Group, 2018). For instance, Stout and Billings (2002)

state that "an improperly meshed model will never provide accurate transient response, regardless of the time stepping".

As much of the theory to establish convergence and stability of numerical methods has been created for specific cases, it is of limited application (especially to non-linear problems, such as thermal problems with phase-change), hence it often needs to be combined with numerical experimentation (Causon and Mingham, 2010). Although there are some rules of thumb for meshing and, in transient problems, for choosing time steps for finite element schemes (Abbasi et al., 2013), the usual engineering practice involves using a trial-and-error approach to choose the mesh and time steps, which requires skill and experience (GEO-SLOPE International Ltd., 2014). The order of magnitude $\mathcal{O}$ of the truncation error in a numerical scheme may be used to check that a scheme is working properly, e.g. if the order is linear in space, $\mathcal{O}(\Delta x)$, the error should decrease linearly when the mesh size is reduced linearly (Recktenwald, 2004).

The fact that the appropriate time step is dependent on the mesh size further complicates modelling. As presented in chapter 4.2, the time step is dependent upon the chosen mesh: even for problems without phase change, explicit methods have stability issues when the time step is larger than the critical time step for a certain mesh (see Equation (4.8)). ANSYS (2004) (*https://www.ansys.com/*), the owner of a Finite Element software very widely used in engineering problems, recommends using smaller time steps for phase-change thermal problems.

4.4.1.1. Mesh quality and evaluation

Itasca Consulting Group (2018) defines a good mesh as the one which allows "to solve the problem at the expected level of accuracy within the time available for the project". According to Altair university (n.d.), the suitable mesh (regarding accuracy) to be used in a numerical model is the one whose results do not significantly change if it is refined. There are several methods for mesh generation, which yield meshes of different elements and quality (see e.g. the review in Owen (1998)).

Meshes can be classified in structured and unstructured meshes. Structured meshes are regular, contain typically well-shaped elements and are computationally more efficient than unstructured meshes (Itasca Consulting Group, 2018). Studying the comparative performance of structured and unstructured meshes has been suggested by Zavaleta Camacho (2017).

As much of the research on meshing for numerical methods has been performed for mechanical simulations, it makes sense to use parallelisms between the mechanical and thermal numerical analyses, as shown e.g. in Table 4.1.

Table 4.1: Analogies between thermal and structural analyses (Akin, 2009)

Thermal analysis item, [units], symbol	**Structural analysis item, [units], symbol***
Unknown: Temperature [K], T	Unknown: Displacements [m], u
Gradient: Temperature Gradient [K/m], ∇T	Gradient: Strains (m/m), ε
Flux: Heat flux [W/m^2), q	Flux: Stresses [N/m^2], σ
Source: Heat Source for point, line, surface, volume [W], [W/m], [W/m^2], [W/m^3], Q	Source: Force for point, line, surface, volume [N], [N/m], [N/m^2], [N/m^3], Q
Restraint: Prescribed temperature [K], T	Restraint: Prescribed displacement [m], u
Reaction: Heat flow resultant [W], Q	Reaction: Force component [N], Q
Material Property: Thermal conductivity [W/m K], k	Material Property: Elastic modulus [N/m2], E
Material Law: Fourier's law	Material Law: Hooke's law

**Note: Several of these symbols, which are used in the table above in the context of structural analysis, are used otherwise in the rest of this thesis (see List of Symbols).*

Areas with high stresses in mechanical analysis (Altair university, n.d.) or analogously a steep thermal flux and temperature gradient in thermal simulations need a finer and preferably structured mesh. Also areas in which the heat flux will change rapidly should be finely meshed (Akin, 2009). Areas of numerical difficulties in thermal simulations include e.g. the freeze pipes if simulated as punctual sources (lines in 3D models or points in 2D models), which pose a similar case of singularity (Tounsi et al., 2019) to stress concentration under a punctual load in mechanical analysis (see Table 4.1). A graded mesh can be used so that there is a fine mesh in those sensitive areas in order to achieve good results, while limiting the increase of the computing time (Stout and Billings, 2002).

It is also important to choose the most suitable element type, considering the boundary conditions, geometry and required accuracy (Altair university, n.d.). A structured hexahedral mesh usually gives the best results regarding accuracy, although it can be more time-consuming to create (Itasca Consulting Group, 2018). With respect to the order of the elements, lower-order elements are recommended for problems with phase change (ANSYS, 2004).

In order to set the requirements for meshing, to improve the mesh and to control its quality, mesh quality metrics are used (Knupp, 2001). A metric for an element is a scalar function which depends on the node coordinates and provides a measure of some geometrical property of the element (Knupp, 2001). Numerous measures of mesh quality have been proposed, e.g. element volume, aspect ratio, skew, angles, stretching or orientation (Knupp, 2001). A specially interesting metric is the Jacobian matrix because it contains information regarding the volume, shape and orientation of an element (Knupp, 2001). “Good” elements are usually regular elements, i.e. equilateral or symmetrical (Pébay, 2002). Another relevant approach is the Grid Convergence Index proposed by Roache (1993) in order to improve the comparability between grids.

There exist automatized programmes to evaluate metric quality, such as the Verdict Geometric Quality Library (Knupp et al., 2006) and there are numerous academic papers written on mesh optimisation, such as Dompierre et al. (1998). In FLAC3D, there are three metrics for controlling the quality of the elements (Abbasi et al., 2013):

- Aspect ratio: "ratio of the longest edge of an element to either its shortest edge or the shortest distance from a corner node to the opposing edge".
- Orthogonality: "the ratio of the smallest angle to the largest angle"
- Face planarity

4.4.1.2. Meshes and time steps used in engineering projects and theoretical studies

A review of the meshes and time steps in different studies and projects reported in the literature was performed. The results are shown in Table 4.2 and Figure 4.6. It can be concluded from this table and graph that the meshes used in papers written by the theoretical researchers with the aim of checking the accuracy of numerical methods tend to be significantly smaller (in the order of a few centimetres) with respect to the ones used by practitioners who apply them to engineering projects (several decimetres). Furthermore, in the latter, there is usually no justification of the chosen discretisation. There is no known method to choose "appropriate" mesh size, so it is common practice to do it by trial and error (GEO-SLOPE International Ltd., 2014). Choosing a mesh which produces sufficiently accurate results and at the same time requires an acceptable computing time and RAM memory is a critical task for the numerical modeller. For instance, finer mesh is reported to produce a large increase in computation time (unknown, n.d.-a). Another aspect which should be considered is that areas where phase change is occurring and with high temperature gradients may require finer meshes: see e.g. Nakano and Brown (1971), who use meshes of approximately 2 cm in those areas, gradually increasing it to 1 m in less critical areas.Not only the spatial discretisation but also time steps should be carefully chosen (P.E.Frivik, 1981); too large steps may cause instability or accuracy problems. It is known that "very small time steps are often needed for accurate solutions" (Rizwan-uddin, 1998) (Savovic and Caldwell, 2009). As the time step is seldom reported in the publications on actual engineering projects, it is not possible to compare the size of the time steps between theoretical and practical papers from the data in Table 4.2 and Figure 4.6. However, according to the experience of the author, it is probable that the time steps typically used in engineering practice are generally larger than the ones used for theoretical studies.

Table 4.2: Meshes and time steps used in different publications

Paper nº	Study or project name and dimensions	Paper author	Mesh	Time step
1	Experiment (30 cm length, 72 hours)	Jame and Norum (1980)	0.01 to 2.5 cm	0.001 to 0.4 hours
2	Experiment (ca. 75 cm length, ca. 72 hours)	Vitel et al. (2016)	Approx. 5-10 cm	0.024 hours
3	Mathematical discussion (200 grid intervals, 0.25 total time)	Javierre et al. (2006)	0.0005 (no units)	$5x10^{-4}$ to $9x10^{-5}$ (no units)
4	Verification of FLAC thermal capabilities, line source, without phase change (length 500 m, 360 days).	Itasca Consulting Group (n.d.-a)	Graded, 1 m to 40 m	2 h
5	Verification against analytical solution (50 days)	Voller and Cross (1981)	10, 12.5 cm	1 h (explicit algorithm) 108 h (implicit algorithm)
6	Verification of TEMP/W against analytical solution (10 m, 100 days)	GEO-SLOPE International Ltd. (n.d.)	1 – 20 cm	10 days (these steps may be subdivided by the program)
7	Verification against analytical solution (20 m, 24 h)	Nakano and Brown (1971)	0.2 – 100 cm	2.4 h
8	Verification against an experiment (15 cm, 2 h)	Scheerlinck et al. (1997)	1.25 x 0.83 x 0.25 cm	10 s
9	Verification of an analytical solution (model of 4m radius)	Cai et al. (2018)	Approx. 2 – 29 cm	unknown
10	Development of customised numerical code (6x8m model, 48 days)	Zhu and Michalowski (2005)	Approx. 6 – 110 cm	unknown
11	Design of AGF for cross passage in Shanghai metro	Wang et al. (2015)	Approx. 50 cm	unknown
12	Design of AGF for metro station in Naples	Viggiani and De Sanctis (2009)	35-60 cm and upwards	unknown
13	Design of AGF for mine shaft in Russia	Franz (2014)	Approx. 50 cm	unknown
14	Design of AGF for metro of Naples	Colombo (2010)	Approx. 10 – 50 cm	unknown

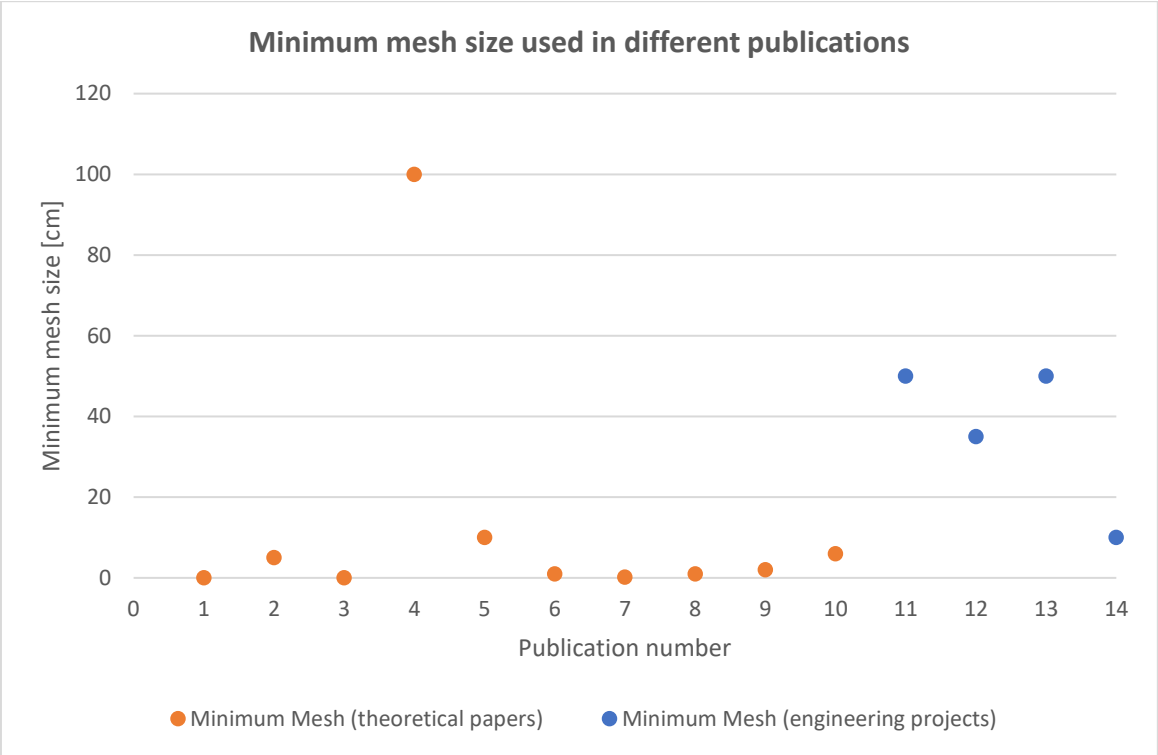

Figure 4.6: Minimum mesh size used in theoretical / model verification papers and in engineering projects

4.4.2. Phase change missing and overflowing

The numerical methods developed for phase-change problems often account for a sharp phase-change. However, allowing for a gradual release of the latent heat over a range of temperatures is usually more realistic and improves the stability of the method (Pentland and Fredlund, 2001). Even so, if the half phase change range, ε, is too small and the time steps are too large, the enthalpy scheme may "skip" or may overestimate the effects of the latent heat (Voller, 1996) (Tao and Zheng, 2009). The origin of the problem is that, for instance, in the case that the temperature of an element changes within one time step from $T \geq T_f + \varepsilon$ to $T_f - \varepsilon < T < T_f + \varepsilon$, then the scheme applies a specific heat capacity which is not correct for the whole time step, simulating too high or too low latent heat effects.

It is not physically accurate, when simulating an abrupt phase change, that more than one element in the direction of the freeze front changes phase in any given time step. Thus, similarly to the stability criterion applied in Causon and Mingham (2010) to the advection differential equation, a condition for the heat transfer equation with phase change would be $\Delta t \leq \Delta x / |v_g|$ (v_g represents the flow velocity in the original equation for advection). When applied to the advection equation, $C = v_g \cdot \Delta t / \Delta x$ is called the Courant number, and schemes are often stable for $|C| \leq 1$ (Causon and Mingham, 2010). For the heat transfer equation with phase change, v_g would represent the speed of propagation of the freeze front. Furthermore, the time step should be somewhat smaller than what is given by the previous condition, i.e. a certain "safety factor", which has to be determined testing the numerical method, should be applied (Causon and Mingham, 2010).

A solution to the problems of phase change missing and overflowing was proposed by Tao and Zheng (2009). They propose a so-called backwards calculating time step method, which computes the largest possible time step required to avoid these issues and recalculates the system with it. They demonstrate that this method has lower phase-change errors and shows a more regular behaviour than the fixed-time-step and variable-time-step methods, which tend to overestimate the velocity of the freezing process.

4.4.3. Sharp and gradual phase change in phase change problems

As described in chapter 2.3.1, in general, materials which are not a pure substance, such as soil or metallic alloys, change phase at a temperature range and instead of a sharp interface, a mushy region appears. These problems are generally solved by using a fixed grid scheme and the enthalpy method. The simplest approach is to define a function of unfrozen water content, which can be directly related to the enthalpy (Voller, 1996). The release of latent heat in natural ground can be described by unfrozen water functions which are usually non-linear (see e.g. Lunardini (1988) and Schüller (2015)) and which are typically derived from laboratory tests or literature values. Typical unfrozen water content functions for different soils are shown in Figure 2.9. For the purposes of this thesis, a linear unfrozen water function is a reasonable approach.

Numerical methods generally perform better for smooth problems, i.e. problems without singularities. That is, computationally it is more stable to simulate a gradual phase change with a "mushy" region than a sharp phase change with an infinitesimally thin interface and an abrupt change in apparent heat capacity (Alekseev et al., 2018). Therefore, even for materials with near-sharp phase change (such as granular soils), a temperature range for phase change may be introduced for computational reasons, which has been proved to be more stable and sufficiently accurate for engineering (Nakano and Brown, 1971). Furthermore, the effect of gradual phase change in cohesive soils has an impact in the temperature distribution which could be of practical importance.

4.4.4. Initialisation and boundaries of the numerical model

Numerical methods are prone to instabilities at the beginning of the calculation, as the model starts at non-equilibrium conditions, e.g. with very large temperature gradients. That is why it is common to use analytical solutions as an initial condition for numerical schemes until a certain (small) time has elapsed (Mitchell and Vynnycky, 2009). Indeed, the sudden temperature change and large gradient caused by the initial condition tend to produce numerical instabilities and error, which may be prevented by using as the initial boundary condition the exact analytical solution (if available) for a certain time after the initial time (Nakano and Brown, 1971), also applied in Furzeland (1980).

In order to avoid boundary effects in a numerical model with finite dimensions, the size of the model has to be sufficiently large so that the boundaries do not significantly affect the temperature field in the relevant region. Alternatively, if there is an available analytical solution, it may be applied at the boundary.

4.5. Introduction to numerical software for Stefan problems

There are a few numerical software packages capable of solving thermal ground freezing problems. Some of the most common are presented in Table 4.3, along with exemplary publications in which they were used.

A comparison of the results from four different software packages was performed in Alekseev et al. (2018) and found FROST3D to generate the most accurate results. However, the numerical calculations were performed with different meshes in the four models, which may impair the comparability of the results.

Table 4.3: Overview of software packages for ground freezing design

Software	Developer	Used for thermal calculations in ground freezing in	Comments
TEMP/W	GeoStudio	Sopko (n.d.-a), Sopko (n.d.-b), Chang and Lacy (2008), Hentrich and Franz (2015), Shawn et al. (2016) and Yan et al. (2017)	Finite Element Method, Apparent heat capacity method, only for 2D problems.
Plaxis Thermal Flow	Bentley Systems, Inc. (previously Plaxis BV)	-	Finite Element Method, Apparent heat capacity method.
ABAQUS	Dassault Systèmes	Zhu and Michalowski (2005), Viggiani and De Sanctis (2009), Colombo (2010) and Cai et al. (2018)	Finite Element Method, method to simulate phase change can be customised. Apparent heat capacity.
SHEMAT	RWTH Aachen	Baier (2008) and Schüller (2015)	Finite Difference Method, Apparent heat capacity method. Used up to date only in academical work (to the author's knowledge).
FLAC3D	Itasca Consulting Group	Wang et al. (2015), Kang et al. (2016) and Bock (2018)	Finite Difference Method, method to simulate phase change can be customised. Apparent heat capacity method may be used.
ANSYS	ANSYS, Inc.	Chris K W Leung (2012), Lam and Pang (2014), Alekseev et al. (2018), Song et al. (2018) and Alzoubi et al. (2019)	Finite Element Method.
TH-Model	ETH Zurich	Sres (2009)	Finite Element Method, Apparent heat capacity method.

			Used up to date only in academical work (to the author's knowledge).
JOBFEM	KTH, Royal Institute of Technology, Stockholm	Johansson (2009)	Finite Element Method.
Comsol Multiphysics	COMSOL	Manassero et al. (2008), Alekseev et al. (2018), Tounsi et al. (2019), Wang et al. (2019), Qi et al. (2020), Zhelnin et al. (2020), Zhelnin et al. (2021)	Finite Element Method.
MATLAB	Mathworks	Xu et al. (2020) and Zueter et al. (2021)	Finite Difference Method, enthalpy formulation.
SV Office 2009, SVHEAT module	SoilVision Systems Ltd.	Alekseev et al. (2018)	Finite Element Method.
FROST3D	Simmakers Ltd.	Alekseev et al. (2018)	Finite Difference Method.

4.5.1. Introduction to FLAC3D

FLAC3D (Fast Lagrangian Analysis of Continua) is a commercial numerical software from the developer Itasca Consulting Group, Inc, based in Minneapolis, USA. It is widely used to solve geotechnical, thermal and hydrogeological problems in engineering projects, especially in soil and rock engineering. It is capable of performing complex calculations coupling the mechanical, thermal and hydraulic fields (THM simulations), determining e.g. thermal stresses, stresses due to frost heaving, heat transfer combined with groundwater flows and other coupling effects. The thermal capabilities of FLAC3D include conduction and advection. FLAC3D has also been applied to ground freezing projects, see for example Kang et al. (2016) or Bock (2018).

FLAC3D is a quite versatile software (Bock, 2018) in the sense that many of the parameters, solving algorithms, mesh, time steps etc. may be steered through the built-in programming language FISH. Moreover, the results can be accessed and operated, e.g. to create custom graphics or export tables, via FISH. This flexibility and easy adaptation of the numerical code was the main reason why it was chosen as the numerical simulation tool for this thesis. FLAC3D is programmed to solve thermal problems without phase change. On the other side, the simulation of the phase change for ground freezing needs to be fully programmed by the user. This provides an excellent framework for the present thesis to investigate ways to model the phase change, as well as their accuracy and efficiency.

With respect to the solving algorithm, Itasca Consulting Group (n.d.-b) states the following (referring to the 2D version of the programme, FLAC):

> "The explicit formulation used in FLAC may be slow in some circumstances, but it is very tolerant of extreme nonlinearities and offers a straightforward framework in which to implement complex physics. The method provides a flexible way to simulate complex, 2D systems involving transient, nonlinear heat, fluid and solid coupling."

Further details on the solving algorithm in FLAC3D can be found in the FLAC3D thermal analysis manual in Itasca Consulting Group (n.d.-a). FLAC3D can use two solving algorithms: explicit and implicit. For the explicit scheme to be stable, which is first order accurate, the time steps must be below a certain value. The critical time step is a measure of the time that takes for the diffusion "front" to travel through the element (zone) (Itasca Consulting Group, n.d.-a). For the case without coupling with groundwater flow (and without considering phase change), Equation (4.16) is given by Itasca Consulting Group (n.d.-a) to determine the critical time step:

$$\Delta t_{cr} = \frac{1}{m}\frac{L_c^2}{\alpha} \tag{4.16}$$

where:

Δt_{cr}: critical time step

m: constant, larger than one, which depends on the geometrical discretisation

$L_c = \frac{volume\ of\ solid\ of\ one\ element}{surface\ area\ \text{of one element}\ exchanging\ heat}$: smallest characteristic length of any zone

α: thermal diffusivity

The implicit method in FLAC3D is based on the (second order) Crank-Nicholson method and is stable for any time step (Itasca Consulting Group, n.d.-b). However, it involves solving simultaneous equations at each time step. FLAC3D solves these equations by using the Jacobi method, which, in turn, converges only for time steps below a certain value (Itasca Consulting Group, n.d.-a).

Itasca Consulting Group (n.d.-a) provides some recommendations for choosing between the explicit and implicit methods. For instance, the explicit method tends to be used at the beginning of the simulation or when the model is perturbed, while the implicit method is rather used for the more stable period of the simulation. Regarding computational effort and efficiency, they also give some hints: the implicit method requires more memory and at least three iterations per time step, each of which takes a similar calculation effort as the explicit method for one time step. However, it may be possible to use a much larger time step with the implicit method or it may have higher accuracy for the same time step. It is also highlighted that the critical time steps for coupled mechanical or hydraulic simulations may differ from the one in Equation (4.16).

5. Establishment of the accuracy and limits of numerical methods for thermal calculations with phase change

It is well known that numerical schemes must be verified (Causon and Mingham, 2010). As explained in chapter 3, comparing the results of a numerical program against the exact analytical solution of the PDE is a typical way of checking the accuracy and correctness of the numerical method. This has been done for Stefan problems in several papers, see e.g. Karabenli et al. (2016), Vitel et al. (2016), Alekseev et al. (2018) and FROST 3D (2018). The absolute error of a magnitude obtained from the numerical model can then be defined as the magnitude of that result minus the corresponding exact result obtained from the exact analytical solution.

The usual procedure in engineering practice when utilizing numerical programs is to check that the results are plausible, but a detailed, systematic sensitivity analysis is seldom performed during the course of engineering projects due to time constraints. On the other side, sensitivity studies have been performed in the framework of research regarding the effect of soil properties and freeze pipe positioning, e.g. in Ziegler et al. (2010), Schüller (2015) and Hu et al. (2016a). Parametric studies considering the freeze system geometry, the properties of the coolant or its flow rate can be found in Vitel et al. (2015). However, there is a scarcity of published comprehensive sensitivity studies and systematic calibration checks on the numerical parameters themselves (as an exception to this, Tounsi et al. (2019) performed some sensitivity analyses for different meshes and punctual and surface source types).

When modelling a ground freezing process in a real project, the design is often performed without all the required parameters being available and sometimes based on data of uncertain quality. Consequently, the design engineer must necessarily use engineering judgement to make reasonable assumptions on the missing or uncertain parameters. These assumptions are additional causes of potential inaccuracies, so it is not easy to check the accuracy of the numerical model itself during the design stage. Putting up experiments to check numerical models is also challenging, as it requires significant resources. Indeed, most of the experiments done in this regard are limited in dimensions (usually no larger than 1 m) and duration (a few days at the most), see e.g. Ständer (1967), Scheerlinck et al. (1997) or Sres (2009). Moreover, discrepancies between the experimental results and the numerical simulations may arise from various sources, like for instance inaccuracies in the estimation of the seepage velocity, the initial ground temperature or the thermal parameters of the ground, e.g. in Pimentel et al. (2011). While these sources of error, whose nature is external to the model, may be the causes of some part of the errors in the results, the accuracy of the numerical model itself should also be reviewed. To this extent, comparing the numerical results with the ones of exact analytical solutions seems to be a suitable path to take.

Therefore, the main objectives of this chapter are checking the accuracy of the model without external error sources, evaluating its sensitivity to the numerical parameters and

investigating its accuracy limits. Numerical models with different parameters and conditions (mesh size, time steps, type of source, type of elements, model size, solving algorithm, etc.) will be run to find out under which conditions the numerical solution is correct, sufficiently precise and stable for freezing problems (such sensitivity analyses have also been used e.g. in Ayasoufi (2004) for time step optimisation). Exact analytical solutions known for "simple" problems (mainly Neumann's solution for the one-dimensional problem) will be used in order to check the sensitivity and accuracy of the numerical model. This approach has already been applied e.g. in Baier (2008) and Alekseev et al. (2018). Several verifications will be performed with different initial and boundary conditions. The main ground thermal parameters which affect the conductive freezing process (latent heat of fusion, specific heat capacity and thermal conductivity) according to Jumikis (1966) (from Johansson (2009)) will also be varied in the different models. Further studies have been done to assess the influence of the numerical parameters on the computing time of the models, the numerical predictions for power consumption, the comparison with the exact solution from Carslaw and Jaeger (1959) and the applicability of the numerical code to a large-scale engineering model. In this thesis, only the freezing case was evaluated, as FLAC3D does not admit negative values of specific heat, which would be required to model the thawing case with the apparent heat capacity method. An overview of the verifications performed and the numerical parameters considered, along with some additional studies, is presented in Table 5.1.

Table 5.1: Numerical parameters and physical properties for the sensitivity analyses and additional studies

Numerical parameter	**Chapter**	**Range of values**
Model boundaries	5.2	5 – 50 m length
Mesh Size	5.3, 5.9, 5.10	1 – 400 cm
Time step	5.4, 5.9, 5.10	1 – 12,800 s
Frequency of execution of "freeze code"	5.5, 5.9, 5.10	1 – 3.2 x 10^6 s
Abrupt / Gradual phase change modelling	5.8	0.1 – 4ºC
Structured / unstructured mesh	5.12	Structured & unstructured meshes
Type of elements	5.12	Triangular & rectangular prisms
Punctual / surface source	5.16	Source radius 0.1 – 10^6 cm
Explicit / Implicit algorithm	5.11	Explicit & implicit
Physical property	**Chapter**	**Range of values**
Thermal properties	5.3, 5.8	water & soil properties
Initial temperature gradient	5.6, 5.8	10, 55 & 250 ºC
Stefan number (latent heat)	5.7	0, 79.71, 797.1 cal/g

Additional studies	**Chapter**	-
Predictions for power consumption	5.13	-
Effects of numerical parameters on computing time	5.14	-
Comparison with the solution from Carslaw and Jaeger (1959)	5.15	-
Applicability to a large-scale engineering model	5.17	-

5.1. Bases of the numerical sensitivity analyses in FLAC3D

The numerical code programmed by the author in FLAC3D is based on the enthalpy method (specifically on the apparent heat capacity variant of the method), because of its flexibility and programmability, as described in chapter 4.3.2.1. The code consists of several blocks. The first one defines the geometry of the model (size, length, width, shape, etc.) and creates the mesh. For the verification of the code, a relatively simple geometry needs to be used for which an exact analytical solution is available. The semi-infinite slab was chosen, for which the Neumann solution exists, so that the accuracy of the simulations could be checked against this exact analytical solution. This exact solution has been contrasted against real data for example in Takashi et al. (1979). The geometry of the model for the 1 cm mesh is shown in Figure 5.1. The width and height of the model can be selected arbitrarily, due to the symmetry of the Neumann problem and to the fact that the boundaries of the model are adiabatic. Both dimensions were chosen to be 100 cm. Based on the results of the analytical solution for a thermal time of 10 days, it was concluded that a 500 cm long model would be sufficiently long to prevent the boundary from having a significant effect on the calculations. Additionally, it was hypothesized that using a larger mesh in the zones further away from the origin (x=0, where the thermal source or “cold plane” is located), would not have a significant effect on the results, but would expedite the computing time significantly. These two hypotheses are confirmed based on numerical experiments in chapter 5.2. For most of the models, a thermal time of 10 or 365 days was selected for the simulation.

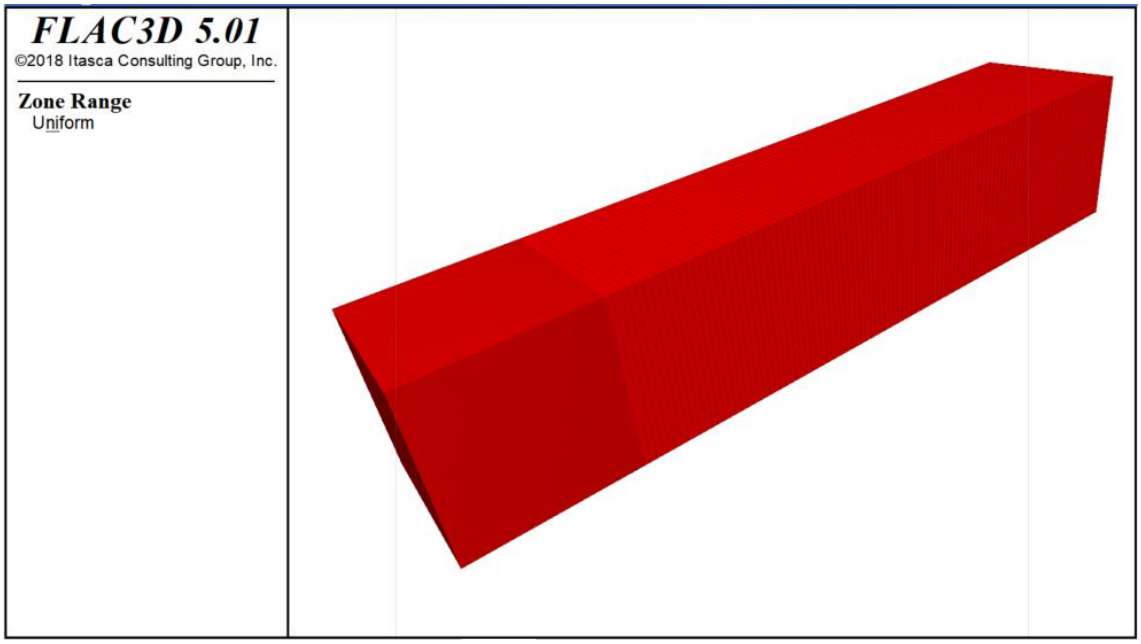

Figure 5.1: Geometry of the semi-infinite slab used in FLAC3D (with 1 cm mesh in the area near the source, left side)

In the second block of the code, the material properties (density, specific heat capacity, thermal conductivity, latent heat, etc.) are determined. For the analysed Problems 1 to 4, which are defined below, the properties of water and ice listed in Table 5.2 were used:

Table 5.2: Thermal properties of water and ice used in Problems 1 to 4

Thermal property	Value
Specific heat capacity (unfrozen)	1 cal/g/ºC
Specific heat capacity (frozen)	0.501 cal/g/ºC
Thermal conductivity (unfrozen)	0.00144 cal/(s cm ºC)
Thermal conductivity (frozen)	0.0053 cal/(s cm ºC)
Latent heat	79.71 cal/g
Phase-change temperature	0ºC
Phase change range	0 to -0.1ºC (range of 0.1ºC, simulating an abrupt phase change)

As FLAC3D does not include an integrated phase-change simulation tool, the user needs to program a customised routine in order to simulate the effects of the phase change process (see Itasca Consulting Group (n.d.-d) or Zhu and Michalowski (2005) for an example of such a routine for mechanical calculations). In this case, the apparent heat capacity method was implemented in the routine due to its flexibility. Thus, the next block of code (the "freeze block") defines how the effects of the phase change are modelled. This block is regularly called by the program every certain number of time steps, which can be determined by the user. In principle, the program is instructed to go through every zone in the model and check if its temperature is above or below the previously defined phase-change temperature. In the case that the temperature in the zone is below the phase-change temperature, the program checks whether the zone is already in the status

"freezing" (i.e. it has already started changing phase) or not. If it is not yet in the "freezing" status, the zone's thermal parameters (specific heat capacity and thermal conductivity) are changed from the unfrozen properties to the "freezing" properties. The thermal conductivity is set to the average of the frozen and unfrozen thermal conductivities. With respect to the heat capacity, based on the apparent heat capacity method, the effect of the latent heat is taken into account by adding the latent heat divided by the phase change range to the average specific heat capacity. The numerical simulations are effectively being performed considering this apparent heat capacity in the zones which are in the status "freezing". When the zone is already in this status, the amount of latent heat introduced via the increase of the specific heat capacity is added up in every iteration, stored in a variable and controlled until it reaches the total latent heat to be introduced for the zone considered. Once that happens, the status of the zone is changed by the program to "already frozen", and the thermal properties (specific heat capacity and thermal conductivity) are updated to the frozen properties. The different statuses of the zones are illustrated by the model in Figure 5.2.

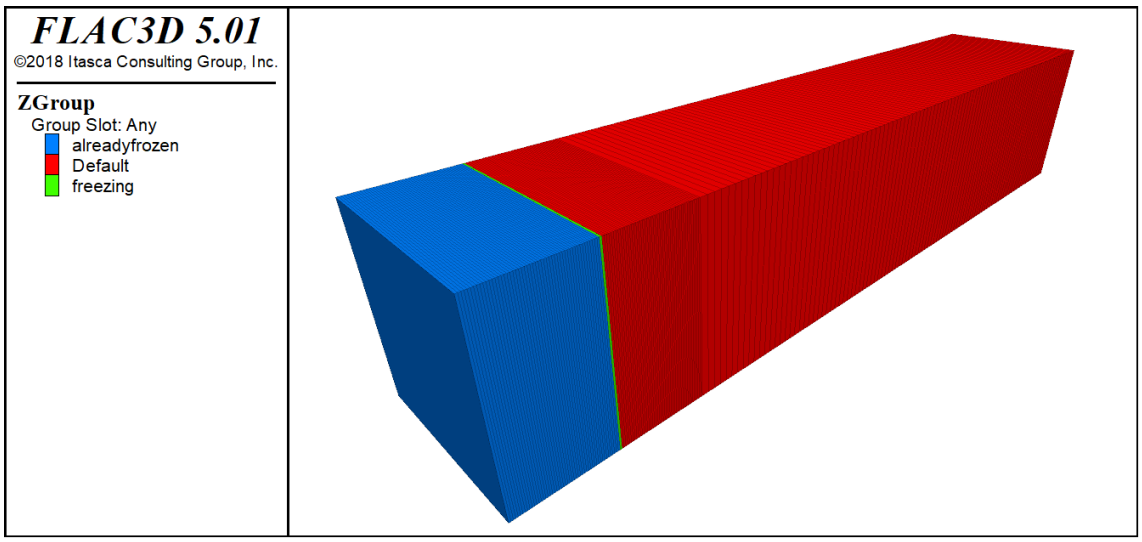

Figure 5.2: Model with already frozen, freezing and unfrozen zones (unfrozen zones shown as "default")

The subsequent code blocks are mainly used for the interpretation of the results of the model. They create the required tables and graphs and import the results from the exact analytical calculations previously performed with Maple 2018, a widely used symbolic and numeric mathematics software. Finally, a block containing the "solve" command is included in the code, which is called to start the numerical simulation.

Six thermal Problems with different boundary conditions were analysed:

- Problem 1: This problem was taken as the base case. The boundary conditions were assumed in the range of the typical temperatures for the artificial ground freezing process with brine. Thus, the model starts at a uniform temperature of +20ºC (which can be considered to be inside the range of typical ground temperatures) and the "cold boundary" is at a constant temperature of -35ºC (typical brine temperature, e.g. when using a calcium chloride brine, see chapter 2.2). Sensitivity analyses

regarding the mesh size, time step and period of execution of the "freeze block" are performed in chapters 5.3, 5.4 and 5.5, respectively.

- Problem 2: A second, more extreme case, was chosen applying a high ground temperature of 50ºC, which may occur at high depths of several hundreds or thousands of meters below ground. Furthermore, the temperature of the "cold boundary" was chosen to be -200ºC, which can be considered representative for nitrogen freezing (see chapter 2.2). The aim of this problem is to check the sensitivity of the model against the initial temperature difference, which in this case is 250/55=4.54 times larger than in the previous model. It may be suspected that such a large thermal gradient may produce numerical instabilities in the model and reduce its accuracy. This Problem is studied in chapter 5.6.
- Problem 3: A third case with the same temperatures as in Problem 2 and with an extreme latent heat 10 times higher than water was simulated in chapter 5.7 in order to check the model's sensitivity to the amount of latent heat. This extremely high latent heat may also be suspected to produce instabilities.
- Problem 4: A model without phase change (linear model) was evaluated in chapter 5.7 in order to isolate the errors that the numerical model already produces without any phase change from the additional errors caused by the simulation of the phase change. Naturally, lower errors are expected in this model.
- Problem 5: The thermal characteristics in Table 5.3 and a small maximum temperature gradient (source temperature of -6ºC, initial temperature of 4ºC) are assumed for this Problem (see chapter 5.8). The other boundary conditions are the same as defined for Problem 1, including the phase-change range between 0ºC and -0.1ºC.
- Problem 6: This is a case based on Problem 5, with a more gradual phase change (gradual phase change over a range of 4ºC, between 0ºC and -4ºC). This Problem is used to check the effect of the abruptness or graduality of the phase change. This model should give more accurate results than the model with abrupt phase-change, as the abruptness may create numerical instabilities and it therefore usually negatively affects the accuracy of numerical models. The material properties considered for Problems 5 and 6 are the ones listed in Table 5.3:

Table 5.3: Thermal properties used in Problems 5 and 6

Thermal property	Value
Specific heat capacity (unfrozen)	0.165 cal/g/ºC
Specific heat capacity (freezing/mushy region)	0.165 cal/g/ºC
Specific heat capacity (frozen)	0.165 cal/g/ºC
Thermal conductivity (unfrozen)	0.00578 cal/(s cm ºC)
Thermal conductivity (freezing/mushy region)	0.00703 cal/(s cm ºC)
Thermal conductivity (frozen)	0.00828 cal/(s cm ºC)
Water content	20%

Residual unfrozen water content	7.82%
Latent heat of water	79.71 cal/g
Phase-change temperature	0ºC
Phase change range	0 to -0.1ºC (abrupt phase change) – Problem 5 0 to -4ºC (gradual phase change) – Problem 6

Several models with different numerical parameters were simulated for these six problems. In order to keep track of the different models and parameters evaluated, the following naming convention was developed. From this point on, the models are named in the thesis following this convention:

Naming convention for numerical models:

MH*a*-TS*b*-UF*c*-TE*d*-SO*e*-SC*f*-ST*g*-TP*h*-AG*i*-*j*_*k*

The meanings of the variables (the lower-case letters in italics) are as follows:

- MH*a*: variable *a* is the mesh size, in cm.
- TS*b*: variable *b* is the time step, in seconds.
- UF*c*: variable *c* is the update period (every how many time steps) with which the "freeze block" routine is executed.
- TE*d*: variable *d* is the type of elements ("h" for rectangular prisms and "t" for triangular prisms).
- SO*e*: variable *e* stands for the source type ("s" for surface, "p" for punctual).
- SC*f*: variable *f* is the type of phase change ("a" for abrupt, "g" for gradual).
- ST*g*: variable *g* represents the presence or not of phase change ("p" for problems with phase change, "n" for problems without phase change).
- TP*h*: variable *h* is the maximum temperature difference (initial temperature of the ground minus temperature of the "cold boundary").
- AG*i*: variable *i* stands for the solving algorithm, ("E" for explicit, "I" for implicit).
- *j*: variable *j* represents the geometry of the model ("NE" for Neumann, "CY" for single freeze pipe, "fw" for freeze wall and "fc" for freeze circle).
- *k*: variable *k* is used for additional parameters changed in the models, e.g. larger models, models with a longer computed thermal time or models without any latent heat (shown as LHT=0).

An example of a model name following this convention is presented below:

MH1-TS1-UF1-TEh-SOs-SCa-STp-TP250-AGE-NE_LHT=0

In order to compare the accuracies of the different models studied, the following data sets, among others, were retrieved from the models, tabulated and plotted into graphs:

- Temperature versus time graph for the point at x=2 cm: T(2,t) for t=0 to 10 days
- Temperature versus time graph for the point at x=10 cm: T(10,t) for t=0 to 10 days
- Temperature versus time graph for the point at x=25 cm: T(25,t) for t=0 to 10 days

- Temperature versus time graph for the point at x=60 cm: T(60,t) for t=0 to 10 days
- Position of the freeze front versus time: X(t) for t=0 to 10 days
- Temperature versus distance graph for t =10 days = 864,000 s: T(x,864'000) for x=0 to 500 cm

In addition to analysing the accuracy of the model, it is imperative to evaluate the computing time, as the available time for design and simulations is usually limited in engineering projects. In order to provide a reliable comparable standard of the computing times cited in this thesis, a benchmark data file, *"timing-test-simple.f3dat"*, from chapter 7 of Itasca Consulting Group (n.d.-c), was run. The results obtained with the computers used in this thesis for the calculations are shown in Table 5.4 in italics, along with results for other benchmark computers provided by Itasca Consulting Group (n.d.-c). The numerical simulations with FLAC3D in this thesis were generally performed with the laptop Asus UX360UAK, with the exception of the ones in chapters 5.10 and 9.2.3, for which the computer Dell Precision 7530 was used.

Table 5.4:
Benchmark of computers and processors for FLAC3D calculations, based on Itasca Consulting Group (n.d.-c)

Computer	**Processor Name**	**Number of Processors**	**Cores**	**Threads**	**Operating System**	**Calculation speed (kzones / sec)**
ZT Affinity	Intel Pentium D	1	2	2	Win-7 64 SP1	170
HP ProBook 4530S	Intel Core i5-2410M	1	2	4	Win-7 64 SP1	680
DELL Optiplex 790	i7-2600	1	4	8	Win XP SP3	1450
Custom	Intel Xeon x5680	2	6	24	Win-Server 64 SP2	2121
Asus UX360UAK	*Intel Core i5-7200U*	*1*	*2*	*4*	*Windows 20 Home, V.1903*	*669.5*
Dell Precision 7530	*Intel(R) Xeon(R) E-2176M*	*1*	*6*	*12*	*Win-10 Enterprise*	*2332*

5.2. Preliminary model checks: boundary and far-field mesh size effects

Several preliminary model checks were performed in order to optimise the simulation time. First, it was confirmed that the numerical model, calculated using certain reference values of the numerical parameters (in this case a mesh size of 1 cm, a time step of 1 s, etc.) can be very accurate, generating errors of less than 1ºC for temperatures and 1 cm for the freeze front. It was also checked that a model with a length of 5 m instead of 50 m to simulate Problem 2 (which is the problem, of the six problems defined in the previous chapter, in which the freeze front advances the fastest) does not provide less accurate results for a thermal time of up to 10 days. Then, it was checked that a coarser mesh from a distance of 1 m of the cold source onwards would give results (for a model simulated until a thermal

time of 10 days) which do not significantly defer from the ones which would be obtained with a completely uniform mesh over the whole length of the model (see the average errors in Table 5.5). However, significant computing time would be saved by using the first mesh.

To this extent, three models were compared and the hypotheses confirmed. This can be appreciated in Figure 5.3, Figure 5.4 and Table 5.5. Figure 5.5 shows in more detail that the additional error because of these simplifications (boundary effect of the boundary at x=500 cm) is reduced and very localized in the area near the phase-change front. The relative error is small, considering that the initial gradient in these models was 250ºC. The absolute error of about 5ºC of the mesh with a larger mesh size from 100 cm onwards shown in Figure 5.5 is due to the phase-change interface having already reached the model area with a coarser mesh. Taking care of avoiding that the phase-change interface reaches the coarser mesh in the next chapters, this approach with a graded mesh and a reduced model length will be used.

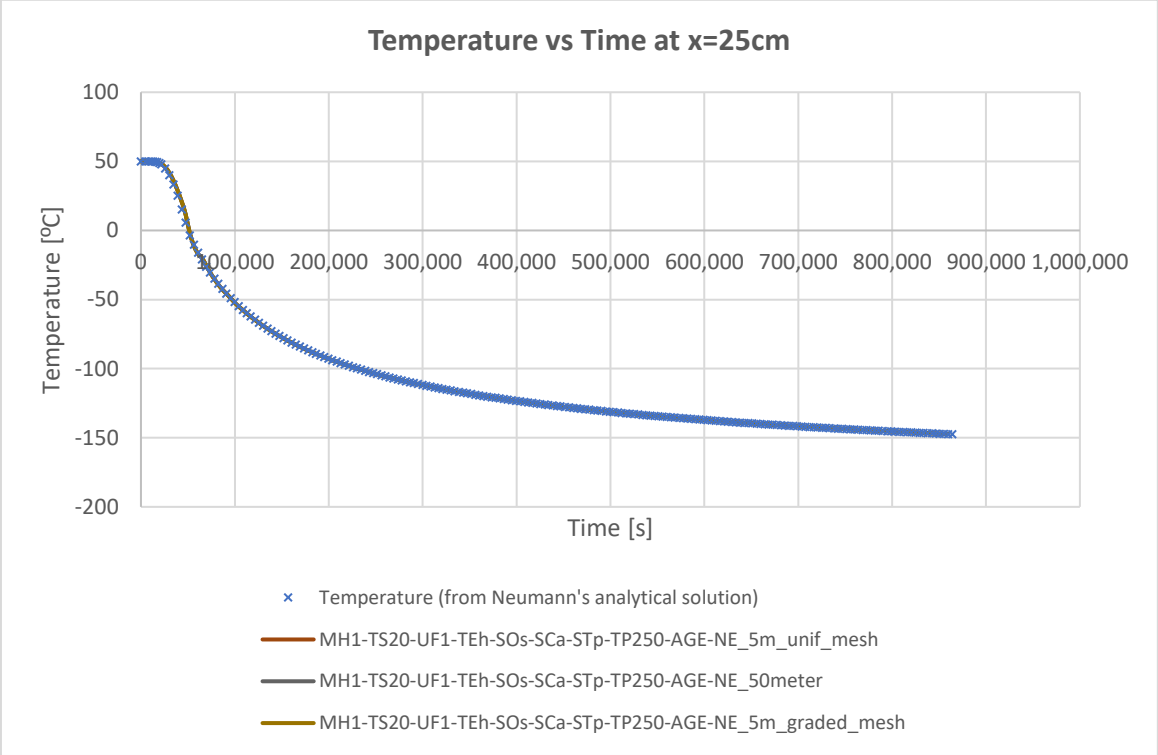

Figure 5.3: Temperature vs time at x=25cm, preliminary model checks, Problem 2

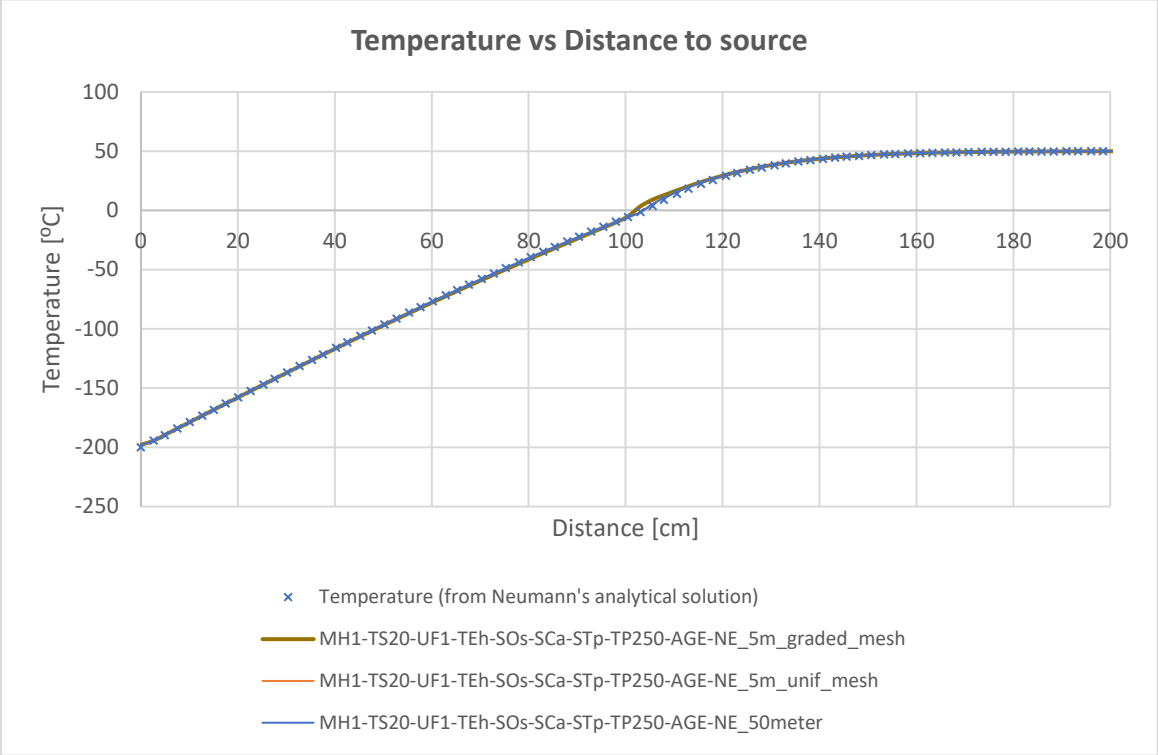

Figure 5.4: Temperature vs distance to source at t=10 days, preliminary model checks, Problem 2

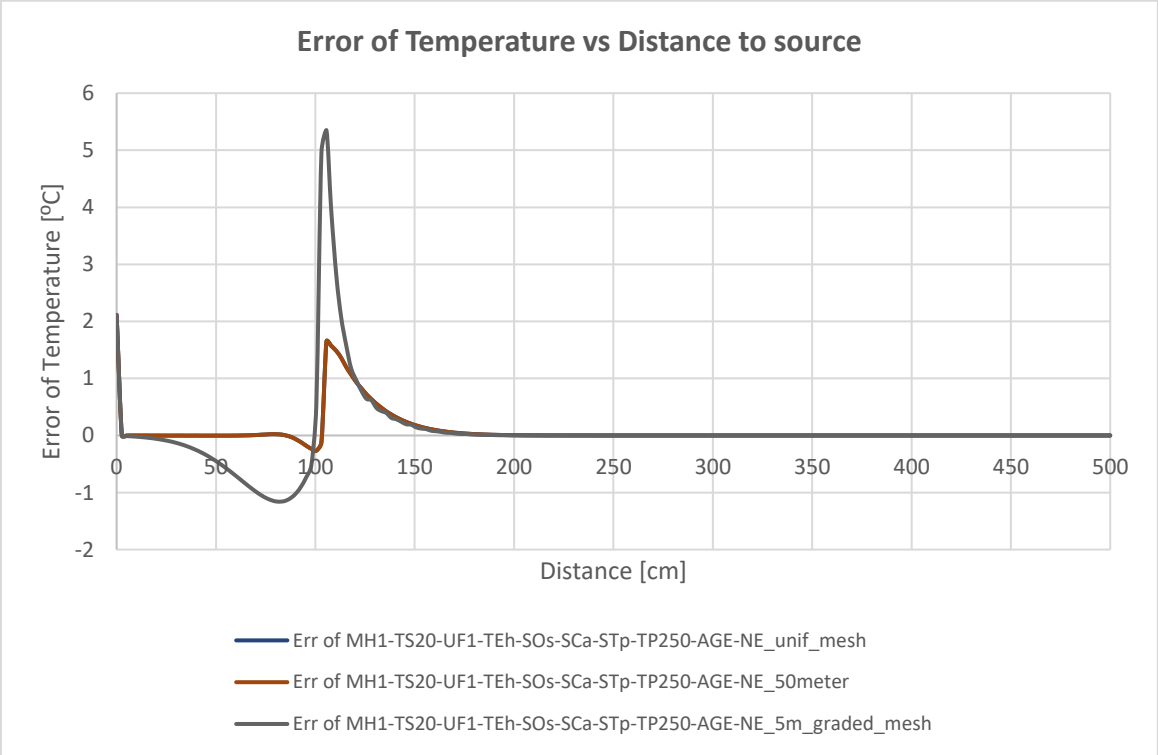

Figure 5.5: Error of temperature vs distance to source at t=10 days, preliminary model checks, Problem 2
Note: both models with uniform meshes yield nearly the same results, so their graphs overlap.

Table 5.5: Average of absolute values of errors, preliminary model checks, Problem 2

Average of absolute values of errors / Computing time	Units	Average absolute error of MH1-TS20-UF1-TEh-SOs-SCa-STp-TP250-AGE-NE_5m_unif_mesh (5 m total length)	Average absolute error of MH1-TS20-UF1-TEh-SOs-SCa-STp-TP250-AGE-NE_50meter	Average absolute error of MH1-TS20-UF1-TEh-SOs-SCa-STp-TP250-AGE-NE_5m_graded_mesh (broadening mesh after 1 m, 5 m total length)
T(10 cm, t)	[ºC]	0.17	0.17	0.17
T(25 cm, t)	[ºC]	0.88	0.88	0.88
T(60 cm, t)	[ºC]	0.39	0.39	0.41
X(t)	[cm]	0.57	0.57	0.61
T(x, 10 days)	[ºC]	0.09	0.09	0.25
Computing time	[s]	0:03:31	0:33:56	0:01:13

5.3. Mesh-size sensitivity analysis

As already explained in the previous chapters, the mesh size may have a significant effect on the accuracy of the results. To test this hypothesis, six models with different mesh sizes of 1, 2, 5, 10, 25 and 50 cm in the near field of the cold source (100 cm) were run for Problem 1. The time step was fixed at 1 s and the freeze routine was executed every time step.

The model MH1-TS1-UF1-TEh-SOs-SCa-STp-TP55-AGE-NE, which has the smallest mesh size of 1 cm and should therefore be the most accurate of the evaluated models, has been taken as a basis to compare the others to. A typical view of the temperature in the model after 10 days is presented in Figure 5.6.

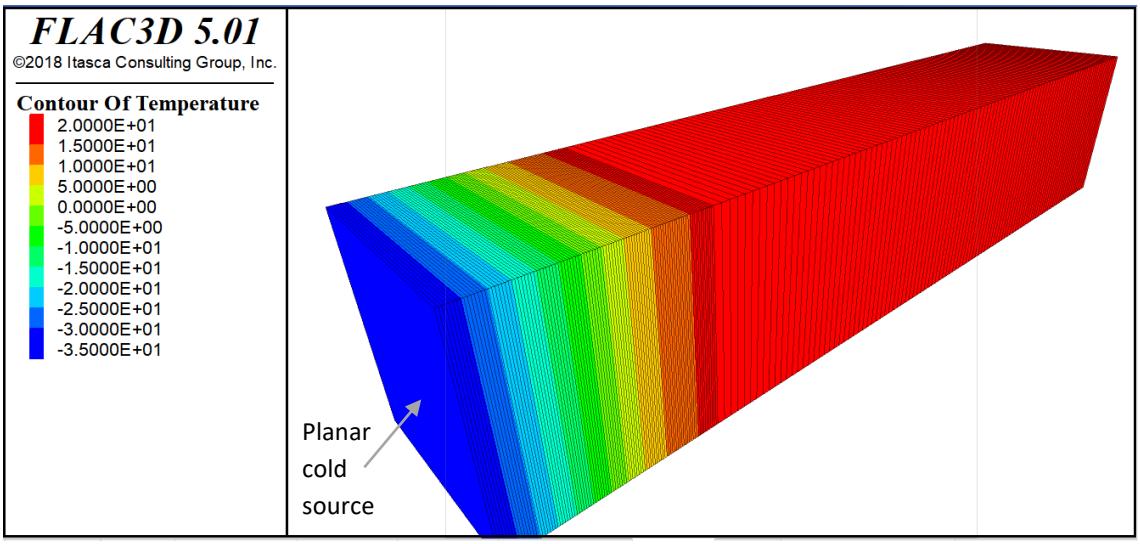

Figure 5.6: Isometric view of temperature contour in the model

Figure 5.7 shows the temperature history in the point of study which is nearest to the source (2 cm away). It can be appreciated that the models with mesh sizes of 1 and 2 cm deliver reasonably accurate results. The 5 cm-mesh provides somewhat unstable results until about $1x10^5$ seconds (roughly above 1 day), but its accuracy improves afterwards (see Figure 5.8). The other three models with coarser meshes generate graphs with very marked "numerical steps", which is typical of the enthalpy method (see chapter 4.3.2.1 and Furzeland (1980), Voller and Cross (1981), Basu and Date (1988) and Mackenzie and Robertson (2000)). For instance, in the model with a mesh size of 25 cm, the maximum errors appear after about 3 days of thermal time and amount to approximately 12 cm for the position of the freeze front (see Figure 5.11 and Figure 5.12) and 25ºC for the temperature at the point 25 cm away from the thermal source (see Figure 5.9 and Figure 5.10).

On the long term, the models tend to stabilize, and the errors tend to decrease after a certain time. Accordingly, the timeframe of interest to the designer and the duration of the project (several weeks, months or years) have to be weighed in when deciding which mesh size to choose. For instance, if long timeframes are of interest, coarser meshes may deliver results which are accurate enough. The stabilisation of the errors with increasing thermal time can be seen in Figure 5.8, Figure 5.10 and Figure 5.12. Indeed, the largest errors tend to occur near the position of the freeze front. The errors at a certain point in the model increase at the beginning of the freezing process as the phase change interface approaches that point, then they reach the maximum when the interface is approximately at that point and finally, they decrease and the numerical results tend to converge with the exact solution. This can be clearly appreciated in Figure 5.10 (the largest errors at a distance of 25 cm from the front occur at $t \approx 3\ days$, which is the time when the freeze front is at $x \approx 25\ cm$) and Figure 5.13 (the largest errors occur at $x \approx 50\ cm$, the position where the freeze front is at $t = 10\ days$). This effect is also apparent in the results from Alekseev et al. (2018).

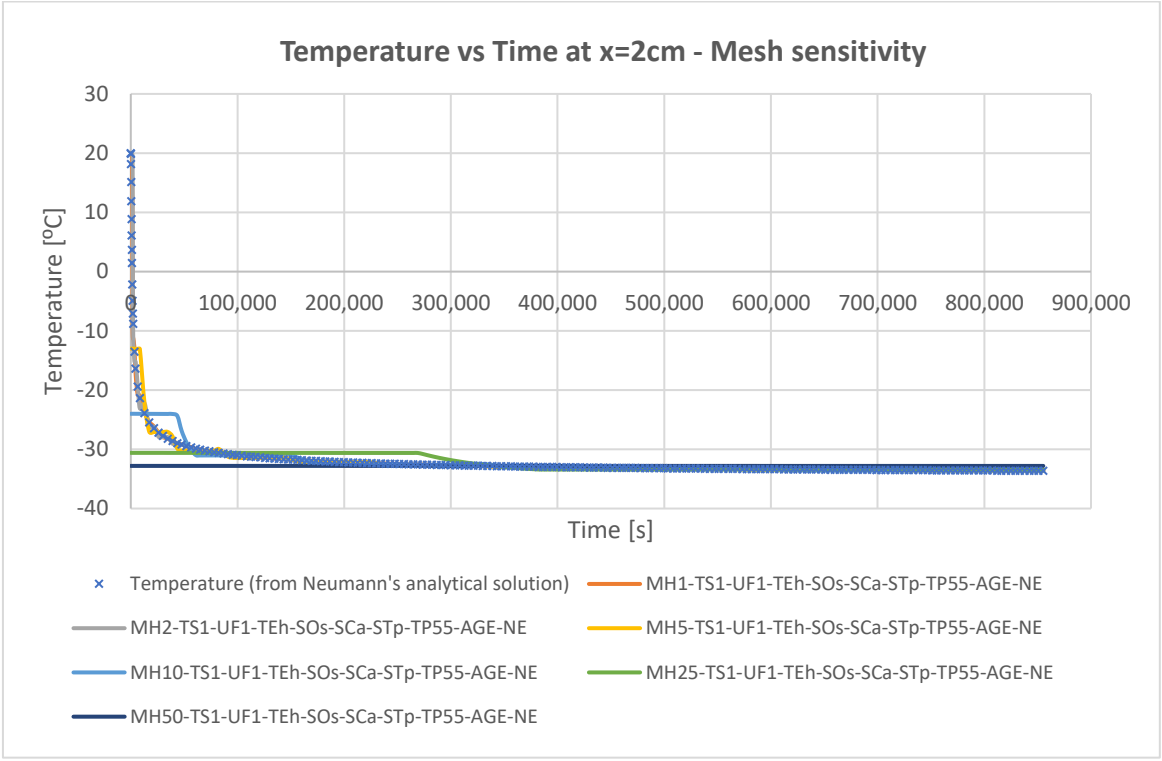

Figure 5.7: Temperature vs time at x=2cm, mesh sensitivity for Problem 1

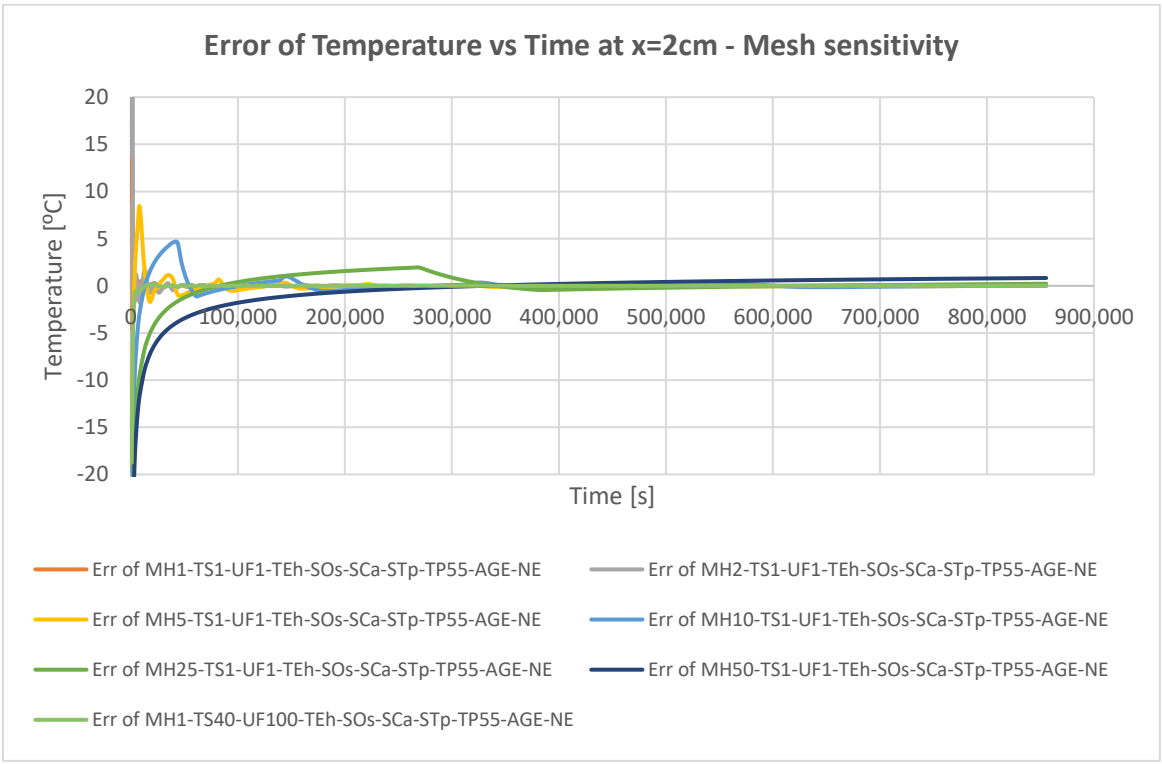

Figure 5.8: Error of temperature vs time at x=2cm, mesh sensitivity for Problem 1

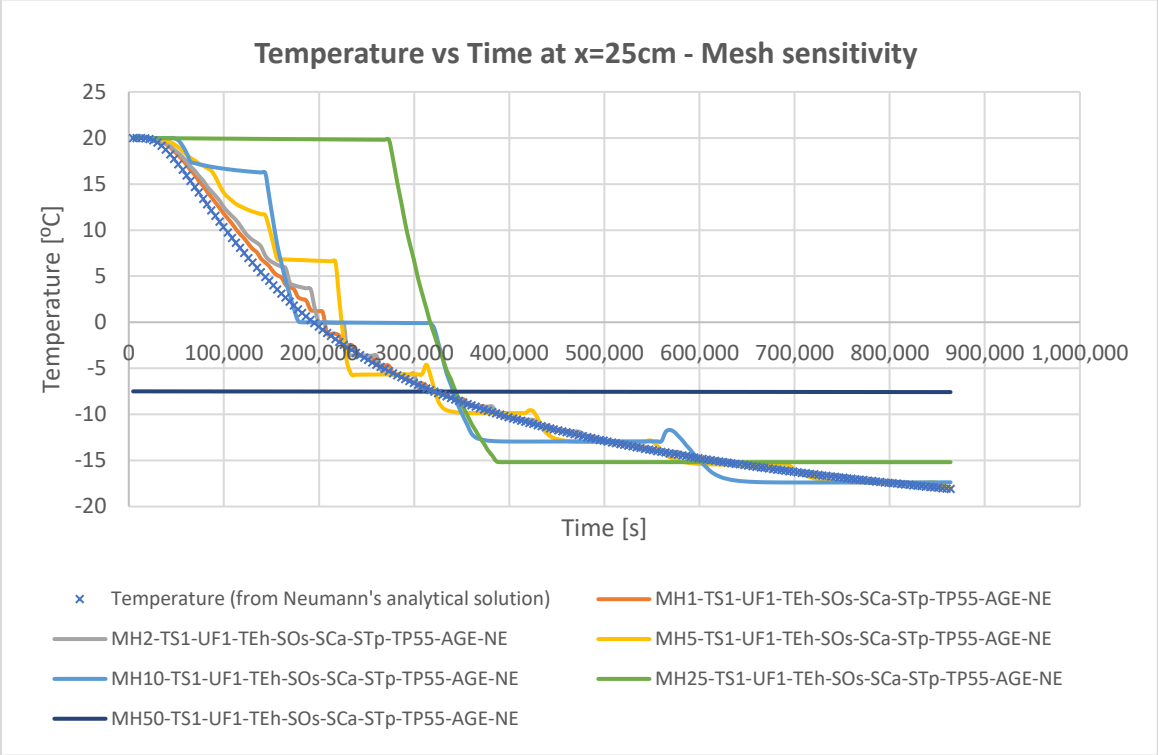

Figure 5.9: Temperature vs time at x=25cm, mesh sensitivity for Problem 1

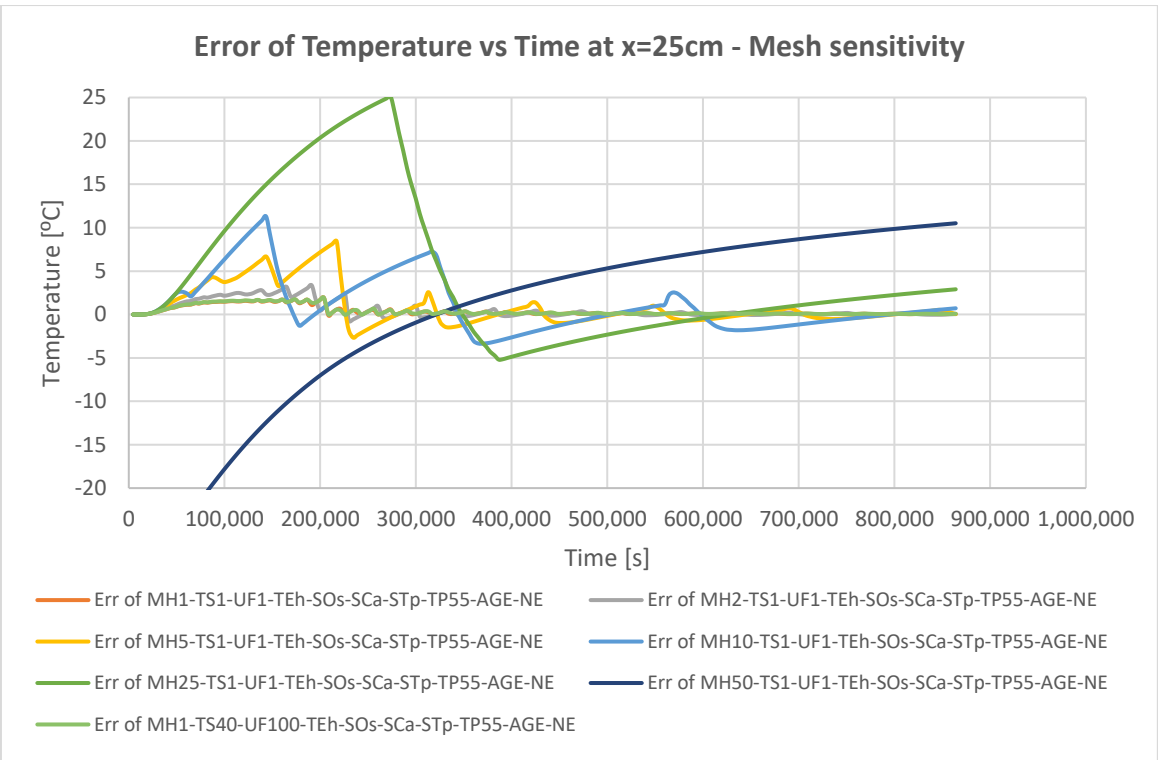

Figure 5.10: Error of temperature vs time at x=25cm, mesh sensitivity for Problem 1

A result of practical importance is the position of the freeze front. It can be appreciated in Figure 5.11 that, similarly to the other graphs, the only two models which approximate the

analytical curve consistently with very high accuracy are the 1 cm and 2 cm mesh models. It is also interesting to notice that the majority of the models underestimate the advance of the phase-change front most of the time (see Figure 5.11 and Figure 5.12).

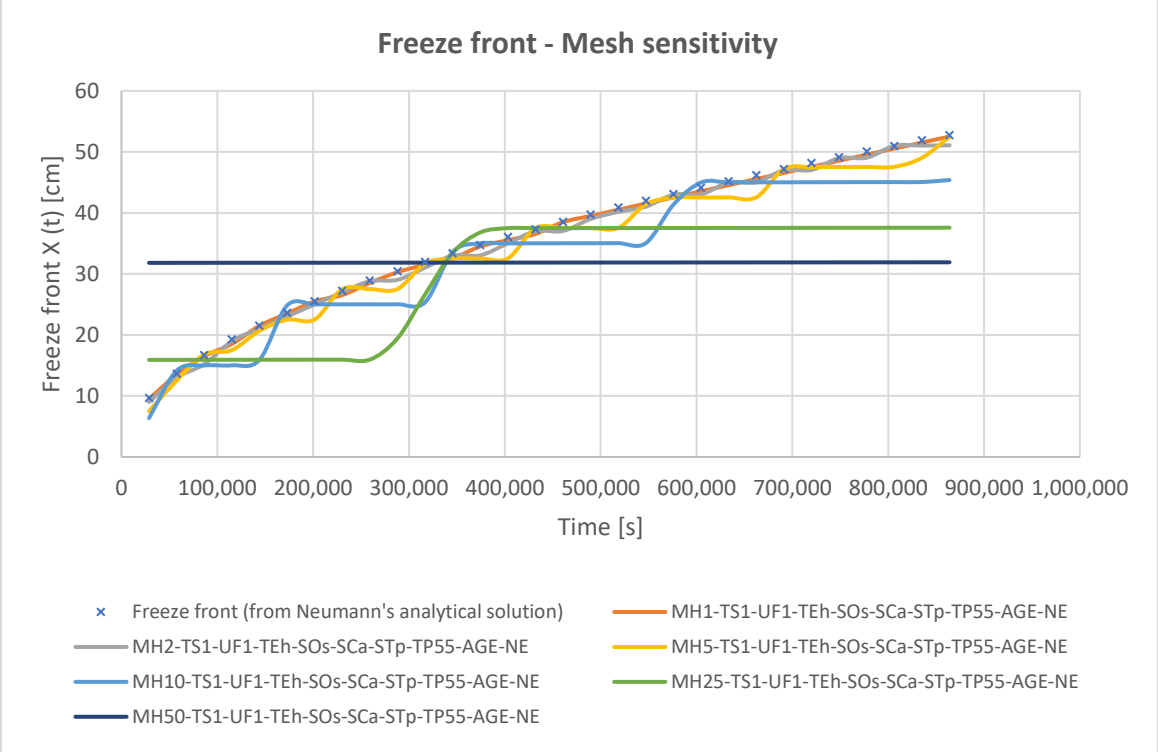

Figure 5.11: Freeze front, mesh sensitivity for Problem 1

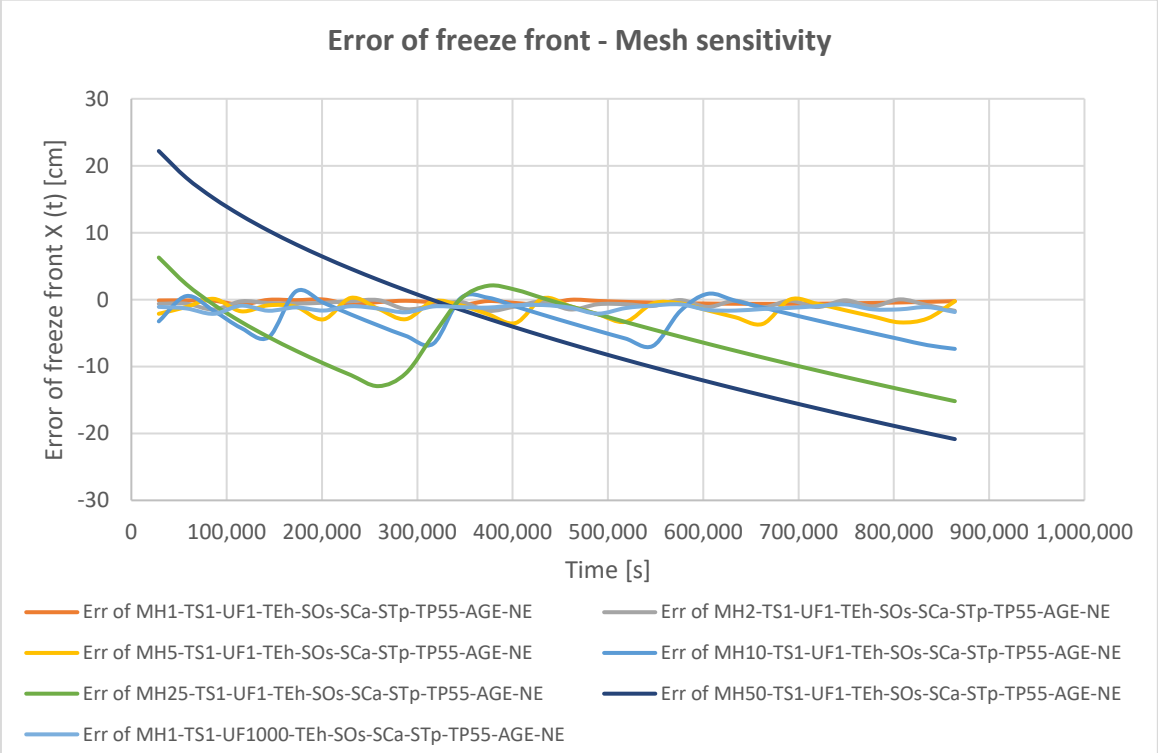

Figure 5.12: Error of freeze front, mesh sensitivity for Problem 1

In the temperature versus space graph (Figure 5.13), the numerical oscillations are not visible (in any of the models). Again, the 1 cm and 2 cm-mesh models appear to have a very high accuracy.

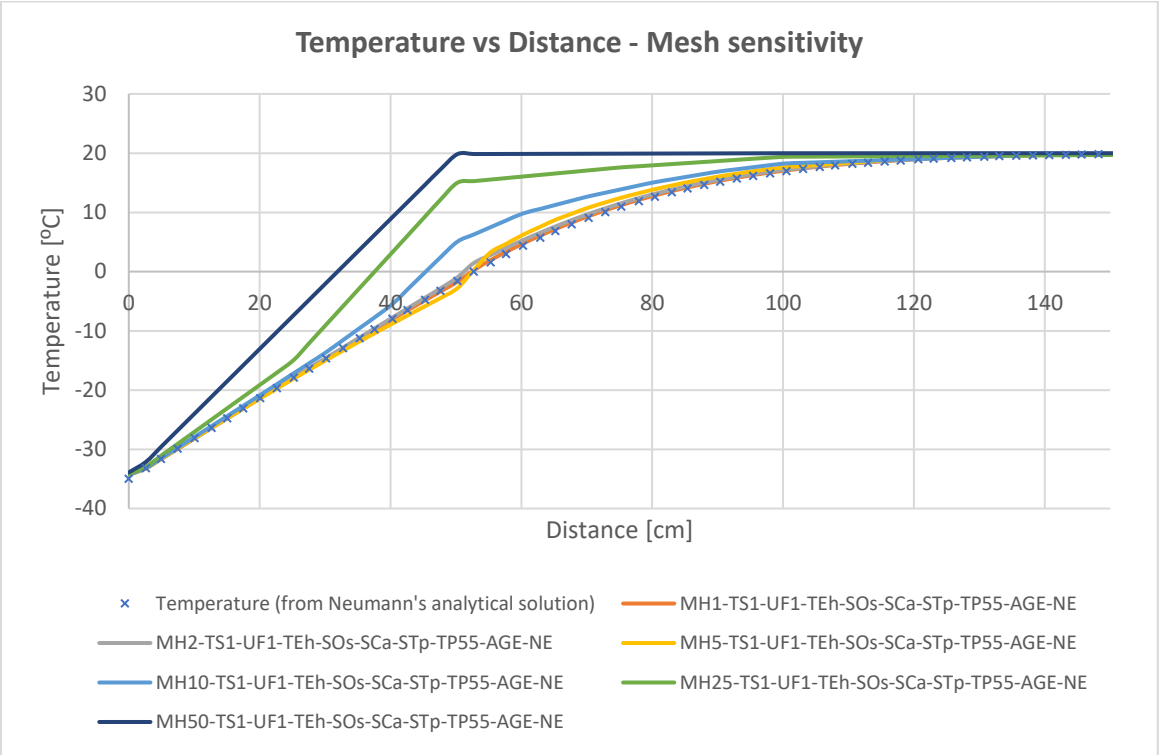

Figure 5.13: Temperature vs distance, t=10 days, mesh sensitivity for Problem 1

A quantitative overview of the average of the absolute values of errors for this Problem 1 is given by Table 5.6. The average of the absolute values of the errors (the absolute value was taken to avoid compensating positive and negative errors) was calculated over the thermal time computed (in this case 10 days) or over the model length (in this case 500 cm). It should be noticed that the models with mesh sizes of 1 and 2 cm have average errors of less than 1 ºC, which is usually acceptable for practical applications. However, their computing times are quite high, even for a relatively small model as the one used. The models with the largest meshes produced errors several times larger, while reducing the required computing time also several times.

Table 5.6: Average of absolute values of errors, mesh sensitivity, Problem 1

Average of absolute values of errors / Computing time	**Units**	**MH1-TS1-UF1-TEh-SOs-SCa-STp-TP55-AGE-NE**	**MH2-TS1-UF1-TEh-SOs-SCa-STp-TP55-AGE-NE**	**MH5-TS1-UF1-TEh-SOs-SCa-STp-TP55-AGE-NE**	**MH10-TS1-UF1-TEh-SOs-SCa-STp-TP55-AGE-NE**	**MH25-TS1-UF1-TEh-SOs-SCa-STp-TP55-AGE-NE**	**MH50-TS1-UF1-TEh-SOs-SCa-STp-TP55-AGE-NE**
T(2 cm, t)	[ºC]	0.39	0.68	1.39	2.26	3.08	3.51
T(10 cm, t)	[ºC]	0.12	0.27	0.75	1.50	4.48	6.30
T(25 cm, t)	[ºC]	0.35	0.54	1.36	2.12	5.86	8.13
T(60 cm, t)	[ºC]	0.30	0.55	1.22	2.17	4.14	6.11
X(t)	[cm]	0.40	0.73	1.61	3.28	6.88	10.92
T(x, 10 days)	[ºC]	0.04	0.09	0.19	0.52	1.40	2.19
Computing time	[s]	0:29:27	0:16:24	0:08:25	0:05:27	0:03:43	0:03:16

Note: The smaller the average error the better the accuracy. Errors are highlighted in a colour scale from green (smallest) to red (largest).

5.4. Time-step sensitivity analysis

According to the literature (see chapters 4.4.1 and 4.4.1.2), the time step used to discretise the time may also have a very significant impact on the accuracy of the numerical model. In this chapter, models with time steps of 1, 5, 10, 20 and 40 seconds (and the smallest mesh of 1 cm used in the previous chapter) were run. The critical time step for the 1 cm mesh, i.e. the largest time step with which the explicit method is stable, is 45.365 seconds according to FLAC3D, and provides similar results to the 40-second time step. In general, all these models provide very accurate results, with significantly shorter computing times for the larger (though sub-critical) time steps. Equations (4.13) and (4.16) (with $m = 2$), yield a time step of 47.26 seconds for the frozen phase (which is the most restrictive one in terms of critical time step), a similar result to the critical time step of 45.365 seconds detected by FLAC3D.

Exemplarily, the evolution of the temperature at x=25 cm is presented in Figure 5.14. The high accuracy of all five models can be appreciated.

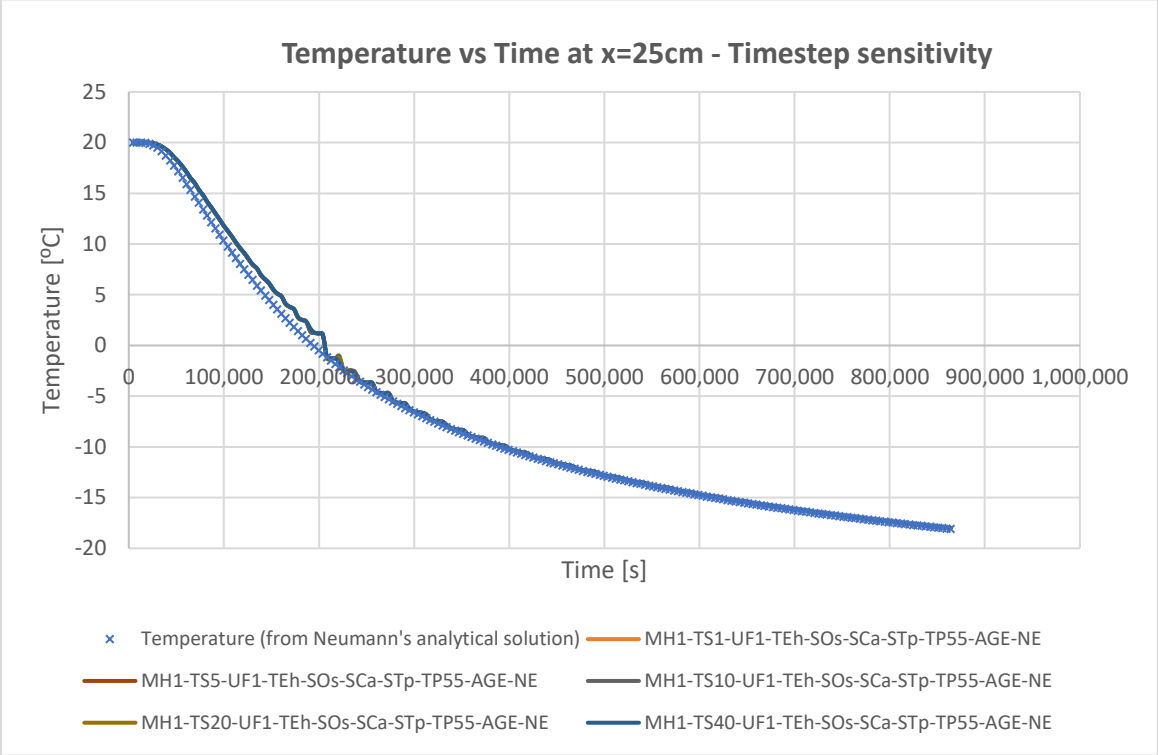

Figure 5.14: Temperature vs time at x=25cm, time-step sensitivity for Problem 1

As shown in Figure 5.15, the freeze front is also accurately calculated with any of these models.

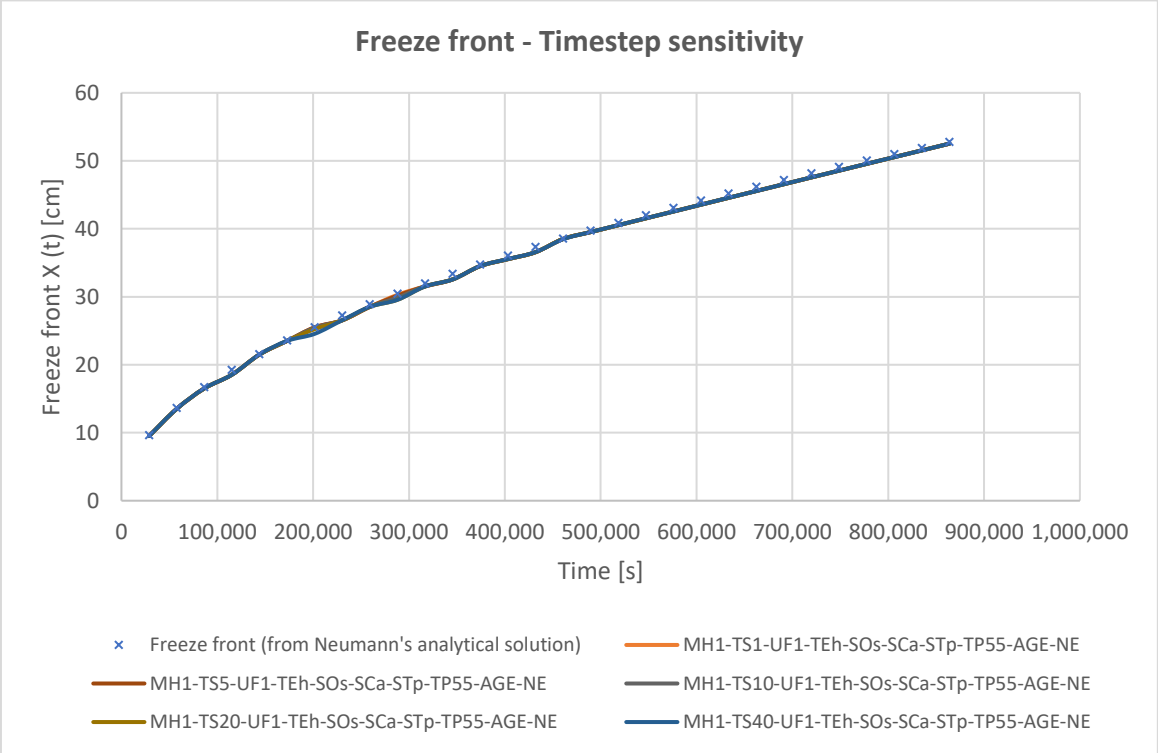

Figure 5.15: Freeze front, time-step sensitivity for Problem 1

The main conclusion which can be extracted from these results is that, for the 1 cm mesh, all the models which were run have a very high accuracy, contrarily to the differences in computing time between them, which are very significant. Consequently, the largest stable time step should be used, in order to spare computing time. This can be appreciated in Table 5.7 and Table 5.8.

Table 5.7: Average of absolute values of errors, time-step sensitivity with 1 cm mesh size, Problem 1

Average of absolute values of errors / Computing time	**Units**	**MH1-TS1-UF1-TEh-SOs-SCa-STp-TP55-AGE-NE**	**MH1-TS5-UF1-TEh-SOs-SCa-STp-TP55-AGE-NE**	**MH1-TS10-UF1-TEh-SOs-SCa-STp-TP55-AGE-NE**	**MH1-TS20-UF1-TEh-SOs-SCa-STp-TP55-AGE-NE**	**MH1-TS40-UF1-TEh-SOs-SCa-STp-TP55-AGE-NE**
T(2 cm, t)	[ºC]	0.39	0.35	0.35	0.38	1.03
T(10 cm, t)	[ºC]	0.12	0.12	0.11	0.11	0.12
T(25 cm, t)	[ºC]	0.35	0.35	0.36	0.37	0.37
T(60 cm, t)	[ºC]	0.30	0.30	0.31	0.31	0.31
X(t)	[cm]	0.40	0.40	0.41	0.43	0.45
T(x, 10 days)	[ºC]	0.04	0.04	0.04	0.04	0.04
Computing time	[s]	0:29:27	0:06:49	0:03:38	0:01:48	0:01:01

Table 5.8 presents the results of models with mesh sizes of 1, 5 and 10 cm, calculated for different time steps. It shows a very interesting effect: while the errors of the different models remain practically constant when increasing the time step for a certain mesh size, the computing time is reduced up to 97-98% for the larger time step compared to the smaller one.

Table 5.8: Average of absolute values of errors, time-step sensitivity with different mesh sizes, Problem 1

Average of absolute values of errors / Computing time	**Units**	**MH1-TS1-UF1-TEh-SOs-SCa-STp-TP55-AGE-NE**	**MH1-TS40-UF1-TEh-SOs-SCa-STp-TP55-AGE-NE**	**MH5-TS1-UF1-TEh-SOs-SCa-STp-TP55-AGE-NE**	**MH5-TS200-UF1-TEh-SOs-SCa-STp-TP55-AGE-NE**	**MH10-TS1-UF1-TEh-SOs-SCa-STp-TP55-AGE-NE**	**MH10-TS400-UF1-TEh-SOs-SCa-STp-TP55-AGE-NE**
T(2 cm, t)	[ºC]	0.39	1.03	1.39	1.51	2.26	2.02
T(10 cm, t)	[ºC]	0.12	0.12	0.75	0.78	1.50	1.36
T(25 cm, t)	[ºC]	0.35	0.37	1.36	1.38	2.12	2.10
T(60 cm, t)	[ºC]	0.30	0.31	1.22	1.24	2.17	2.18
X(t)	[cm]	0.40	0.45	1.61	1.73	3.28	3.30
T(x, 10 days)	[ºC]	0.04	0.04	0.19	0.19	0.52	0.54
Computing time	[s]	0:29:27	0:01:01	0:08:25	0:00:11	0:05:27	0:00:07

5.5. Sensitivity to the period of execution of the “freeze block”

The zone properties (unfrozen / freezing / already frozen) are only updated at certain intervals of time, when the “freeze block” of code is executed. The sensitivity of the model to this is evaluated in this chapter. To this aim, models with 1-second time steps were run in which the “freeze block” was executed every 1, 10, 100 and 1,000 steps. An additional model was executed with a 40-second time step and the execution of the “freeze block” every 100 steps (i.e. every 4,000 seconds). The accuracy of the results remains in a similar order of magnitude to the base case; however, the computing time is heavily reduced (see Table 5.9 and Table 5.10). The advance of the freeze front according to the different models is presented in Figure 5.16.

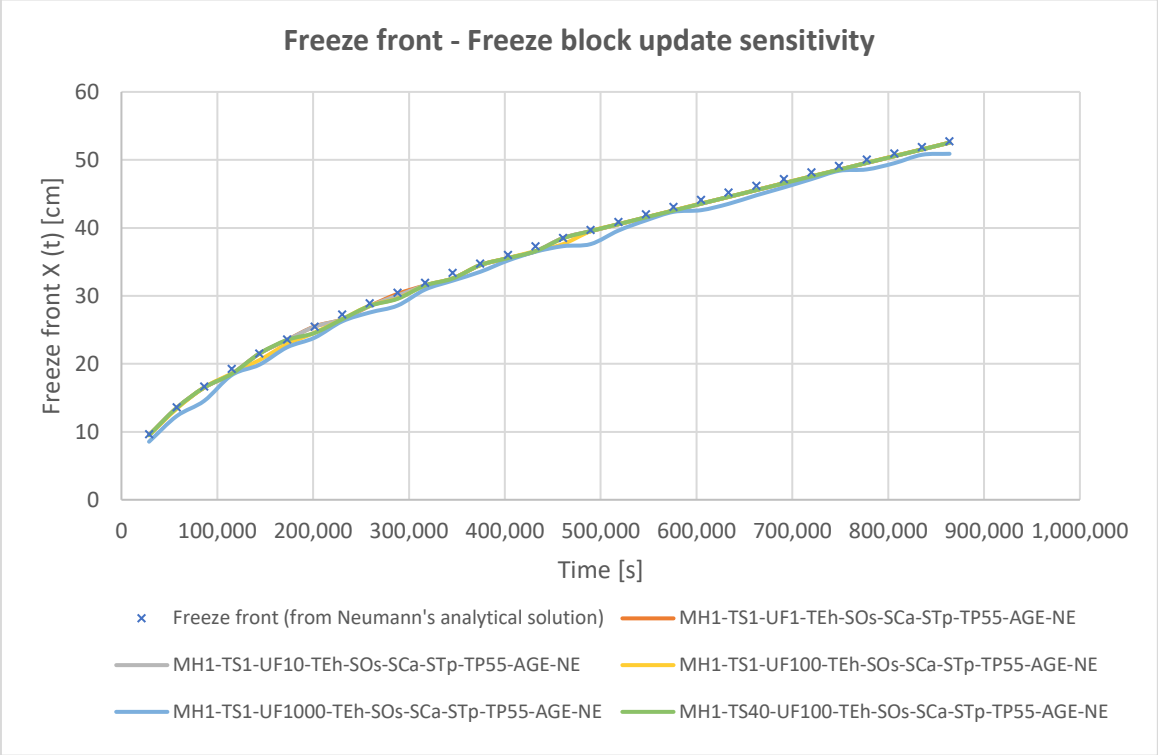

Figure 5.16: Freeze front, freeze block update sensitivity, Problem 1

Table 5.9: Average of absolute values of errors, freeze block update sensitivity, Problem 1

Average of absolute values of errors / Computing time	**Units**	**MH1-TS1-UF1-TEh-SOs-SCa-STp-TP55-AGE-NE**	**MH1-TS1-UF10-TEh-SOs-SCa-STp-TP55-AGE-NE**	**MH1-TS1-UF100-TEh-SOs-SCa-STp-TP55-AGE-NE**	**MH1-TS1-UF1000-TEh-SOs-SCa-STp-TP55-AGE-NE**
T(2 cm, t)	[ºC]	0.39	0.40	0.42	0.48
T(10 cm, t)	[ºC]	0.12	0.12	0.13	0.38
T(25 cm, t)	[ºC]	0.35	0.36	0.40	0.78
T(60 cm, t)	[ºC]	0.30	0.33	0.35	0.46
X(t)	[cm]	0.40	0.41	0.52	1.29
T(x, 10 days)	[ºC]	0.04	0.04	0.24	0.10
Computing time	[s]	0:29:27	0:07:32	0:05:02	0:04:01

Table 5.10: Average of absolute values of errors, freeze block update sensitivity and time step sensitivity, Problem 1

Average of absolute values of errors / Computing time	**Units**	**MH1-TS1-UF1-TEh-SOs-SCa-STp-TP55-AGE-NE**	**MH1-TS40-UF1-TEh-SOs-SCa-STp-TP55-AGE-NE**	**MH1-TS40-UF100-TEh-SOs-SCa-STp-TP55-AGE-NE**
T(2 cm, t)	[ºC]	0.39	1.03	1.12
T(10 cm, t)	[ºC]	0.12	0.12	0.21
T(25 cm, t)	[ºC]	0.35	0.37	0.37
T(60 cm, t)	[ºC]	0.30	0.31	0.41
X(t)	[cm]	0.40	0.45	0.45
T(x, 10 days)	[ºC]	0.04	0.04	0.04
Computing time	[s]	0:29:27	0:01:01	0:00:47

5.6. Effect of the initial temperature gradient on the accuracy

To study the effect of the initial temperature gradient on the accuracy of the model, Problem 2 was created, which has an initial temperature difference (source temperature minus initial ground temperature) about 4.5 times larger than Problem 1. All the other parameters have been chosen as in Problem 1. Thus, the accuracy of the models of the base case (Problem 1) and the Problem 2 can be compared. An overview of the errors of the models for Problem 2 is provided in Table 5.11. In Table 5.12 it can be appreciated that the error in Problem 2 is generally higher than in Problem 1, for all the models. However, it is usually in the same order of magnitude and it has increased by a lower factor than the gradient increase. The median of the ratio of the errors is 245%, i.e. Problem 2 has errors which are typically about 2.45 times larger than the errors in Problem 1. Of special interest are the models with a time step of 40 seconds and the one executing the "freeze block" every 1,000 seconds, which produced relatively accurate results for Problem 1, but whose results are significantly less accurate for Problem 2. This can be explained in that the higher temperature gradient requires a smaller time step and a more frequent update of the "freeze status" of the zones in order to reduce the errors. Finally, the computing time does not appear to have a clear relationship with the initial temperature gradient.

Table 5.11: Average of absolute values of errors, different models, Problem 2

Average of absolute values of errors / Computing time Model	T(2 cm, t)	T(10 cm, t)	T(25 cm, t)	T(60 cm, t)	X(t)	T(x, 10 days)	Computing time
Units	[°C]	[°C]	[°C]	[°C]	[cm]	[°C]	[s]
MH1-TS1-UF1-TEh-SOs-SCa-STp-TP250-AGE-NE	0.3	0.28	0.24	0.42	0.5	0.18	0:29:37
MH2-TS1-UF1-TEh-SOs-SCa-STp-TP250-AGE-NE	1.11	0.45	0.48	0.96	0.9	0.4	0:24:59
MH5-TS1-UF1-TEh-SOs-SCa-STp-TP250-AGE-NE	3.45	0.96	1.29	1.93	1.55	0.3	0:13:08
MH10-TS1-UF1-TEh-SOs-SCa-STp-TP250-AGE-NE	5.97	3.19	2.19	3.43	2.5	0.82	0:07:08
MH25-TS1-UF1-TEh-SOs-SCa-STp-TP250-AGE-NE	8.43	11.23	8.15	6.57	4.81	3.66	0:06:00
MH50-TS1-UF1-TEh-SOs-SCa-STp-TP250-AGE-NE	10.04	18.74	20.92	16.71	10.53	7.12	0:05:19
MH1-TS5-UF1-TEh-SOs-SCa-STp-TP250-AGE-NE	0.42	0.26	0.93	0.81	0.54	0.26	0:05:57
MH1-TS10-UF1-TEh-SOs-SCa-STp-TP250-AGE-NE	0.94	0.33	0.92	0.81	0.58	0.26	0:02:12
MH1-TS20-UF1-TEh-SOs-SCa-STp-TP250-AGE-NE	2.02	0.17	0.88	0.8	0.61	0.25	0:01:13
MH1-TS40-UF1-TEh-SOs-SCa-STp-TP250-AGE-NE	4.78	8.99	13.11	13.79	9.4	2.63	0:00:38
MH5-TS200-UF1-TEh-SOs-SCa-STp-TP250-AGE-NE	5.84	4.19	1.86	2.18	1.7	0.22	0:00:09
MH10-TS400-UF1-TEh-SOs-SCa-STp-TP250-AGE-NE	6.18	5.22	2.42	3.56	2.61	0.91	0:00:07
MH20-TS800-UF1-TEh-SOs-SCa-STp-TP250-AGE-NE	7.19	9.76	6.36	5.48	3.97	2.67	0:00:07
MH1-TS1-UF10-TEh-SOs-SCa-STp-TP250-AGE-NE	0.33	0.24	0.22	0.42	0.58	0.26	0:05:32
MH1-TS1-UF100-TEh-SOs-SCa-STp-TP250-AGE-NE	1.38	0.54	0.42	0.65	0.77	0.24	0:04:07
MH1-TS1-UF1000-TEh-SOs-SCa-STp-TP250-AGE-NE	3.64	3.23	4.1	5.01	3.79	0.85	0:05:23
MH1-TS40-UF100-TEh-SOs-SCa-STp-TP250-AGE-NE	4.78	8.99	13.11	13.79	9.4	2.63	0:00:17

Table 5.12: Ratios of average of absolute values of errors and computing times, Problem 2 to Problem 1 (TP250/TP55)

Ratio of Error of Problem 2 / Problem 1 / Model	T(2 cm, t)	T(10 cm, t)	T(25 cm, t)	T(60 cm, t)	X(t)	T(x, 10 days)	Computing time
MH1-TS1-UF1-TEh-SOs-SCa-STp-TP250/TP55-AGE-NE	78%	238%	67%	139%	125%	481%	101%
MH2-TS1-UF1-TEh-SOs-SCa-STp-TP250/TP55-AGE-NE	164%	170%	88%	173%	124%	447%	152%
MH5-TS1-UF1-TEh-SOs-SCa-STp-TP250/TP55-AGE-NE	249%	128%	95%	159%	96%	161%	156%
MH10-TS1-UF1-TEh-SOs-SCa-STp-TP250/TP55-AGE-NE	264%	212%	103%	159%	76%	157%	131%
MH25-TS1-UF1-TEh-SOs-SCa-STp-TP250/TP55-AGE-NE	274%	251%	139%	159%	70%	261%	161%
MH50-TS1-UF1-TEh-SOs-SCa-STp-TP250/TP55-AGE-NE	287%	297%	257%	273%	96%	326%	163%
MH1-TS5-UF1-TEh-SOs-SCa-STp-TP250/TP55-AGE-NE	120%	223%	262%	266%	133%	697%	87%
MH1-TS10-UF1-TEh-SOs-SCa-STp-TP250/TP55-AGE-NE	266%	286%	255%	263%	139%	690%	61%
MH1-TS20-UF1-TEh-SOs-SCa-STp-TP250/TP55-AGE-NE	531%	149%	241%	257%	142%	675%	68%
MH1-TS40-UF1-TEh-SOs-SCa-STp-TP250/TP55-AGE-NE	464%	7,705%	3,572%	4,391%	2,092%	6,777%	62%
MH5-TS200-UF1-TEh-SOs-SCa-STp-TP250/TP55-AGE-NE	386%	534%	134%	175%	98%	116%	82%
MH10-TS400-UF1-TEh-SOs-SCa-STp-TP250/TP55-AGE-NE	305%	385%	115%	163%	79%	169%	100%
MH20-TS800-UF1-TEh-SOs-SCa-STp-TP250/TP55-AGE-NE	269%	268%	163%	167%	87%	445%	100%
MH1-TS1-UF10-TEh-SOs-SCa-STp-TP250/TP55-AGE-NE	83%	205%	60%	129%	141%	692%	73%
MH1-TS1-UF100-TEh-SOs-SCa-STp-TP250/TP55-AGE-NE	331%	412%	104%	185%	148%	102%	82%
MH1-TS1-UF1000-TEh-SOs-SCa-STp-TP250/TP55-AGE-NE	762%	843%	526%	1093%	293%	811%	134%
MH1-TS40-UF100-TEh-SOs-SCa-STp-TP250/TP55-AGE-NE	425%	4,262%	3,572%	3,376%	2,092%	6,777%	36%
Average of models (TP250/TP55)	**309%**	**975%**	**574%**	**678%**	**355%**	**1,164%**	**103%**
Median of models (TP250/TP55)	**274%**	**268%**	**139%**	**175%**	**125%**	**447%**	**100%**

5.7. Effect of the Stefan number and amount of latent heat on the accuracy

In order to evaluate the effect of the amount of latent heat, which is the major parameter which makes the model non-linear and poses numerical difficulties, two additional problems were studied. First, in order to eliminate the non-linearities, a model without phase change was created (Problem 4). As it was expected, the simulation results are smoother, and no steps or fluctuations are observed (see Figure 5.17). Furthermore, the accuracy of the results tends to be higher than in the models which simulate phase change (see Table 5.13). However, in the models with larger time steps and/or mesh size, the accuracy in the very near field of the "cold source" is worse than in the model with phase change. This effect can be explained in that the existence of latent heat slows down the very abrupt effects of the high initial temperature gradient, leading to more accurate numerical results. The computing time was lower for most (but not all) of the models without latent heat, amounting to a median of 75% of the computing time of Problem 2.

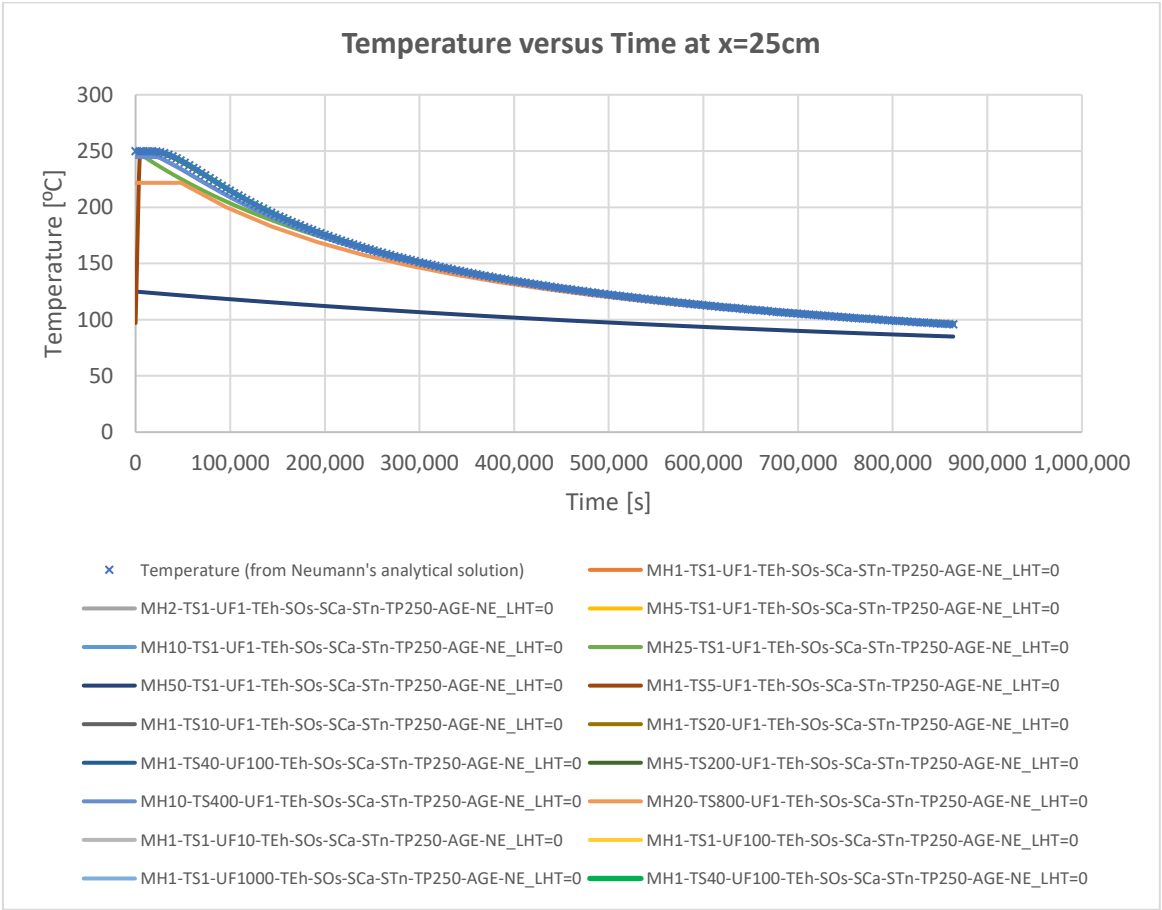

Figure 5.17: Temperature vs time at x=25cm, Problem 4

Table 5.13: Ratios of average of absolute values of errors and computing times, Problem 4 to Problem 2 (STn/p)

Ratio of Error of Problem 4 / Problem 2 / Model	T(2 cm, t)	T(10 cm, t)	T(25 cm, t)	T(60 cm, t)	T(x, 10 days)	Computing time
MH1-TS1-UF1-TEh-SOs-SCa-STn/p-TP250-AGE-NE	23%	4%	2%	1%	200%	18%
MH2-TS1-UF1-TEh-SOs-SCa-STn/p-TP250-AGE-NE	23%	10%	15%	2%	87%	21%
MH5-TS1-UF1-TEh-SOs-SCa-STn/p-TP250-AGE-NE	136%	29%	10%	5%	113%	33%
MH10-TS1-UF1-TEh-SOs-SCa-STn/p-TP250-AGE-NE	128%	31%	83%	10%	49%	54%
MH25-TS1-UF1-TEh-SOs-SCa-STn/p-TP250-AGE-NE	139%	167%	35%	81%	18%	72%
MH50-TS1-UF1-TEh-SOs-SCa-STn/p-TP250-AGE-NE	154%	197%	206%	82%	36%	68%
MH1-TS5-UF1-TEh-SOs-SCa-STn/p-TP250-AGE-NE	32%	4%	83%	1%	137%	15%
MH1-TS10-UF1-TEh-SOs-SCa-STn/p-TP250-AGE-NE	37%	3%	1%	1%	137%	22%
MH1-TS20-UF1-TEh-SOs-SCa-STn/p-TP250-AGE-NE	50%	7%	1%	1%	138%	75%
MH1-TS40-UF100-TEh-SOs-SCa-STn/p-TP250-AGE-NE	48%	0%	0%	0%	13%	76%
MH5-TS200-UF1-TEh-SOs-SCa-STn/p-TP250-AGE-NE	110%	35%	7%	4%	145%	100%
MH10-TS400-UF1-TEh-SOs-SCa-STn/p-TP250-AGE-NE	138%	76%	80%	10%	41%	114%
MH20-TS800-UF1-TEh-SOs-SCa-STn/p-TP250-AGE-NE	153%	153%	96%	26%	18%	129%
MH1-TS1-UF10-TEh-SOs-SCa-STn/p-TP250-AGE-NE	21%	5%	2%	1%	138%	137%
MH1-TS1-UF100-TEh-SOs-SCa-STn/p-TP250-AGE-NE	5%	2%	1%	1%	145%	179%
MH1-TS1-UF1000-TEh-SOs-SCa-STn/p-TP250-AGE-NE	2%	0%	0%	0%	41%	138%
MH1-TS40-UF100-TEh-SOs-SCa-STn/p-TP250-AGE-NE	48%	0%	0%	0%	13%	94%
Average of models (STn/p)	**73%**	**43%**	**37%**	**13%**	**86%**	**79%**
Median of models (STn/p)	**48%**	**7%**	**7%**	**1%**	**87%**	**75%**

A case with a latent heat 10 times higher than in the Problem 2, named Problem 3, was also studied. In this problem, as the effect of the phase change is more pronounced, the errors are expected to be higher. Indeed, this prediction is confirmed for the temperature-time graphs (the absolute values of the errors of Problem 3 being in average about 255% of the ones of Problem 2). The temperature profile over distance also presents a higher error for Problem 3, while the freeze front has a lower average error, about 66% of the average errors of Problem 2. The computing time is about 42% higher on average. The detailed results are presented in Table 5.13.

Table 5.14: Ratios of average of absolute values of errors and computing times, Problem 3 to Problem 2 (LHTx10/LHTx1)

Ratio of Error of Problem 3 / Problem 2 / Model	T(2 cm, t)	T(10 cm, t)	T(25 cm, t)	T(60 cm, t)	X(t)	T(x, 10 days)	Computing time
MH1-TS1-UF1-TEh-SOs-SCa-STp-TP250-AGE-NE_ LHTx10/LHTx1	480%	272%	549%	205%	45%	104%	126%
MH2-TS1-UF1-TEh-SOs-SCa-STp-TP250-AGE-NE_ LHTx10/LHTx1	293%	380%	541%	182%	57%	89%	74%
MH5-TS1-UF1-TEh-SOs-SCa-STp-TP250-AGE-NE_ LHTx10/LHTx1	178%	475%	579%	219%	81%	365%	76%
MH10-TS1-UF1-TEh-SOs-SCa-STp-TP250-AGE-NE_ LHTx10/LHTx1	178%	487%	538%	216%	103%	176%	141%
MH25-TS1-UF1-TEh-SOs-SCa-STp-TP250-AGE-NE_ LHTx10/LHTx1	182%	302%	649%	181%	153%	129%	121%
MH50-TS1-UF1-TEh-SOs-SCa-STp-TP250-AGE-NE_ LHTx10/LHTx1	162%	200%	225%	77%	101%	51%	113%
MH1-TS5-UF1-TEh-SOs-SCa-STp-TP250-AGE-NE_ LHTx10/LHTx1	305%	476%	148%	284%	42%	195%	228%
MH1-TS10-UF1-TEh-SOs-SCa-STp-TP250-AGE-NE_ LHTx10/LHTx1	235%	435%	147%	285%	42%	196%	16%
MH1-TS20-UF1-TEh-SOs-SCa-STp-TP250-AGE-NE_ LHTx10/LHTx1	38%	404%	150%	274%	38%	72%	258%
MH1-TS40-UF1-TEh-SOs-SCa-STp-TP250-AGE-NE_ LHTx10/LHTx1	117%	82%	54%	8%	17%	34%	195%
MH5-TS200-UF1-TEh-SOs-SCa-STp-TP250-AGE-NE_ LHTx10/LHTx1	107%	105%	403%	251%	72%	492%	200%
MH10-TS400-UF1-TEh-SOs-SCa-STp-TP250-AGE-NE_ LHTx10/LHTx1	173%	300%	480%	243%	100%	161%	200%
MH20-TS800-UF1-TEh-SOs-SCa-STp-TP250-AGE-NE_ LHTx10/LHTx1	210%	345%	600%	229%	173%	70%	186%
MH1-TS1-UF10-TEh-SOs-SCa-STp-TP250-AGE-NE_ LHTx10/LHTx1	433%	312%	597%	203%	41%	71%	147%
MH1-TS1-UF100-TEh-SOs-SCa-STp-TP250-AGE-NE_ LHTx10/LHTx1	118%	138%	312%	125%	32%	68%	106%
MH1-TS1-UF1000-TEh-SOs-SCa-STp-TP250-AGE-NE_ LHTx10/LHTx1	74%	71%	55%	10%	16%	42%	127%
MH1-TS40-UF100-TEh-SOs-SCa-STp-TP250-AGE-NE_ LHTx10/LHTx1	123%	82%	54%	7%	17%	34%	94%
Average of models (LHTx10/LHTx1)	**200%**	**286%**	**358%**	**176%**	**66%**	**138%**	**142%**
Median of models (LHTx10/LHTx1)	**178%**	**302%**	**403%**	**205%**	**45%**	**89%**	**127%**

5.8. Abrupt and gradual phase change

Two models with identical thermal parameters and boundary conditions except for the phase-change ranges (Problems 5 and 6, see chapter 5.1) were run and compared. A phase change range of 0.1ºC was chosen to simulate the abrupt phase change (Problem 5), as it is not possible to numerically simulate a phase-change range of 0ºC with the enthalpy method. A phase-change range of 4ºC was defined for the case with gradual phase change (Problem 6). The Neumann formula and the solution for gradual phase change by Lunardini described in chapter 3.2.2 were used to check the accuracy of the respective numerical models. The material properties used are different than for the other problems and are defined in chapter 5.1.

The results indicate, as expected, that a material with gradual phase change leads to smoother numerical results and smaller oscillations in the progress of the freeze front (compare Figure 5.18 and Figure 5.19). This effect can also be observed in the temperature-time graphs (Figure 5.20 and Figure 5.21), which usually display large oscillations and steps, typical of the enthalpy method, but in the case of the gradual phase change, the oscillations practically disappear.

With respect to the errors of the models, Table 5.15 presents the ratios of the average of the absolute values of errors of Problem 6 (gradual phase change) to Problem 5 (abrupt phase change). It can be observed that in most cases, the results of Problem 6 are more accurate, although this accuracy improvement varies widely. For instance, Problem 6 is, on average across the different models, less accurate than Problem 5 regarding the prediction of the freeze front. On the other hand, the model with gradual phase change consistently takes longer to compute (up to twice as long), which may be caused by the fact that the zones in the numerical model stay in the freezing state during more time steps, which makes the computing routine slower, as the status of a higher number of zones has to be evaluated.

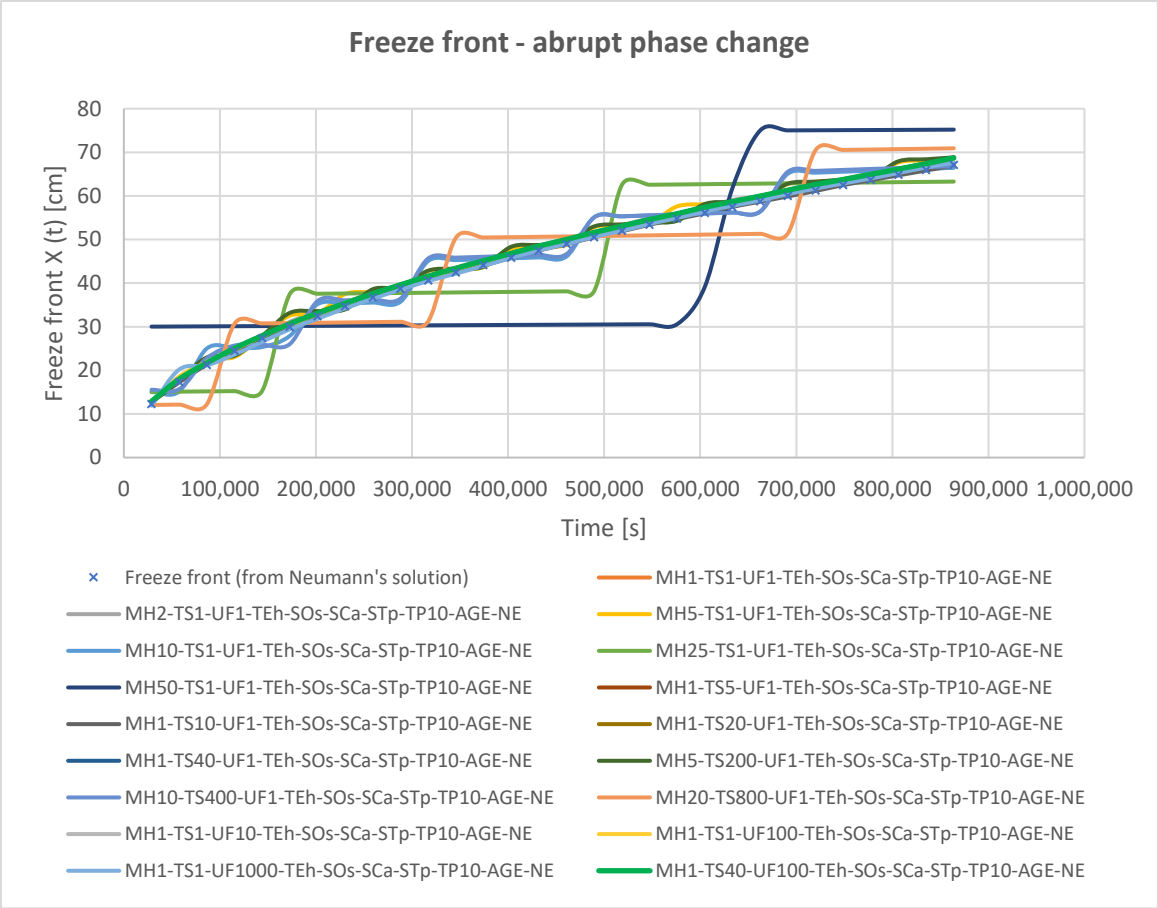

Figure 5.18: Freeze front for Problem 5 (abrupt phase change)

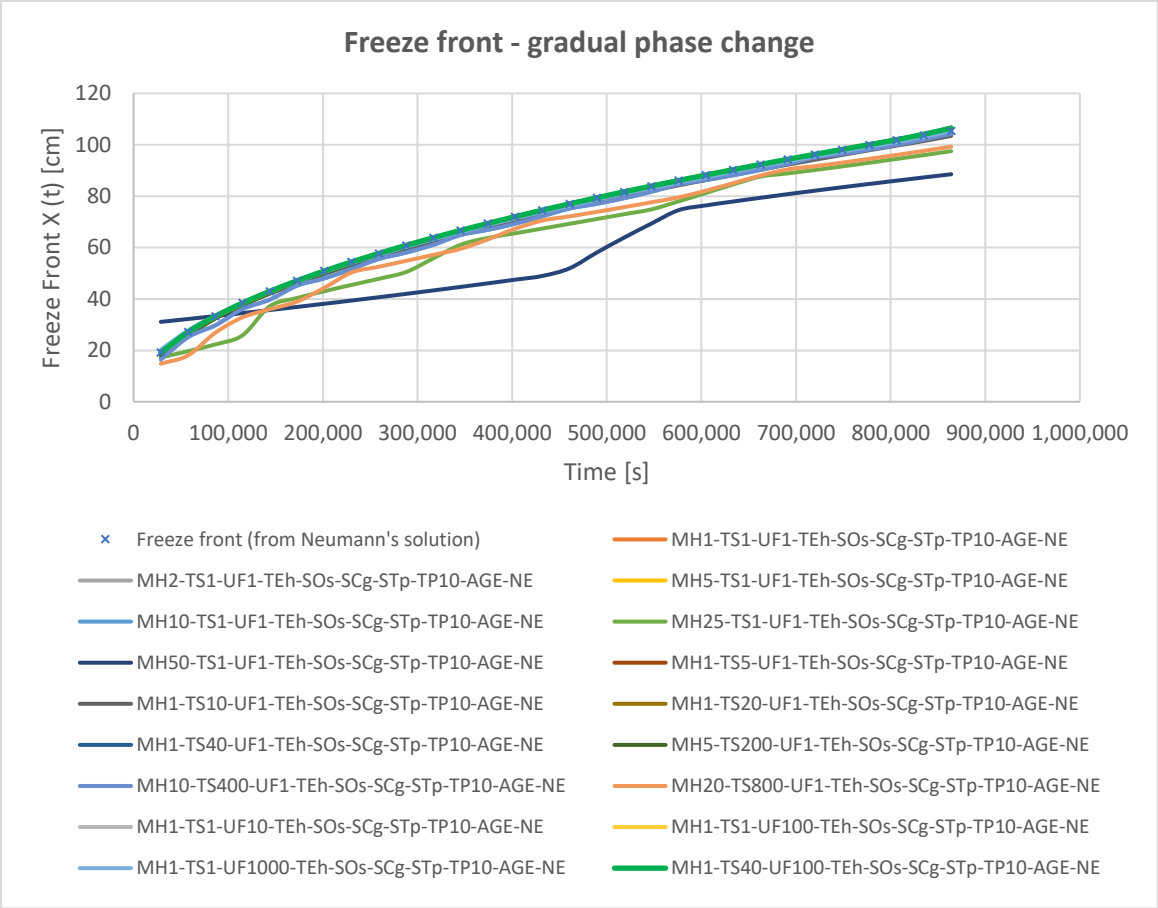

Figure 5.19: Freeze front for Problem 6 (gradual phase change)

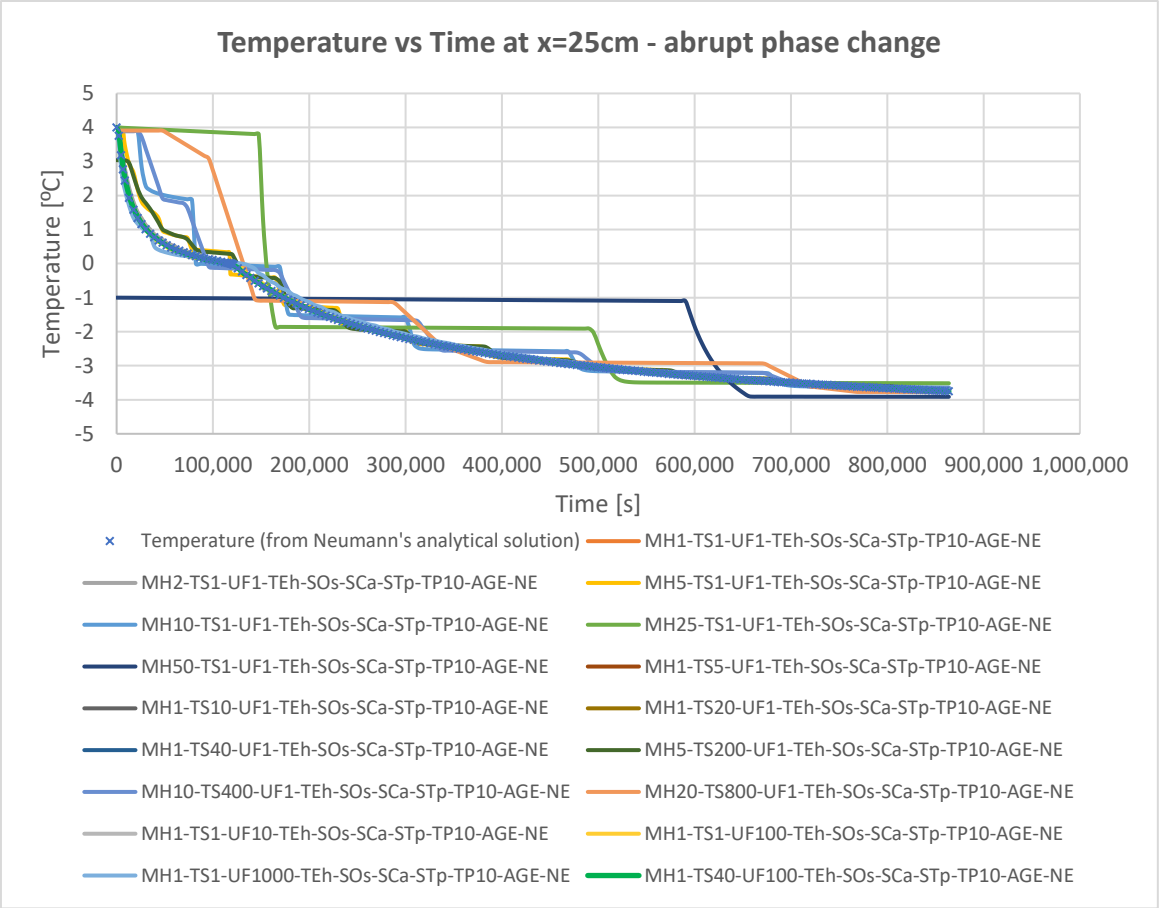

Figure 5.20: Temperature vs time at x=25cm, Problem 5 (abrupt phase change)

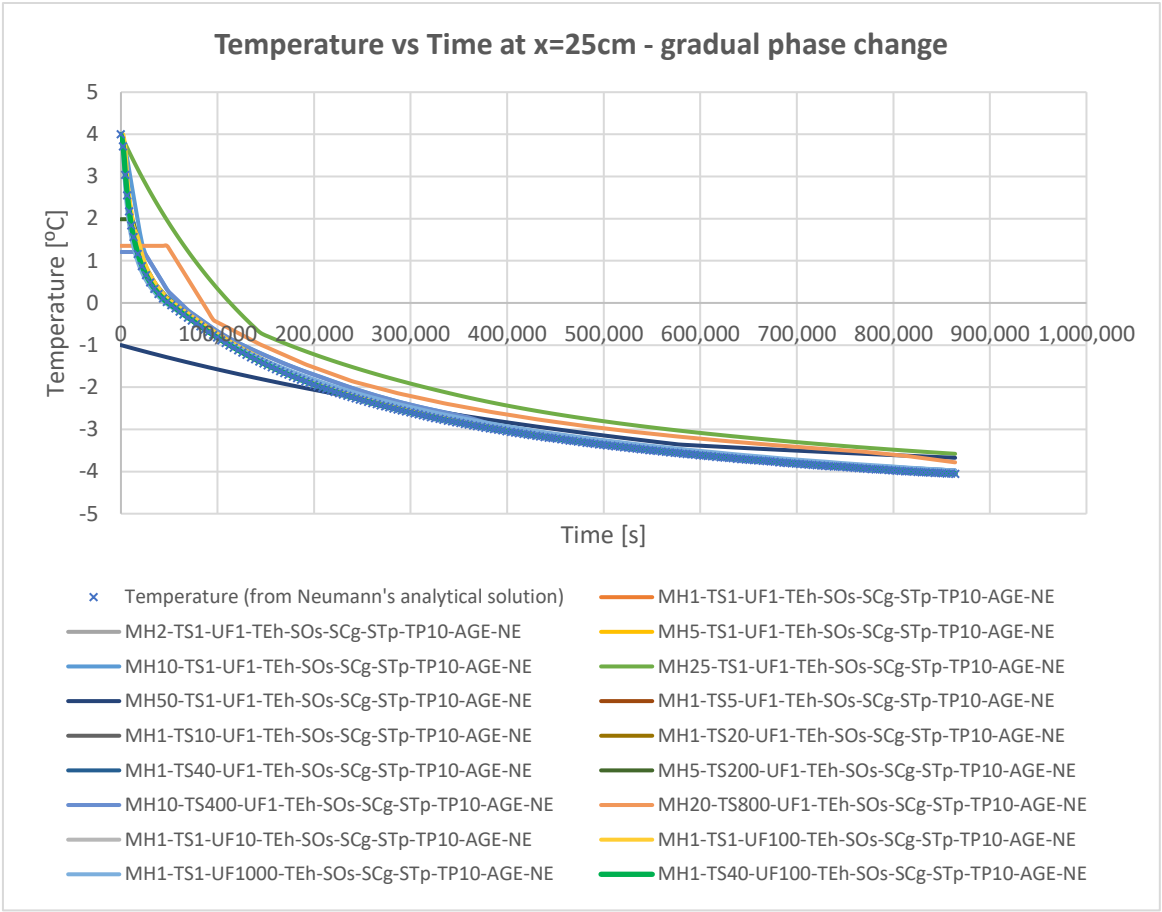

Figure 5.21: Temperature vs time at x=25cm, Problem 6 (gradual phase change)

Table 5.15: Ratios of average of absolute values of errors and computing times, Problem 6 to Problem 5 (SCg/SCa)

Ratios of Error of Problem 6 / Problem 5 / Model	Te_ti_2cm	T(10 cm, t)	T(25 cm, t)	T(60 cm, t)	X(t)	T(x, 10 days)	Computing time
MH1-TS1-UF1-TEh-SOs-SCg/SCa-STp-TP10-AGE-NE	50%	32%	18%	11%	11%	43%	185%
MH2-TS1-UF1-TEh-SOs-SCg/SCa-STp-TP10-AGE-NE	61%	35%	25%	17%	10%	45%	126%
MH5-TS1-UF1-TEh-SOs-SCg/SCa-STp-TP10-AGE-NE	82%	54%	35%	27%	43%	25%	124%
MH10-TS1-UF1-TEh-SOs-SCg/SCa-STp-TP10-AGE-NE	89%	87%	49%	30%	100%	25%	115%
MH25-TS1-UF1-TEh-SOs-SCg/SCa-STp-TP10-AGE-NE	88%	88%	76%	32%	137%	31%	102%
MH50-TS1-UF1-TEh-SOs-SCg/SCa-STp-TP10-AGE-NE	79%	65%	41%	40%	124%	44%	97%
MH1-TS5-UF1-TEh-SOs-SCg/SCa-STp-TP10-AGE-NE	80%	35%	20%	11%	11%	43%	119%
MH1-TS10-UF1-TEh-SOs-SCg/SCa-STp-TP10-AGE-NE	117%	49%	21%	11%	1,836%	141%	129%
MH1-TS20-UF1-TEh-SOs-SCg/SCa-STp-TP10-AGE-NE	126%	73%	22%	11%	13%	130%	125%
MH1-TS40-UF1-TEh-SOs-SCg/SCa-STp-TP10-AGE-NE	126%	73%	22%	11%	11%	53%	140%
MH5-TS200-UF1-TEh-SOs-SCg/SCa-STp-TP10-AGE-NE	88%	123%	53%	32%	44%	27%	138%
MH10-TS400-UF1-TEh-SOs-SCg/SCa-STp-TP10-AGE-NE	108%	88%	56%	36%	95%	27%	150%
MH20-TS800-UF1-TEh-SOs-SCg/SCa-STp-TP10-AGE-NE	98%	121%	76%	35%	114%	39%	233%
MH1-TS1-UF10-TEh-SOs-SCg/SCa-STp-TP10-AGE-NE	130%	224%	209%	42%	14%	44%	123%
MH1-TS1-UF100-TEh-SOs-SCg/SCa-STp-TP10-AGE-NE	128%	227%	491%	80%	28%	50%	105%
MH1-TS1-UF1000-TEh-SOs-SCg/SCa-STp-TP10-AGE-NE	94%	140%	112%	133%	141%	132%	119%
MH1-TS40-UF100-TEh-SOs-SCg/SCa-STp-TP10-AGE-NE	126%	73%	22%	11%	11%	53%	105%
Average of models (SCg/SCa)	**98%**	**93%**	**79%**	**34%**	**161%**	**56%**	**131%**
Median of models (SCg/SCa)	**94%**	**73%**	**41%**	**30%**	**43%**	**44%**	**124%**

5.9. Scalability of the models: thermal time of 365 days

In this chapter, it is investigated to which extent the results of the previous chapters, which have been evaluated for a total thermal time of 10 days, can be extrapolated to the usual dimensions in engineering projects. For instance, practical orders of magnitude of space and time could be a few meters of frozen ground and several weeks or months to a few years, respectively. For this purpose, several simulations for Problem 2 have been executed for a longer thermal time of 365 days and with a larger model, which is 50 m long, to avoid boundary effects. In this case, only a selection of the previous simulations has been run due to the longer computing times required.

The results are qualitatively analogous to the ones in the previous chapters, indicating that the models converge to the exact analytical solution for long times. In general, as observed before, the models do not diverge from the exact solution, but they oscillate around it, eventually converging to it. Specially the temperature-time diagrams exhibit this effect. Once the freeze front has passed a certain location in space, the oscillations tend to decrease with time. Exemplarily, the temperature-time diagram at a distance of 2.5 m from the source is shown in Figure 5.22. The corresponding errors are presented in Figure 5.23. It is interesting to notice that the errors of the temperature-time diagram at x=2.50 m reach their maximum at the time of $5 \cdot 10^6$ seconds, when the interface is around that same position. Indeed, the freeze-front diagram in Figure 5.24 confirms that the front is at x=2.50 m at a time of 5,011,200 seconds. This temporal coincidence of the maximum errors and the freeze front occurs in the temperature-time graphs for other locations as well. The profile of temperature versus space also confirms this, as it can be observed that the maximum errors occur in the position located about 600 cm from the source, where the front is situated (see Figure 5.25).

The limits and the different computing efficiencies of the numerical simulations can be best appreciated in Table 5.16. Regarding the mesh sensitivity, the results of the 10 cm mesh and 1 second time step with execution of the freeze block every step have average errors under 1ºC for the temperature and under 5 cm for the freeze front. However, the calculation time for the model was nearly two days. The models with 25 cm and 50 cm mesh size and a time step of 1 second decrease the calculation time to 30 and 11 hours, respectively, but at the cost of increasing the errors to 2ºC / 7.5 cm and 5ºC / 10 cm. As already shown in chapter 5.4, it can be noticed also here that increasing the time step dramatically for the 10 cm and 50 cm mesh size models, from 1 second to 400 s and 1,600 s, respectively, had a minimal impact on the accuracy of the models, supporting again the thesis that the largest stable time step should be used for the explicit method.

Interestingly, much more accurate results (with errors below 0.1ºC and 0.6 cm) than with the 10 cm mesh and 1 second time step can be obtained by choosing a 1 cm mesh and a larger time step of 20 seconds. In addition, this model, which was the most accurate of the ones assessed, took just above 5 hours to calculate, i.e. it was about 9 times quicker than the first one which used a 1 cm mesh, a 1 s time step and freeze block execution every time

step. Very high accuracies in the same order of magnitude were obtained with the models using a 1 cm mesh and a 1 s time step but updating the freeze / no-freeze status of the model zones every 10 or 100 steps. However, these models took above 29 and 13 hours to run, respectively. The model with a mesh size of 5 cm and a time step of 200 seconds also reached very good accuracies (average errors under 0.3ºC / 3 cm for the freeze front), while taking a comparatively low computing time of 26 minutes.

In practical projects, an accuracy of 1-2ºC for the temperature and of 10-20 cm for the position of the freeze front may be considered as a reasonable target for the desired accuracy of the models. Thus, in this example, all the models but the two models with 50 cm mesh size (i.e. MH50-TS1-UF1-TEh-SOs-SCa-STp-TP250-AGE-NE and MH50-TS1600-UF1-TEh-SOs-SCa-STp-TP250-AGE-NE) would be considered to fulfil the accuracy target on average. Nevertheless, a word of cautiousness is required here: the local accuracy in the areas where the freezing process is occurring is usually several orders of magnitude lower than the average accuracy. In fact, the maximum error is under the limits defined above only for the two most accurate models (i.e. MH1-TS20-UF1-TEh-SOs-SCa-STp-TP250-AGE-NE and MH1-TS1-UF10-TEh-SOs-SCa-STp-TP250-AGE-NE) and even they produce maximum errors of about 4ºC in the point at a distance of 25 cm from the source (see Table 5.17).

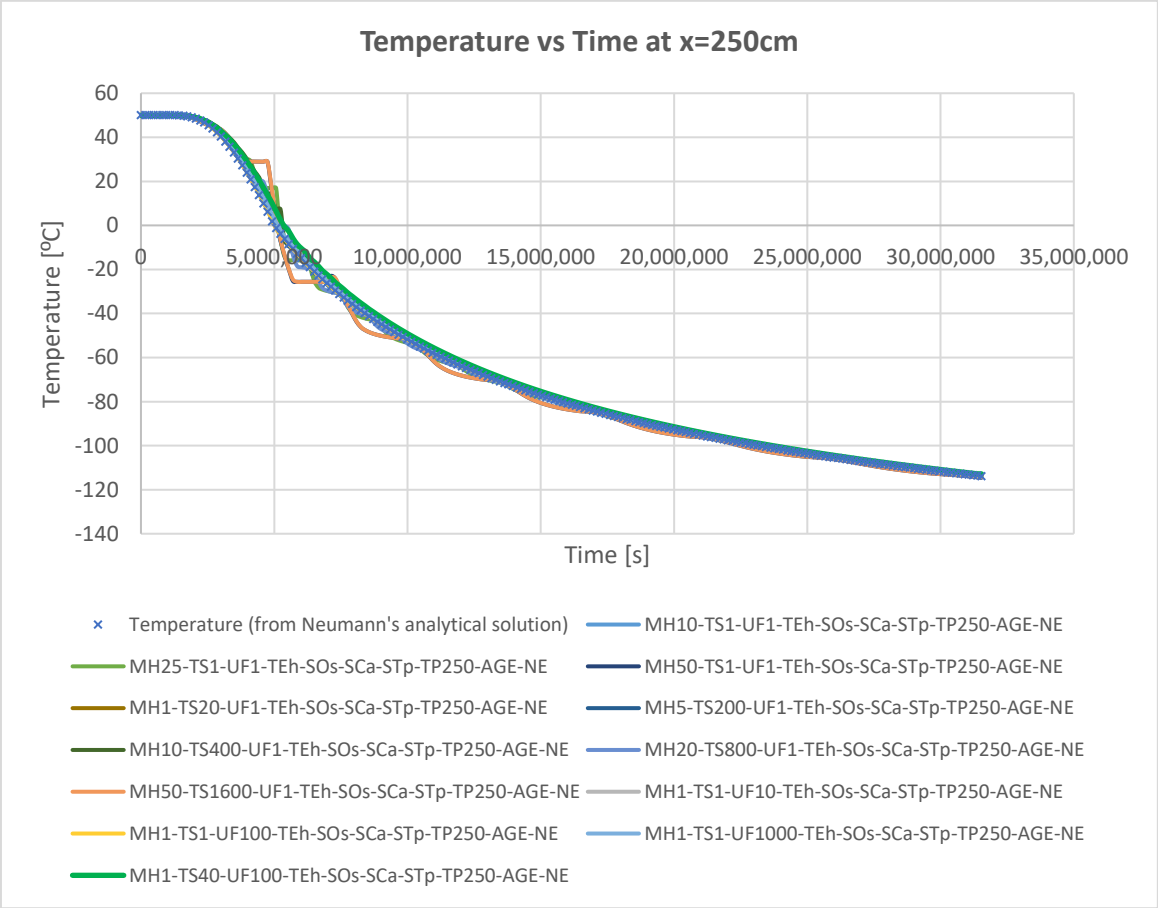

Figure 5.22: Temperature vs time at x=250cm, total time of 365 days, Problem 2

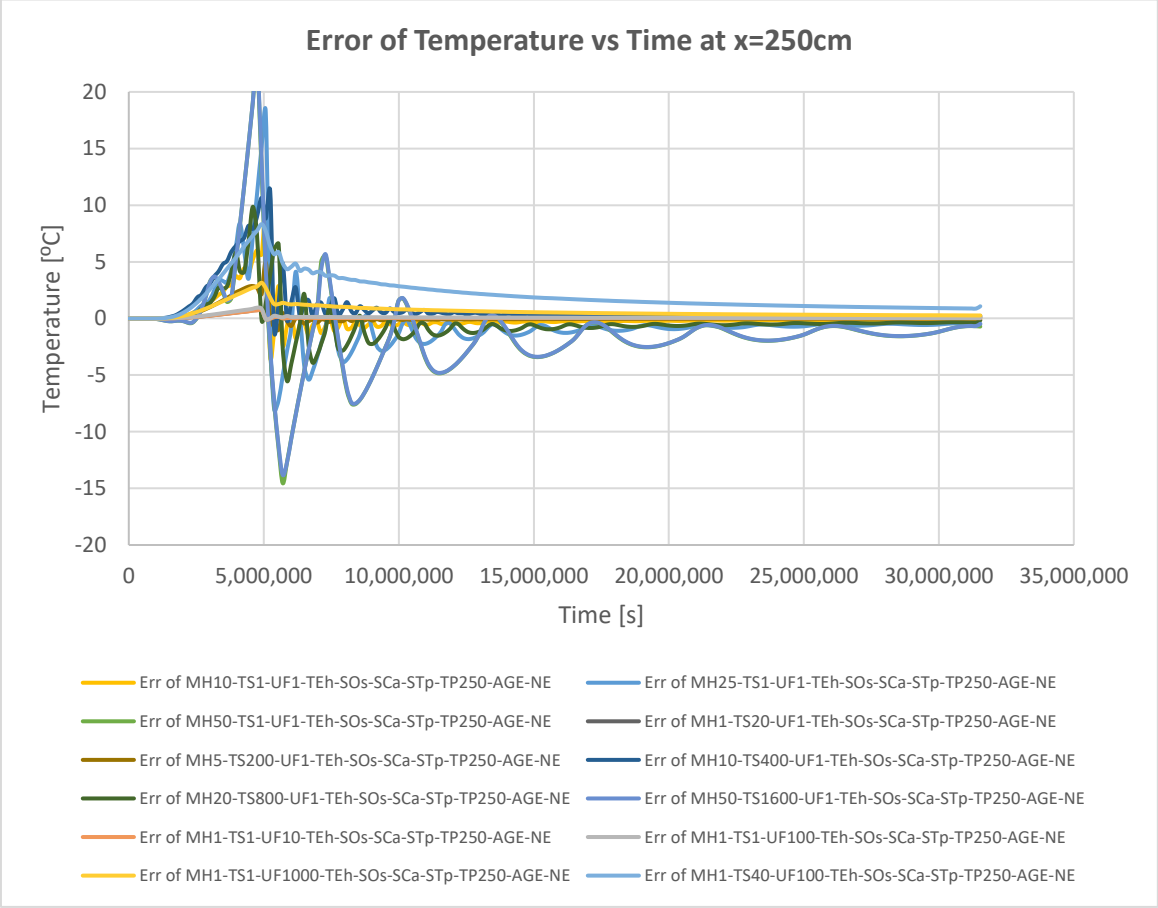

Figure 5.23: Error of temperature vs time at x=250cm, total time of 365 days, Problem 2

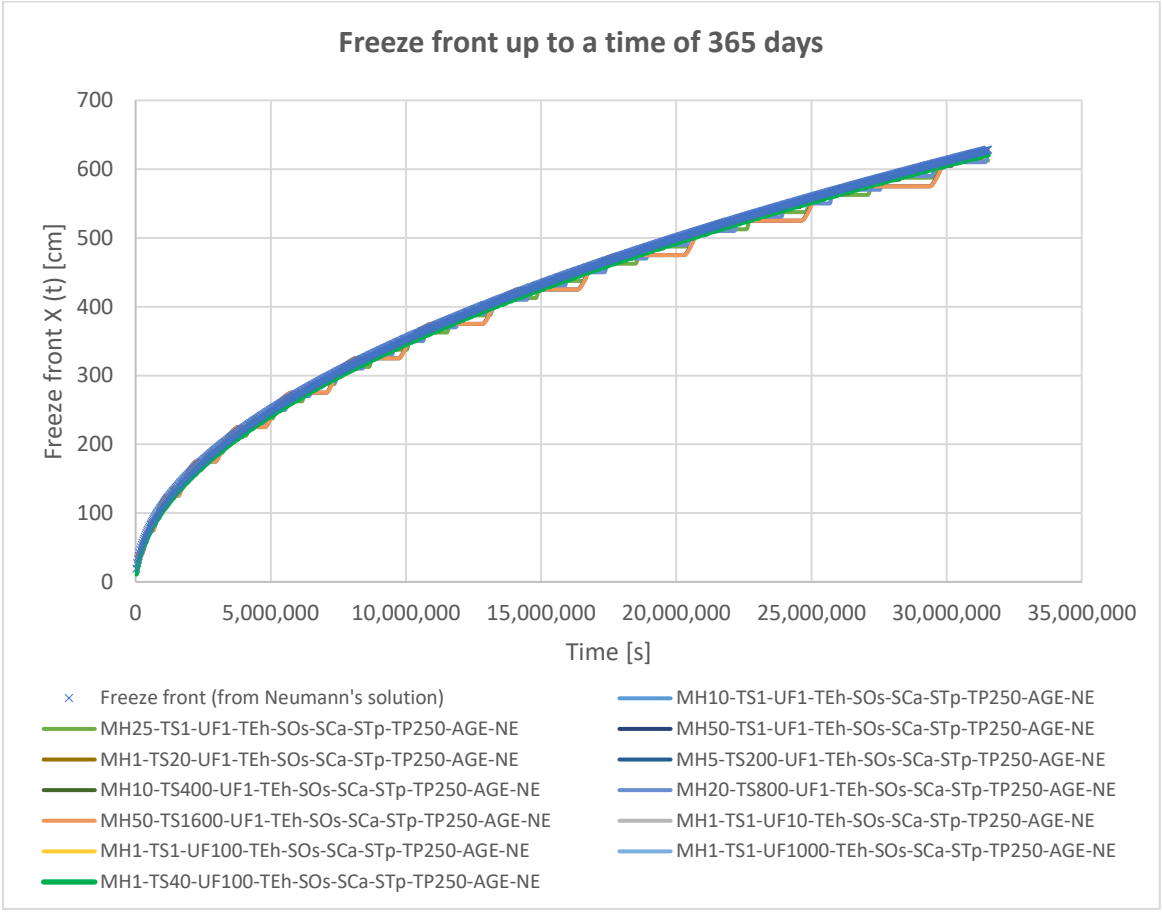

Figure 5.24: Freeze front, total time of 365 days, Problem 2

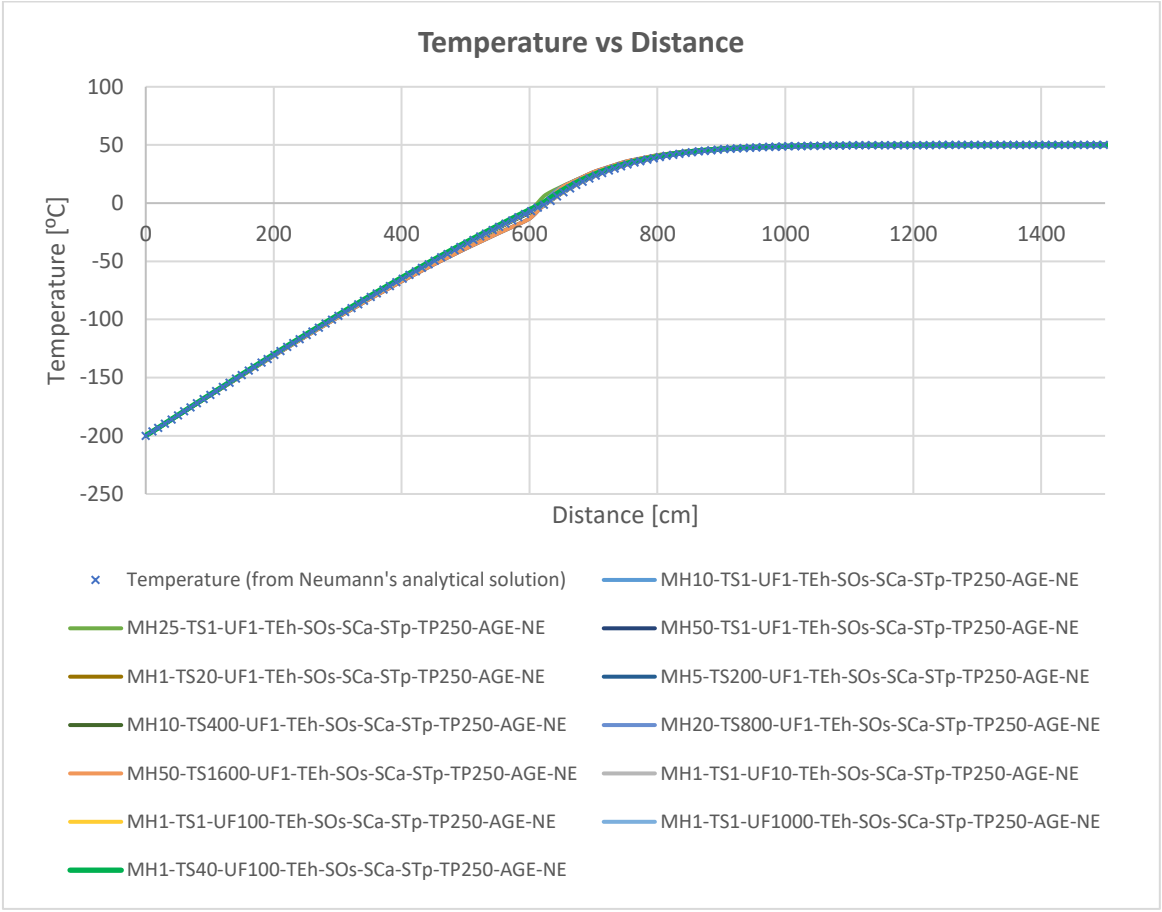

Figure 5.25: Temperature vs distance, t=365 days, Problem 2

Table 5.16: Average of absolute values of errors, computing time, number of zones and number of time steps, 365 days, Problem 2

Average of absolute values of errors / Model	T(25 cm, t)	T(100 cm, t)	T(250 cm, t)	T(600 cm, t)	X(t)	T(x, 365 days)*	Computing time	Nº of zones	Nº of steps
Units	[ºC]	[ºC]	[ºC]	[ºC]	[cm]	[ºC]	[s]		
MH10-TS1-UF1-TEh-SOs-SCa-STp-TP250-AGE-NE	0.47	0.45	0.59	0.89	4.5	0.23	45:44:46	500	31,536,000
MH25-TS1-UF1-TEh-SOs-SCa-STp-TP250-AGE-NE	1.84	0.98	1.48	1.82	7.52	0.59	30:03:54	240	31,536,000
MH50-TS1-UF1-TEh-SOs-SCa-STp-TP250-AGE-NE	5.19	1.56	2.58	2.81	10.11	0.91	11:08:45	100	31,536,000
MH1-TS20-UF1-TEh-SOs-SCa-STp-TP250-AGE-NE	0.07	0.05	0.07	0.08	0.6	0.03	5:18:54	1,400	1,576,800
MH5-TS200-UF1-TEh-SOs-SCa-STp-TP250-AGE-NE	0.3	0.2	0.24	0.49	2.78	0.11	0:26:16	600	157,680
MH10-TS400-UF1-TEh-SOs-SCa-STp-TP250-AGE-NE	1	0.92	0.89	1.15	4.6	0.22	0:15:06	500	78,840
MH20-TS800-UF1-TEh-SOs-SCa-STp-TP250-AGE-NE	1.54	0.78	1.08	1.56	6.99	0.45	0:10:58	250	39,420
MH50-TS1600-UF1-TEh-SOs-SCa-STp-TP250-AGE-NE	5.16	1.54	2.57	2.82	10.18	0.91	0:04:43	100	19,710
MH1-TS1-UF10-TEh-SOs-SCa-STp-TP250-AGE-NE	0.06	0.05	0.06	0.08	0.58	0.02	29:41:44	1,400	31,536,000
MH1-TS1-UF100-TEh-SOs-SCa-STp-TP250-AGE-NE	0.13	0.08	0.11	0.1	0.78	0.04	13:28:53	1,200	31,536,000
MH1-TS1-UF1000-TEh-SOs-SCa-STp-TP250-AGE-NE	0.88	0.56	0.63	0.37	2.85	0.16	14:32:44	1,400	31,536,000
MH1-TS40-UF100-TEh-SOs-SCa-STp-TP250-AGE-NE	2.31	1.76	2.04	1.05	8.18	0.51	0:27:19	1,400	788,400

**Note: Averages calculated for the first 2,000 cm from the source.*

Table 5.17: Maximum of absolute values of errors, 365 days, Problem 2

Model / Maximum of absolute values of errors	T(25 cm, t)	T(100 cm, t)	T(250 cm, t)	T(600 cm, t)	X(t)	T(x, 365 days)*
Units	[ºC]	[ºC]	[ºC]	[ºC]	[cm]	[ºC]
MH10-TS1-UF1-TEh-SOs-SCa-STp-TP250-AGE-NE	17.5	16.9	8.7	4.1	9.7	2.3
MH25-TS1-UF1-TEh-SOs-SCa-STp-TP250-AGE-NE	59.4	20.8	18.2	9.6	20.1	7.7
MH50-TS1-UF1-TEh-SOs-SCa-STp-TP250-AGE-NE	125	21	22.8	16	31.4	6
MH1-TS20-UF1-TEh-SOs-SCa-STp-TP250-AGE-NE	4.3	1.8	0.7	0.4	0.9	0.3
MH5-TS200-UF1-TEh-SOs-SCa-STp-TP250-AGE-NE	14.5	9.1	4.9	2.2	5.3	1.5
MH10-TS400-UF1-TEh-SOs-SCa-STp-TP250-AGE-NE	16.2	23.2	11.2	4.8	9.8	2.4
MH20-TS800-UF1-TEh-SOs-SCa-STp-TP250-AGE-NE	29.1	16.4	9.9	7.7	17.1	5.5
MH50-TS1600-UF1-TEh-SOs-SCa-STp-TP250-AGE-NE	125	20.3	22.8	16	31.7	6.1
MH1-TS1-UF10-TEh-SOs-SCa-STp-TP250-AGE-NE	3.8	1.8	0.7	0.3	0.9	0.3
MH1-TS1-UF100-TEh-SOs-SCa-STp-TP250-AGE-NE	9.8	2.2	0.9	0.4	1.1	0.3
MH1-TS1-UF1000-TEh-SOs-SCa-STp-TP250-AGE-NE	26.4	8.6	3.2	1.2	3.1	1
MH1-TS40-UF100-TEh-SOs-SCa-STp-TP250-AGE-NE	53	19.8	8.3	3.2	8.4	2.8

**Note: Averages calculated for the first 2,000 cm from the source.*

5.10. Scalability of the models: large mesh sizes, large time steps and low update frequency

This chapter has the aim to test models with much larger meshes, time steps and freeze intervals than the ones used in the previous chapters. For this reason, another set of models was run for a thermal time of 365 days for Problem 1, with larger meshes and longer intervals between freeze status updates than in previous chapters. The time steps chosen correspond approximately to the respective critical time step (which vary with the mesh size) for most of the models. The reason is that, as shown in chapter 5.4, the accuracy does not significantly depend on the time step when using the explicit algorithm, as long as it stays under the critical time step.

With regard to the extreme time steps used in this chapter, it could be thought that they have a negative influence on the accuracy of the results. As the problem is considered to have a sharp phase-change interface, it is not physically accurate that more than one element in the direction of the freeze front changes phase in any given time step. Thus, an analogous stability criterion to the one applied in Causon and Mingham (2010) to the advection differential equation, $\Delta t \leq \Delta x / |v_g|$, (see also chapter 4.4.2) could be applied. This would imply that the time step should not be larger than the mesh size divided by the speed of freeze front propagation. This suggested criterion, however, does not seem to be too restrictive for freezing calculations: taking the average propagation speed for the first 100 cm from Figure 5.27, and the model with the largest mesh (400 cm) and time step (12,800 s), the equation would be as follows: $\Delta t \leq \frac{400}{\left|\frac{100}{311000}\right|} = 1.244 \cdot 10^6$ seconds, which is much larger than the largest chosen time step of 12,800 s.

The results and errors of the calculations, presented in Figures 5.26 to 5.29 and Table 5.18, show that the accuracy of the results is low when the meshes and freeze intervals are too large. In fact, average errors as large as 6ºC for certain temperature histories and 86 cm for the freeze front are generated by the model with the 200 cm mesh size (see Table 5.19). Updating the freeze status at a very low frequency also decreases the accuracy of the model, e.g., using an update interval of 300 time steps and a time step of 1,600 seconds (i.e. updating the freeze status every approx. 5.5 days), generates errors in the temperature of about 2-5ºC and freeze front errors of about 50 cm (see Table 5.20). Interestingly, in this case, the errors do not appear to increase for update intervals larger than 300 time steps (for the same time step of 1,600 s).

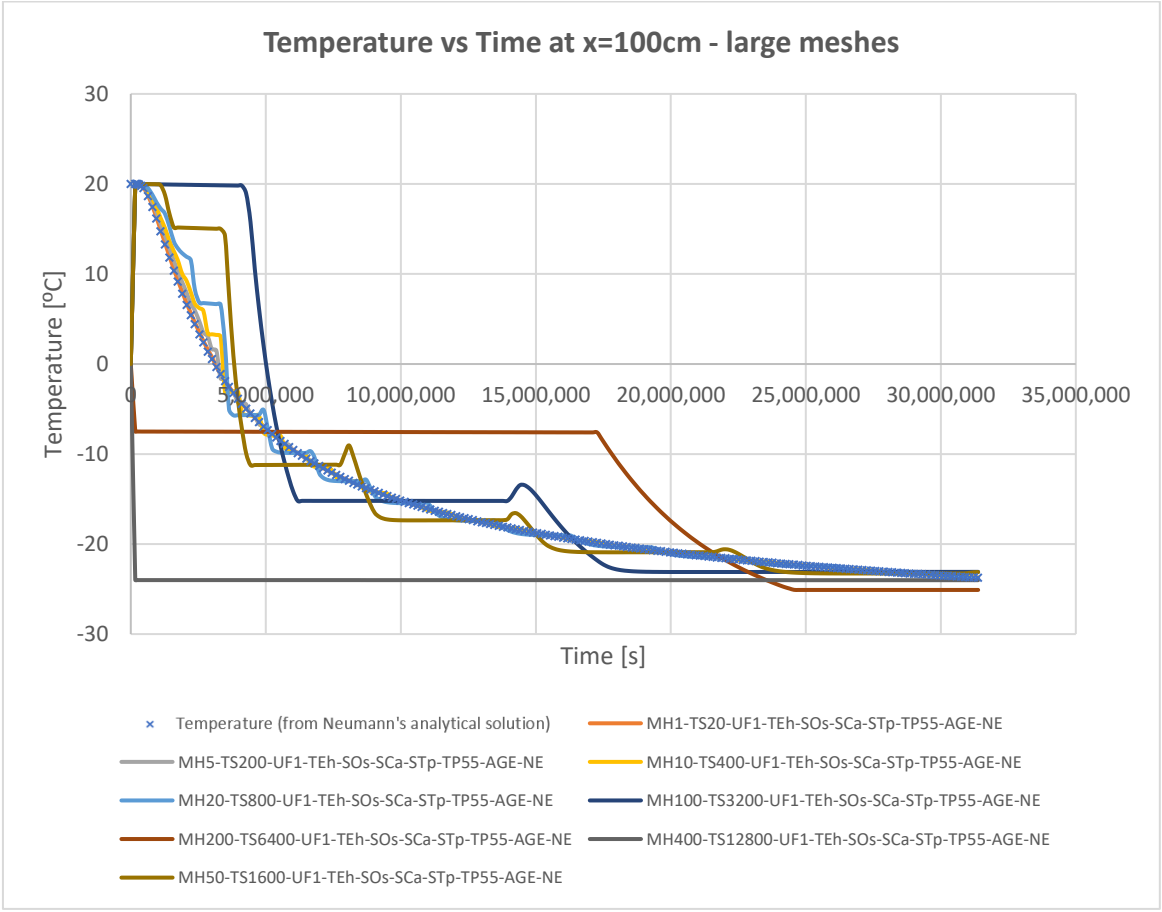

Figure 5.26: Temperature vs time, x = 100 cm, large mesh sizes

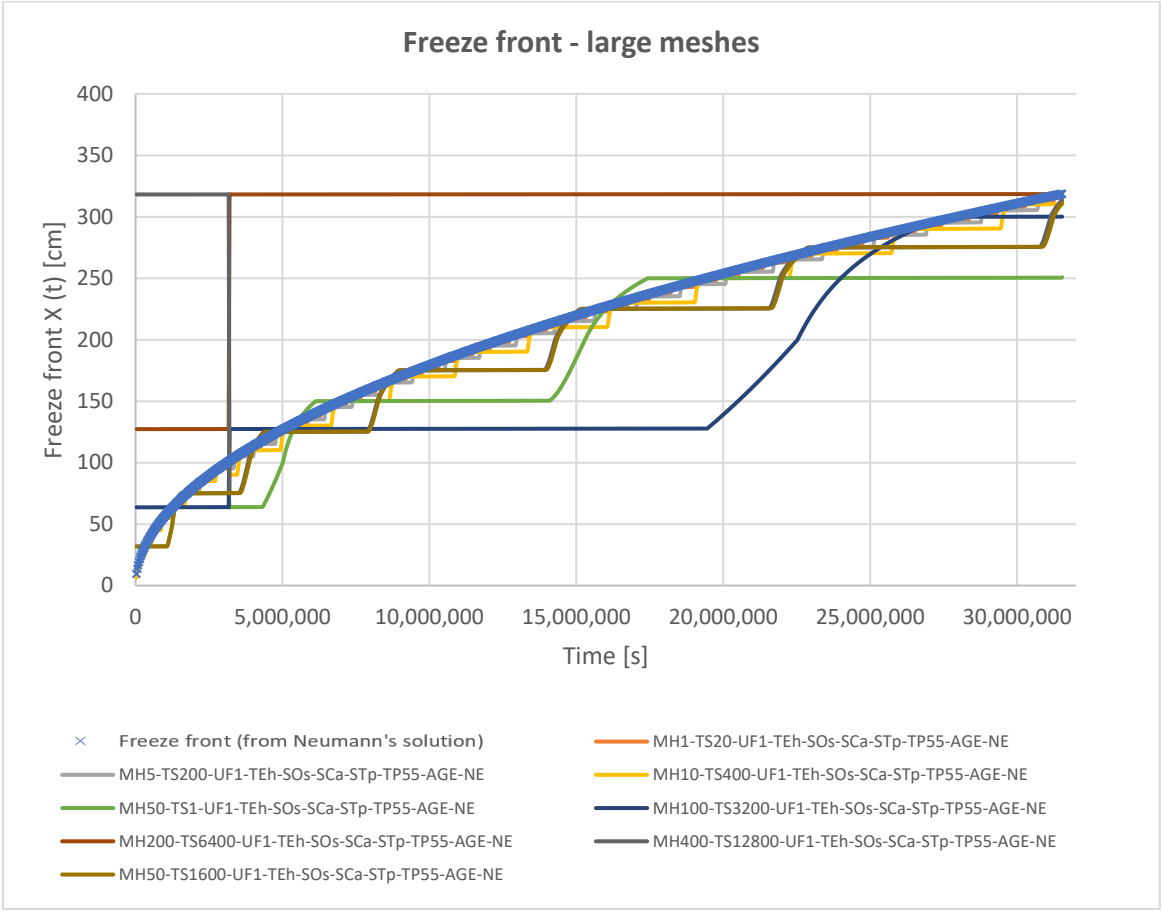

Figure 5.27: Freeze front, large mesh sizes

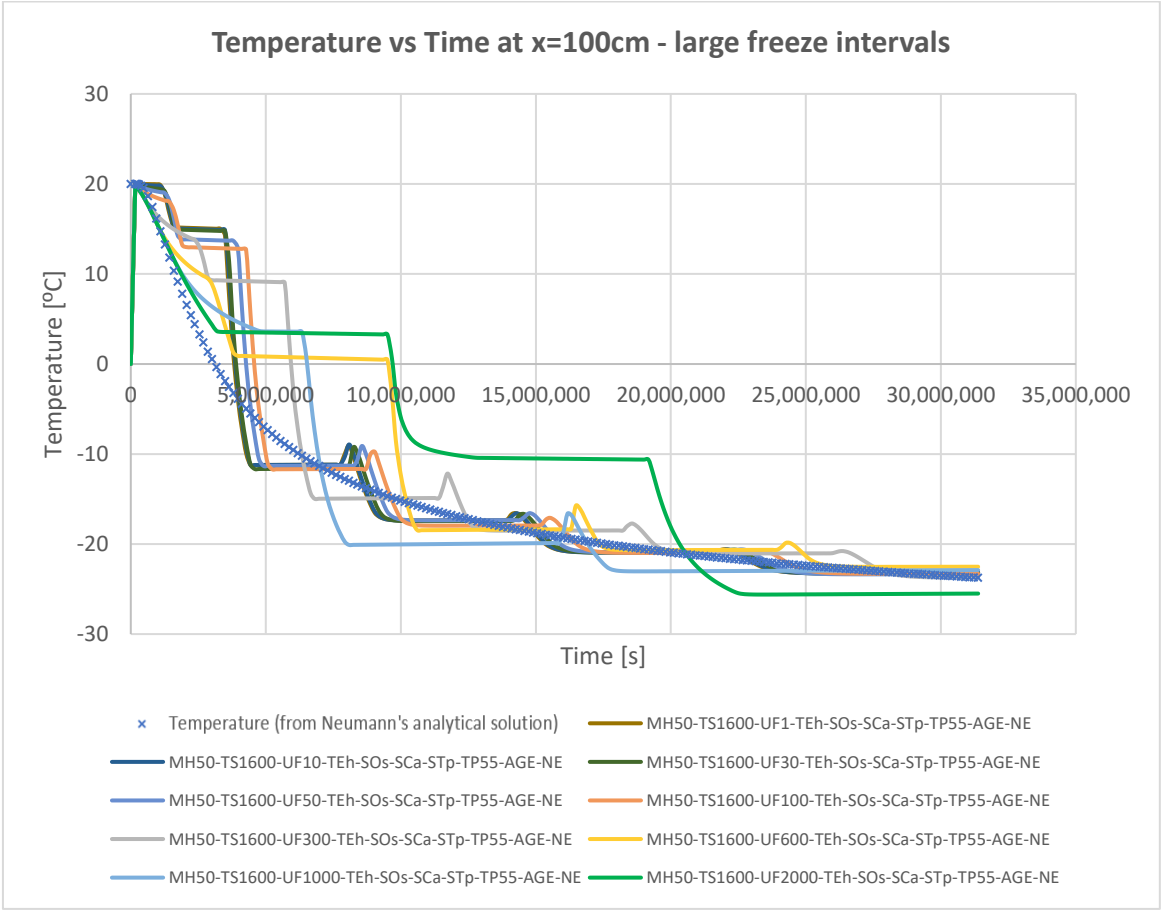

Figure 5.28: Temperature versus time, x = 100 cm, large freeze intervals

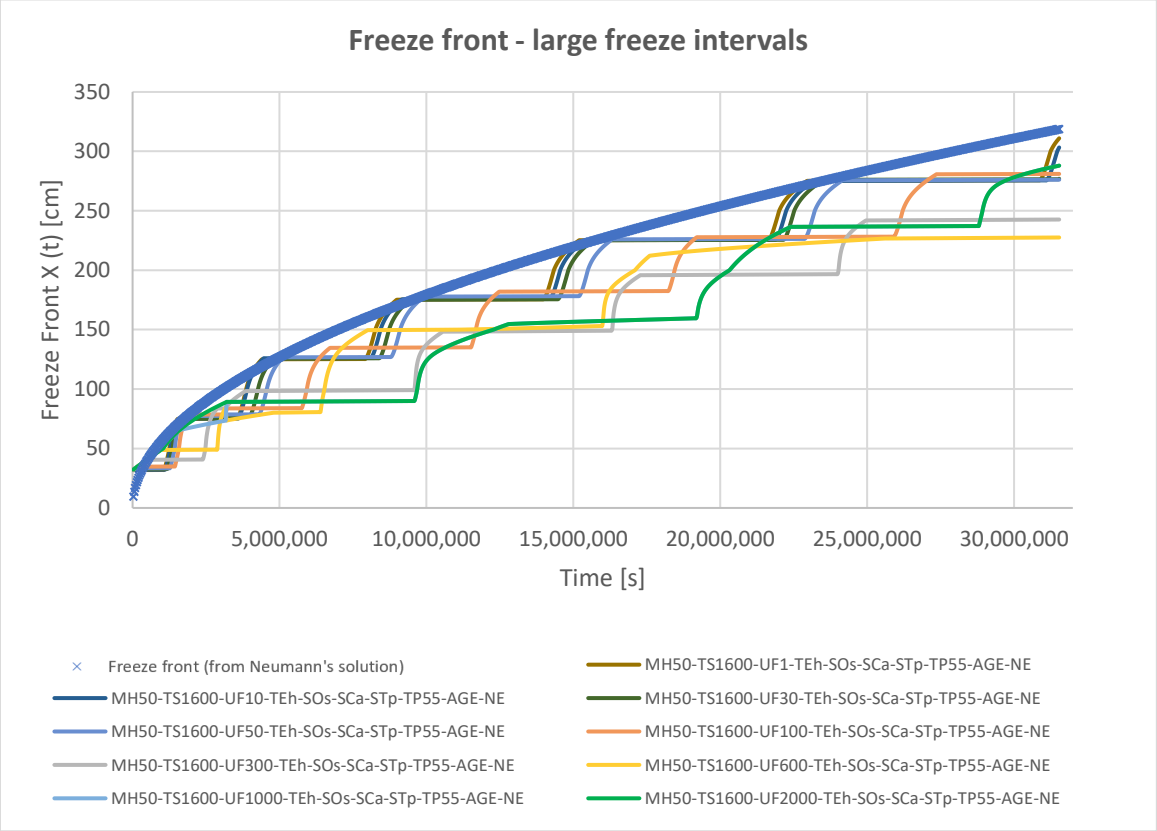

Figure 5.29: Freeze front, large freeze intervals

Table 5.18: Average of absolute values of errors, mesh size sensitivity (large meshes), 365 days, Problem 1

Average of absolute values of errors / Computing time	T(25 cm, t)	T(100 cm, t)	T(250 cm, t)	T(600 cm, t)	X(t)	T(x, 365 days)*	Computing time**
Units	[ºC]	[ºC]	[ºC]	[ºC]	[cm]	[ºC]	[s]
MH1-TS20-UF1-TEh-SOs-SCa-STp-TP55-AGE-NE	0.13	0.12	0.13	0.1	1.98	0	2:03:22
MH5-TS200-UF1-TEh-SOs-SCa-STp-TP55-AGE-NE	0.29	0.23	0.35	0.13	4.02	0.04	0:05:36
MH10-TS400-UF1-TEh-SOs-SCa-STp-TP55-AGE-NE	0.4	0.4	0.65	0.17	7.31	0.09	0:03:19
MH20-TS800-UF1-TEh-SOs-SCa-STp-TP55-AGE-NE	0.61	0.77	1.18	0.22	15.65	0.19	0:02:30
MH50-TS1-UF1-TEh-SOs-SCa-STp-TP55-AGE-NE	1.95	1.77	2.84	0.26	28.09	0.45	5:20:33
MH100-TS3200-UF1-TEh-SOs-SCa-STp-TP55-AGE-NE	3.34	3.5	3.81	0.51	47.69	1.34	0:01:59
MH200-TS6400-UF1-TEh-SOs-SCa-STp-TP55-AGE-NE	4.6	6.83	6.11	0.69	86.51	0.91	0:02:09
MH400-TS12800-UF1-TEh-SOs-SCa-STp-TP55-AGE-NE	5.5	9.53	12.67	0.89	40.3	0.66	0:02:08

**Note: Averages calculated for the first 2,000 cm from the source. **Note: These models were calculated with a different computer, so the computing time is not comparable to the models in other chapters.*

Table 5.19: Average of absolute values of errors, freeze interval sensitivity (large intervals), 365 days, Problem 1

Average of absolute values of errors / Computing time	T(25 cm, t)	T(100 cm, t)	T(250 cm, t)	T(600 cm, t)	X(t)	T(x, 365 days)*	Computing time**
Units	[ºC]	[ºC]	[ºC]	[ºC]	[cm]	[ºC]	[s]
MH50-TS1600-UF1-TEh-SOs-SCa-STp-TP55-AGE-NE	1.92	1.86	2.94	0.36	16.66	0.45	0:02:09
MH50-TS1600-UF10-TEh-SOs-SCa-STp-TP55-AGE-NE	1.93	1.88	2.96	0.36	17.62	0.48	0:02:01
MH50-TS1600-UF30-TEh-SOs-SCa-STp-TP55-AGE-NE	1.99	1.88	3.01	0.37	19.3	0.57	0:02:00
MH50-TS1600-UF50-TEh-SOs-SCa-STp-TP55-AGE-NE	2.02	1.95	3.16	0.38	21.76	0.69	0:02:00
MH50-TS1600-UF100-TEh-SOs-SCa-STp-TP55-AGE-NE	2.08	2.04	3.28	0.38	33.6	0.71	0:02:00
MH50-TS1600-UF300-TEh-SOs-SCa-STp-TP55-AGE-NE	2.32	2.64	4.22	0.41	51.75	0.62	0:02:00
MH50-TS1600-UF600-TEh-SOs-SCa-STp-TP55-AGE-NE	2.45	3.22	4.85	0.36	46.5	1.02	0:01:59
MH50-TS1600-UF1000-TEh-SOs-SCa-STp-TP55-AGE-NE	2.96	2.99	4.11	0.3	49.45	1.13	0:01:59
MH50-TS1600-UF2000-TEh-SOs-SCa-STp-TP55-AGE-NE	3.87	6.41	4.43	0.37	49.02	0.77	0:02:00

**Note: Averages calculated for the first 2,000 cm from the source. **Note: These models were calculated with a different computer, so the computing time is not comparable to the models in other chapters.*

5.11. Explicit and implicit solving algorithms

The numerical simulations in the previous chapters have been performed with the explicit algorithm. In this chapter, the influence of using the explicit versus the implicit algorithm is analysed, taking Problem 1 as a basis. First, the previous simulations with the same numerical meshes and time steps were tried with the implicit algorithm, but FLAC3D automatically changes to the explicit algorithm if the implicit one is not required, i.e. if the explicit algorithm is stable for the defined mesh size and time step. Thus, several calculations with fixed time steps larger than the critical time step for the explicit method were executed with the implicit method. The results have reasonable accuracy for even relatively large time steps, although the errors eventually increase, mainly due to the update of the freeze code block becoming too seldom in time. This effect is specially illustrated by the model MH1-TS200-UF1000-TEh-SOs-SCa-STp-TP55-AGI-NE, in which the update is done only every 200,000 seconds (every 1,000 steps, the step duration being 200 seconds). In this case, the results no longer converge to the exact solution (see Figure 5.31 and Figure 5.32). The explanation is that, in the first calculation step of 200,000 seconds (about 2.3 days), several zones in the model lower their temperature far below the freeze point. After the first step, the thermal properties of these zones are changed by the "freeze block" of the code, so their apparent heat capacity becomes comparatively large in order to account for the effect of the latent heat. However, in the second step, their

temperature is not significantly lowered for two reasons: their temperature is already quite low (due to their cooling during the long first step of 200,000 seconds), so that the equilibrium can be found without lowering it in a large amount and they have a high apparent heat capacity. This leads to these zones becoming "stuck" in the "freezing" status (shown as blue zones in the left side of Figure 5.30, which should have progressed to the status "already frozen") and to the model not converging to the temperatures predicted by the exact solution over time (at least not in the simulated first 10 days). This also explains the high errors produced by this model (see Table 5.20). These numerical issues were not observed in chapter 5.5, where the sensitivity of other models to the update frequency of the "freeze block" was also studied. This is probably because the update frequency in those models was not as large as the one modelled in the present chapter. An important lesson can be taken from this: numerical calculations of Stefan problems do have limitations and care should be taken to use appropriate numerical parameters and check the plausibility of the results.

It is possible to achieve lower calculation times with the implicit method than with the explicit method by using larger time steps than the critical time step, while maintaining relatively low errors (see Table 5.21), which may be sufficiently good for practical purposes. If that table is compared with the results presented in the tables in chapters 5.2, 5.3 and 5.4, it is found that the computing time to achieve a similar accuracy tends to be lower by using the implicit method. This result may, however, be influenced by the fact that the explicit method was not always used with the critical time step. Indeed, for similar time steps (explicit method with a time step slightly below the critical one and the implicit method with a time step slightly above the critical one), the errors and the computing time are very similar (see Table 5.21). The errors of the models calculated with the implicit method generally increase with larger mesh and time steps (see Table 5.21).

The fact that the time steps of the implicit method can be chosen to be larger than in the explicit method is specially advantageous for models with variable mesh size in which some of the elements are very small, thus requiring a very small critical time step and long computing time for the explicit method (such as for example the model in chapter 5.17).

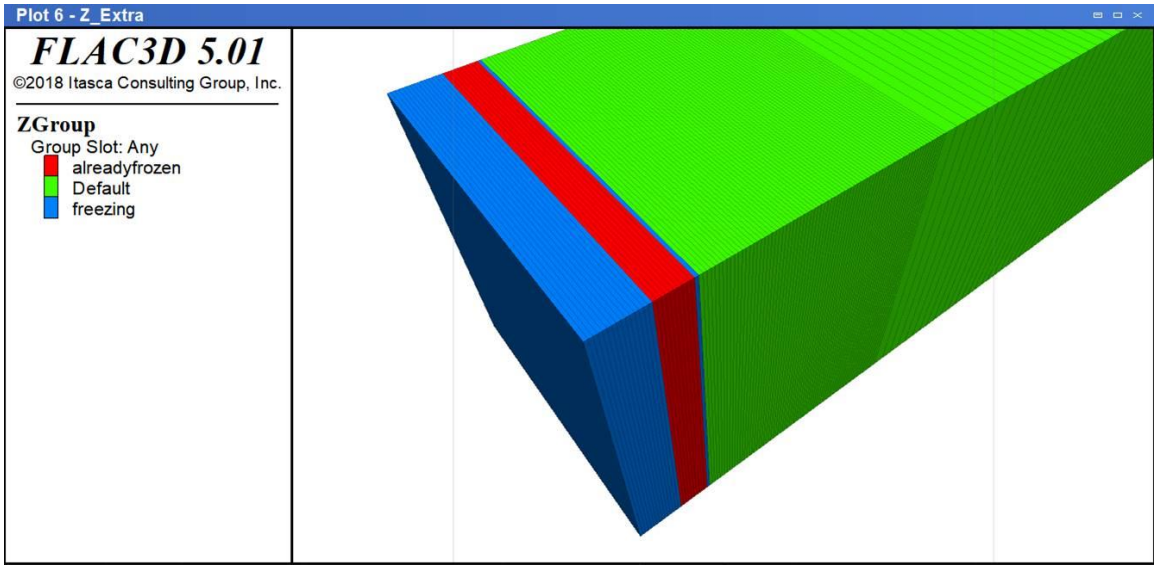

Figure 5.30: Overview of model MH1-TS200-UF1000-TEh-SOs-SCa-STp-TP55-AGI-NE showing the blue zones on the left "stuck" in the freezing status

An overview of the results obtained with the implicit algorithm is presented in Figure 5.31 and Figure 5.32.

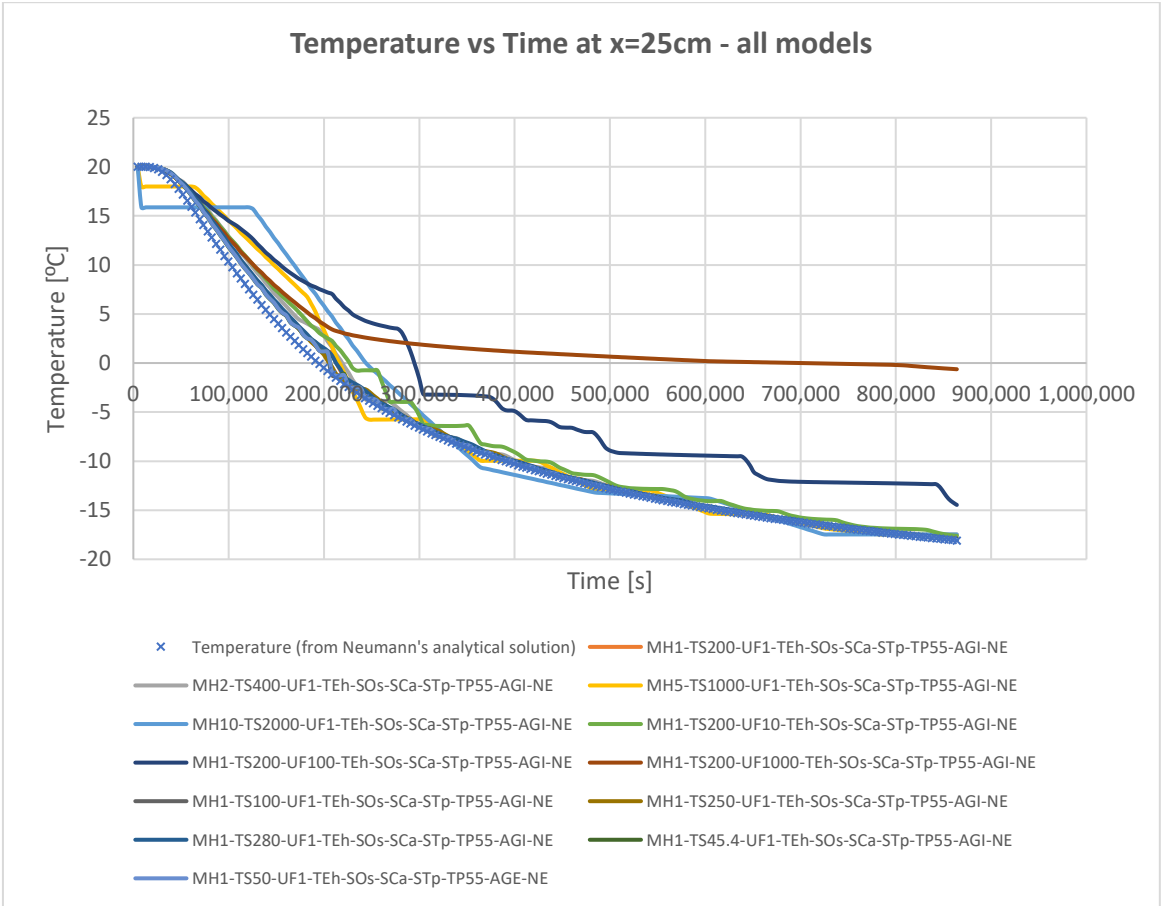

Figure 5.31: Temperature vs time, x=25cm, Problem 1, implicit algorithm

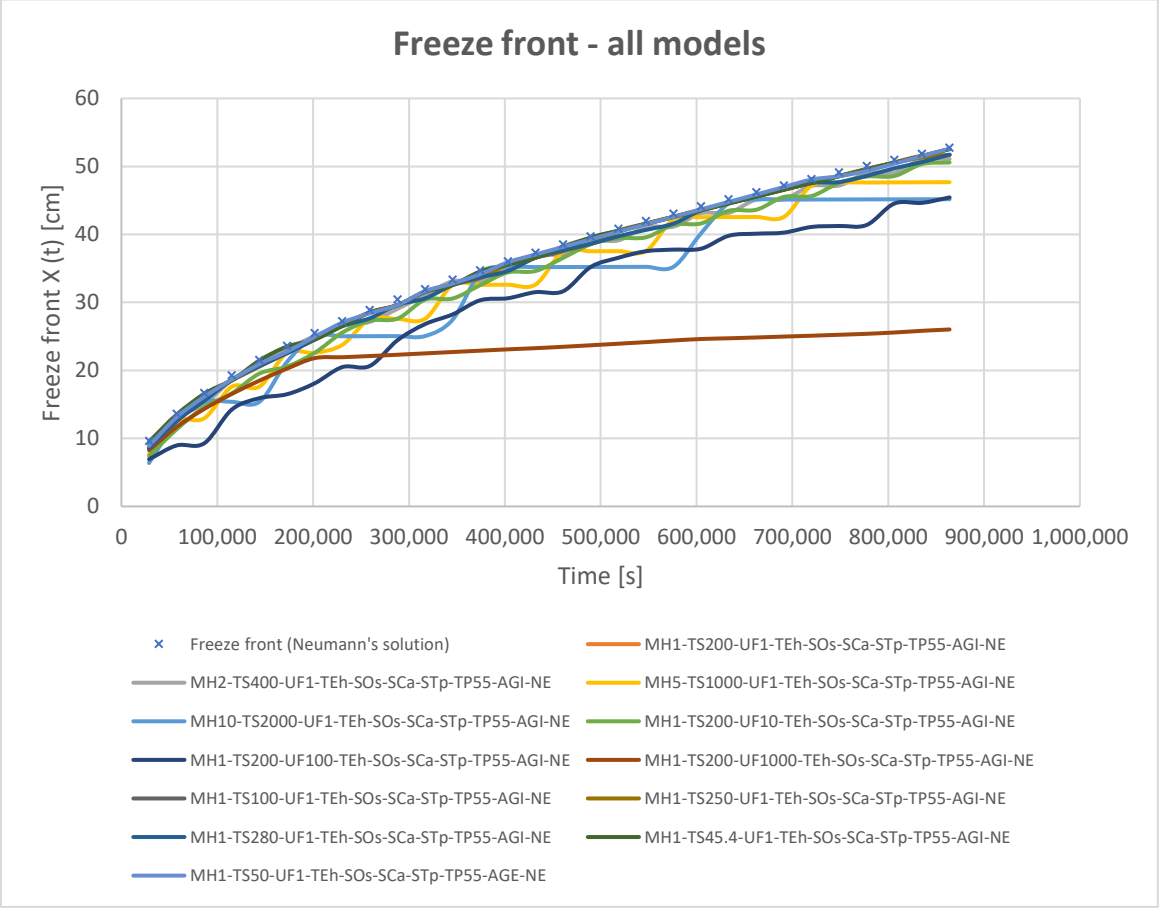

Figure 5.32: Freeze front, Problem 1, implicit algorithm

Table 5.20: Comparison of the accuracies of the explicit and implicit methods, critical time step

Average of absolute values of errors / Computing time	**Units**	**Implicit Model (calculated with the critical time step of the explicit method): MH1-TS45.4-UF1-TEh-SOs-SCa-STp-TP55-AGI-NE**	**Explicit Model (calculated with the critical time step): MH1-TS45.365-UF1-TEh-SOs-SCa-STp-TP55-AGE-NE**
T(2 cm, t)	[ºC]	1.09	1.16
T(10 cm, t)	[ºC]	0.20	0.11
T(25 cm, t)	[ºC]	0.37	0.46
T(60 cm, t)	[ºC]	0.41	0.34
X(t)	[cm]	0.46	0.46
T(x, 10 days)	[ºC]	0.04	0.04
Computing time	[s]	0:01:04	0:00:54

Table 5.21: Average of absolute values of errors and computing time, Problem 1, implicit method

Sensitivity study	**Average of absolute values of errors / Computing time** / **Model** / **Units**	**T(2 cm, t)**	**T(10 cm, t)**	**T(25 cm, t)**	**T(60 cm, t)**	**X(t)**	**T(x, 10 days)**	**Computing time**
		[ºC]	**[ºC]**	**[ºC]**	**[ºC]**	**[cm]**	**[ºC]**	**[s]**
Mesh sensitivity, TS=1s	MH1-TS200-UF1-TEh-SOs-SCa-STp-TP55-AGI-NE	1.75	0.33	0.48	0.36	0.71	0.06	0:00:22
	MH2-TS400-UF1-TEh-SOs-SCa-STp-TP55-AGI-NE	2	0.67	0.68	0.62	1.13	0.1	0:00:13
	MH5-TS1000-UF1-TEh-SOs-SCa-STp-TP55-AGI-NE	2.41	2.21	1.12	1.27	2.71	0.33	0:00:18
	MH10-TS2000-UF1-TEh-SOs-SCa-STp-TP55-AGI-NE	2.6	2.97	1.89	2.26	3.8	0.55	0:00:08
Time step sensitivity, MS=1cm	MH1-TS45.4-UF1-TEh-SOs-SCa-STp-TP55-AGI-NE	1.09	0.2	0.37	0.41	0.46	0.04	0:01:04
	MH1-TS100-UF1-TEh-SOs-SCa-STp-TP55-AGI-NE	1.36	0.13	0.41	0.33	0.55	0.04	0:00:45
	MH1-TS250-UF1-TEh-SOs-SCa-STp-TP55-AGI-NE	1.78	0.44	0.47	0.37	0.7	0.07	0:00:37
	MH1-TS280-UF1-TEh-SOs-SCa-STp-TP55-AGI-NE	1.85	0.54	0.56	0.39	1	0.07	0:00:25
Update freeze interval sensitivity	MH1-TS200-UF10-TEh-SOs-SCa-STp-TP55-AGI-NE	2.16	1	1.24	0.63	2.1	0.13	0:00:10
	MH1-TS200-UF100-TEh-SOs-SCa-STp-TP55-AGI-NE	2.87	3.64	4.68	1.53	6.05	0.56	0:00:13
	MH1-TS200-UF1000-TEh-SOs-SCa-STp-TP55-AGI-NE	3.07	7.28	9.97	2.34	13.85	1.76	0:00:12

5.12. Unstructured versus structured meshes

In addition to the size of the mesh, its shape and regularity may have an influence on the accuracy of the results. The subject of unstructured and structured meshes for numerical modelling was introduced in chapter 4.4.1.1. In the prior chapters, only structured meshes featuring regular rectangular prisms of the same size (within every region of the model) have been used for the models. In order to evaluate the effect of unstructured versus structured meshes on the accuracy of the models, unstructured meshes were generated in the program Phase 2 from Rocscience Inc. Then, they were extruded using the convertor F2F, a free software which creates three dimensional zones for FLAC3D by extruding meshes from 2D finite element software (Geraili Mikola, 2015). Finally, they were imported into FLAC3D. Two unstructured meshes were generated, one with prisms whose bases are irregular quadrilaterals (presented in Figure 5.33) and one with irregular triangular prisms (presented in Figure 5.34). The structured meshes used are presented in Figure 5.35 and Figure 5.36.

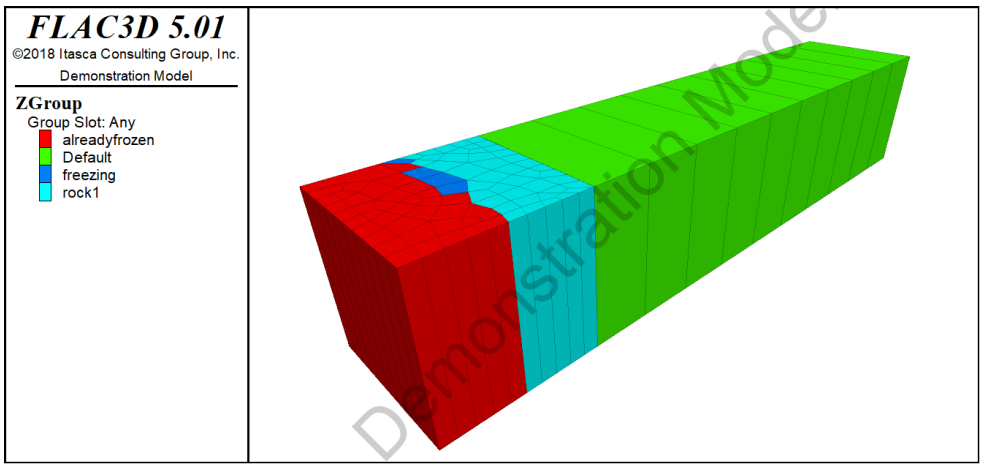

Figure 5.33: Overview of freezing progress, model MH10 -TS40-UF1-TEh-SOs-SCa-STp-TP55-AGE-NE_UNSTR, unstructured mesh with quadrilateral prisms

Note: The areas defined as "Default" and "rock1" have both the properties of the unfrozen material

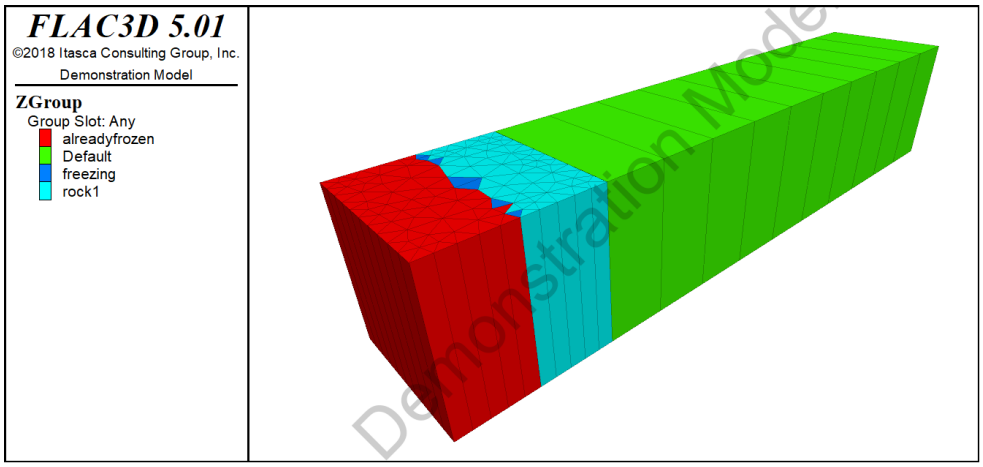

Figure 5.34: Overview of freezing progress, model MH10-TS40-UF1-TEt-SOs-SCa-STp-TP55-AGE-NE_UNSTR, unstructured mesh with triangular prisms

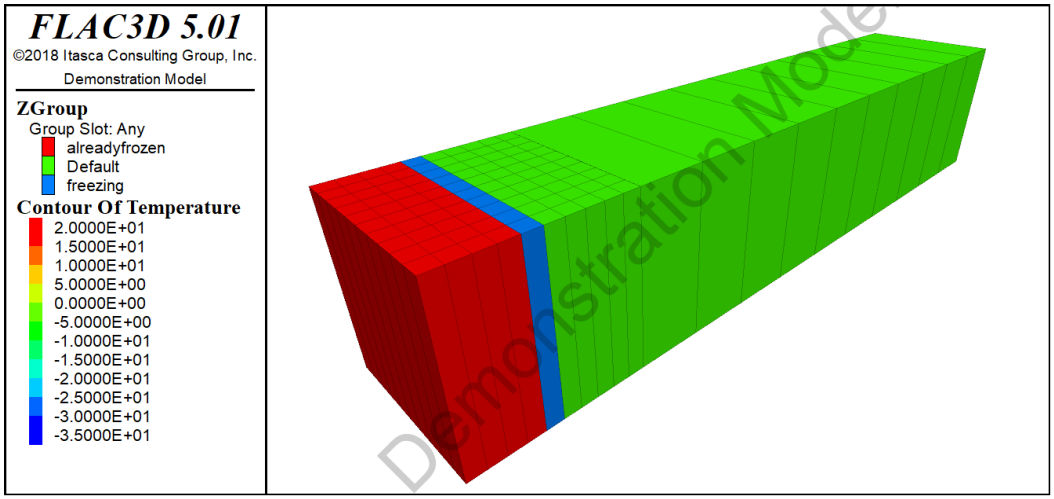

Figure 5.35: Overview of freezing progress, model MH10-TS40-UF1-TEh-SOs-SCa-STp-TP55-AGE-NE_STR, structured mesh

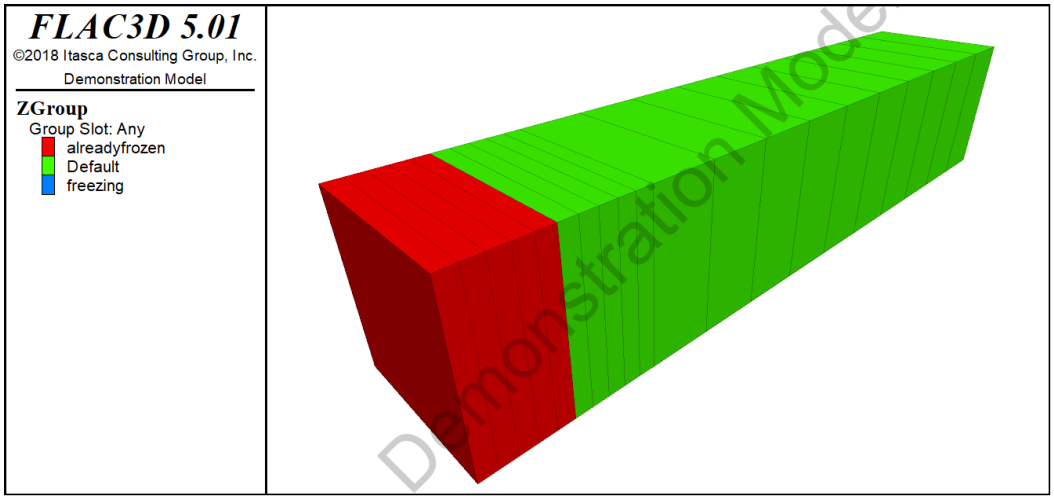

Figure 5.36: Overview of freezing progress, model MH10-TS40-UF1-TEh-SOs-SCa-STp-TP55-AGE-NE-STR-1elem, structured mesh with a reduced number of elements

Interestingly, the results of the models with unstructured meshes have lower errors than those with structured meshes, which contradicts the usual understanding that structured meshes generally yield results of higher quality (see e.g. Itasca Consulting Group (2018)). For instance, when models with the same mesh size of 10 cm are compared, the plateaux which appear in the freeze front versus time graphs are less marked for the models with unstructured meshes and the accuracy is better than in the models with structured meshes, as presented in Figure 5.37 and Table 5.22. The errors are between 10-50% lower with the unstructured mesh with quadrilateral prisms than with the structured meshes, even with a number of zones 10% lower than the structured mesh (i.e. zone volumes about 10% larger, which release 10% more latent heat each). Concordantly, the computing time is about 10% lower than with the structured model. The model with triangular prisms has an even better accuracy than the one with rectangular prisms, although this is probably at least partially due to it having nearly twice as many zones as the structured mesh. The reason for the unstructured meshes delivering better results than structured meshes could be that in the

structured model all the zones in a row (parallel to the freeze front) freeze during a single time step, producing large plateaux as a result of their latent heat being released simultaneously, while in the unstructured mesh, the zones freeze at different time steps, generating smaller plateaux. This can be appreciated by comparing Figure 5.33, Figure 5.34 and Figure 5.35. For the same reason, the model with structured mesh and a reduced number of elements provides the same results as the structured one with more elements.

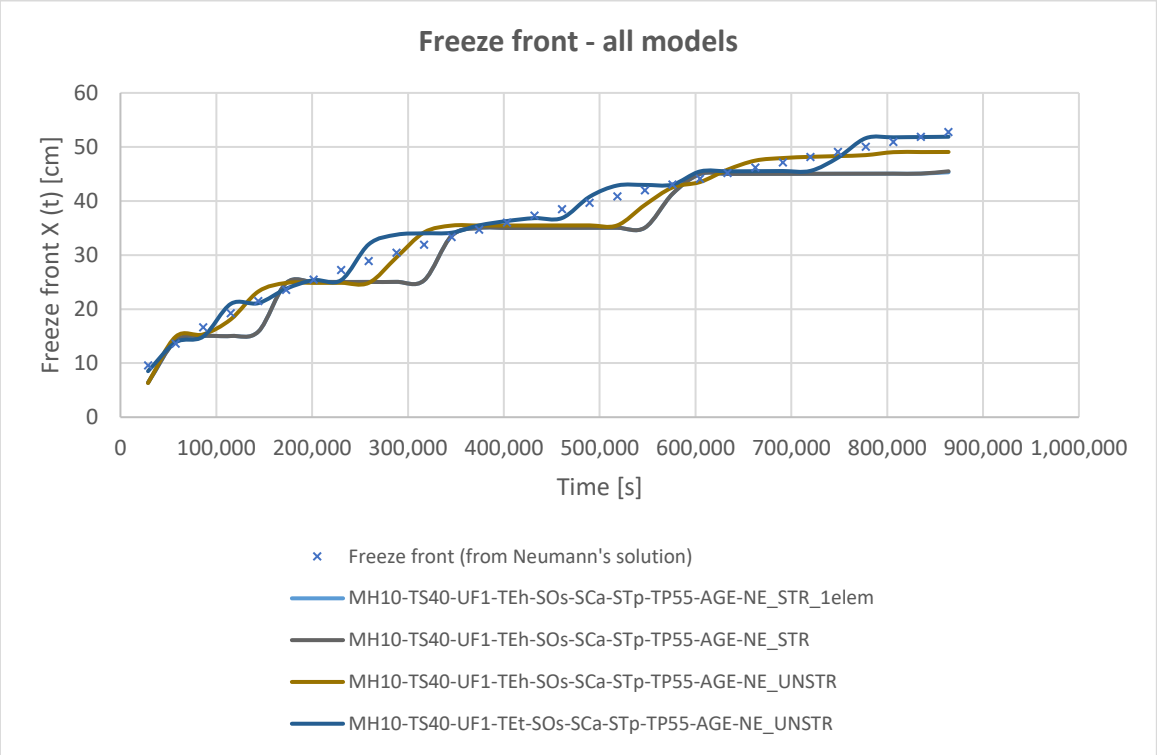

Figure 5.37: Freeze front, Problem 1, structured and unstructured meshes

Note: both structured meshes yield nearly the same results, so their graphs overlap.

Table 5.22: Average of absolute values of errors, Problem 1, structured versus unstructured meshes

Average of absolute values of errors / Computing time / Nº of elements	**Units**	**MH10-TS40-UF1-TEh-SOs-SCa-STp-TP55-AGE-NE_STR_1elem**	**MH10-TS40-UF1-TEh-SOs-SCa-STp-TP55-AGE-NE_STR**	**MH10-TS40-UF1-TEh-SOs-SCa-STp-TP55-AGE-NE_UNSTR**	**MH10-TS40-UF1-TEt-SOs-SCa-STp-TP55-AGE-NE_UNSTR**
Te_ti_2cm	[ºC]	2.26	2.26	2.19	1.87
T(10 cm, t)	[ºC]	1.50	1.50	1.29	0.52
T(25 cm, t)	[ºC]	2.13	2.13	1.81	0.78
T(60 cm, t)	[ºC]	2.17	2.15	1.52	0.72
X(t)	[cm]	3.28	3.27	1.85	1.16
T(x, 10 days)	[ºC]	0.53	0.57	0.26	0.13
Number of elements in the model	[-]	20	110	100	202
Computing time	[s]	0:00:20	0:01:29	0:01:17	0:01:40

5.13. Power consumption

The previous chapters have focused on the study of the accuracy of the numerical model by comparing the resulting temperature field with Neumann's solution. This chapter deals with the accuracy of the power consumption predicted by the numerical model. The calculation of the power consumption is required for example to dimension the freezing station for artificial ground freezing projects. The energy flux which is absorbed by the material is equivalent to the power consumption of the source (which in engineering projects is typically a freeze pipe). In the case of a planar source with a semi-infinite space, this flux can be calculated exactly based on the Neumann's analytical solution. This makes it possible to have a benchmark to compare the results of the numerical model also in terms of thermal flux. The power is calculated from the Neumann solution by applying the following Equation (5.1) at the position of the source $x = 0$:

$$P(x,t) = -k_1 \cdot \frac{\partial T(x,t)}{\partial x} \tag{5.1}$$

where $P(x,t)$ is the flux per unit surface.

The results and errors for the power of the source in Problem 1 from the numerical simulation are presented in Figure 5.38 and Figure 5.39, respectively. This flux has a similar accuracy to the temperatures, which were presented in chapter 5.3. This is logical, because the flux is proportional to the derivative of the temperature with respect to the space coordinate (see Equation (5.1) above).

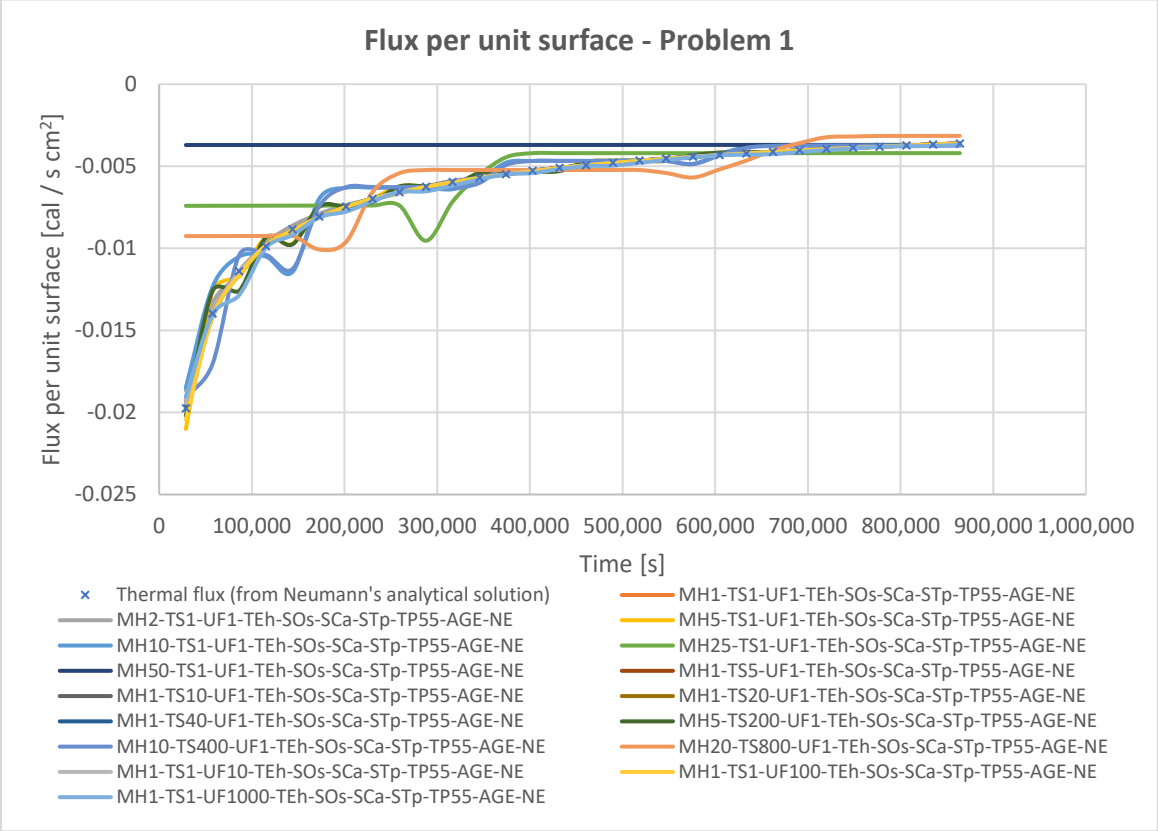

Figure 5.38: Flux per unit surface, Problem 1

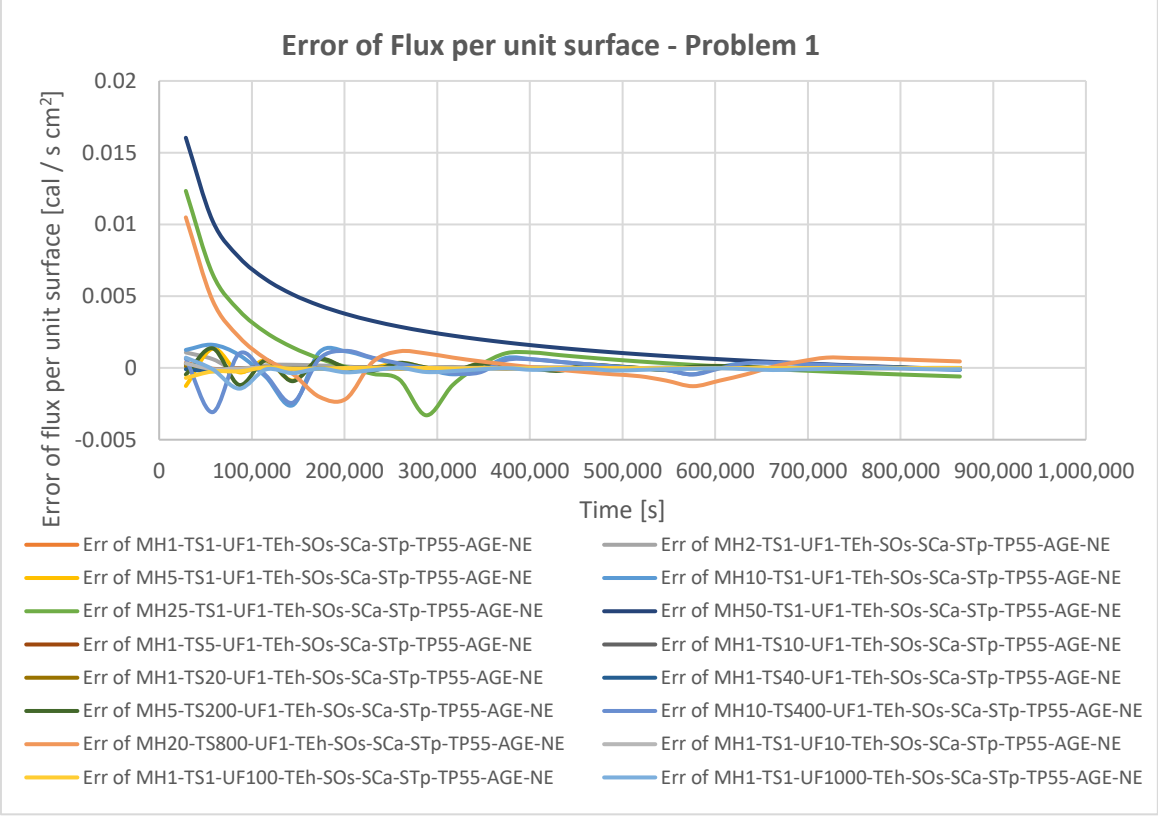

Figure 5.39: Error of flux per unit surface, Problem 1

5.14. Study of the Computing time

The computing time required for the calculation of the model has been analysed for the model MH1-TS40-UF10-TEh-SOs-SCa-STp-TP250-AGE-NE for a thermal time of 10 days. To start this study, some factors which could be suspected *a priori* to affect the computing time were selected. The first factor which could affect the computing time per time step is the temperature gradient, which decreases steadily during the calculation. It could have an influence on the computing time because higher gradients tend to make the model more unstable and further away from equilibrium, so it may take the numerical scheme more time to reach the equilibrium. The temperature gradient, i.e. the temperature difference divided by the distance, from the origin (source location) to the freeze front was chosen as a proxy measure of the overall temperature gradient. The computing time per time step is the computing time which the computer needed to compute one time step of the transient analysis. The temperature gradient defined before is depicted versus the computing time per time step in Figure 5.40, which does not show a clear correlation between them.

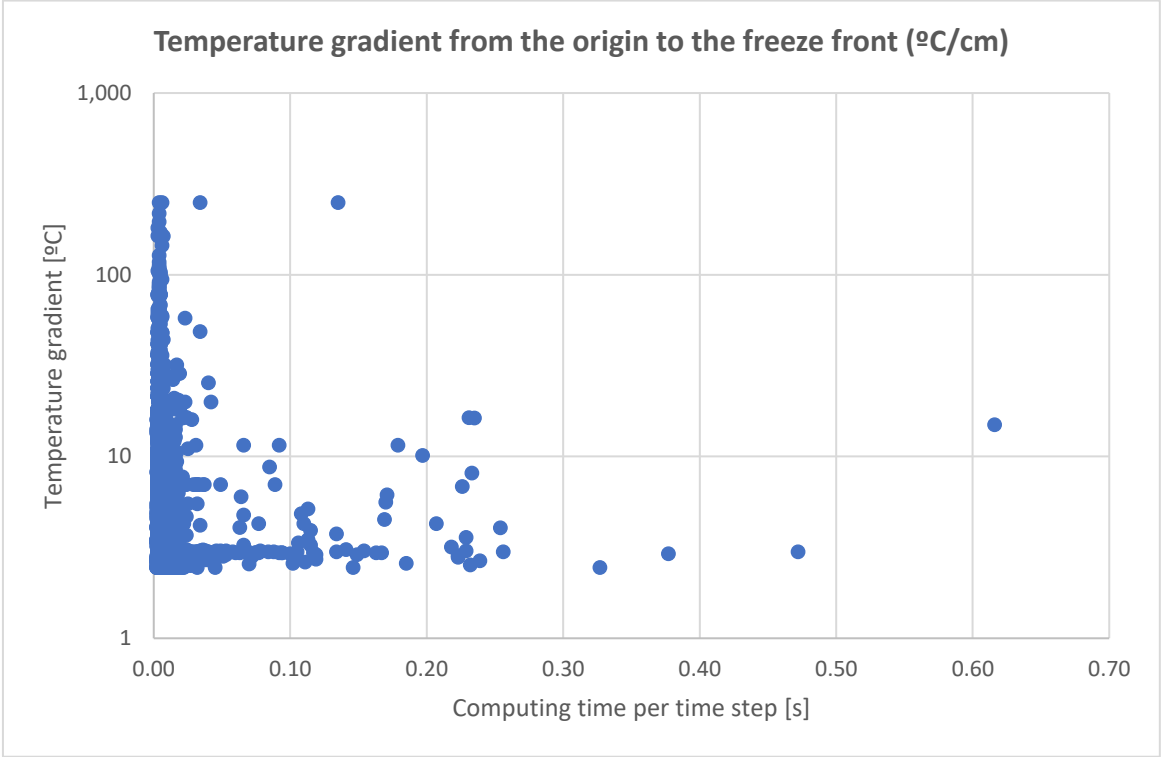

Figure 5.40: Temperature gradient from the origin to the freeze front vs computing time per time step

Another factor that may influence the computing time is the total thermal time the model is run for. The accumulated computing time is presented in Figure 5.41 versus the thermal time. It appears to be a clear linear correlation between them. That is, the computing time per time step (shown in Figure 5.42) does not seem to decrease with the advance of the simulation, but it tends to be stable instead. The average time to compute 1 time step is in the order of 5.59 milliseconds.

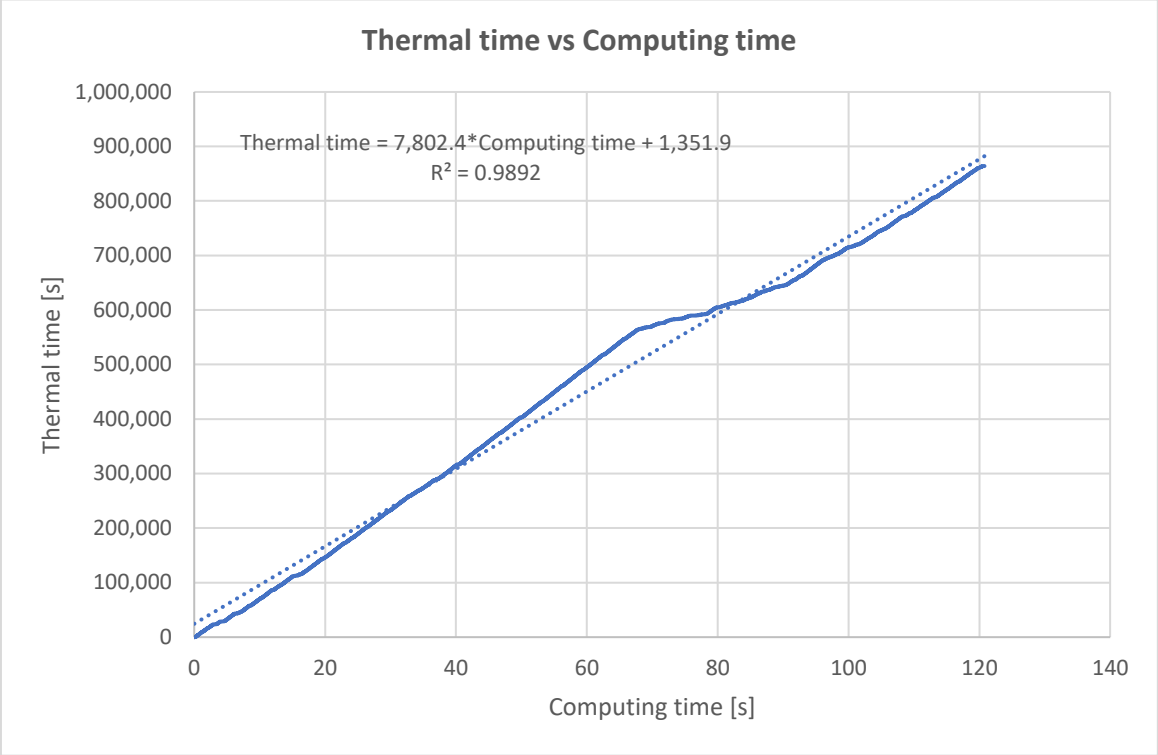

Figure 5.41: Thermal time vs computing time

Yet another factor which *a priori* could be supposed to influence the computing time per time step is the execution or not of the code block which freezes the elements, and the number of elements (zones) changing phase. The time to compute the freeze block for the model with 804 gridpoints (nodes) is about 1 millisecond, which is about 18% of the average computing time per time step. From the model it was observed that there are very slow time steps at intervals, which are caused by the update of the graphs in FLAC3D and the export of data and graphic files. To review the effects of the freeze block execution, a model without export files was computed in order to filter out their effect on the computing time. The computing time per time step and the times where phase change of any zone happened are plotted in Figure 5.42. From this figure, no clear relationship between the phase change happening and a longer computing time in the time step directly afterwards can be derived. There are indeed some time steps which take longer to compute, but they are not necessarily the steps directly after a phase change. Nevertheless, the number of times the freezing status is updated does influence the total computing time, as shown for example in Table 5.9 in chapter 5.5.

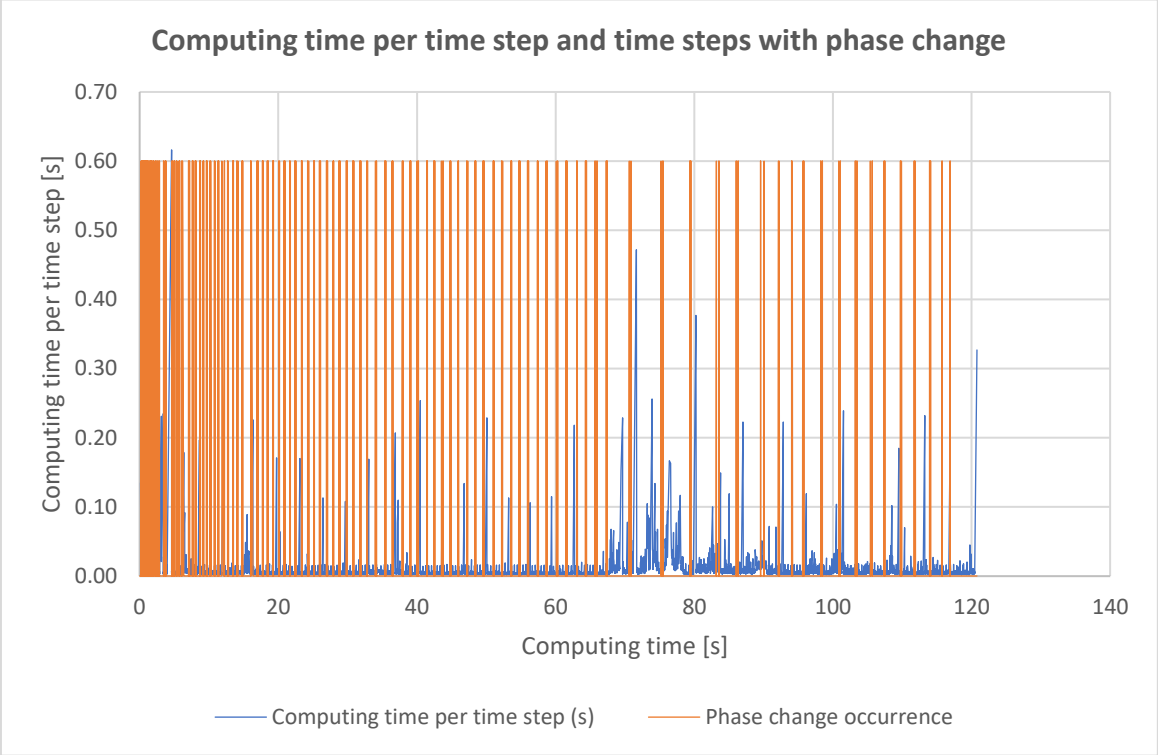

Figure 5.42: Computing time per time step and time steps with phase change occurrence

5.15. Assessment of the accuracy of the numerical model by comparison with Carslaw's solution for the punctual flux source

In this chapter, the solution of Carslaw and Jaeger (1959) presented in chapter 3.2.3 is taken as an additional benchmark against which the results of the numerical model are compared. An overview of the model employed, which makes use of the radial symmetry of the problem and has a mesh size of 1 cm in the area near the cooling source, is presented in Figure 5.43.

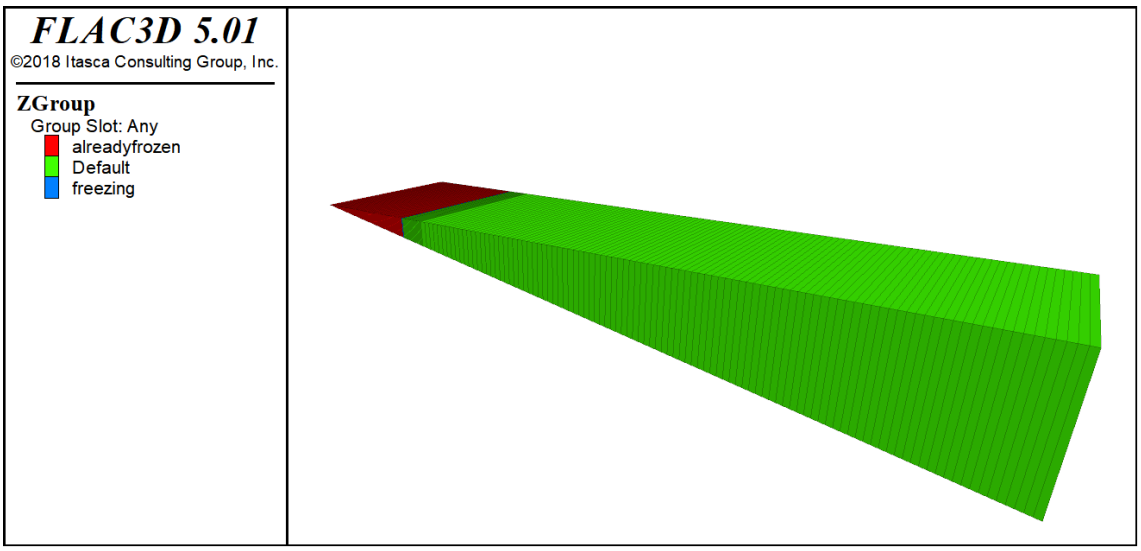

Figure 5.43: Cylindrical model with constant-flux source

The material properties and boundary conditions of Problem 1 were used. A constant flux of 1 $cal/(s \cdot cm)$ at the axis of the cylinder was considered. This boundary condition is applied in the numerical model as punctual sources in the two nodes located in the axis. As the cylinder section is 1 cm thick and spans an angle of 10º, the punctual sources used have a value of $\frac{1}{\left(2 \cdot \frac{360}{10}\right)} = 0.0139\ cal/s$ for each of the two nodes in the axis.

The numerical and analytical results for the temperature profile along the cylinder radius after 10 days are shown in Figure 5.44. The temperature-time graphs are presented in Figure 5.45. The accuracy of the numerical model is considerably lower than for the Neumann problem considered in the previous chapters. For example, the temperature at a distance of 10 cm from the source shows errors of about 5ºC after 10 days. One potential reason for these higher errors could be the use of punctual sources, which tend to create instabilities in numerical calculations (analogously to for example punctual forces applied in a structural model). Another reason may be the use of a heat flux source instead of a constant temperature boundary. In fact, according to the analytical solution from Carslaw and Jaeger (1959), the flux source produces a temperature of minus infinite at the cylinder axis, which cannot be correctly represented by a numerical model.

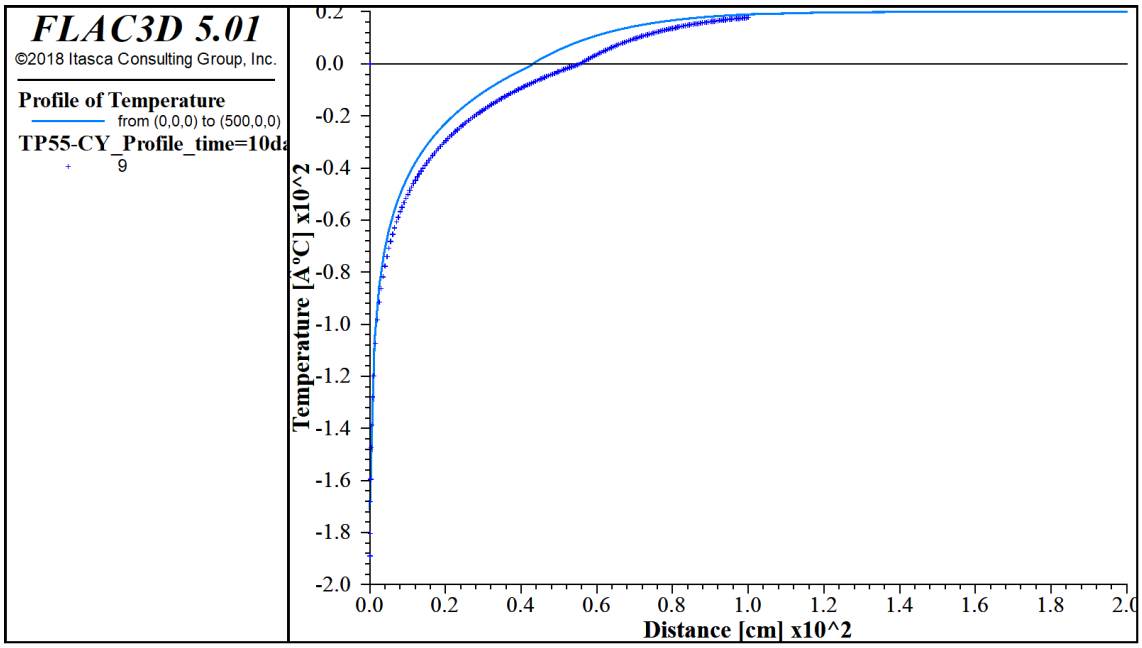

Figure 5.44: Temperature versus distance along the radius, t=10 days, comparison of the numerical results (shown as a continuous line) and analytical results (shown as crosses)

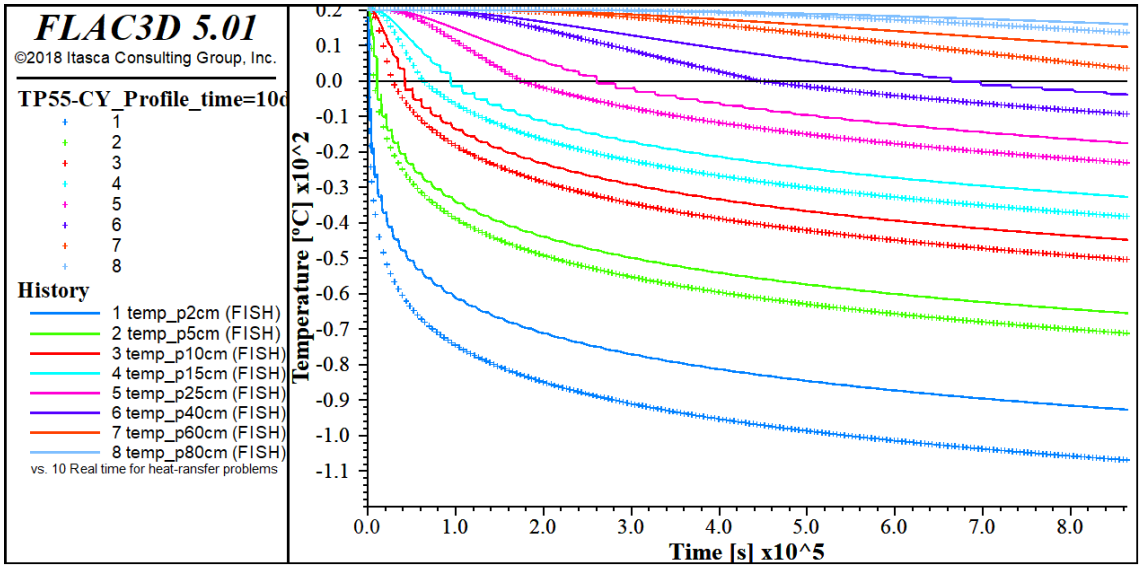

Figure 5.45: Temperature versus time, comparison of the numerical results (shown as a continuous line) and analytical results (shown as crosses)

5.16. Punctual versus surface source

Freeze pipes are sometimes modelled in engineering models as punctual sources in order to simplify the model, see e.g. GEO-SLOPE International Ltd. (2014) and Hentrich and Franz (2015). To evaluate the accuracy of this approach, a single-freeze-pipe problem (Problem 7, defined in chapter 6.1) was simulated with various freeze pipe radii, ranging from 0.1 to 8 cm. Indeed, there are very significant differences in the results: the freezing progress is much slower in the models with smaller freeze pipe diameters (see Figure 5.46). Furthermore, the numerical model with a punctual source (just the two gridpoints at the origin with the fixed source temperature) generated an even slower freeze front progress than the small radii. As an additional benchmark, the analytical solution from Ständer, which has been proved to be very accurate for the single-freeze-pipe problem (see chapter 6), was evaluated for different freeze-pipe radii.

The fact that the models with a smaller freeze pipe radius exhibit a slower freezing progress can be explained because the perimeter of the pipe, which is where the heat transfer to the ground takes place, is linearly proportional to the pipe radius, leading to a slower heat transfer in these models.

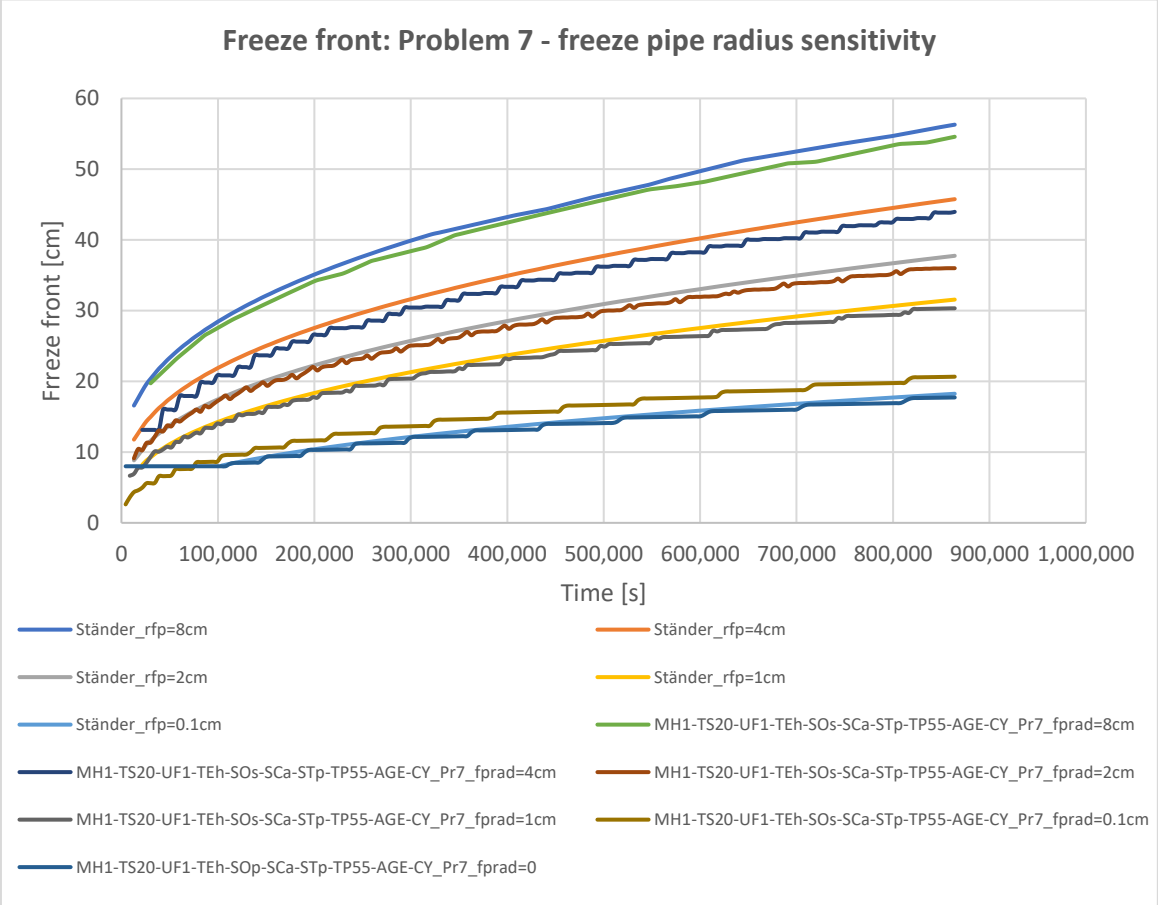

Figure 5.46: Freeze front progress, freeze pipe radius sensitivity (graph origin at r=0)

An additional planar (Neumann) model was run, which can be considered as a model with a freeze pipe of infinite radius. Ständer's solution was computed for a freeze pipe radius of 1 million centimetres (10 km), which is a circle so large that it could be considered a "plane source" and thus matches the Neumann model quite well. To be able to represent the results from this model and to provide an easier comparison of the freezing progress between the different models, Figure 5.47 was created. In this figure, the data from the "plane source model" are displayed together with the same data from the previous figure, but the origin of the graph has been moved to the corresponding freeze pipe radius of each model. In this figure it is again apparent that the freeze pipe radius has a high influence on the freeze wall advance, even when measured from the freeze pipe outwards.

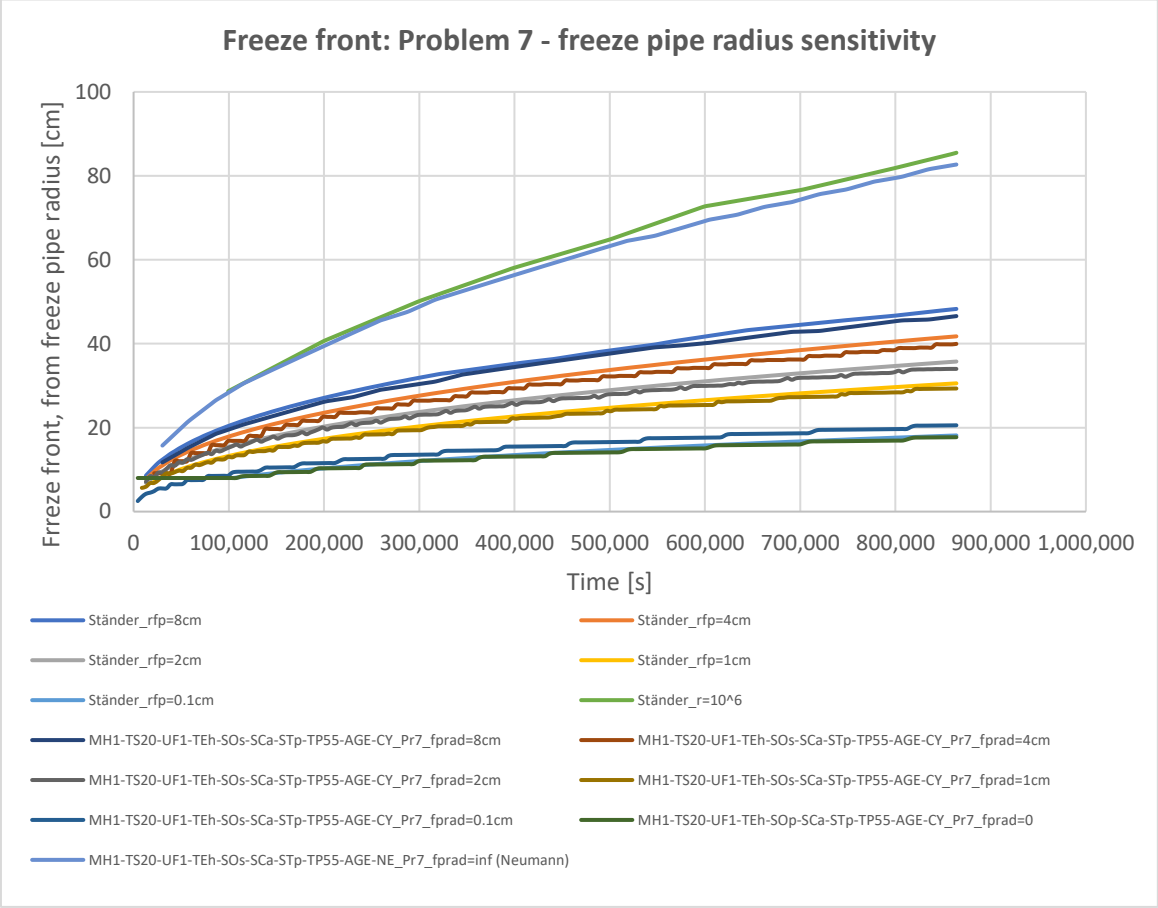

Figure 5.47: Freeze front progress, freeze pipe radius sensitivity (graph origin at r=freeze pipe radius)

5.17. Large-scale engineering model

Until this point, the models evaluated have been of a relatively small scale in order to be able to run a large number of experimental models in a reasonably short time. They have been mainly used to verify the accuracy of the model. However, it could be the case that the custom computing code programmed to simulate the phase change based on the enthalpy method may lead to impractically long computing times for models of the scale typically required for engineering purposes. In order to evaluate the usability of the method for practical engineering cases, a large-scale model with a size of 40x40x100 m and 45 freeze pipes was calculated for a total thermal time of one year. This model could be used for example to simulate a 100 m deep, 8 m diameter, freeze shaft. It was discretised with a large number of gridpoints (540,956) and zones (576,000), although the mesh size is larger than the ones used in the previous chapters. An overview of the model is presented in Figure 5.48, where the freeze circle and the effects of the external model boundaries can be appreciated. The duration of the time steps was between 292 and 1,600 seconds, with a total of 107,430 time steps. Still, the computing time was less than one week, even using a light laptop (see Table 5.4) which is in the low range of the computing capacity nowadays available to professional engineers. This can be considered as a reasonable computing time

for engineering purposes. Consequently, it can be concluded that the enthalpy method as implemented in the custom code can be practicable for large-scale engineering models.

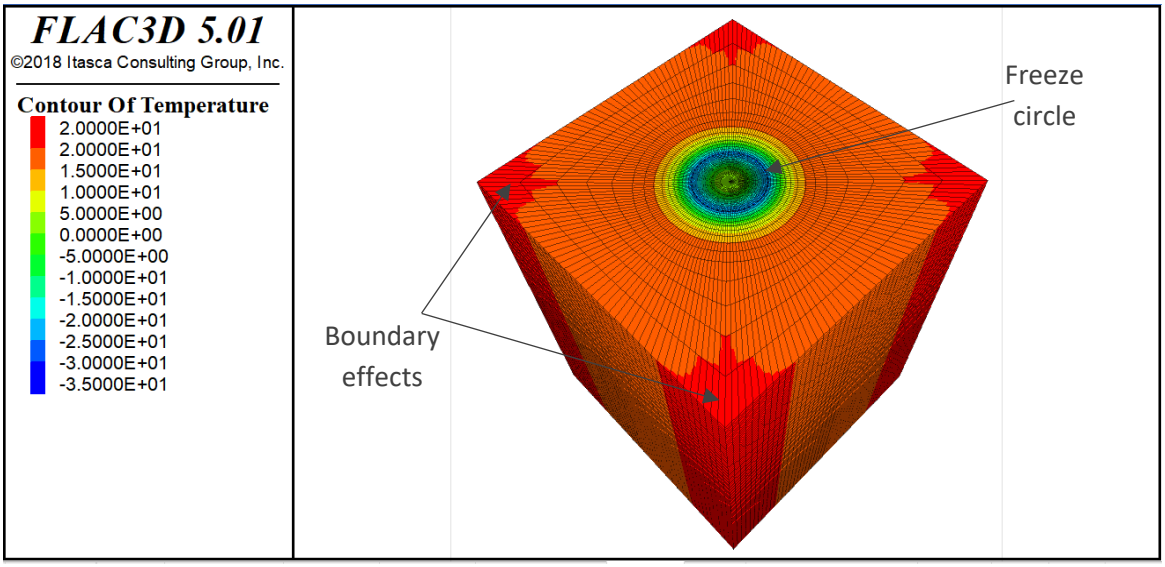

Figure 5.48: Large-scale numerical model, MHxx-TS20-UF1-TEh-SOs-SCa-STp-TP55-AGI-Wall_Pr7c_fulldepth

6. Evaluation of the accuracy and applicability of existing approximate analytical solutions for ground freezing thermal design

According to Lunardini (1981), "[for] approximate methods, the absolute accuracy of the results, […], is unknown without validation", which is why these approximate analytical methods should be validated against either reliable verified numerical models, or controlled experiments. In this chapter, the freeze front positions provided by the five approximate analytical solutions presented in chapter 3.4.1 have been compared to the results from numerical models analogue to the ones verified in chapter 5. Since these analytical solutions just provide the position of the freeze front with respect to time, additional comparisons, e.g. in terms of the temperature evolution versus time or position are not possible.

6.1. Bases of the verification of the analytical solutions

Problems with significantly different boundary conditions which may affect the accuracy and applicability of the analytical solutions have been used to evaluate them. The problems have the material parameters listed in Table 6.1 below, which could be representative of a sandy soil:

Table 6.1: Thermal properties used in Problems 7 to 12

Thermal property	Value
Specific heat capacity (unfrozen)	0.7019 cal/g/ºC
Specific heat capacity (frozen)	0.5256 cal/g/ºC
Thermal conductivity (unfrozen)	0.004545 cal/(s cm ºC)
Thermal conductivity (frozen)	0.007608 cal/(s cm ºC)
Density	2.664 g/cm^3
Water content	0.21 $g_{water}/g_{dry\ soil}$
Latent heat of water	79.71 cal/g
Phase-change temperature	0ºC
Phase change range	0 to -0.1ºC (range of 0.1ºC, simulating an abrupt phase change)

The Problems are defined as follows:

- Problem 7: Base case, with the boundary conditions listed below (representative for ground freezing with brine). The following Problems are variations of this problem, with the indicated changes.
  - Initial temperature: 20ºC
  - Temperature of freeze pipe (source temperature): -35ºC
  - Phase-change temperature: 0ºC

- Problem 8: Case with extreme temperature gradient: initial temperature of 50ºC, freeze-pipe temperature of -200ºC (representative for ground freezing with nitrogen).
- Problem 9: Case with extremely high latent heat 10 times higher than the base case and extreme temperatures as defined in Problem 8.
- Problem 10: Linear case, no latent heat (only 0.5 cal/g latent heat in the liquid phase to prevent the analytical formulae from not working) and extreme temperatures as defined in Problem 8.
- Problem 11: Case with a smaller amount of sensible heat compared to the latent heat: initial temperature of 2ºC.
- Problem 12: Phase-change temperature of -21ºC.
- Problem 13: Same boundary conditions as Problem 7 but with the thermal characteristics of water (comparable to Problem 1 but with different geometry, cylindrical geometry instead of planar).

A freeze pipe radius of 8 cm was chosen, which is in the order of magnitude of the freeze pipes which are used in real projects. The model length (the radius of the outside boundary) is 500 cm for the models which were run for a thermal time of 10 days and 5,000 cm for the ones run for 365 days.

The numerical parameters used were a mesh size of 1 cm and a time step of 20 s (model names MH1-TS20-UF1-TEh-SOs-SCa-STp-TPxx-AGE-CY), whose results have been proven to be sufficiently accurate by comparison with Neumann's exact solution in chapter 5.4. It was also established that for these parameters the numerical model converges to the exact solution. Moreover, the errors of the model in the prediction of the freeze front location for Problems 1 to 3 were small, between 0.2 and 0.6 cm. For the calculations with a thermal time of 365 days, the freeze block of the model was updated only every 100 steps (model names MH1-TS20-UF100-TEh-SOs-SCa-STp-TPxx-AGE-CY), which should also be sufficiently accurate, considering the results in chapter 5.5. The geometry of the model is presented in Figure 6.1.

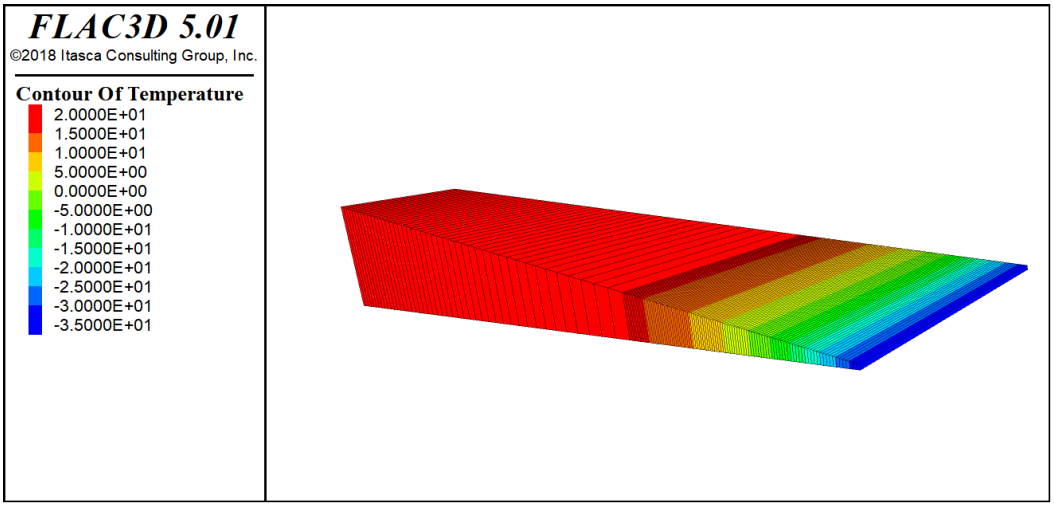

Figure 6.1: Geometry of the cylindrical sector (angle 10º) used in FLAC3D

6.2. Evaluation of the accuracy of the analytical solutions: single freeze pipe

6.2.1. Preliminary model check

In order to reduce the computing time, a model of reduced size (with the geometry of a circular sector instead of the whole circle, see Figure 6.1), which exploits the radial symmetry of the problem, was used in the following chapters. A preliminary check was conducted in order to confirm that its results are very similar to those which would be obtained by using a larger model (e.g. a cylinder quarter, see Figure 6.2). For the freeze front, the results obtained from both models match up to the order of accuracy of the numbers exported, so there is no doubt that the reduced model shown in Figure 6.1 can be used from here on.

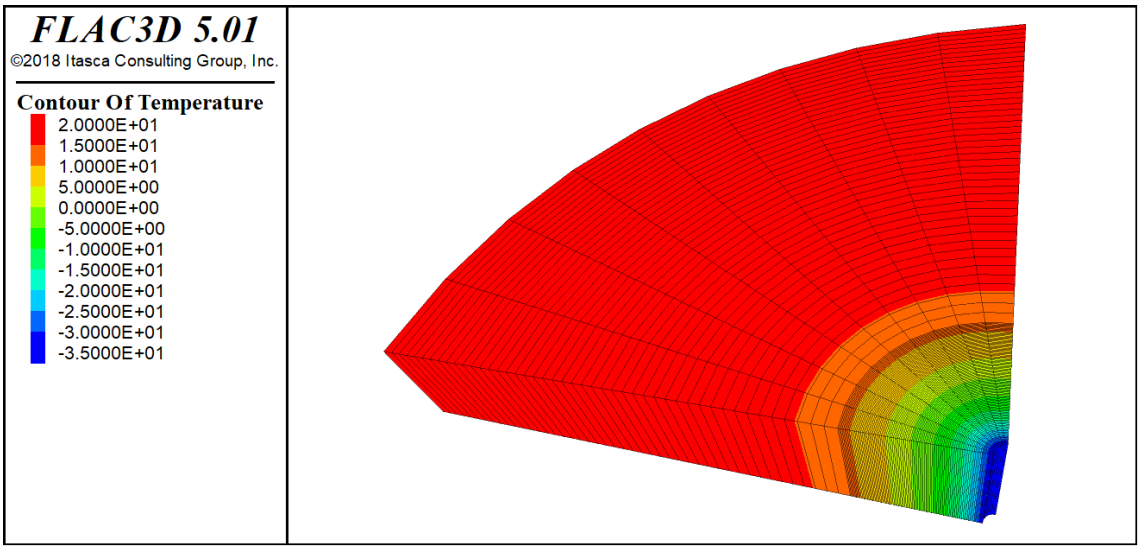

Figure 6.2: Quarter-of-cylinder model

6.2.2. Problem 7: Base case

This problem may be considered representative for brine ground freezing. The progress of the freeze front during the first 10 days according to the analytical and numerical models is presented in Figure 6.3. It is apparent that the Leibenson solution widely overestimates the freeze front advance, which can be explained considering that this solution neglects the sensible heat in the unfrozen area. The Lunardini and Khakimov solutions both underestimate the advance of the freeze front. The Sanger & Sayles and Ständer solutions appear to be the most accurate ones, with an error of just a few centimetres.

However, the situation changes when a time period of 1 year is considered (Figure 6.4). In fact, Ständer's and Khakimov's solutions are still very near to the numerical results (their errors being below 9 cm), but Sanger & Sayles' solution clearly overestimates the freezing progress. It can be observed in Figure 6.5 and Figure 6.6 that the relative errors of Ständer's and Khakimov's solutions appear to be bound for this Problem (i.e. they do not grow with

time or increase slowly, see also Figure 6.5 and Figure 6.6), whereas the errors of the other three solutions significantly grow with time.

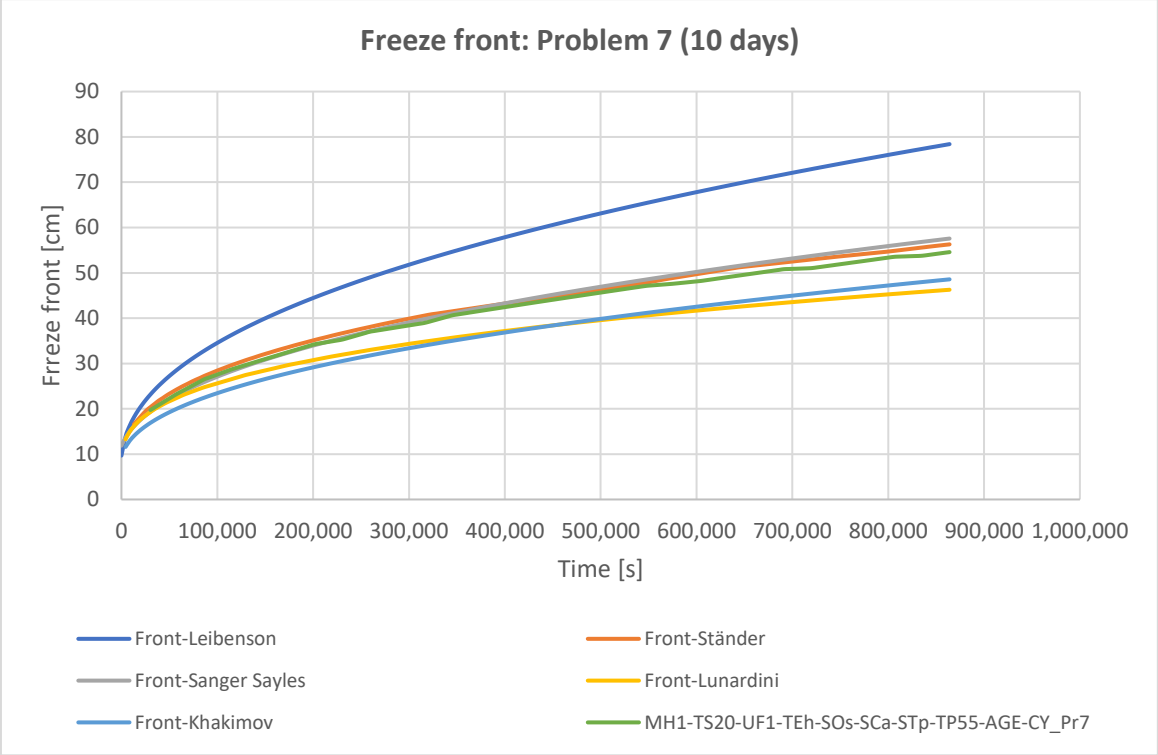

Figure 6.3: Single freeze pipe: freeze front progress, 10 days, Problem 7

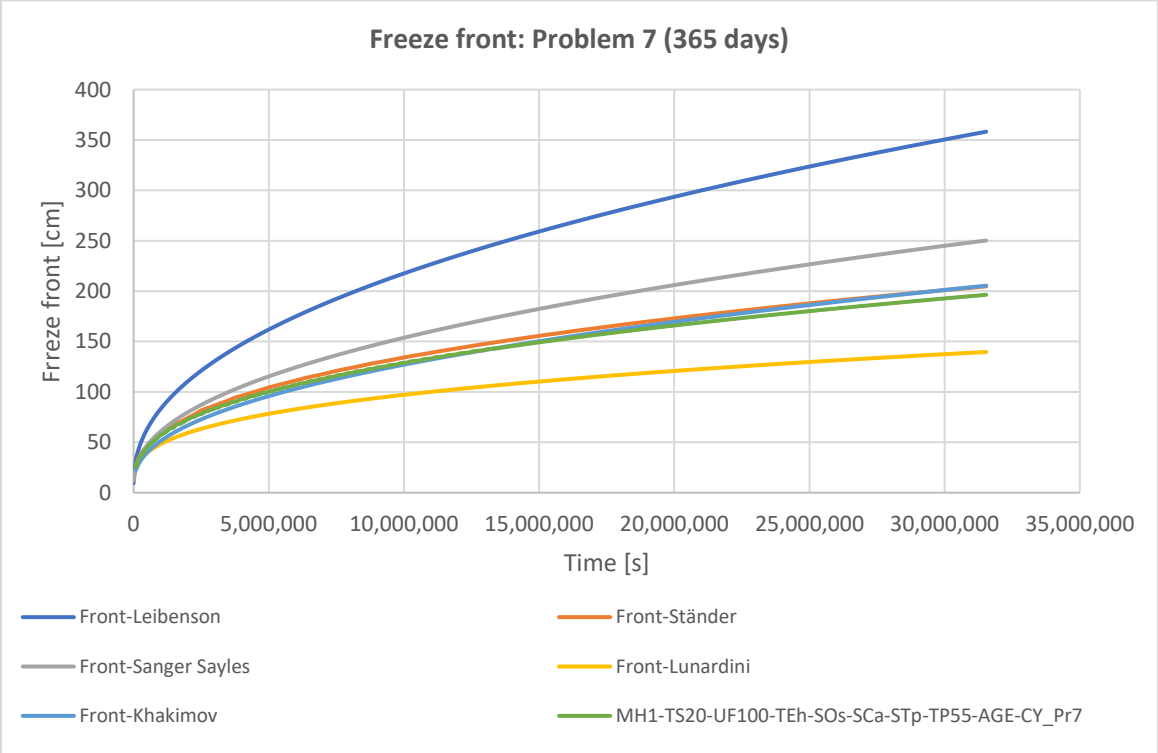

Figure 6.4: Single freeze pipe: freeze front progress, 365 days, Problem 7

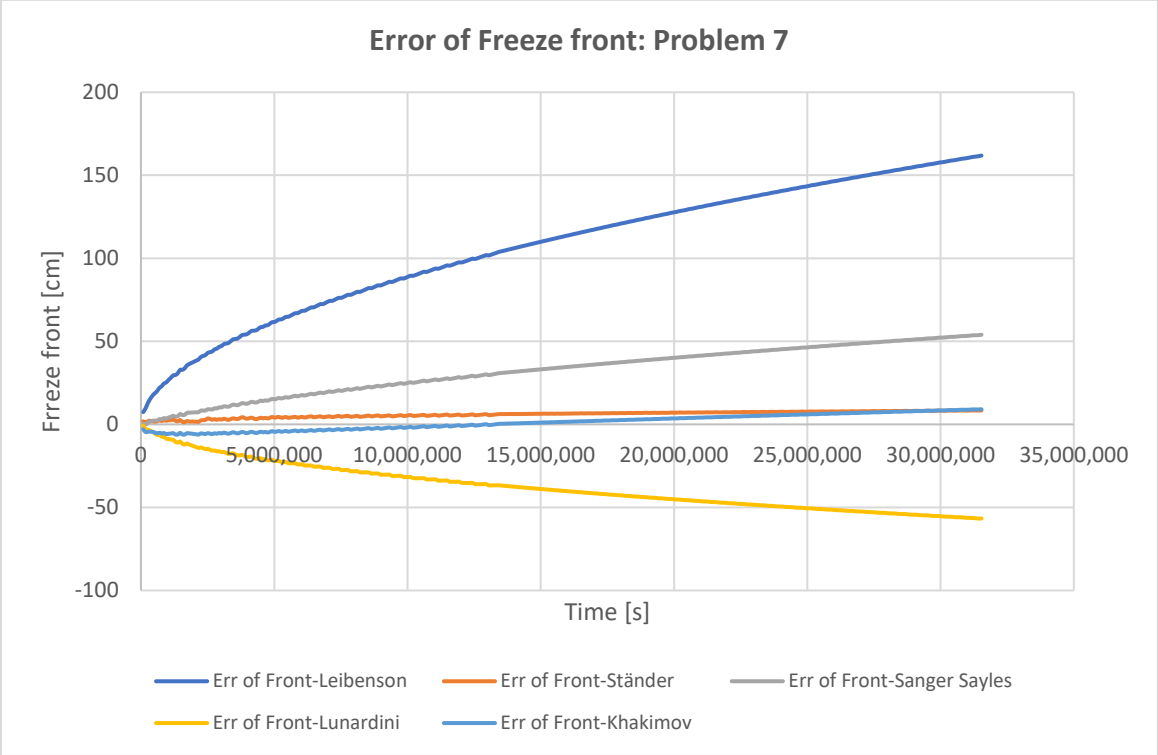

Figure 6.5: Single freeze pipe: error of freeze front progress, Problem 7

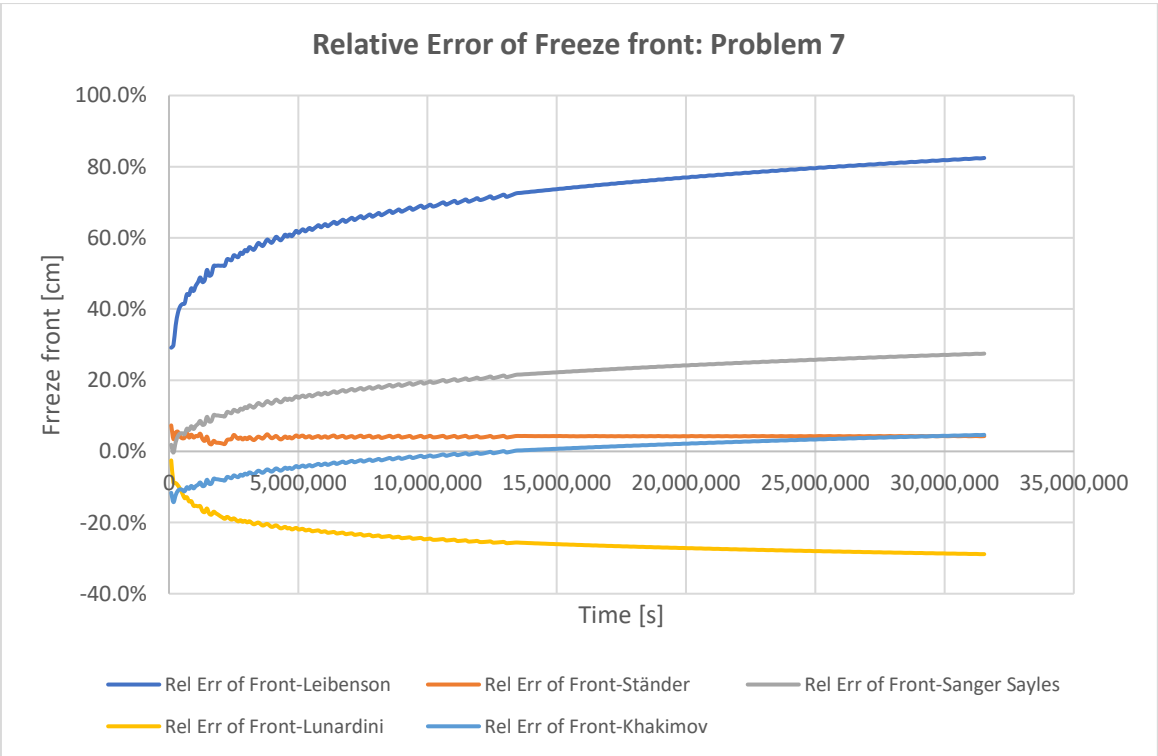

Figure 6.6: Single freeze pipe: relative error of freeze front progress, Problem 7

6.2.3. Problem 8: Case with extreme temperature gradient

This problem has been chosen to evaluate the usability of the analytical solutions for extreme temperature gradients, which may appear for example if nitrogen ground freezing is applied. In this case (see Figure 6.7), Ständer's solution is still the most accurate one (average error of 5.5 cm) and Sanger & Sayles' solution is also quite accurate (average error of 11.3 cm). Considering that the results of the numerical model indicate a freeze front position at 404 cm after 365 days, the relative errors are in the range of 1 to 3%, which is generally good enough for engineering purposes. The absolute errors of these two solutions appear not to grow with time. Khakimov's solution, on the contrary, largely underestimates the freezing progress. Leibenson's solution still has the largest errors, giving a freezing progress which is nearly twice faster than the numerical solution. Lunardini's solution works similarly to the previous case, with an average relative error of -30.8%.

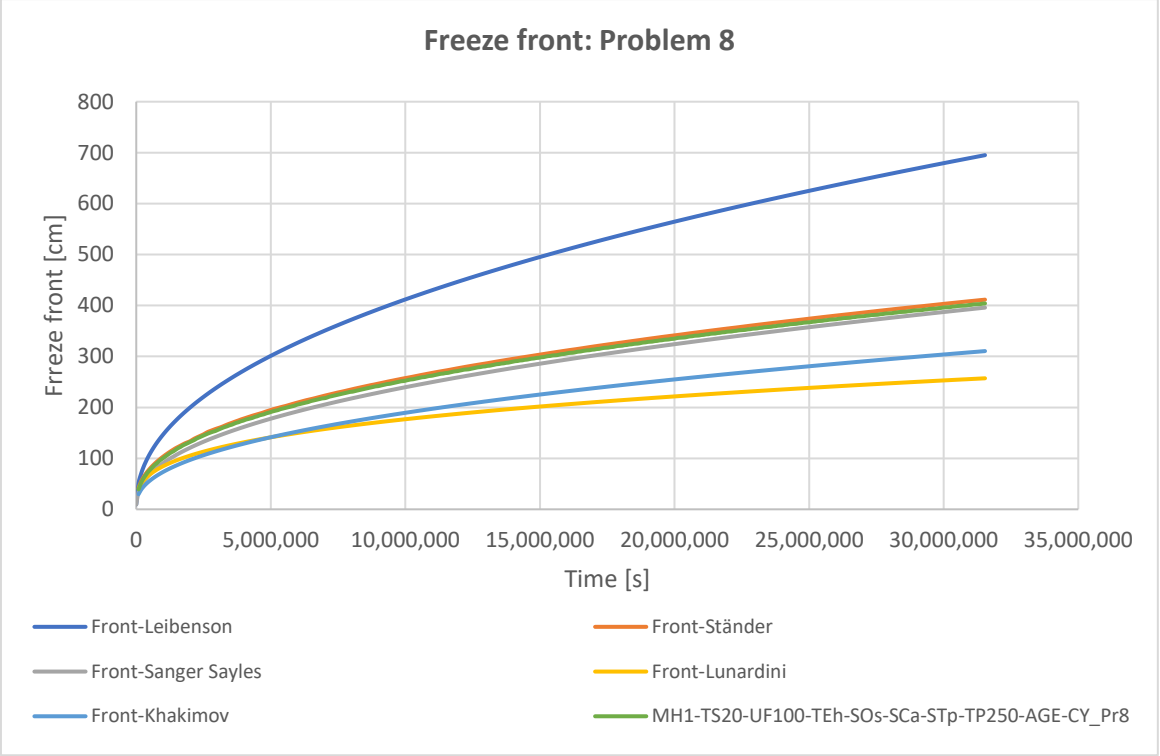

Figure 6.7: Single freeze pipe: freeze front progress, Problem 8

6.2.4. Problem 9: Case with extremely high latent heat

Problem 9 has been chosen to evaluate the sensitivity of the analytical solutions to the extreme case of very high latent heat. The errors for this case are somewhat smaller for most of the solutions, probably due to the fact that the sensible heat to be absorbed by the unfrozen phase between the start of the freezing process and the phase change is smaller in relation to the amount of latent heat released than in Problem 8, which was analysed in the previous chapter. Indeed, sensible heat is absorbed by the unfrozen phase between the initial and the phase-change temperature, before the material starts freezing.

A lower sensible heat to be absorbed from the unfrozen phase, as in this Problem 9, improves the accuracy of the analytical formulae if they do not correctly account for this sensible heat, which is a common problem, see e.g. Ständer (1967). This effect is especially pronounced for Leibenson's solution, for the reason that it completely neglects the sensible heat of the unfrozen area. In fact, Leibenson's solution improves its accuracy for Problem 9 with respect to the previous problems in a very significant amount, lowering its error to just above 20%. An overview of the results for Problem 9 is presented in Figure 6.8.

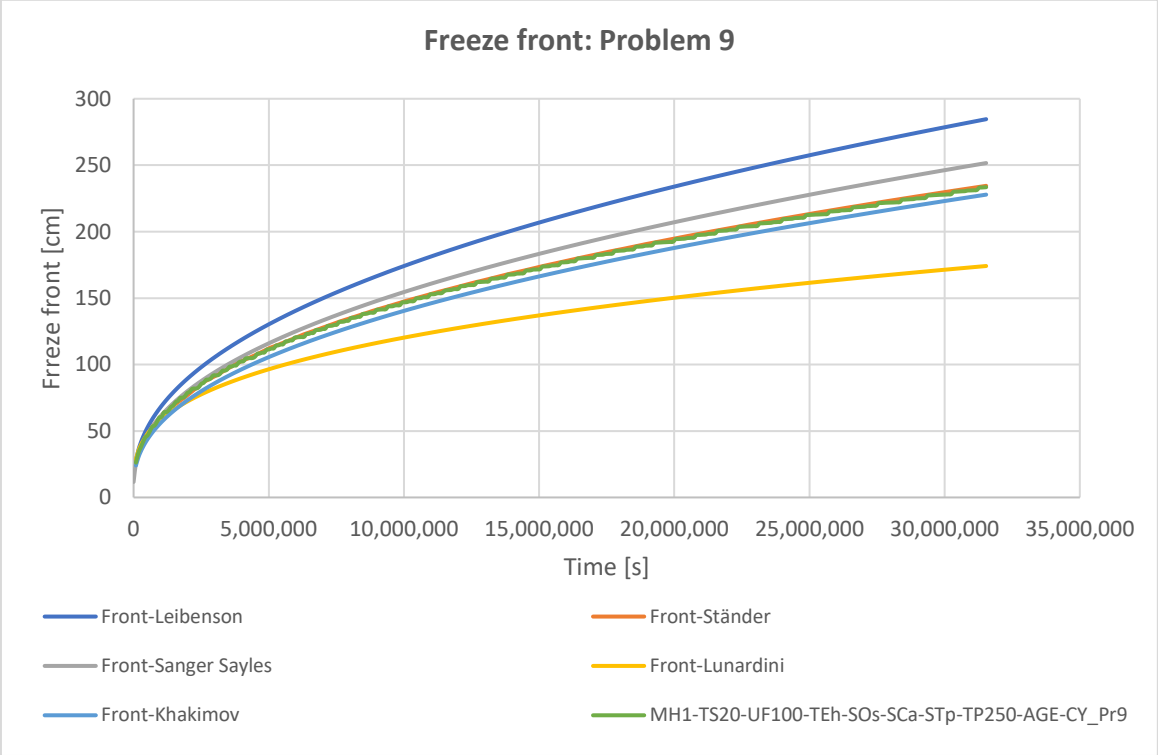

Figure 6.8: Single freeze pipe: freeze front progress, Problem 9

6.2.5. **Problem 10: Linear case (no latent heat)**

This Problem has been defined in order to test the analytical solutions, which were originally generated for phase-change problems, for a case with no latent heat (as described in chapter 6.1, a minimal latent heat of 0.5 cal/g was applied so that the analytical formulae can be computed). In this case, the errors of the Leibenson, Lunardini and Khakimov solutions are higher than in Problem 7, hinting again to the fact that these the formulae do not accurately account for the sensible heat in the unfrozen phase (see Figure 6.9). The Ständer solution again provides very good accuracy (average error of 8.1 cm), and Sanger & Sayles' solution also provides a good accuracy.

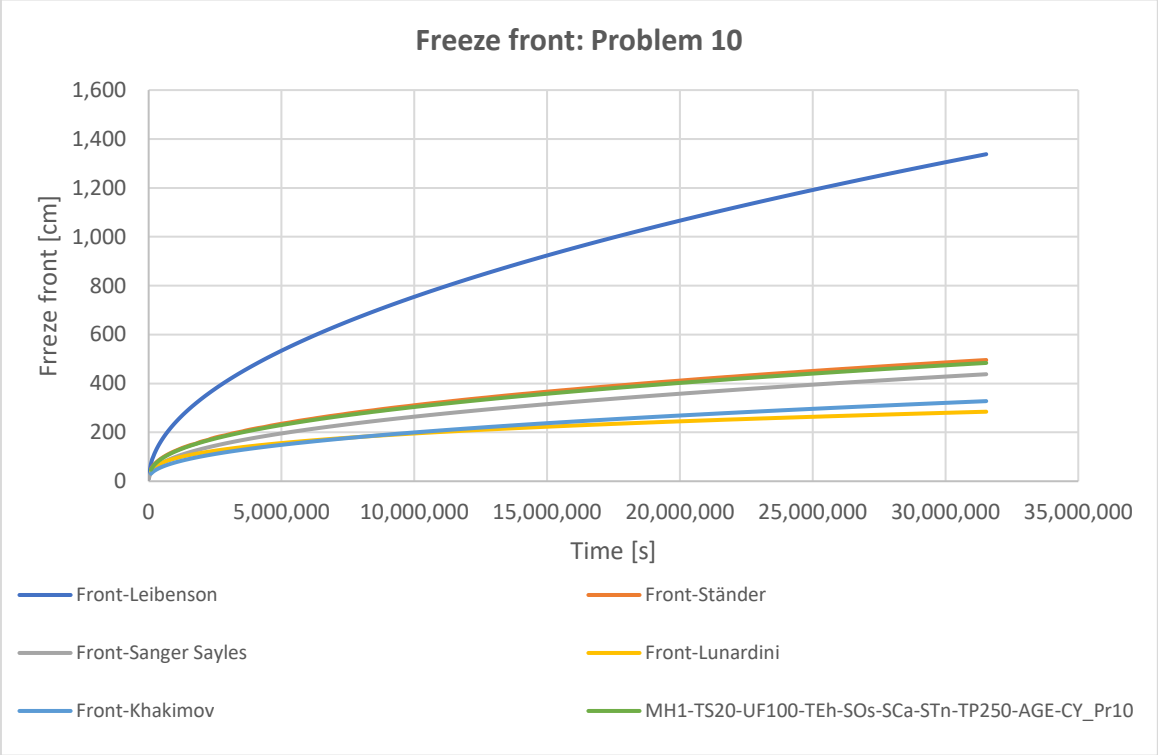

Figure 6.9: Single freeze pipe: freeze front progress, Problem 10

6.2.6. **Problem 11: Initial temperature of 2ºC**

This Problem is representative of brine ground freezing, together with Problem 7, but it serves to test the analytical solutions for a case where the initial temperature is quite near to the phase-change temperature. In this case, the amount of sensible heat to be absorbed by the unfrozen phase before the start of freezing is reduced, and all the solutions studied provide better accuracies than for the previous problems (see Figure 6.10). Again, Ständer's and Sanger & Sayles' solutions provide the lowest and most stable errors, as can be observed from Figure 6.11. It is interesting to highlight that, contrarily to the majority of the solutions considered, the error of Lunardini's solution changes sign, i.e. it overestimates the freezing progress in the first half-year, whereas it underestimates it in the second half-year.

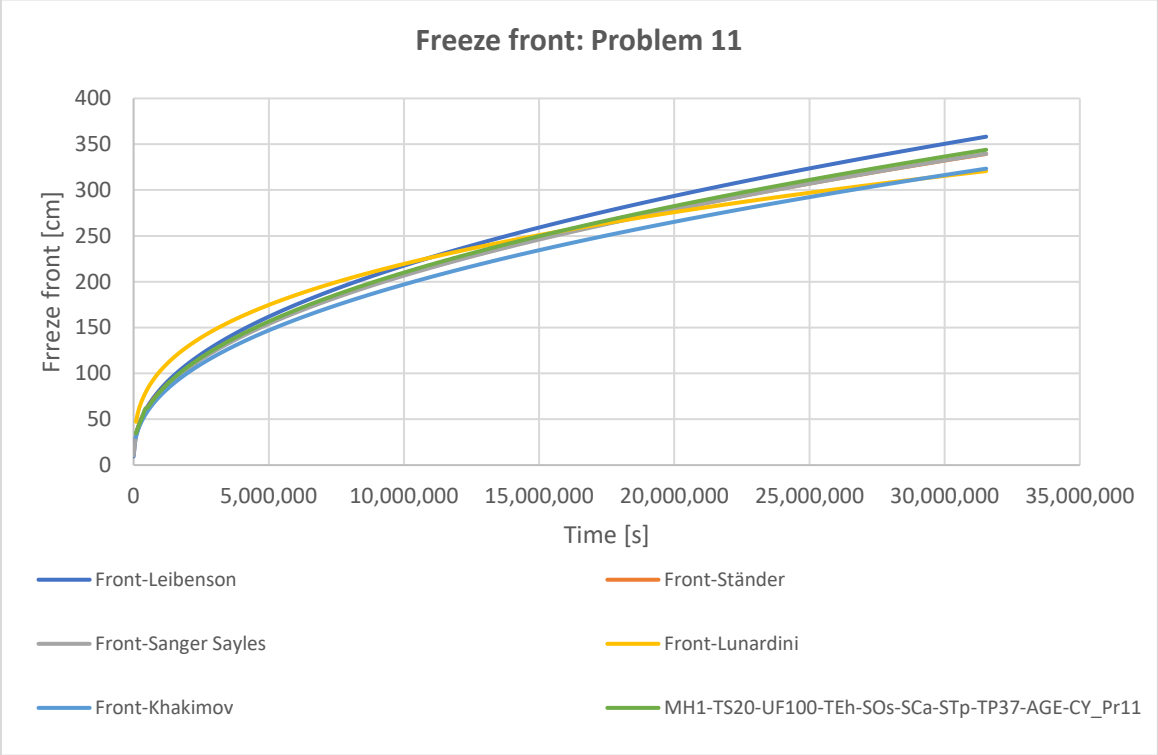

Figure 6.10: Single freeze pipe: freeze front progress, Problem 11

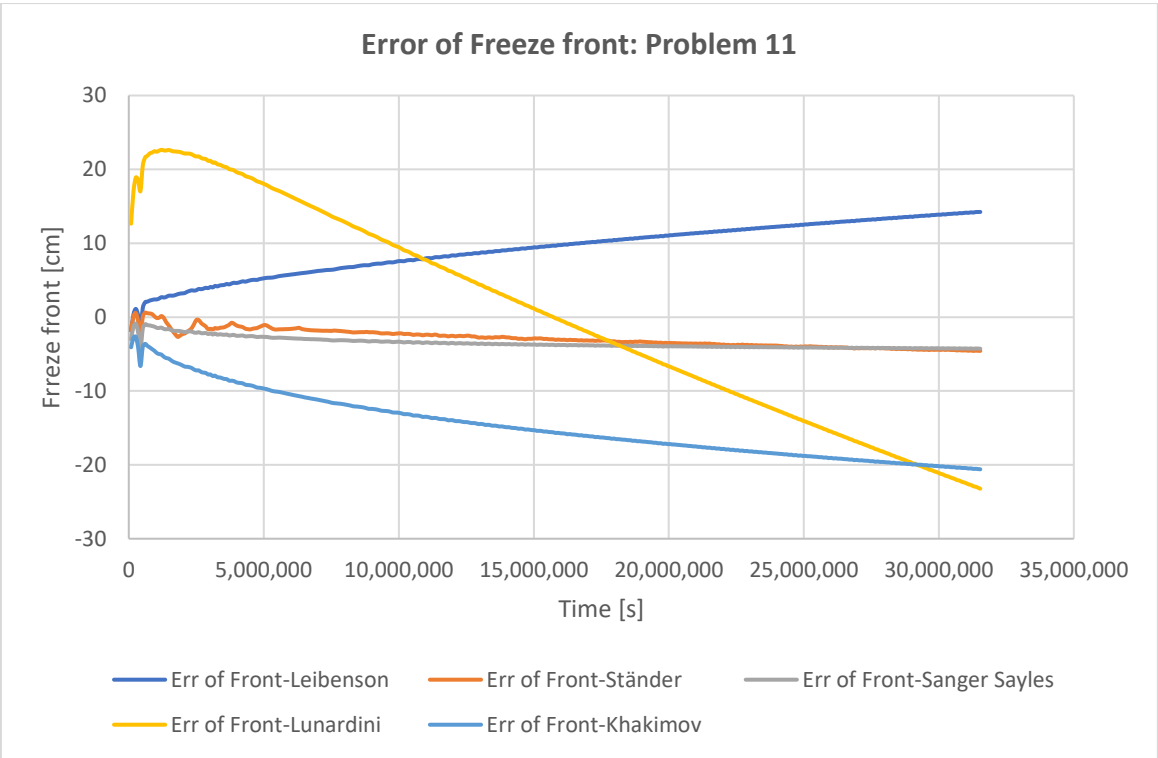

Figure 6.11: Single freeze pipe: error of freeze front progress, Problem 11

6.2.7. Problem 12: Phase-change temperature of -21ºC

This Problem may be representative of brine ground freezing in strata containing salty groundwater, which has a lower phase-change temperature than pure water. In this case, Lunardini's solution is the most accurate one, followed by Ständer's solution, both achieving average errors under 10 cm. However, they both produce relatively high relative errors of more than 25%, which may be because of the higher amount of sensible heat present in the unfrozen phase (because of the larger difference between the initial and phase-change temperatures). The other solutions provide results with extremely high errors (see Figure 6.12).

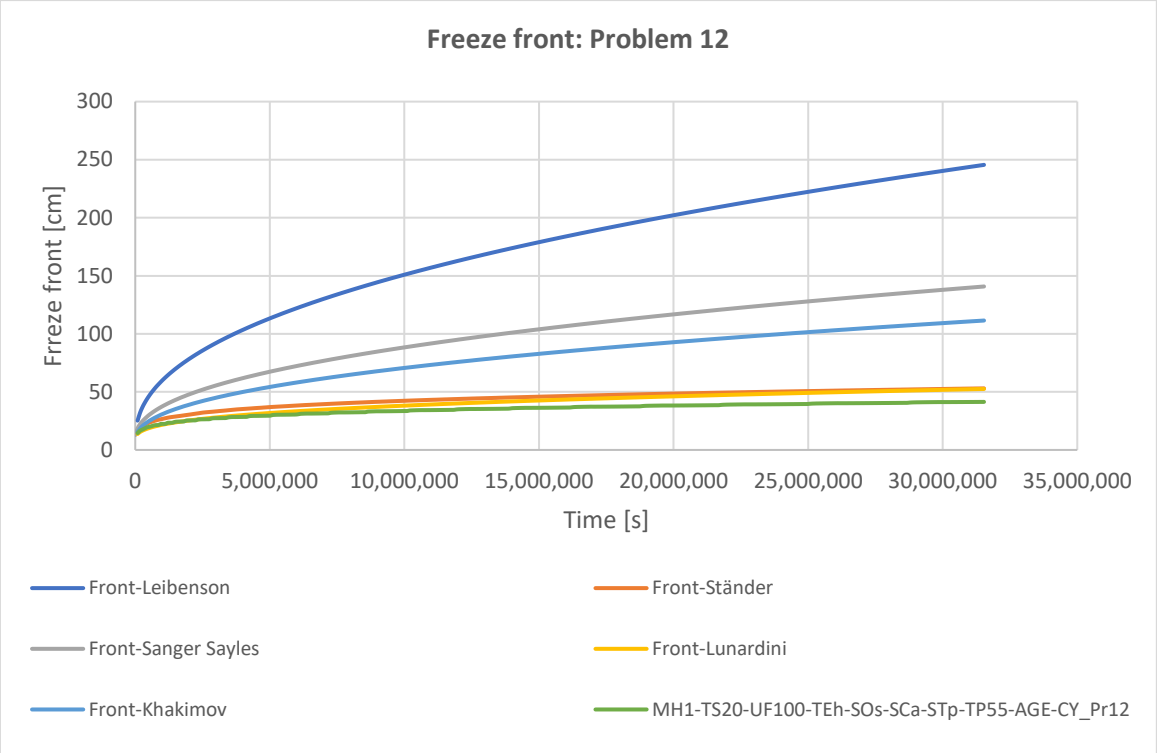

Figure 6.12: Single freeze pipe: freeze front progress, Problem 12

6.2.8. Problem 13: Thermal characteristics of water

This Problem with the thermal characteristics of water was chosen to evaluate the accuracy of the analytical solutions for different thermal properties than the ones used in the previous problems. Ständer's and Sanger & Sayles' solutions are extremely accurate (less than 2 cm average error) in this case. It can be explained because pure water has a much higher proportion of latent heat with respect to sensible heat than the soil whose properties were used in the Problems above. The results for Problem 13 are shown in Figure 6.13.

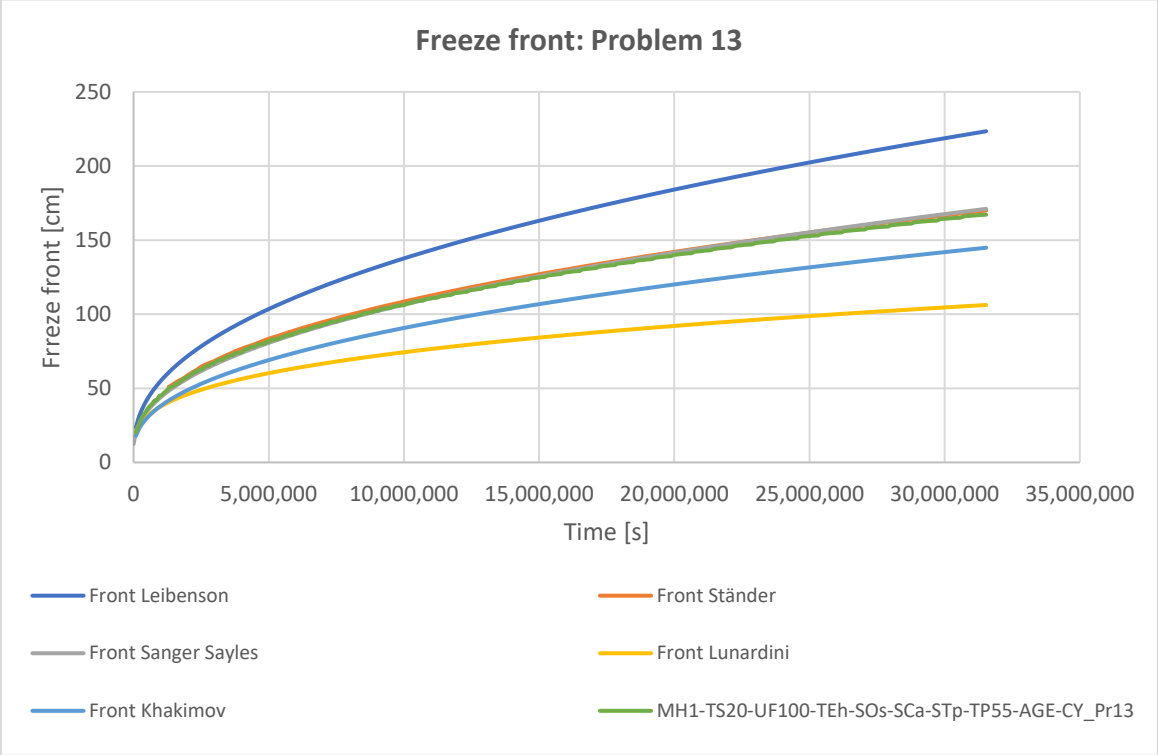

Figure 6.13: Single freeze pipe: freeze front progress, Problem 13

6.2.9. **Comparison of the analytical solutions for the single freeze pipe**

An overview of the accuracy of the five analytical solutions evaluated for the problems previously presented is given in this chapter. It can be observed from Figure 6.14 and Table 6.2 that Leibenson's solution clearly produces the highest errors, while Ständer's solution is consistently the most accurate solution, with average absolute errors of 1 to 10 cm and relative errors lower than 5%, except for Problem 12. Sanger & Sayles' and Khakimov's solutions appear to have accuracies in the same order of magnitude, which vary widely depending on the boundary conditions. Lunardini's solution ranks fourth in accuracy, presenting very variable errors too.

The sign of the errors can be observed in Figure 6.15. It is apparent that Leibenson's, solution generally overestimates the freeze front advance by a large amount, while Lunardini's and Khakimov's solutions tend to underestimate it. Sanger & Sayles' solution under- or overestimates the freezing progress depending on the conditions set in the specific Problem.

A key point to make here is that the errors in the estimation of the freeze front location for a certain time have been considered in this chapter. However, the errors in the estimation of the time to achieve a certain freeze front advance are also of utmost practical significance. For instance, it is important for a design engineer to be able to estimate the required time to achieve the freeze wall thickness required for stability or water-cut purposes. It is essential to notice that for this purpose, due to the shape of the freeze front

versus time curves, the relative errors of the methods are larger than for the freeze front location.

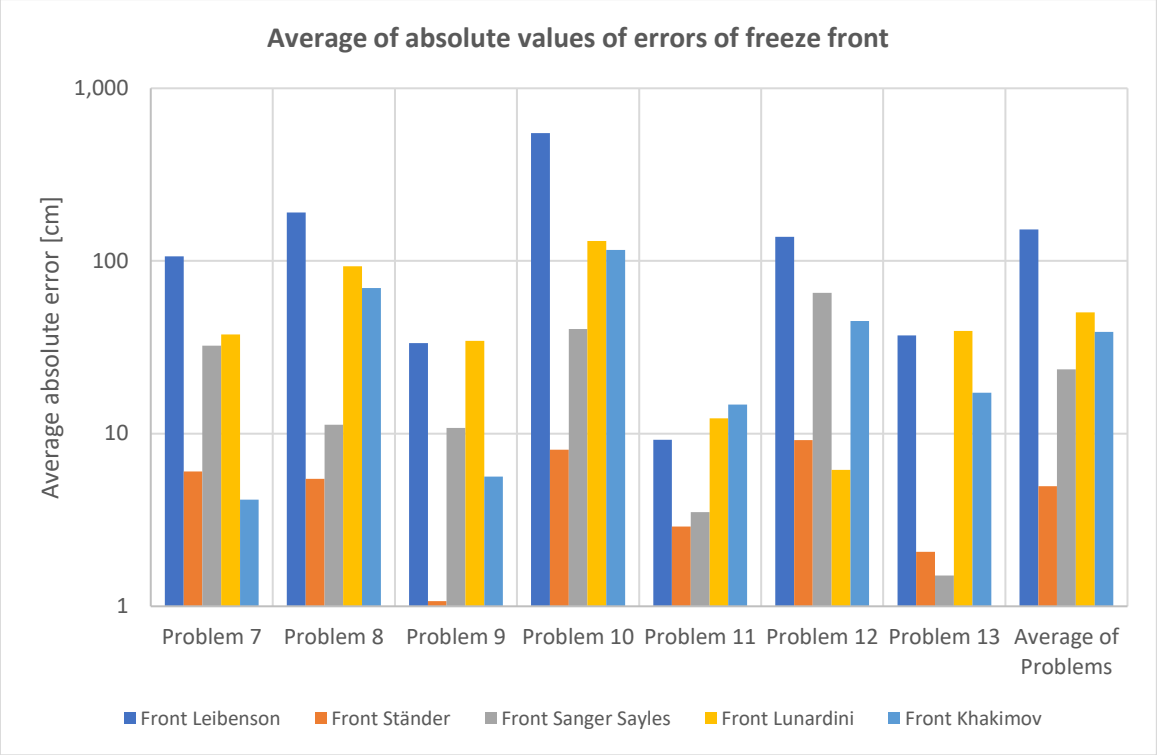

Figure 6.14: Average of absolute values of error in the location of the freeze front, single freeze pipe (logarithmic scale)

Table 6.2: Average of absolute values of errors of freeze front, single freeze pipe, analytical solutions

Average of absolute values of error of X(t)	**Front Leibenson**	**Front Ständer**	**Front Sanger & Sayles**	**Front Lunardini**	**Front Khakimov**	**Average of methods**
Problem 7	106.5	6.0	32.3	37.6	4.2	37.3
Problem 8	191.2	5.5	11.3	93.2	69.7	74.2
Problem 9	33.5	1.1	10.8	34.5	5.6	17.1
Problem 10	549.2	8.1	40.3	130.3	115.6	168.7
Problem 11	9.2	2.9	3.5	12.3	14.7	8.5
Problem 12	137.8	9.2	65.3	6.2	44.9	52.7
Problem 13	37.1	2.1	1.5	39.3	17.3	19.4
Average of the Problems	**152.1**	**5.0**	**23.6**	**50.5**	**38.9**	**53.99**
Median of the Problems	**106.5**	**5.5**	**11.3**	**37.6**	**17.3**	-

As already described in the previous chapters, the Problems where the analytical solutions had the lowest errors were Problems 9 and 11, in which the proportion of sensible heat in the unfrozen region to latent heat released is the lowest. On the other side, the Problem with the highest errors was by far, surprisingly, the linear problem without phase change (Problem 10).

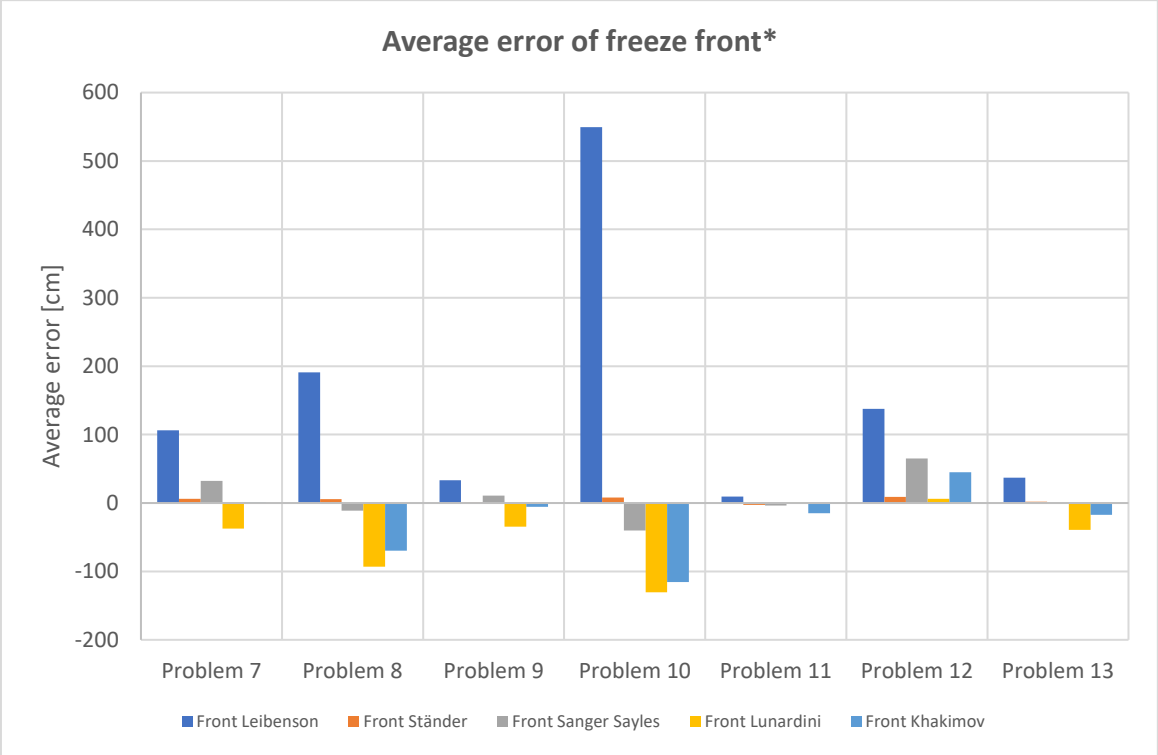

Figure 6.15: Average of errors of the freeze front, single freeze pipe

**Note: The average over time may underestimate the real errors, because negative and positive errors of each problem may be compensated.*

6.3. Evaluation of the accuracy of the analytical solutions: flat freeze wall

In this chapter, the approximate analytical solutions from Ständer and Sanger & Sayles for the freeze wall geometry were compared to numerical simulations performed with analogous models to the ones verified in chapter 5. The implicit method was used to solve these models because the critical time step of the explicit method would be limited by the smallest mesh size, which would imply a considerably longer computing time than with the implicit method. An exemplary image displaying one of the numerical models used, which makes use of the symmetry of the freeze pipe disposition in a freeze wall, can be seen in Figure 6.16.

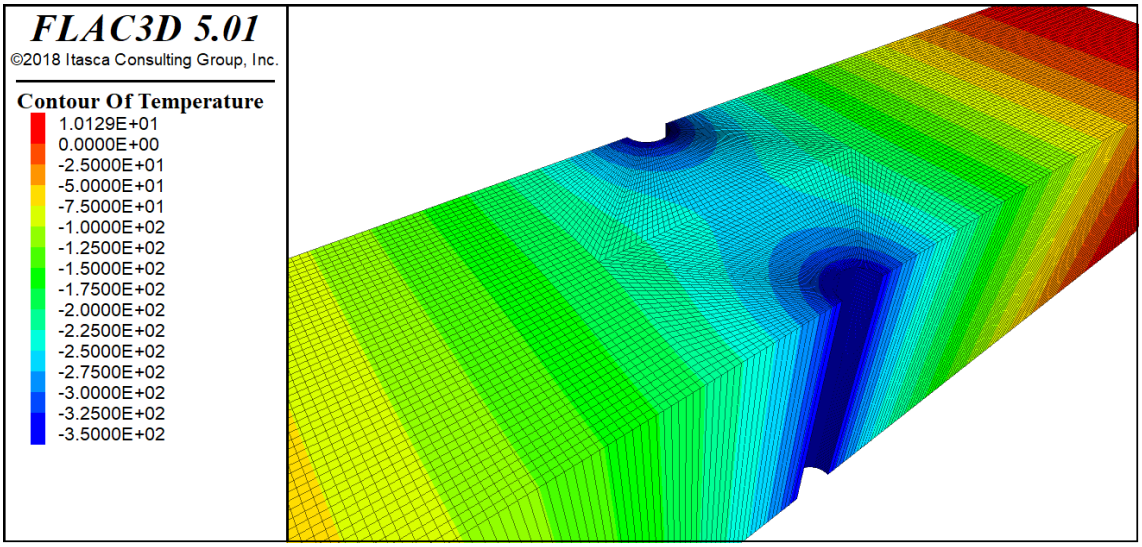

Figure 6.16: Exemplary numerical model for a freeze wall

6.3.1. **Simulated problems - flat freeze wall**

These problems use the same parameters, material characteristics and boundary and initial conditions of Problems 7 to 13 presented in chapter 6.1, but with the freeze wall geometry instead of the single pipe. They are therefore named Problems 7_fw to 13_fw. The separation between freeze pipes was defined as 1 m, which is in the typical order of magnitude for engineering projects.

The results for Problem 7_fw from the numerical simulation, Ständer's solution and Sanger & Sayles' solution are shown in Figure 6.17. It is apparent that the results derived from Ständer's solution coincide very accurately with the results from the numerical model. On the other hand, Sanger & Sayles' solution has an error of about 22% in this case, which may be too high for practical uses.

In Problem 8_fw, the numerical results show a step characteristic of the enthalpy method as a result of the freeze front reaching the area with coarser mesh, however, this does not reduce the overall validity of the comparison with the analytical solutions.

Both Sanger & Sayles' and Ständer's solutions were computed considering the closure time of the freeze wall, which was computed with their respective solutions for the single-freeze-pipe problem.

The following figures 6.17 to 6.23 show the results of the problems calculated for the freeze wall. In general, Ständer provides more accurate results than Sanger & Sayles. A further overview of the results for the different problems is presented in chapter 6.3.2.

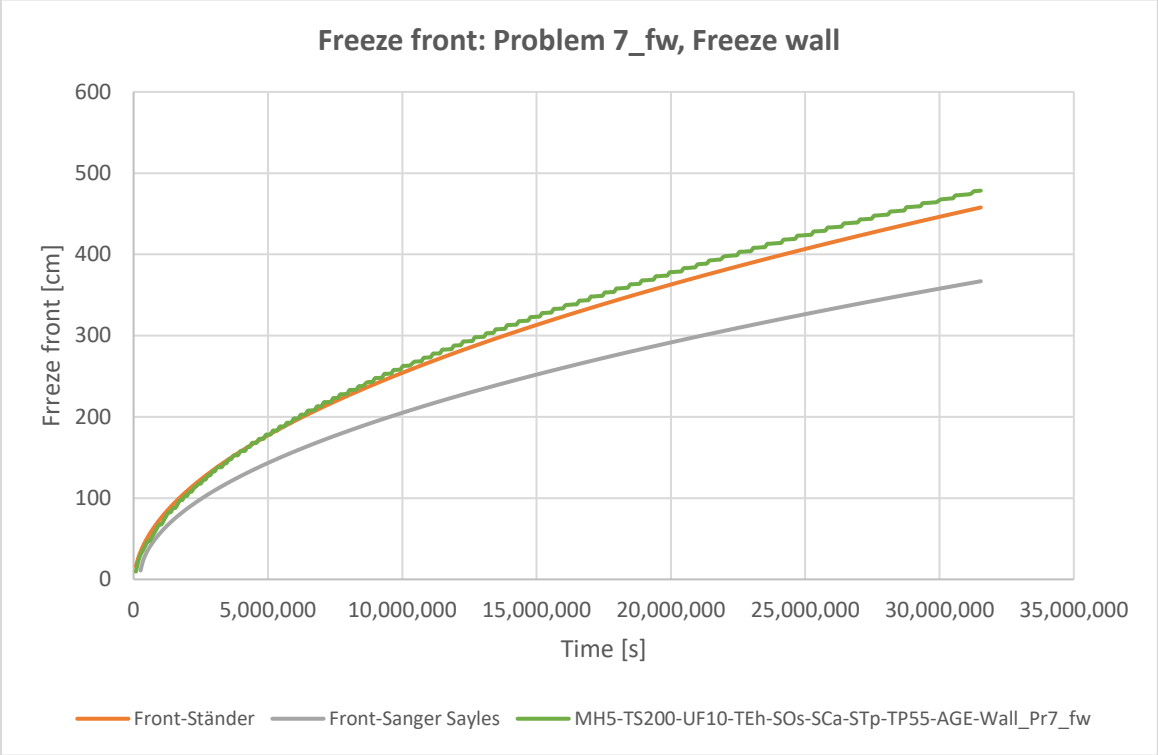

Figure 6.17: Freeze wall: freeze front progress, 365 days, Problem 7_fw

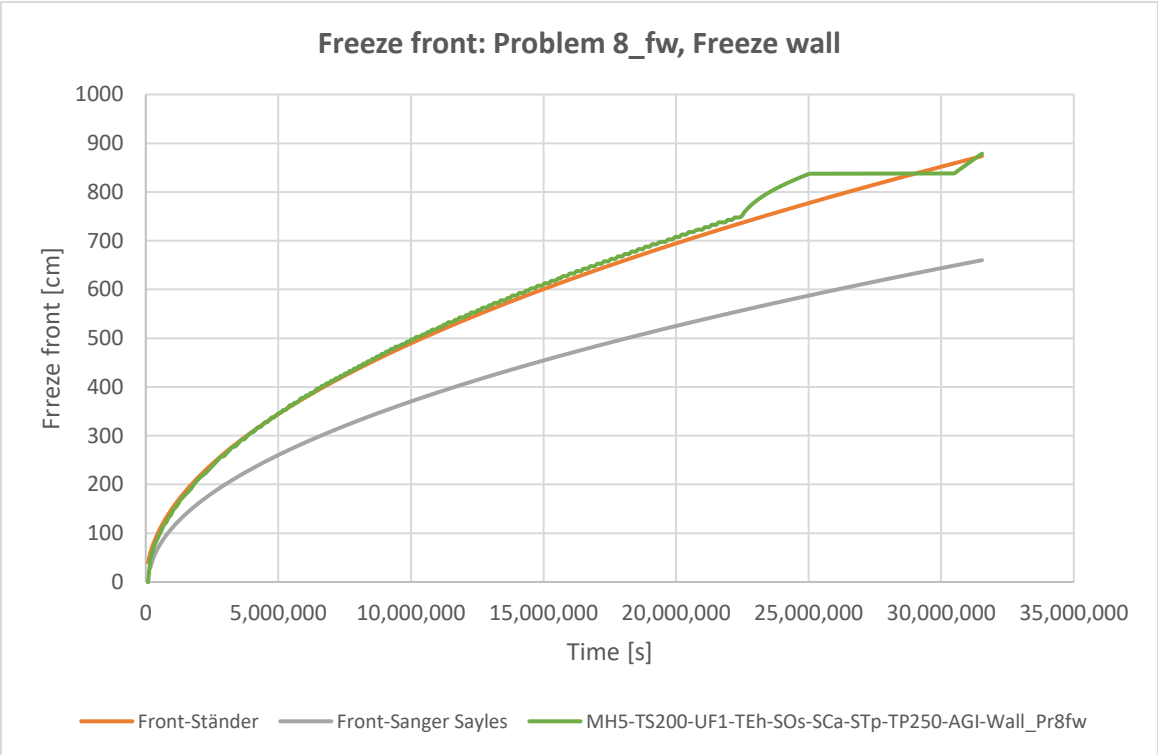

Figure 6.18: Freeze wall: freeze front progress, 365 days, Problem 8_fw

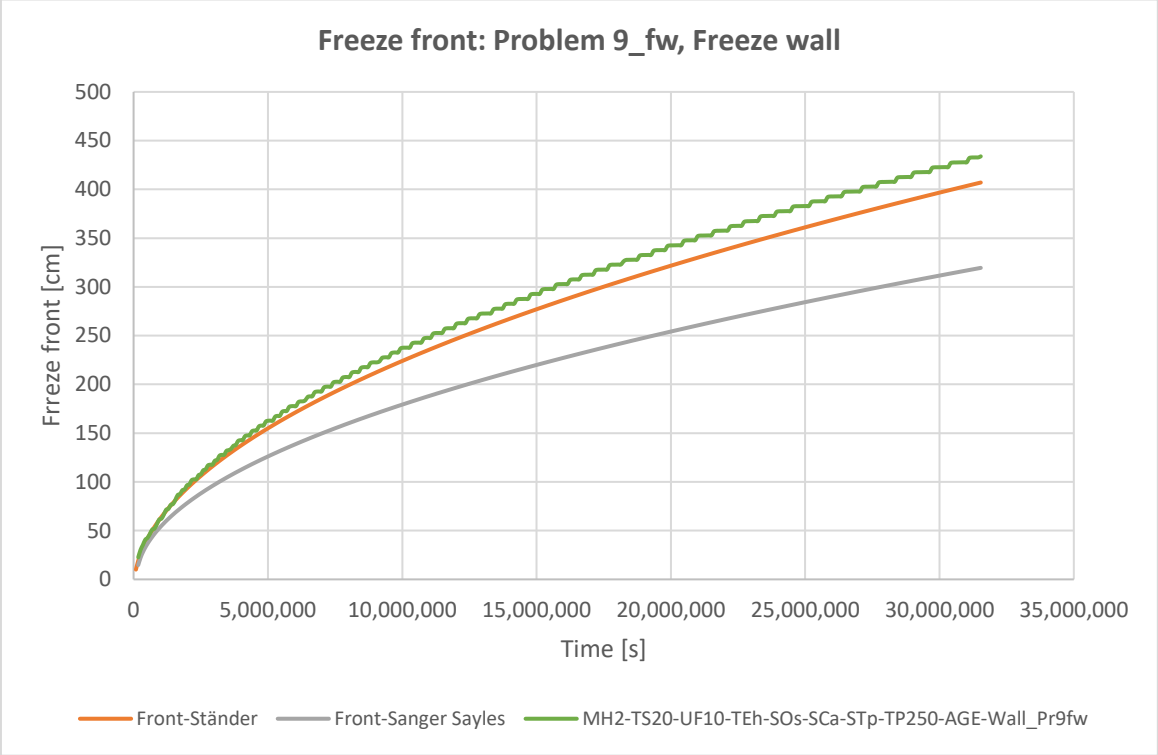

Figure 6.19: Freeze wall: freeze front progress, 365 days, Problem 9_fw

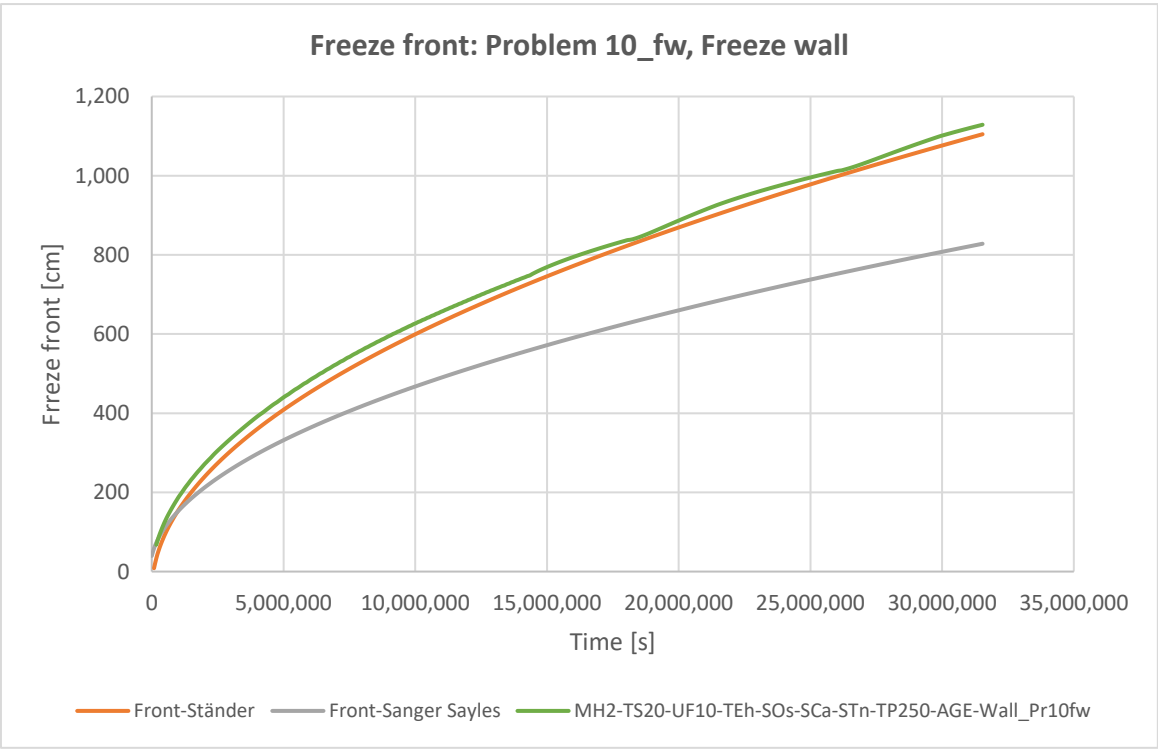

Figure 6.20: Freeze wall: freeze front progress, 365 days, Problem 10_fw

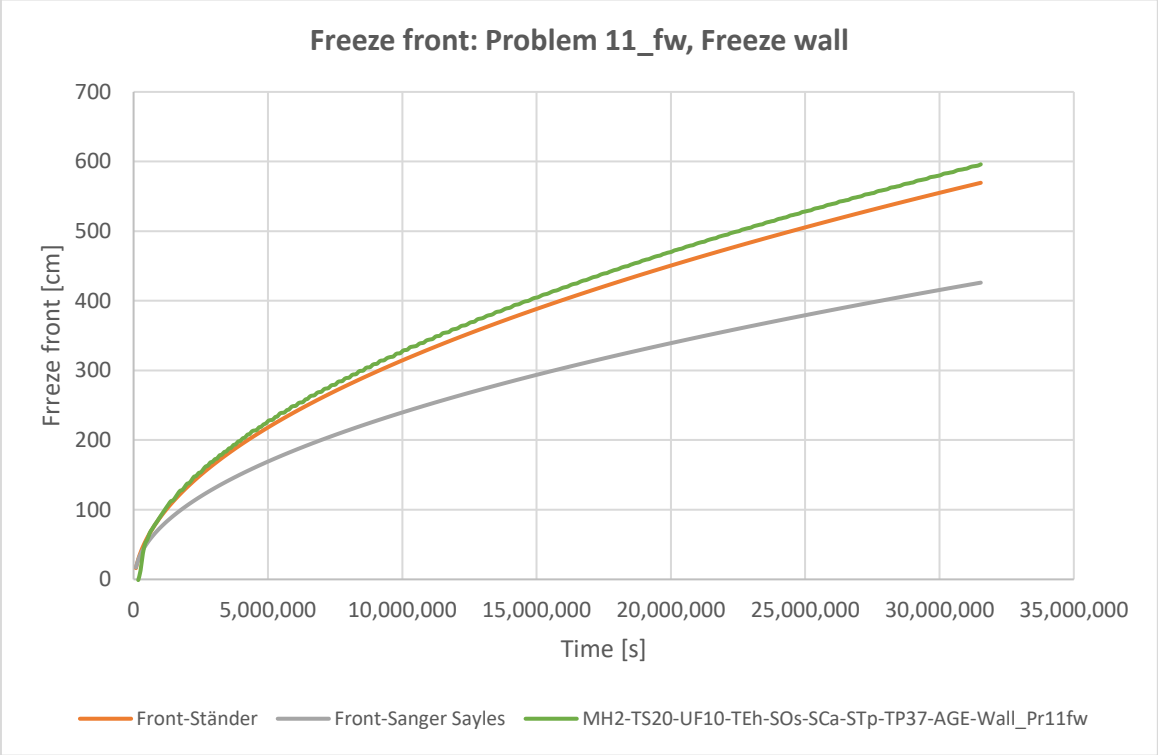

Figure 6.21: Freeze wall: freeze front progress, 365 days, Problem 11_fw

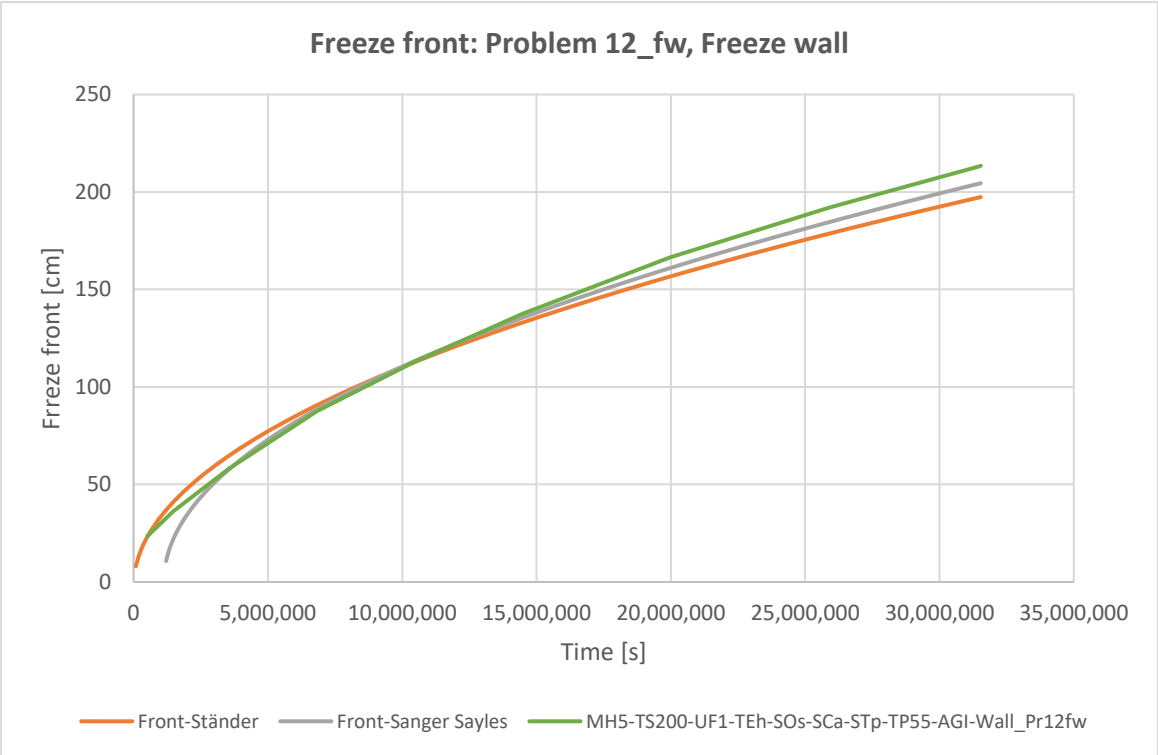

Figure 6.22: Freeze wall: freeze front progress, 365 days, Problem 12_fw

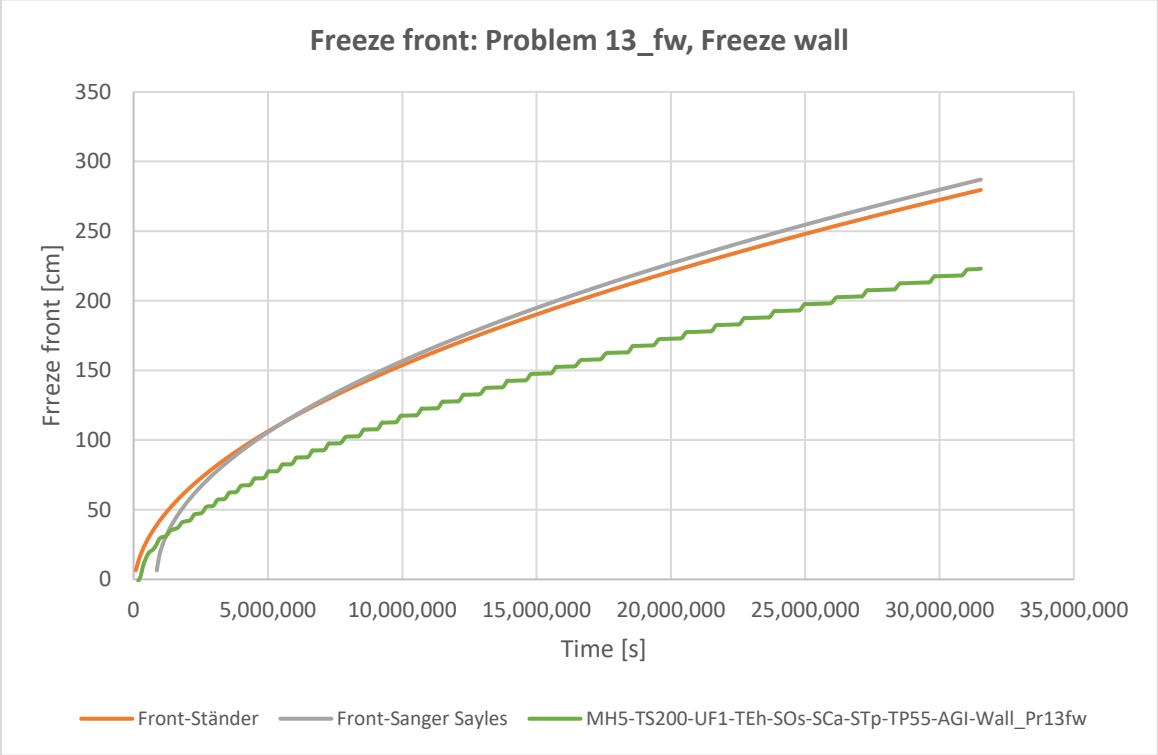

Figure 6.23: Freeze wall: freeze front progress, 365 days, Problem 13_fw

6.3.2. Comparison of the analytical solutions for the flat freeze wall

From the two solutions analysed for the freeze wall geometry, the solution from Ständer consistently generates results of significantly higher accuracy with respect to Sanger & Sayles' solution (see Figure 6.24). Ständer's solution has an accuracy higher than 5.1% for all problems except for Problem 13_fw (which has thermal characteristics of water), while Sanger & Sayles' solution produces errors of up to 32% (see Table 6.3 and Table 6.4). Therefore, Ständer is probably sufficiently accurate for many practical problems, while Sanger & Sayles should be applied with considerable caution.

Overall, both analytical solutions tend to underestimate the freezing progress, as can be observed from Figure 6.25, except for Problem 13_fw (which has a high latent heat due to using water's thermal characteristics).

Table 6.3: Average of absolute values of errors of freeze front, freeze wall, analytical solutions

Average of absolute values of error of X(t)	Front Ständer	Front Sanger & Sayles	Average of methods
Problem 7_fw	8.1	64.2	36.1
Problem 8_fw*	7.6*	126.3*	66.9
Problem 9_fw	15.7	71.0	43.4
Problem 10_fw	23.6	190.5	107.0
Problem 11_fw	16.2	107.7	62.0
Problem 12_fw	7.6	4.2	5.9
Problem 13_fw	42.1	46.3	44.2
Average of Problems	**17.3**	**87.2**	**52.22**
Median of Problems	**15.7**	**71.0**	-

**Note: Errors evaluated only until a thermal time of $2.2x10^6$ seconds.*

Table 6.4: Average of relative errors, freeze wall, analytical solutions

Average of relative errors of X(t)*	Front Ständer	Front Sanger & Sayles
Problem 7_fw	2.2%	-16.1%
Problem 8_fw	0.0%**	-25.1%**
Problem 9_fw	-5.1%	-24.1%
Problem 10_fw	-4.6%	-24.9%
Problem 11_fw	-2.7%	-25.4%
Problem 12_fw	-1.2%	-2.8%
Problem 13_fw	33.7%	31.8%

**Note: The average over time may underestimate the real errors, because negative and positive errors of each problem may be compensated. **Note: Errors evaluated only until a thermal time of $2.2x10^6$ seconds.*

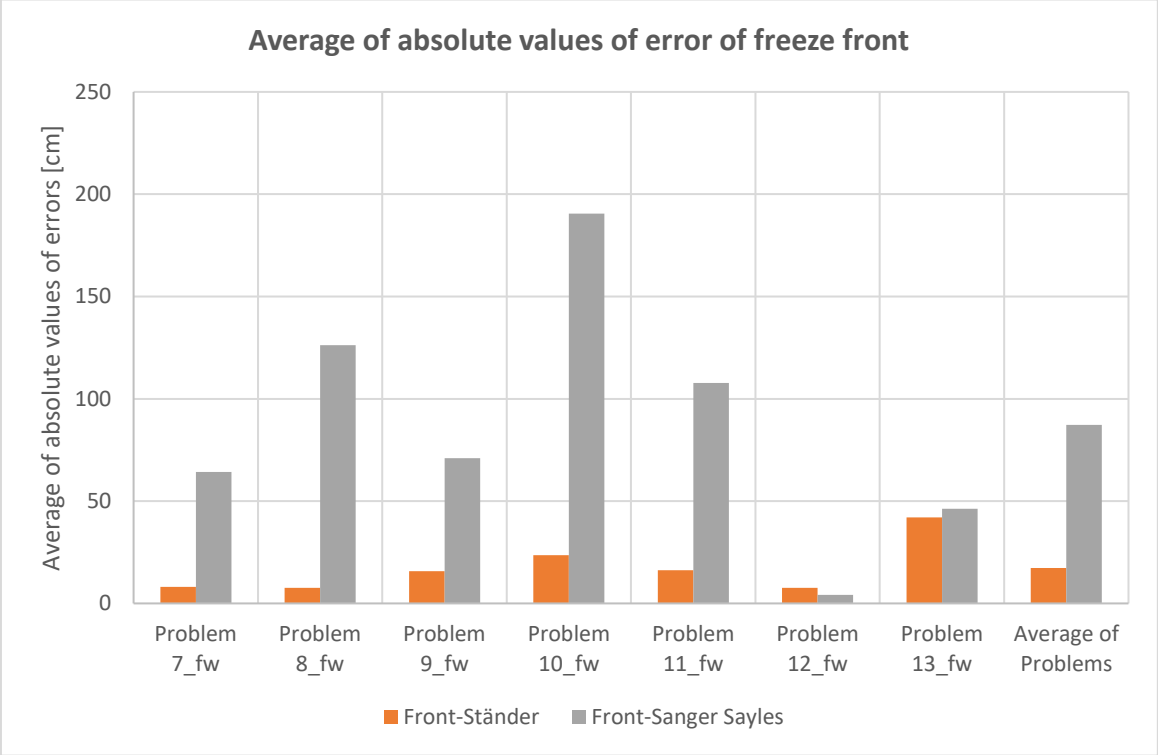

Figure 6.24: Average of absolute values of error in the location of the freeze front, freeze wall problems

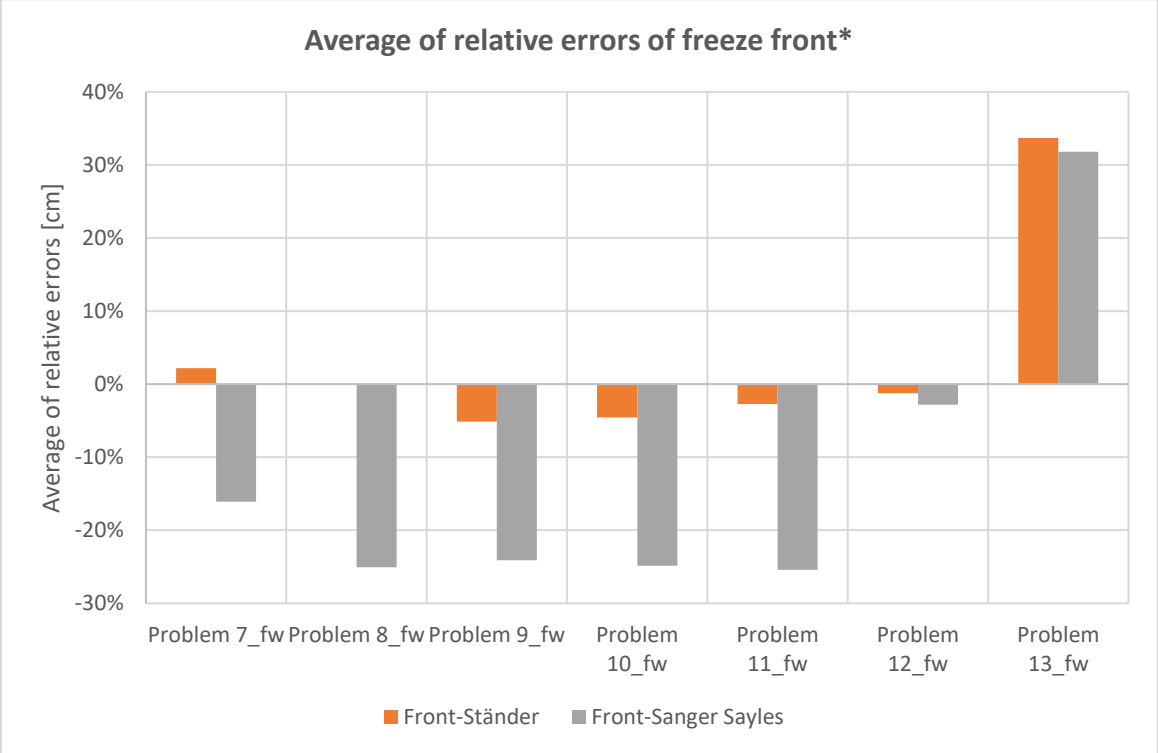

Figure 6.25: Average of relative errors in the location of the freeze front, freeze wall problems

**Note: The average over time may underestimate the real errors, because negative and positive errors of each problem can be compensated.*

6.4. Evaluation of the accuracy of the analytical solutions: freeze circle

In this chapter, numerical simulations with analogue models to the ones verified in chapter 5 were compared to the approximate analytical solutions for the freeze circle geometry from Ständer and Sanger & Sayles. An exemplary image displaying the numerical model used for the freeze circle can be seen in Figure 6.26.

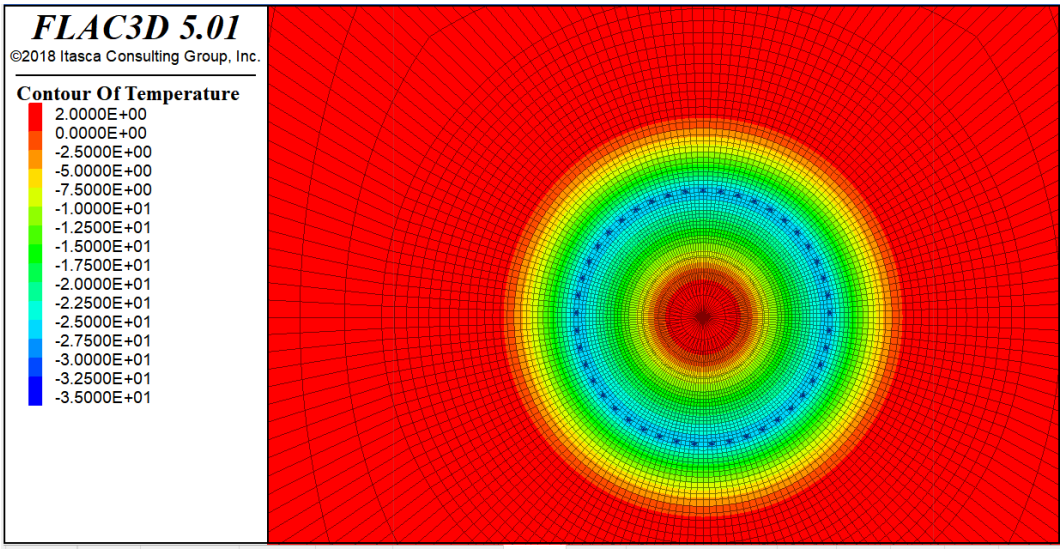

Figure 6.26: Overview of numerical model in FLAC3D for a freeze circle

6.4.1. Simulated problems - freeze circle

These problems use the same parameters, material characteristics, etc. of the problems presented in chapter 6.1, but using the freeze circle geometry instead of the single pipe (thus they are named analogously, with the suffix "_fc"). The geometry is defined by:

- Freeze circle radius of 8.5 m
- Number of pipes in the freeze circle: 45
- Freeze pipe radius of 6.99 cm

The results from the numerical solution and Ständer's and Sanger & Sayles' solutions for Problem 7_fc are shown in Figure 6.27. In this case, the results derived from Sanger & Sayles' solution for the outer freeze front coincide quite well with the numerical solution. For the inner freeze front, they approximate the solution with a larger error. Ständer's solution has a larger error for both the inner and outer freeze front: about 0.6 m for the outer front and approximately 2 m for the inner front after 1 year, which is a very high discrepancy for practical uses.

The results of Sanger & Sayles' and Ständer's solutions are presented including the consideration of the closure time of the freeze circle, which was calculated with their respective solutions for the single-freeze-pipe geometry. For these problems, several plateaux are visible in the numerical results because a larger mesh than in previous problems was chosen in order to limit the computing time. The following figures 6.27 to 6.33 show the results for the problems evaluated. In these figures, the graph origin has been

situated at the centre of the freeze circle instead of at the centre of freeze pipes as in previous chapters. In general, both Sanger & Sayles' and Ständer's solutions provide results of variable accuracy and with high errors. An overview of the results and errors is presented in chapter 6.4.2.

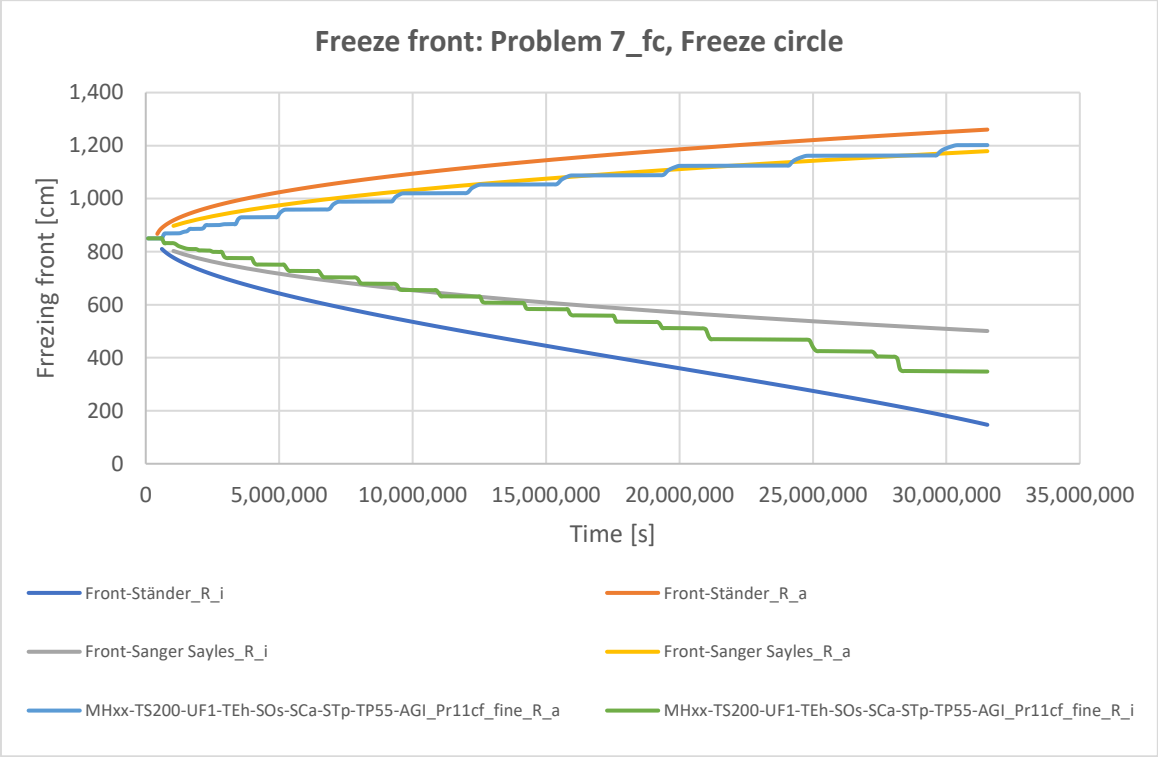

Figure 6.27: Freeze circle: freeze front progress, 365 days, Problem 7_fc

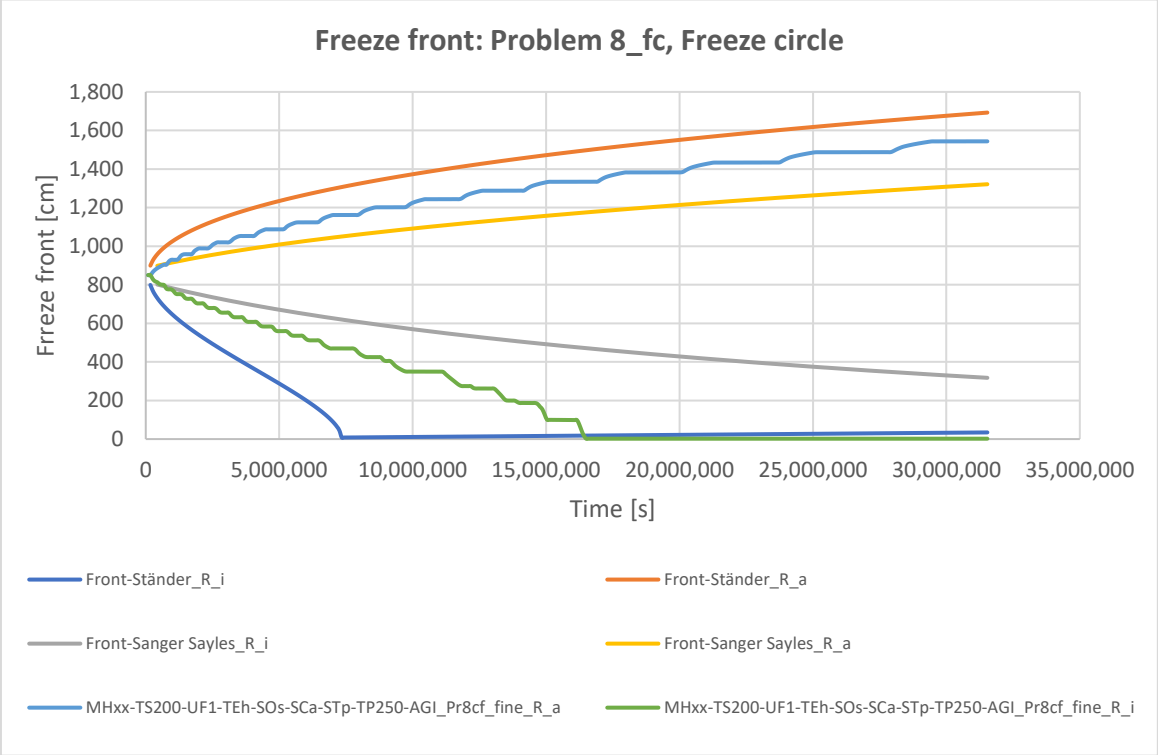

Figure 6.28: Freeze circle: freeze front progress, 365 days, Problem 8_fc

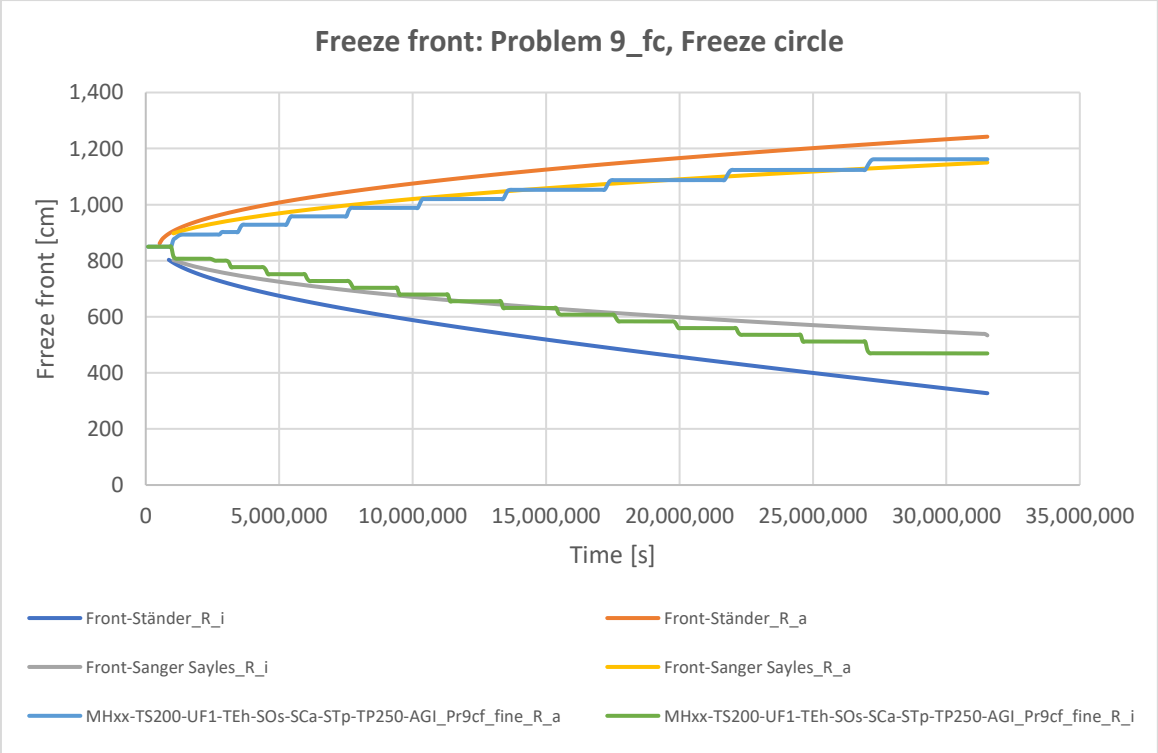

Figure 6.29: Freeze circle: freeze front progress, 365 days, Problem 9_fc

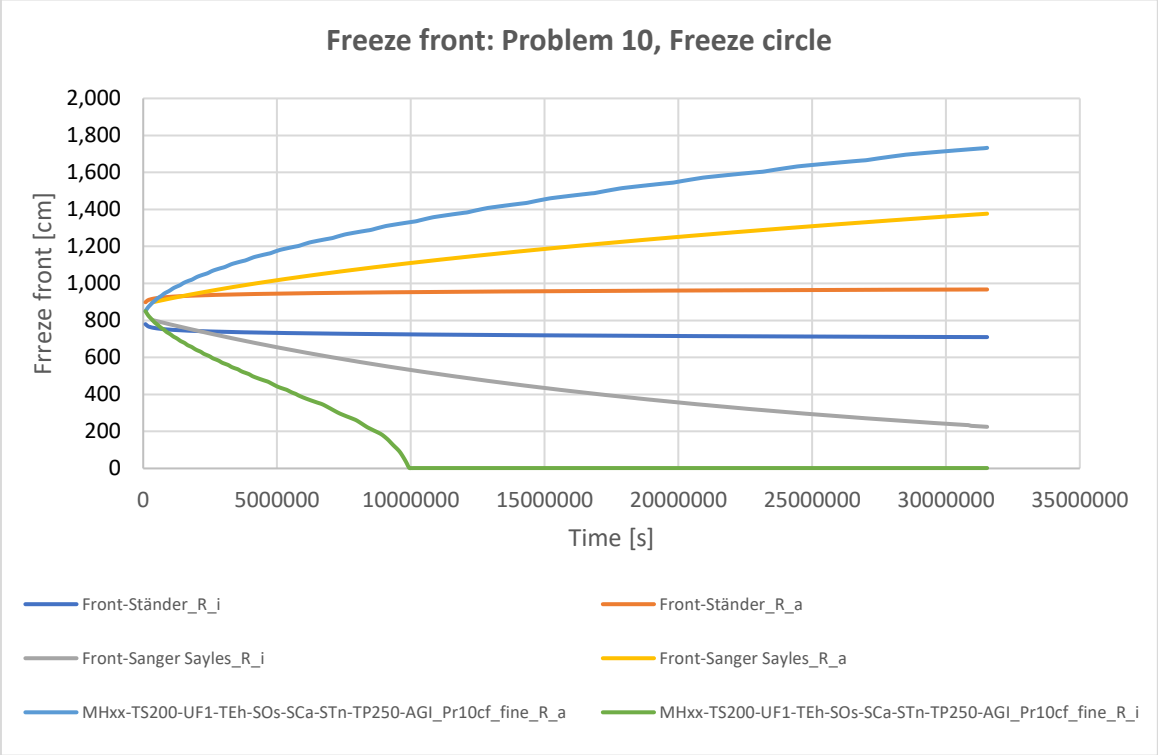

Figure 6.30: Freeze circle: freeze front progress, 365 days, Problem 10_fc

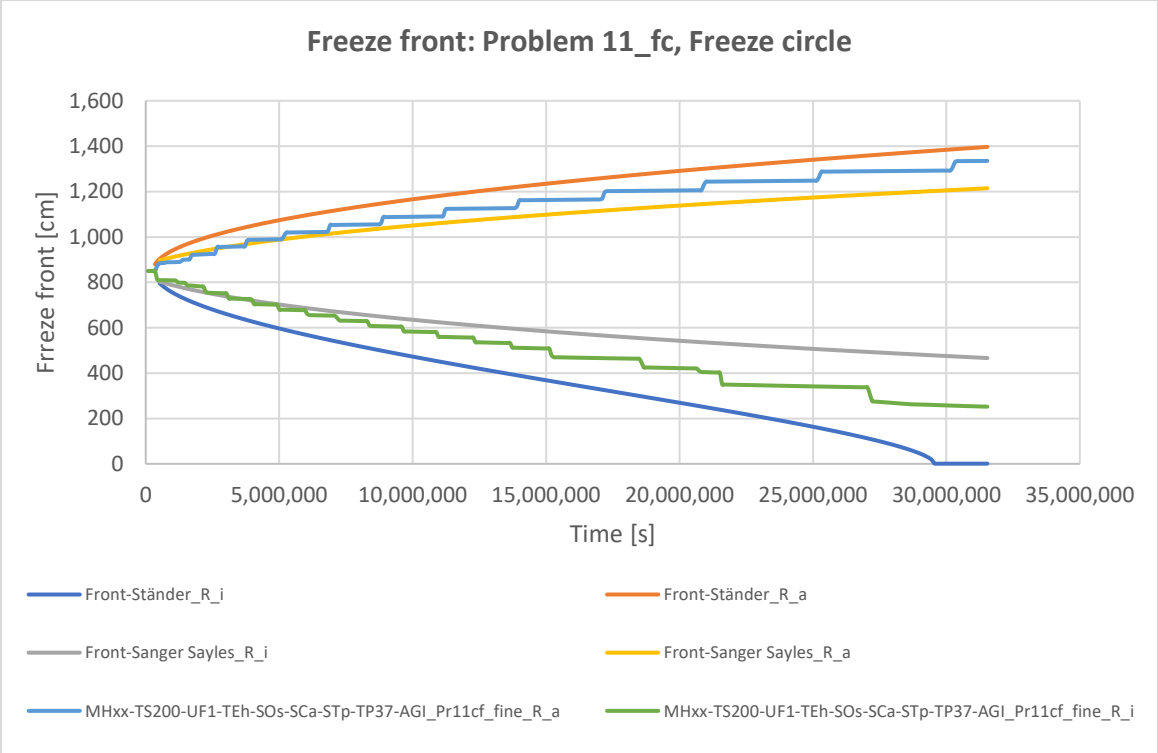

Figure 6.31: Freeze circle: freeze front progress, 365 days, Problem 11_fc

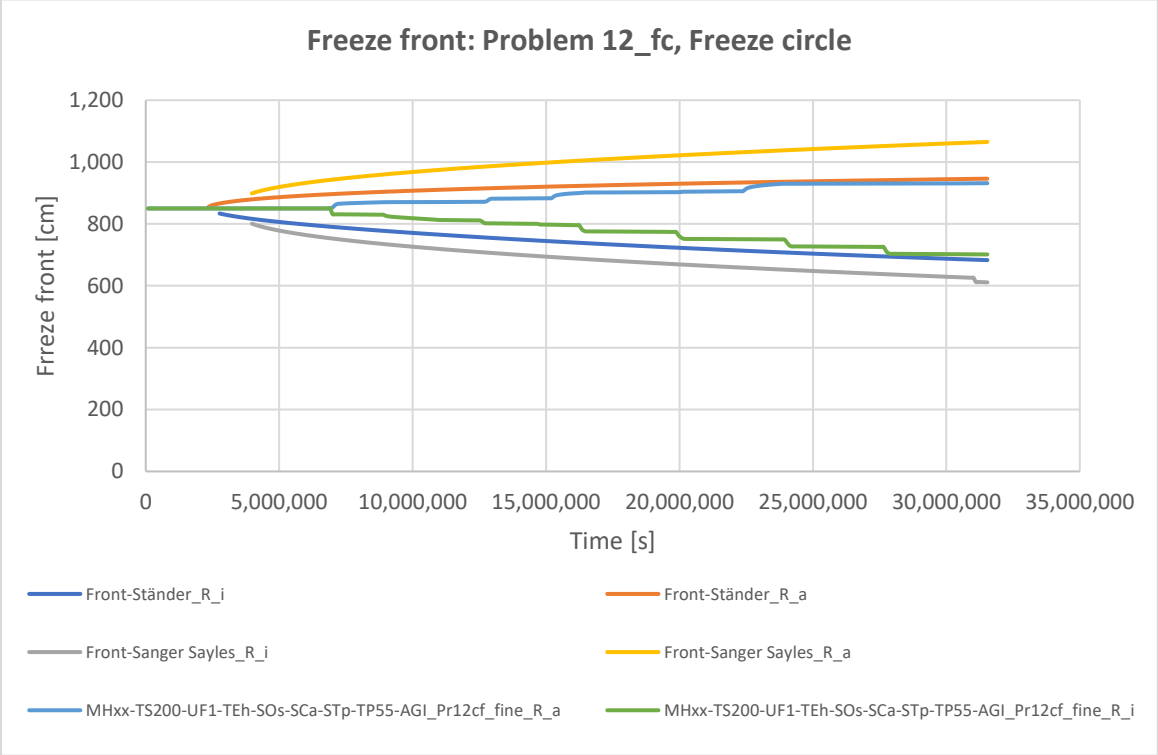

Figure 6.32: Freeze circle: freeze front progress, 365 days, Problem 12_fc

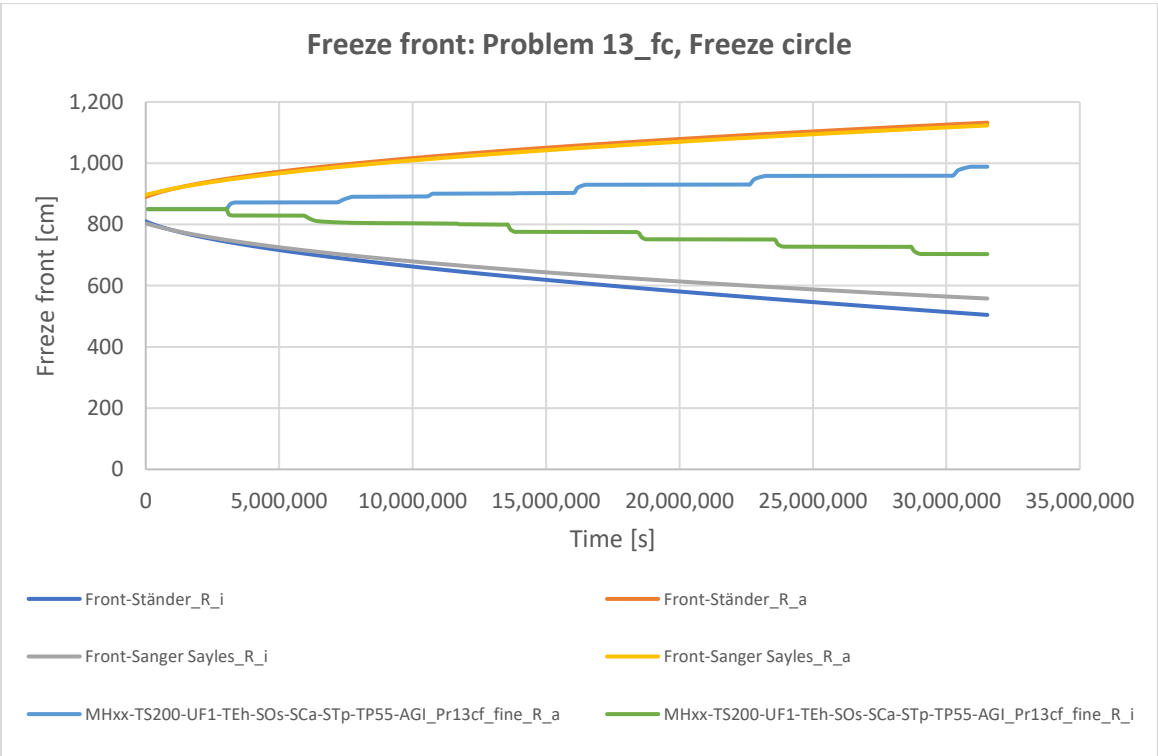

Figure 6.33: Freeze circle: freeze front progress, 365 days, Problem 13_fc

6.4.2. Comparison of the analytical solutions for the freeze circle

The analytical solutions from Ständer (1967) and Sanger and Sayles (1979) for the freeze-circle geometry produce results of very variable accuracy, cf. Figure 6.34 and Figure 6.35. For instance, Sanger & Sayles' solution is relatively accurate for Problem 7_fc and Problem 9_fc, with an average of absolute errors lower than 57 cm, while Ständer produces errors of up to 136 cm and tends to overestimate the speed of the freezing process. For Problem 8_fc and Problem 11_fc, Sanger & Sayles' solution underestimates the freeze front progress, whereas Ständer overestimates it, both of them by a significant amount. For Problem 10_fc, both solutions produce very large errors, underestimating the freeze front progress. It is worth noticing that Ständer's solution yields a much lower freeze front for Problem 10_fc, where the latent heat is negligible, than in Problems 8_fc and 9_fc, where the latent heat was much higher. Therefore, there appears to be a systematic error in Ständer's solution, which should be considered when using it for ground with low water content. For Problem 12_fc, both solutions overestimate the freeze front progress, with Sanger & Sayles producing the higher errors. In the case of Problem 13_fc, both analytical solutions yield results of similar accuracy, also overestimating the freeze front progress.

Considering all problems studied for the freeze circle geometry, Ständer's solution has a better accuracy than Sanger & Sayles' one for the outer freeze front, while it is the other way around for the inner freeze front. In any case, both solutions yield very variable accuracies throughout the problems and should therefore be used with extreme caution (see Table 6.5).

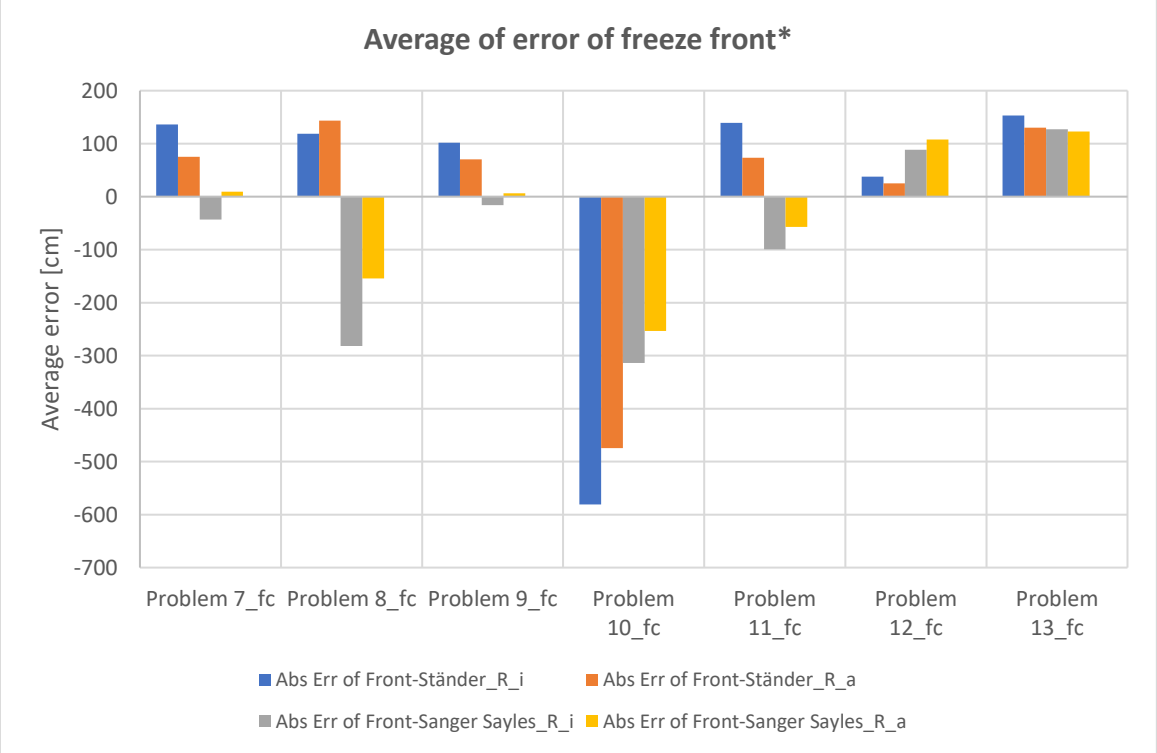

Figure 6.34: Average error of freeze front, freeze circle
**Note: The average over time may underestimate the real errors, because negative and positive errors of each problem can be compensated.*

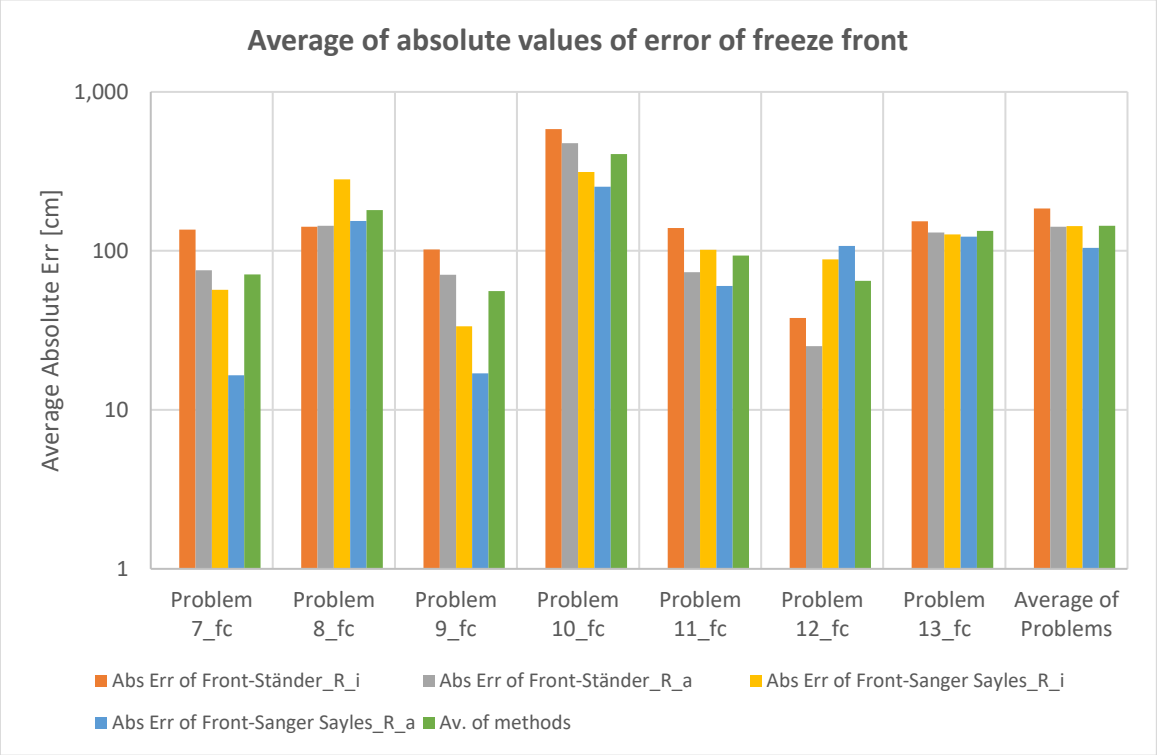

Figure 6.35: Average of absolute values of error of freeze front, freeze circle (logarithmic scale)

Table 6.5: Average of absolute values of errors of freeze front, freeze circle

Average of absolute values of errors of X(t)	Front Ständer, R_i	Front Ständer, R_a	Front Sanger & Sayles, R_i	Front Sanger & Sayles, R_a	Average of methods
Problem 7_fc	136.1	75.4	56.8	16.5	71.2
Problem 8_fc	142.1	143.6	281.9	154.5	180.5
Problem 9_fc	101.9	70.6	33.6	17.0	55.8
Problem 10_fc	582.3	475.2	314.1	253.3	406.2
Problem 11_fc	139.2	73.6	101.8	60.1	93.7
Problem 12_fc	37.9	25.2	88.2	107.6	64.7
Problem 13_fc	153.3	130.4	127.0	123.1	133.5
Average of Problems	**184.7**	**142.0**	**143.3**	**104.6**	**143.65**
Median of Problems	**139.2**	**75.4**	**101.8**	**107.6**	-

6.5. Comparison of the accuracy of the analytical solutions for the different geometries

Approximate analytical solutions for thermal design for three different geometries (single freeze pipe, freeze wall and freeze circle) have been studied. For the first two, Ständer's solution provides generally very accurate results, which can be very useful in engineering practice. Sanger & Sayles' solution provides estimates of variable accuracy, which is dependent on the initial and boundary conditions. Therefore, this solution may produce errors which are too high for practical uses. For the freeze circle, both solutions generate relatively high errors, so they should be used with extreme caution and only for estimation purposes. Therefore, the designer should be conscious of their limitations.

7. Adjustment of Sanger & Sayles' analytical solution for the single freeze pipe geometry

The importance and applicability of approximate analytical methods for thermal calculations in ground freezing design has already been discussed in chapter 3.4. Based on the review of the state of the art of analytical solutions in chapter 3 and the evaluation of the accuracy of the solutions in chapter 6, the necessity of improving the approximate analytical solutions is apparent. In this regard, a new adjusted solution for the single freeze pipe is sought in this chapter, which should be more accurate than the existing solutions and easier to use in engineering practice than Ständer's solution, which is accurate but relatively complex to use.

As Sanger & Sayles' formula for the single freeze pipe has proven to be of very variable accuracy, depending on the conditions of the problem (see chapter 6.2), an attempt to adjust it based on the results of the verified numerical models is made in this chapter.

From the three basic assumptions on which Sanger & Sayles' formula is based, presented in chapter 3.4.1.4, the following one can be argued against, in the view of the author (see Holden (1997) for a discussion on the other assumptions of the formula):

> "The radius of the unfrozen soil affected by the temperature of the freeze pipe [i.e. the temperature penetration depth] can be expressed as a multiple of the frozen soil radius prevailing at the same time. […for the single-pipe case] assume [this multiple] as $a_r = 3$." (Sanger and Sayles, 1979)

The statement above implicitly assumes that the ratio a_r is constant and is not influenced by the duration of the freezing process, the boundary conditions, the initial conditions (freeze-pipe, phase-change and initial ground temperatures), the water content or the thermal properties of the ground (thermal conductivity and specific heat capacity). The assumption $a_r = 3$ for the single freeze pipe case matches the experience from Khakimov (1966). Ständer (1967) questions this assumption, because it is only empirical and not based on physical theory. He also points out that the value of the factor a_r will not be a constant but will depend on the thermal characteristics of the unfrozen ground and therefore the error arising from this simplification is unknown.

Figure 7.1 presents an overview of an exemplary temperature distribution around a freeze pipe, which assumes $a_r = \frac{7.5}{2.5} = 3$.

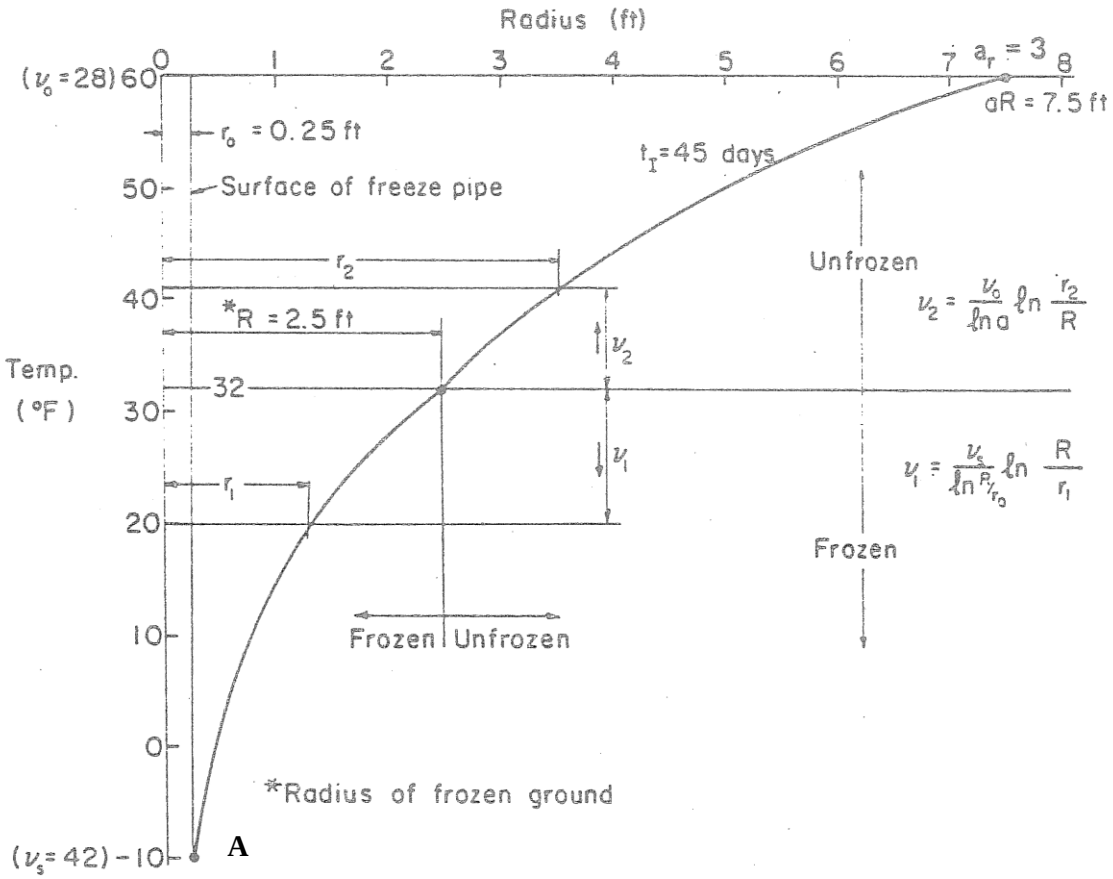

Figure 7.1: Typical temperature distribution around one freeze pipe, adapted from Sanger and Sayles (1979)

Furthermore, the supposition that there exists a point at a finite distance of the pipe whose temperature is not affected by the freeze pipe is mathematically incorrect. Strictly considered, the temperature at any location of the continuum (ground) will change due to the existence of the cooling source (freeze pipe), no matter the distance of the point to the source (even if the temperature change may be extremely small and negligible at large distances to the pipe). This can be observed in the analogous Neumann problem by evaluating the exact solution and obtaining the temperature at long distances from the source. Indeed, the temperature penetration depth is mathematically infinite, so the assumption is intrinsically inaccurate. Therefore, this assumption is difficult to verify. In any case, for practical purposes, the temperature penetration depth could be defined as the radius at which the ground temperature changes by less than an amount considered negligible, taking a "small", arbitrary quantity, e.g. 0.05ºC ($a_{r0.05}$), 0.1ºC ($a_{r0.1}$), 0.2ºC ($a_{r0.2}$) or 0.5ºC ($a_{r0.5}$).

To examine these suppositions, the ratio between the position in which the temperature has changed a small amount and the freeze radius was calculated by means of numerical models for Problems 7 to 12. Figure 7.2 shows the ratios $a_{r0.5}$, $a_{r0.2}$, $a_{r0.1}$ and $a_{r0.05}$ for Problem 7. Based on Figure 7.2, it can be claimed that a_r is not singularly defined, because the quantity considered "negligible" is arbitrary. Moreover, it is also clear that a_r is not constant but

instead it generally grows with time, for example, $a_{r0.1}$ increases from 3.7 to 8.2 for thermal times between 0 and 365 days.

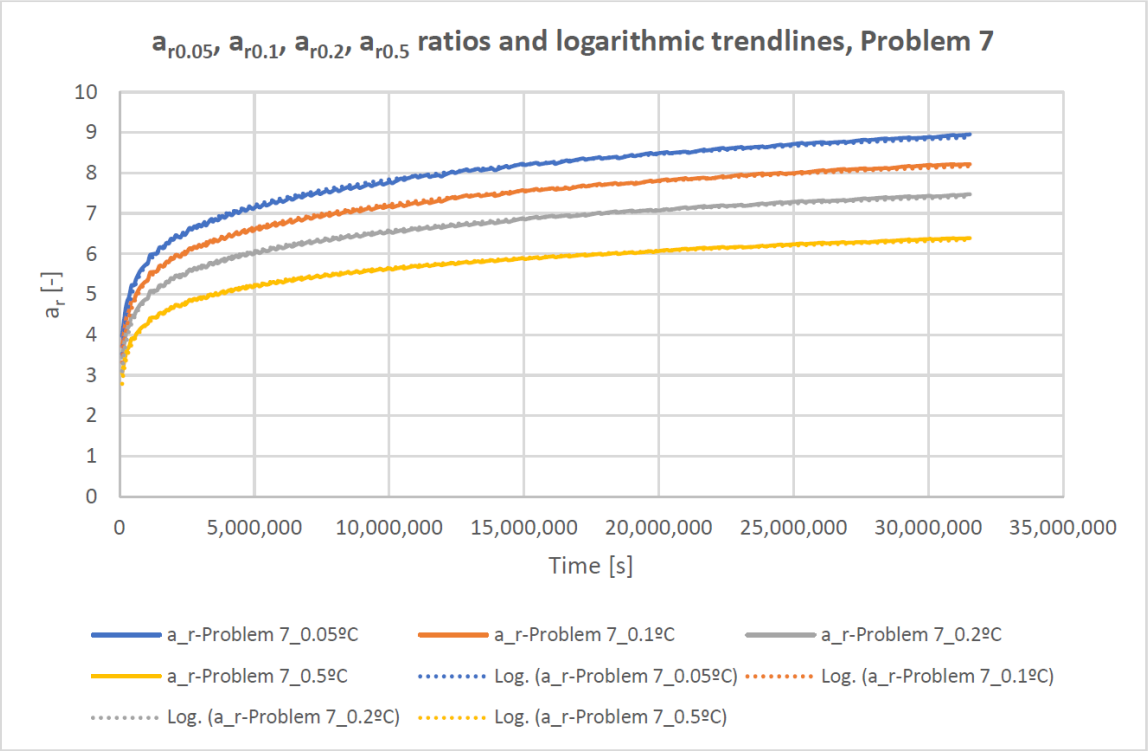

Figure 7.2: $a_{r0.05}$, $a_{r0.1}$, $a_{r0.2}$, $a_{r0.5}$ ratios for Problem 7

The $a_{r0.1}$ ratios for Problems 7 to 12 are shown in Figure 7.3. From this figure, it is apparent that $a_{r0.1}$ (and by extension a_r) varies widely depending on the initial and boundary conditions and other variables of the specific problem. The values of $a_{r0.1}$ for a thermal time of 1 day are between 2.3 and 7, relatively near to Sanger & Sayles' assumption of $a_r = 3$, which was possibly derived from experiences in short times. For longer times, the values of $a_{r0.1}$ are generally higher than at the beginning of the freezing process.

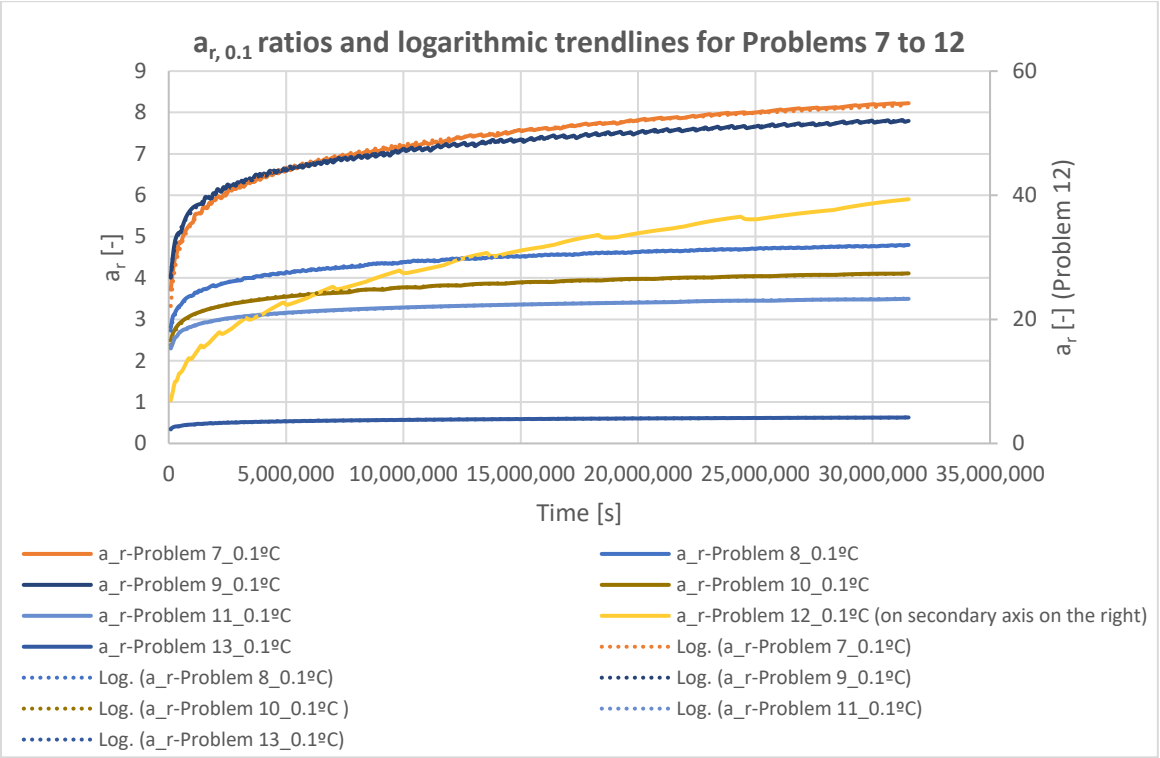

Figure 7.3: $a_{r0.1}$ ratios for Problems 7, 8, 9, 10, 11, 12 and 13

As shown in Figure 7.3, the ratio a_r is not constant, but it depends on several variables of the model. As a qualitative example, a higher freeze pipe temperature, which is nearer to the phase change temperature, would have the effect that point "A" in Figure 7.1 would be higher and the freeze radius "*R" would be smaller compared to the temperature penetration depth, which implies a larger value of a_r. An initial temperature only slightly above the phase-change temperature would, on the contrary, generate a temperature penetration depth only slightly larger than the freeze radius, implying a ratio a_r approaching a_r=1 in the limit when the initial temperature is just infinitesimally above the phase-change temperature (cf. the one-phase Stephan problem). Following this logic, other variables, such as the thermal properties of the ground (thermal conductivity, specific heat capacity, latent heat/water content) or the freeze pipe radius may affect this ratio as well.

7.1. Adjustment of the Sanger & Sayles' solution for a time of 365 days

In order to test the prior hypotheses, the ratio a_r was calculated based on the results of several numerical models, on the condition that Sanger & Sayles' solution with the calculated a_r yields the same freeze radius as the numerical model for a freezing time of one year. The problems evaluated included the ones studied in chapter 6 and several additional ones to further assess the effects of several variables on the Sanger & Sayles solution. Table 7.1 shows the definition of the problems, including the values of the main variables in them.

Table 7.1: Definition of the problems used for the adjustment of Sanger & Sayles' solution

Problem	Short description	T_{II} [ºC]	T_I [ºC]	c_{av} [cal/g/ºC]	k_{av} [cal/(s cm ºC)]	l_s [cal/g]	r_0 [cm]
Base problems							
11	2ºC initial temperature	2	35	0.61	0.0061	13.8	8
7.3	/3 k, x3 c	20	35	1.84	0.0020	13.8	8
8	extreme temperature	50	200	0.61	0.0061	13.8	8
13	water properties	20	35	0.75	0.0034	79.7	8
7	base case	20	35	0.61	0.0061	13.8	8
7.4	-21ºC phase-change temperature, point, -46ºC freeze pipe	41	25	0.61	0.0061	13.8	8
12	-21ºC phase-change temperature	41	14	0.61	0.0061	13.8	8
Latent heat sensitivity							
10	no latent heat	50	200	0.61	0.0061	0.1	8
9	extreme latent heat	50	200	0.61	0.0061	138.3	8
Water content sensitivity							
7.2	Water content = 0.42	20	35	0.61	0.0061	23.6	8
13.1	Water content =1 (soil properties)	20	35	0.61	0.0061	79.7	8
Specific heat capacity and thermal conductivity sensitivity							
7.1	x3 k, /3 c	20	35	0.20	0.0182	13.8	8
7.5	x2 k, /2 c	20	35	0.20	0.0122	13.8	8
7.11	x2k	20	35	0.61	0.0122	13.8	8
7.12	x3k	20	35	0.61	0.0182	13.8	8
7.13	x2c	20	35	1.23	0.0061	13.8	8
7.14	x3c	20	35	1.84	0.0061	13.8	8
7.15	/2k	20	35	0.61	0.0030	13.8	8
7.16	/3k	20	35	0.61	0.0020	13.8	8
7.17	/2c	20	35	0.31	0.0061	13.8	8
7.18	/3c	20	35	0.20	0.0061	13.8	8
Freeze pipe radius sensitivity							
7.19	r_0=4cm	20	35	0.61	0.0061	13.8	4
7.20	r_0=2cm	20	35	0.61	0.0061	13.8	2
7.21	r_0=16cm	20	35	0.61	0.0061	13.8	16

In order to be able to interpolate and extrapolate the calculation of a_r based on the different problems evaluated, a parameter p was created, which is a function of the variables considered and can be correlated with a_r. The parameter p was defined as a multiplication of the monomial functions of the variables considered. The exponents of these monomial functions were calibrated in a way that the coefficient of determination, R^2, of its linear correlation with a_r was maximized (see Equation (7.1)). Other combinations with slightly different values of the exponents may also yield a similarly high coefficient of determination.

$$p = -{T_{II}}^a / {T_I}^b / {c_{av}}^c \cdot {k_{av}}^d \cdot {l_s}^e / {r_0}^f \quad (7.1)$$

where:

$a = 1.0$: exponent of T_{II}

$b = 1.4$: exponent of T_I

$c = 0.4$: exponent of c_{av}

c_{av}: average of frozen and unfrozen specific heat capacities, in $cal/(cm^3 \cdot ºC)$

$d = 0.1$: exponent of k_{av}

$e = 0.0$: exponent of l_s

$f = 0.2$: exponent of r_0

k_{av}: average of frozen and unfrozen thermal conductivities, in $cal/(s \cdot cm \cdot ºC)$

$l_s = \frac{l_{water}\ \omega\ \rho_d}{\rho}$: crystallisation heat of the groundwater, per unit mass of ground, in cal/g

p: calibrated parameter

r_0: radius of freeze pipe, in [cm]

$T_{II} = T_0 - T_f$: initial temperature minus phase-change temperature, in $ºC$

$T_I = T_s - T_f$: freeze-pipe temperature minus phase-change temperature, in $ºC$

The calculated ratios a_r and their correlation with the parameter p are presented in Figure 7.4. According to this figure, the optimal values of a_r, which minimize the error of Sanger & Sayles' solution, vary widely, between 2.47 and 28.5 for the different problems used (see also Table 7.2). If a_r could be estimated based on the conditions of the specific problem before introducing it in Sanger & Sayles' formula, so that it approximates its optimal value, the error produced by this solution would decrease by a significant amount compared to the error produced when using their original assumption $a_r = 3$ without consideration of the particular conditions of the problem. To this aim, the adjusted value of a_r can be estimated based on its correlation with parameter p applying Equation (7.2), which is derived from the correlation in Figure 7.4. This parameter can be calculated previously from the boundary and initial conditions and thermal properties of the ground for the problem at hand by using Equation (7.1). An exemplary application of this procedure is shown in chapter 9.2.

$$a_{r,adjusted} = 54p + 2.0353 \quad (7.2)$$

This approach certainly has several limitations. First, it is still an empirical correlation based on the study of a limited number of specific cases, which is not based on physics (although it may be possible to qualitatively explain the effects of the variables considered, see previous section). Second, there may be additional variables to the ones considered here which could influence the value of a_r. Third, a_r has been optimised based on the

minimisation of the error for a thermal time of 365 days. The dependency of a_r with thermal time, which was proven in Figure 7.3, has not been accounted for yet.

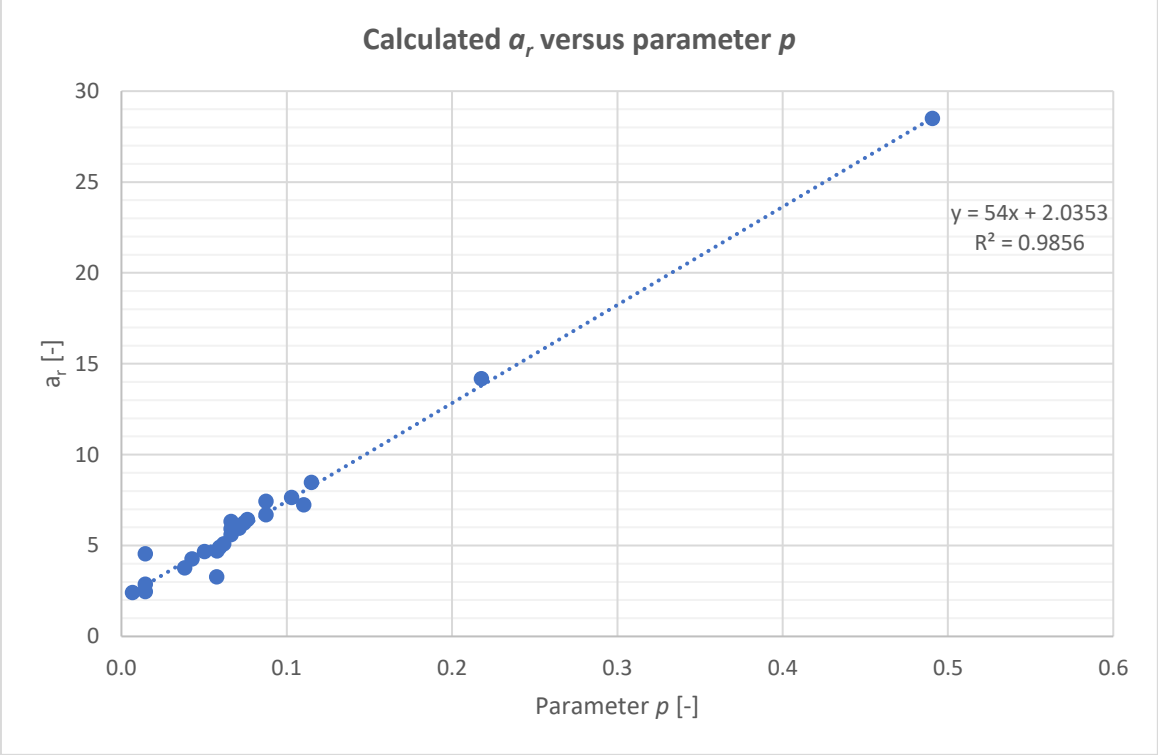

Figure 7.4: Ratio a_r versus the defined parameter "p"

The calculated a_r for the different problems as well as the values of a_r obtained from the correlation with the parameter p (adjusted a_r) are presented in Table 7.2. It can be observed from the table that the error of the adjusted a_r based on the correlation, compared to the calculated value, is small, of about 0.4 in average, much lower than it would be using the original approach of Sanger & Sayles of $a_r = 3$. The relative error ranges from -38% to +58%. Nevertheless, the error of the freeze front estimated with those values is significantly lower (see Table 7.2) and is under 10% for all the problems considered but for Problem 13, which is a quite extreme case, as it considers the properties of water.

Table 7.2: Calculated and adjusted a_r, error of a_r and adjusted freeze front

Problem	Adjusted param. p	Calc. a_r, num. model	Adjusted $a_{r,adj.}$ (from correl.)	Rel. Error of $a_{r,adj.}$	Rel. Error of a_r=3	Freeze radius, 365d, num. [cm]	Freeze radius, 365d, $a_{r,adj.}$ [cm]	Freeze radius, 365d, with a_r=3 [cm]	Rel. Error of freeze Radius, 365d, $a_{r,adj.}$ [cm]	Rel. Error of freeze Radius, 365d, a_r=3 [cm]
11	0.007	2.42	2.39	-1.1%	-25.1%	343	344.2	339.7	0.3%	-1.0%
7.3	0.038	3.77	4.10	8.9%	29.3%	102.5	98.56	113.2	-3.8%	10.5%
8	0.014	2.87	2.82	-1.9%	-6.4%	404	406	395.8	0.5%	-2.0%
13	0.058	3.27	5.15	57.6%	65.8%	167	143.2	171.1	-14.2%	2.5%
7	0.066	5.6	5.62	0.3%	46.8%	195	194.7	250.3	-0.2%	28.4%
7.4	0.218	14.2	13.80	-2.6%	76.2%	77.6	78.85	178.7	1.6%	130.3%
12	0.491	28.5	28.53	0.1%	89.6%	41	40.97	140.8	-0.1%	243.3%
10	0.014	2.47	2.82	14.0%	-7.5%	484	452.2	437.7	-6.6%	-9.6%
9	0.014	4.55	2.82	-38.1%	-4.0%	233	253.8	251.6	8.9%	8.0%
7.2	0.066	5.91	5.62	-4.9%	44.3%	179.2	183	224.8	2.1%	25.5%
13.1	0.066	6.32	5.62	-11.1%	41.4%	168.7	176.6	212.3	4.7%	25.8%
7.1	0.115	8.47	8.24	-2.7%	61.9%	363.2	367.7	502.8	1.2%	38.4%
7.5	0.110	7.23	8.00	10.6%	69.1%	289.9	276.3	393.8	-4.7%	35.8%
7.11	0.071	5.96	5.88	-1.4%	48.3%	254.2	255.9	337.7	0.7%	32.9%
7.12	0.074	6.24	6.03	-3.3%	48.6%	295.7	300.9	403.1	1.8%	36.3%
7.13	0.050	4.67	4.75	1.7%	37.5%	168.1	166.7	204.9	-0.9%	21.9%
7.14	0.043	4.27	4.34	1.7%	31.5%	151.8	150.6	179.1	-0.8%	18.0%
7.15	0.062	5.09	5.38	5.7%	46.7%	152.3	148.5	186.2	-2.5%	22.3%
7.16	0.059	4.9	5.25	7.1%	45.8%	130.9	127	157	-3.0%	19.9%
7.17	0.088	6.7	6.76	0.9%	56.2%	223	222.1	291.4	-0.4%	30.7%
7.18	0.103	7.64	7.60	-0.6%	60.2%	236.6	237.1	311.2	0.2%	31.5%
7.19	0.076	6.42	6.15	-4.2%	49.1%	165	168.7	228.7	2.3%	38.6%
7.20	0.088	7.44	6.76	-9.1%	50.6%	139.8	147.4	211.6	5.4%	51.3%
7.21	0.058	4.7	5.15	9.7%	45.8%	236.6	227.6	278.5	-3.8%	17.7%

The calculated values of a_r which minimise the error of Sanger & Sayles' solution correlate very well with the values of $a_{r0.1}$ obtained directly from the numerical solution (see Figure 7.5). This correlation supports the idea that a_r has a physical meaning, i.e., it is indeed related to the temperature penetration depth, which matches Sanger & Sayles' definition of a_r.

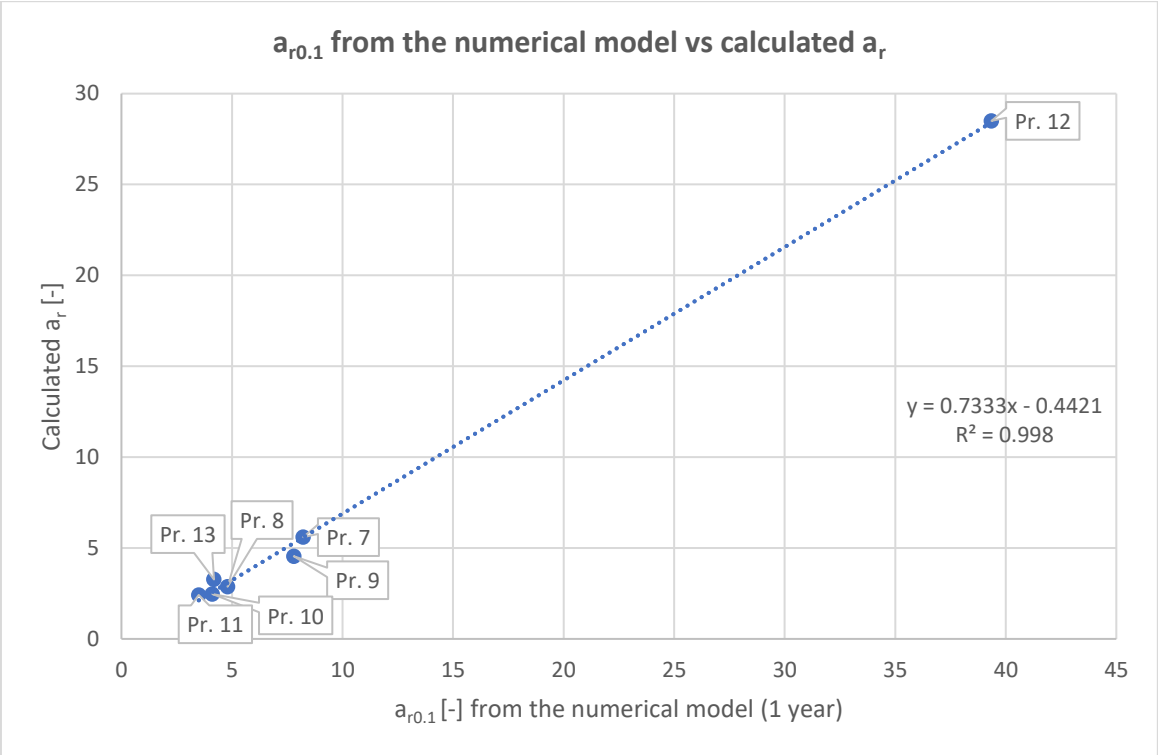

Figure 7.5: Correlation between $a_{r0.1}$ from the numerical model and the calculated a_r, Problems 7 to 13

7.2. Adjustment under consideration of the freezing time

In the previous chapter, the ratio a_r has been calculated and adjusted for different problems for a thermal time of 365 days after the start of the freezing process. Another subject of interest is the change of a_r with time. Indeed, it was already shown in Figure 7.2 and Figure 7.3 that $a_{r0.05}$, $a_{r0.1}$, $a_{r0.2}$ and $a_{r0.5}$ are not constant, but they increase with the freezing progress. The very high correlation with logarithmic trendlines in those figures, where $a_{r0.xx}$ is represented against time, should also be noticed. Therefore, to study this, a_r was calculated for Problem 7 for several time points, again showing a high correlation with logarithmic trendlines, see Figure 7.6.

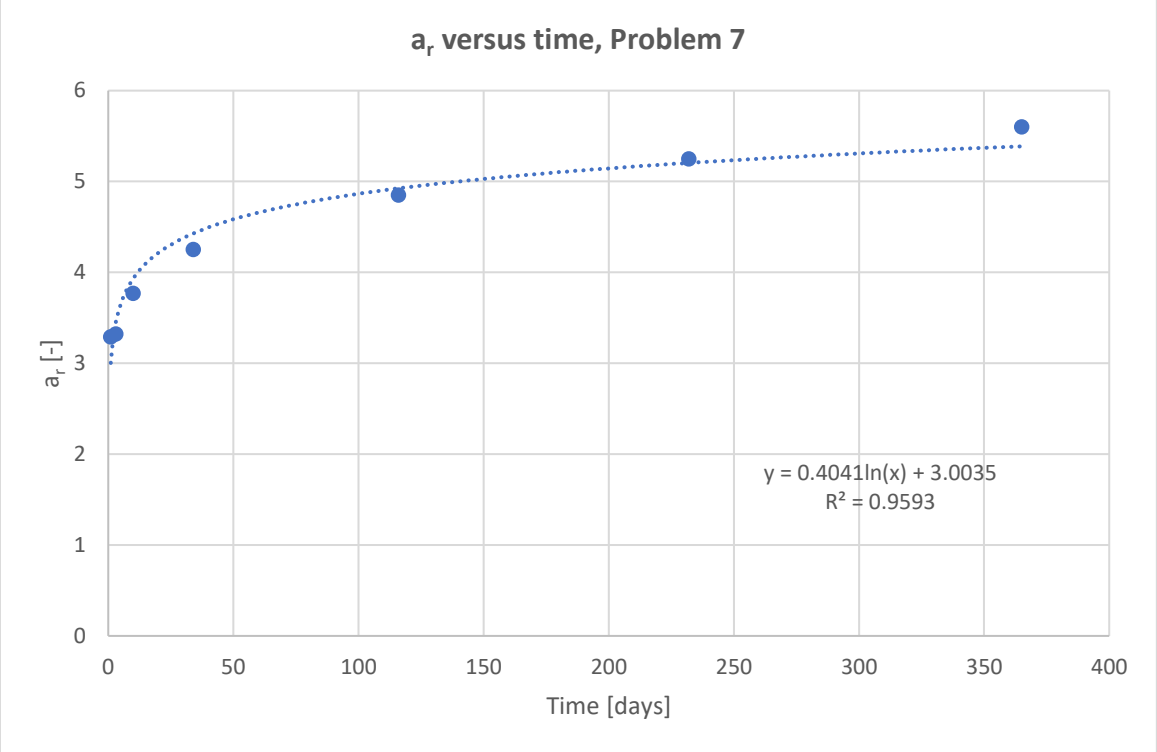

Figure 7.6: Calculated a_r for several time points, Problem 7

Thus, it is apparent that the ratio a_r varies with the thermal time. In order to study this effect, the ratio a_r was calculated using the same method as in the previous chapter for a time of 10 days after the start of the freezing process. The results of using this calculated ratio in the Sanger & Sayles' formula are compared to the ones previously obtained for 365 days and to their original approach of $a_r = 3$ in Figure 7.7. In this case, $a_{r,365d}$ provides a reasonable accuracy, also for shorter times than 365 days. Indeed, it generally produces lower errors than $a_{r,10d}$. The values of $a_{r,365d}$ and $a_{r,10d}$ which have been used in this chapter are the ones calculated directly from the numerical model, and not the ones adjusted from the correlation with parameter p. The reason for this approach is that this allows a better comparability of both, uninfluenced by the additional error of the adjustment based on the correlation between different problems.

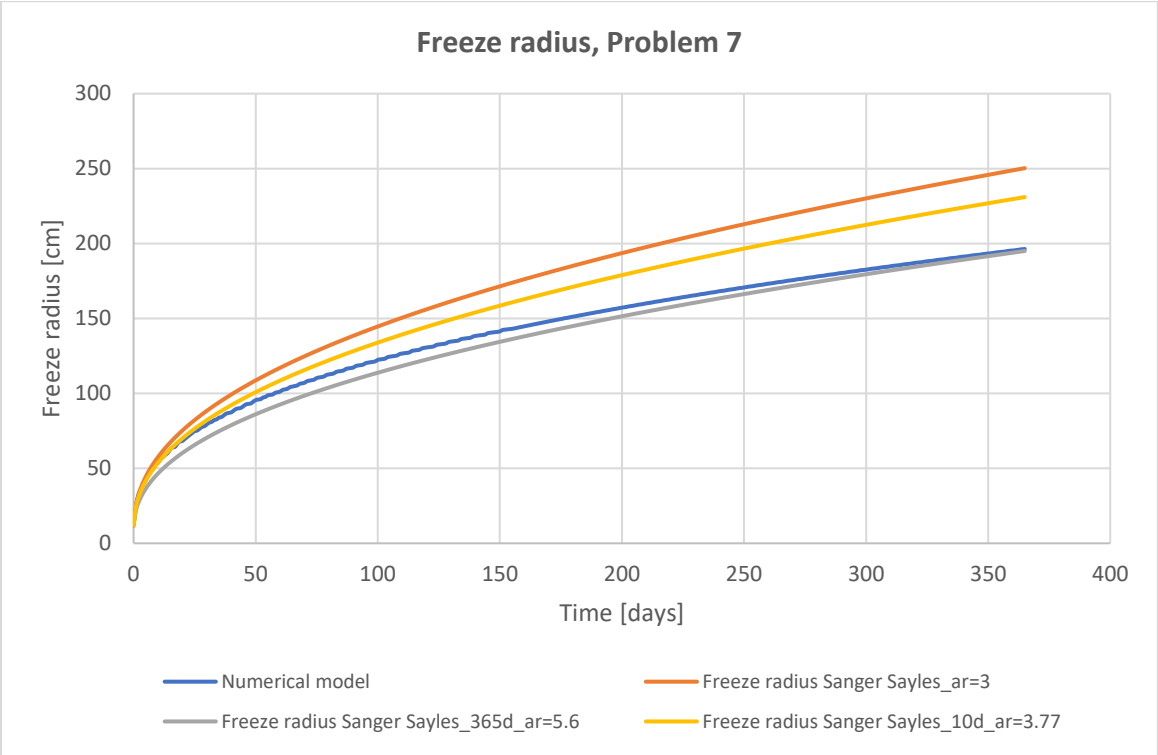

Figure 7.7: Freeze radius, Sanger & Sayles original (a_r = 3) and with a_r calculated for t=365d and t=10d

The calculated ratios $a_{r,365d}$ and $a_{r,10d}$ have been applied to Sanger & Sayles' formula for Problems 7 to 13 and are shown in Table 7.3. As explained before, the ratio a_r increases with time, so $a_{r,365d} > a_{r,10d}$. The ratio $\frac{a_{r,365d}}{a_{r,10d}}$ seems to remain at about 1.15 to 1.5, except for Problem 12, which has a very low freeze temperature of -21ºC. This ratio and the logarithmic trendline shown in Figure 7.6 may be useful for the design engineer in order to adjust a_r for other timeframes. It is also interesting to notice that the original assumption from Sanger & Sayles ($a_r = 3$) is more accurate for a time of 10 days than for 365 days. Hence, they may have made that assumption based on experimental data stemming from short-term experiments.

Table 7.3: Calculated ratio a_r for 365 and 10 days

Problem	**a_{r365d}**	**a_{r10d}**	**Ratio a_{r365d}/a_{r10d}**
7	5.6	3.77	1.49
8	2.87	2.09	1.37
9	4.55	3.38	1.35
10	2.47	1.81	1.36
11	2.42	2.12	1.14
12	28.5	11.5	2.48
13	3.27	2.79	1.17
		Average	**1.48**
		Std. dev.	**0.46**

The calculated ratios $a_{r,365d}$ and $a_{r,10d}$ were introduced into Sanger & Sayles' formula and the average errors of the resulting freeze radius between the start of freezing and 365 days have been evaluated. It is apparent from Table 7.4 and Figure 7.8 that the approach based on $a_{r,365d}$ consistently generates significantly lower errors, which are under 5%, except for Problem 12.

Table 7.4: Average of the relative errors of the freeze radius

Average of the relative errors of X(t)*	**Freeze radius Sanger & Sayles original with $a_r = 3$**	**Freeze radius Sanger & Sayles with $a_{r,365d}$**	**Freeze radius Sanger & Sayles with $a_{r,10d}$**
Problem 7	-20.9%	5.0%	-11.9%
Problem 8	4.6%	2.8%	-8.9%
Problem 9	-5.9%	1.6%	-4.1%
Problem 10	12.4%	3.5%	-11.2%
Problem 11	1.5%	1.5%	-0.2%
Problem 12	-178.4%	12.3%	-43.6%
Problem 13	-0.4%	1.8%	-2.2%

**Note: The average over time may underestimate the real errors, because negative and positive errors of each problem may be compensated.*

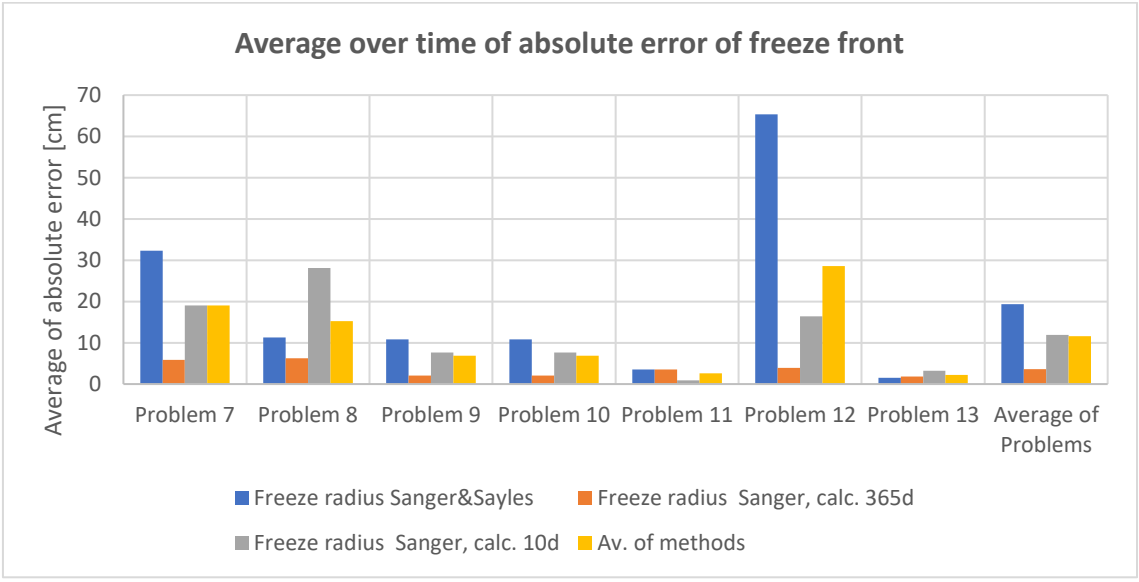

Figure 7.8: Average over time of absolute error of freeze front, original and calculated Sanger & Sayles solutions

8. Comparison of numerical and analytical results against experimental data

The accuracy of the numerical model used with respect to the exact analytical solution of Neumann was studied in chapter 5. In addition to this verification, it has to be checked that the partial differential equation which is being approximated by the numerical model represents the reality sufficiently accurately (Causon and Mingham, 2010). Compared to using data from real projects for model verification, experiments have the advantage that they are performed in a controlled environment under boundary conditions known within the measurement tolerances. Therefore, it is generally recognised that experimental data are a solid base for the verification of numerical models (Alzoubi et al., 2020). However, only a few experiments with sufficient data for model verification can be found in the literature (Schüller, 2015) (Alzoubi et al., 2020). A possible reason is that performing large-scale experiments with a long duration in a similar order of magnitude to real projects is costly, however, real-scale trials are necessary (Pigorini et al., 2012). The experiments have typically been done with small samples in short times, see e.g. Jame and Norum (1980), where 30 cm long tubes were cooled for 72 hours, Ständer (1967), G. Gioda (1994), Neaupane et al. (1999), Song et al. (2018), Alzoubi et al. (2019), Sudisman et al. (2019), Wang et al. (2019), Wang et al. (2020), Zueter et al. (2020) or Zhang et al. (2021)). Recently, a larger experimental model was studied in Qi et al. (2020).

In this chapter, a numerical model analogue to the one evaluated in chapter 5 and the analytical solutions which have been evaluated in chapter 6 are compared to the experimental results in the doctoral thesis from Sres (2009). Sres (2009) performed monitored experiments with one and several freeze pipes, where the temperature was measured at several positions.

8.1. Experiment with a single freeze pipe

Sres (2009) built up a small-scale model with one freeze pipe for experimentation. The model used is depicted in Figure 8.1. The positions of the temperature monitoring sensors in the experimental model are shown in Figure 8.2.

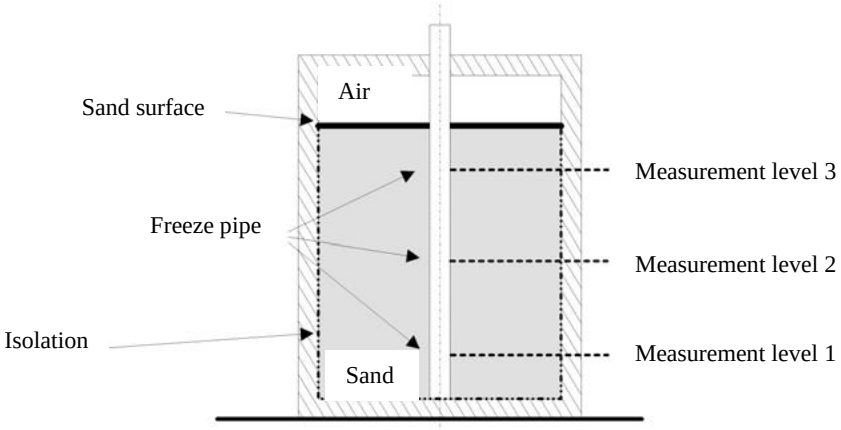

Figure 8.1: Scheme of the experimental model for a single freeze pipe, modified from Sres (2009)

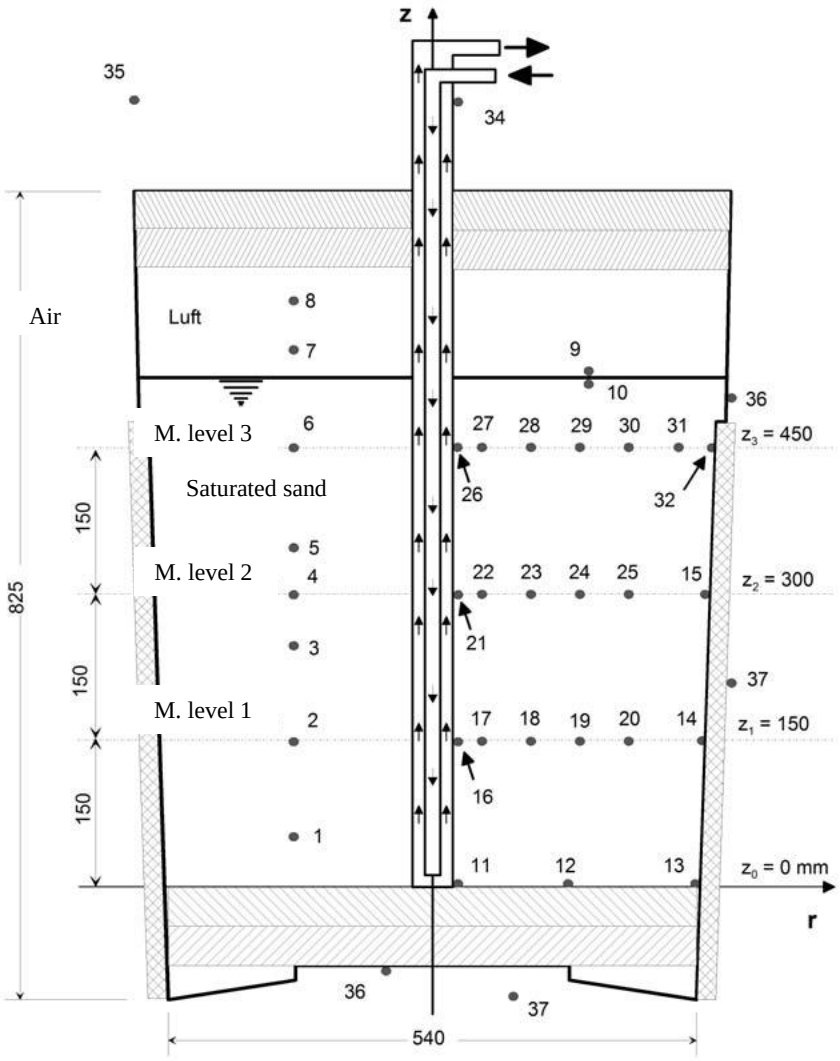

Figure 8.2: Disposition of the temperature monitoring sensors, modified from Sres (2009) (measures in mm)

A numerical model was built up in FLAC3D, taking into consideration the specific boundary conditions of the experiment, such as the change of the freeze pipe wall temperature with time and the temperature at the outside of the cylinder (see Figure 8.3). The numerical parameters (mesh, time steps, etc.) used were similar to the ones from the numerical models evaluated in chapters 5 and 6.

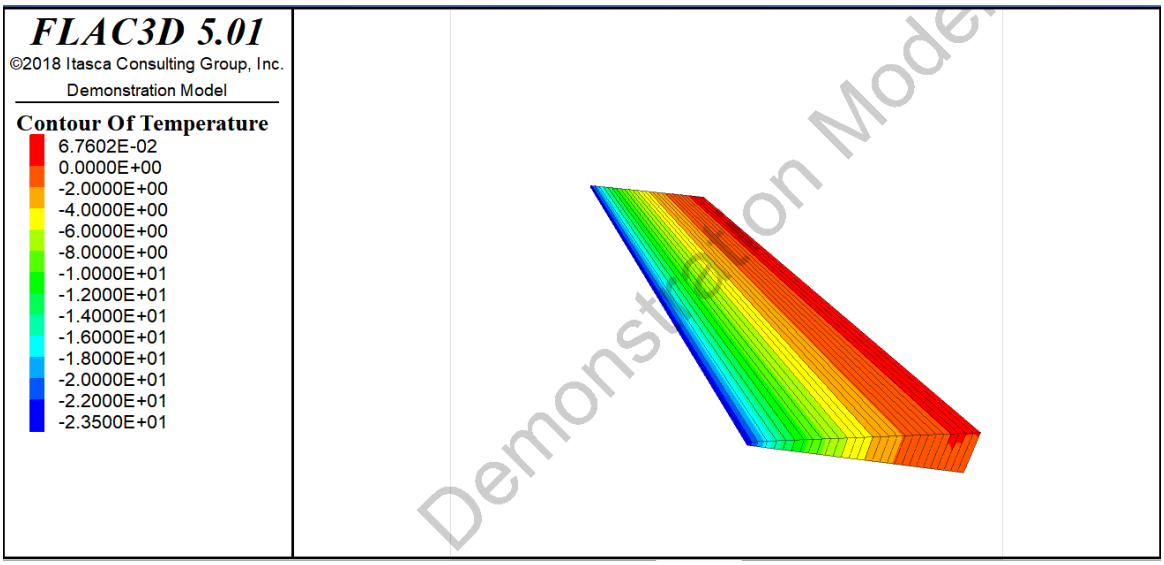

Figure 8.3: Overview of the FLAC3D model for simulation of Sres' experiment with a single freeze pipe

The results from these experiments (see monitoring data in Figure 8.4) have been compared with the results of the numerical model and analytical solutions presented in chapter 6. The comparison of the numerical and the measured data from the second monitoring level shows a good match, with maximum errors of about 2ºC (see Figure 8.5). The higher errors compared to the models in chapter 5 can be explained in that, as it is a real experiment, there are several factors which could not be simulated exactly, among others, the following:

- The temperature at the exterior of the cylinder wall was taken in the numerical model as the temperature measured at the interior of the isolation (from Sres (2009), Figure 8.4).
- The freeze pipe wall temperature was taken from Sres (2009), Figure 8.4, based only on punctual data.
- Other sources of error are for example the errors in the determination of the thermal parameters of the soil and isolation used in the experiment.

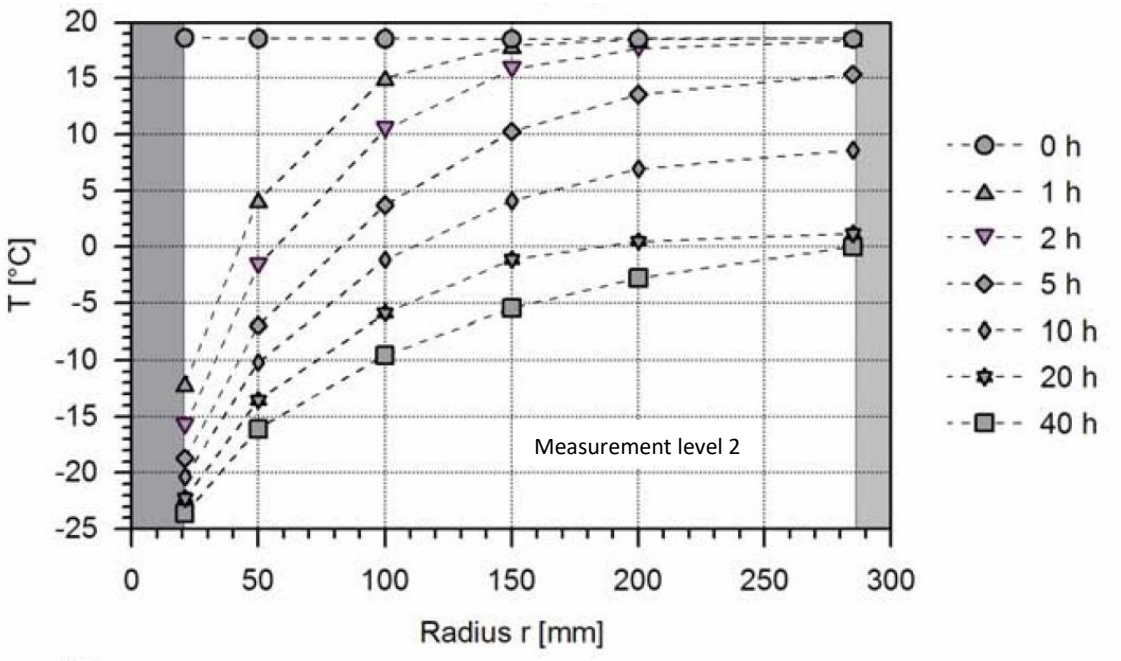

Figure 8.4: Measurement data, single freeze pipe model, modified from Sres (2009)

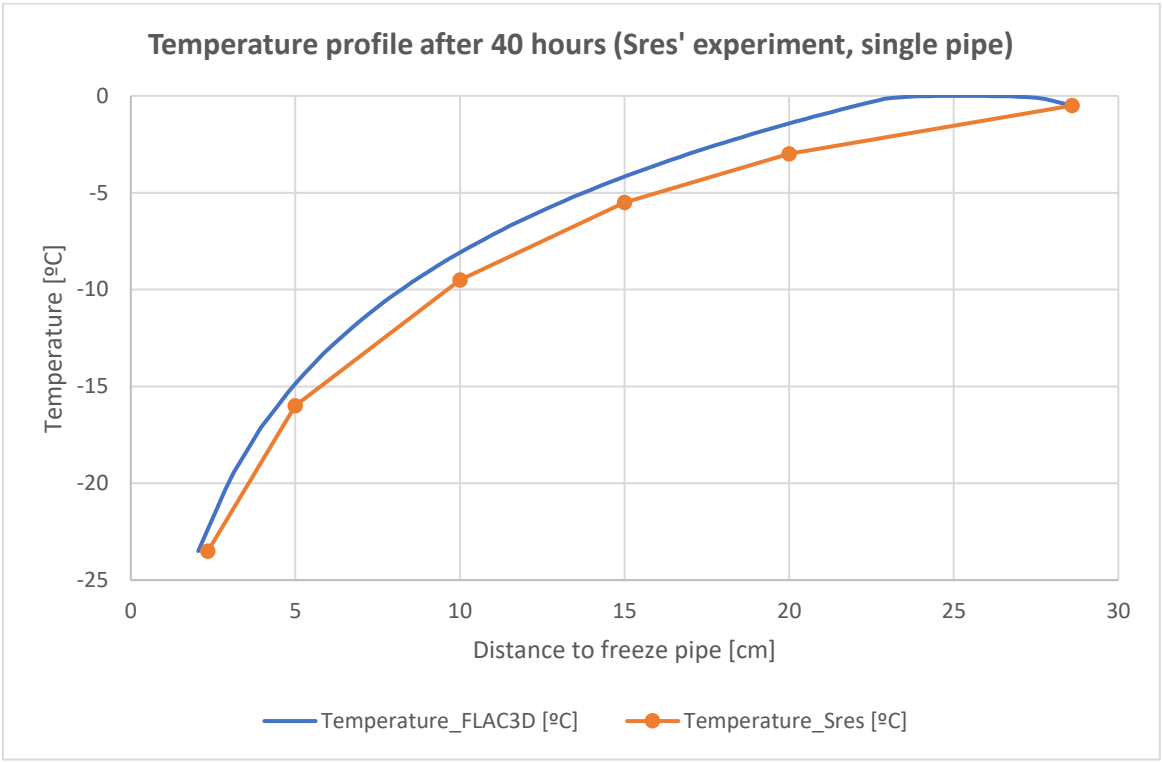

Figure 8.5: Temperature profile after 40 hours, comparison of FLAC3D results vs experimental data from Sres (2009)

The experimental data on the position of the freeze radius with time were derived from Figure 8.4 and compared to the results of the numerical model and of the approximate analytical solutions discussed in chapter 6 (see Figure 8.6). However, it must be highlighted here that the five analytical solutions consider an infinite cylinder of soil. That is, they do not consider the boundary effects of the existing isolation at a finite distance of the freeze

pipe. This is the reason why only at the very start of the process (up to approximately 40,000 seconds), the two generally most accurate solutions (see chapter 6), i.e., Ständer and Sanger & Sayles, match the experimental and numerical results. After that time, the freeze radius moves at a much faster pace than they predict, because the cooling effect of the pipe is being concentrated in a smaller cylinder, as a result of the boundary effect of the isolation. Indeed, the bending of the experimental and numerical graphs at a time between 35,000 and 40,000 seconds due to this effect can be observed in Figure 8.6. A further reason for the mismatch of the analytical and experimental results is that the analytical solutions are based on certain assumptions (e.g. a constant freeze pipe temperature), which is rather inaccurate at the beginning of the freezing process (see e.g. Figure 8.4).

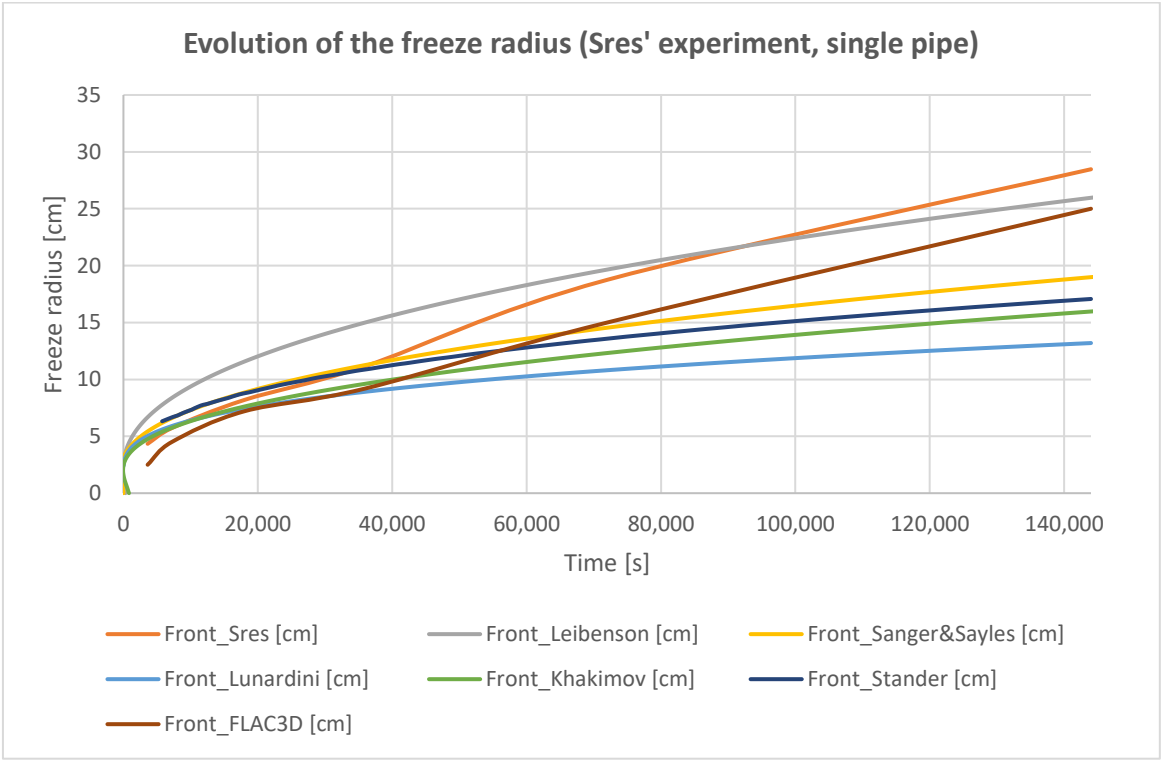

Figure 8.6: Evolution of the freeze radius: experimental data, FLAC3D results and analytical solutions

8.2. Experiment with a row of three freeze pipes (freeze wall)

Sres (2009) also performed an experiment with three freeze pipes in a line, corresponding to the freeze wall arrangement. An overview of this experiment is shown in Figure 8.7.

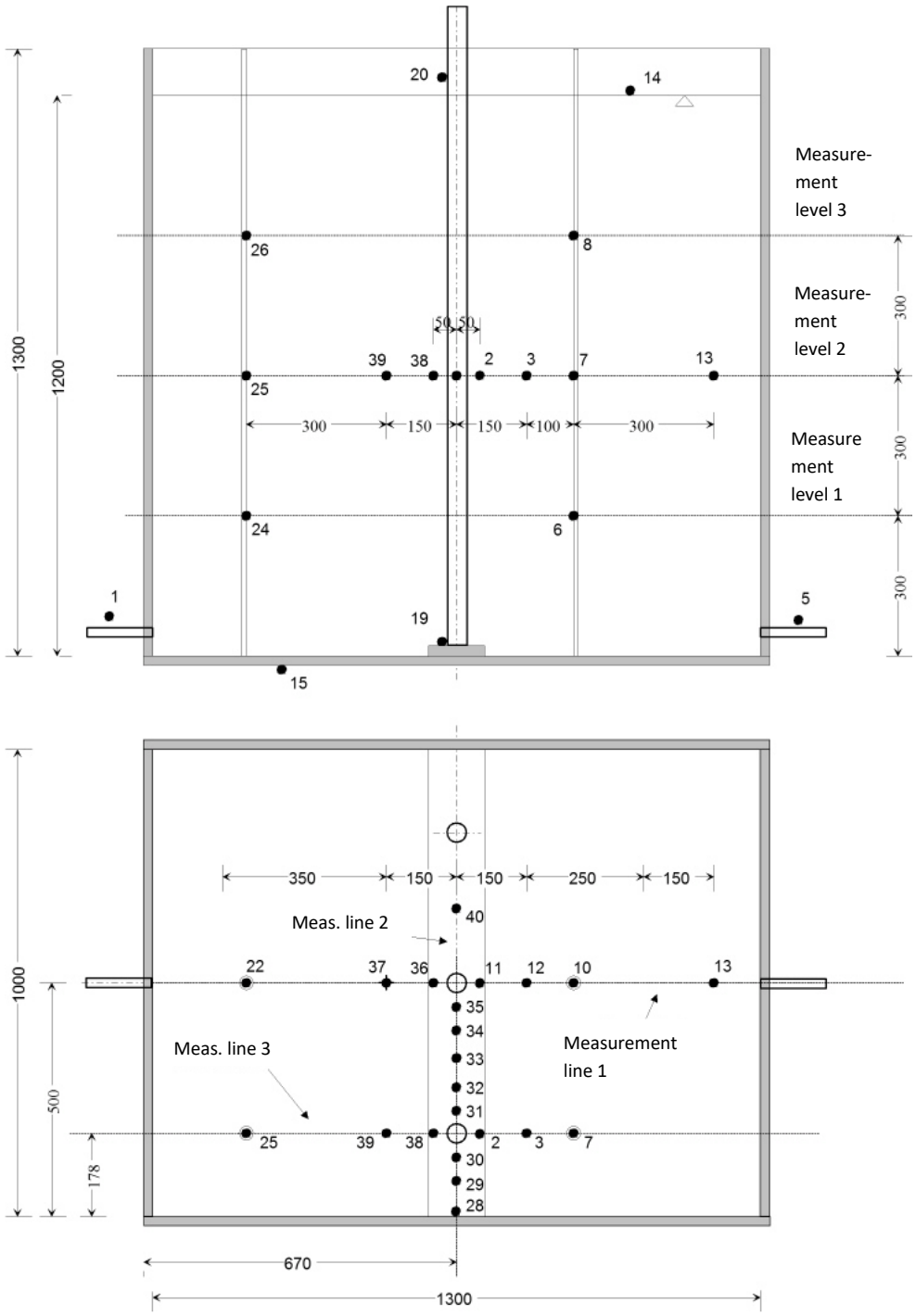

Figure 8.7: Overview of experimental model with several pipes (freeze wall arrangement), modified from Sres (2009)

This experiment was modelled in FLAC3D using the existing symmetry from chapter 6.3, presented in Figure 8.8.

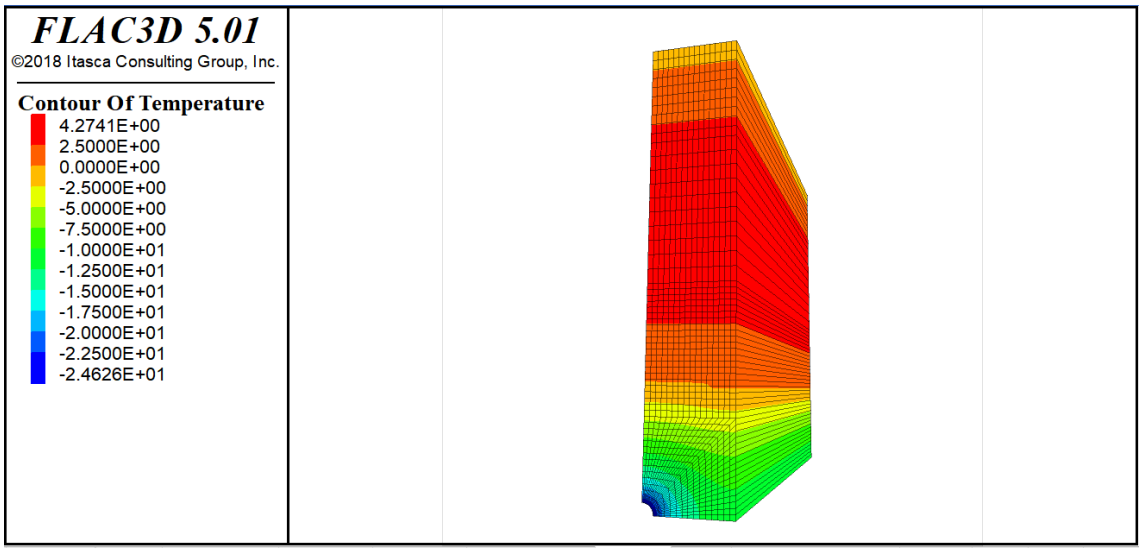

Figure 8.8: FLAC3D model for freeze wall to simulate Sres' experiment with several pipes

The results of the experiments of Sres (2009) and of the numerical model in FLAC3D were compared and are shown in Figure 8.9, Figure 8.10 and Figure 8.11. In general, the results of the numerical model match the data from the experiment very well. In Figure 8.9 there are some differences at the farther distance to the pipe, potentially as a result of uncertainties in the boundary conditions at the outside of the box and in the thermal characteristics of the isolation. However, the numerical model approximates the experimental results with a higher accuracy than for the single freeze pipe experiment, probably due to a comparatively lower effect of the boundary conditions.

The analytical solution from Ständer provides results of a relatively high accuracy, whereas Sanger & Sayles' solution does not match the experimental and numerical results (see Figure 8.11). Interestingly, it can be corrected by moving its start to the origin, which potentially points to an incorrect calculation of the freeze wall formula for short timeframes below the closure time. This can be traced to how Sanger & Sayles' solution for the freeze wall is built up, as the sum of the freezing times for the phases before and after wall closure. In fact, the short duration of the experiment (40 hours) is much shorter than the typical duration of ground freezing projects for which the analytical solution from Sanger & Sayles' is likely to have been originally conceived.

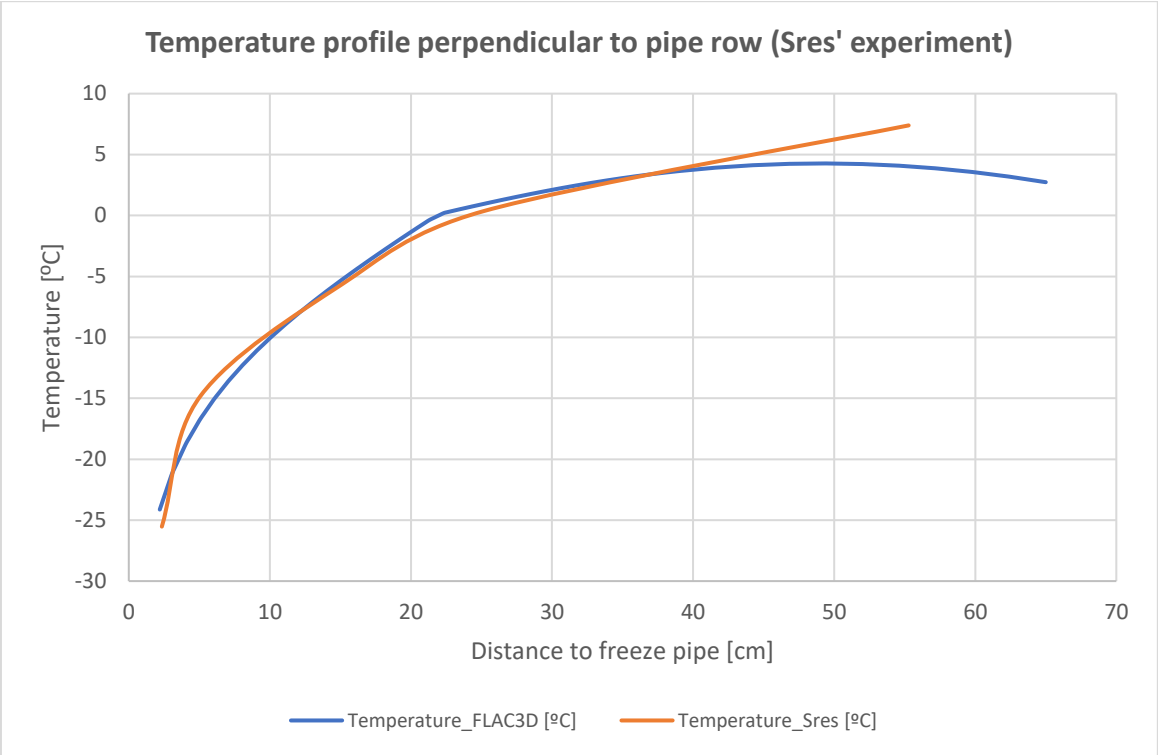

Figure 8.9: Temperature profile perpendicular to pipe row: experimental data and FLAC3D results

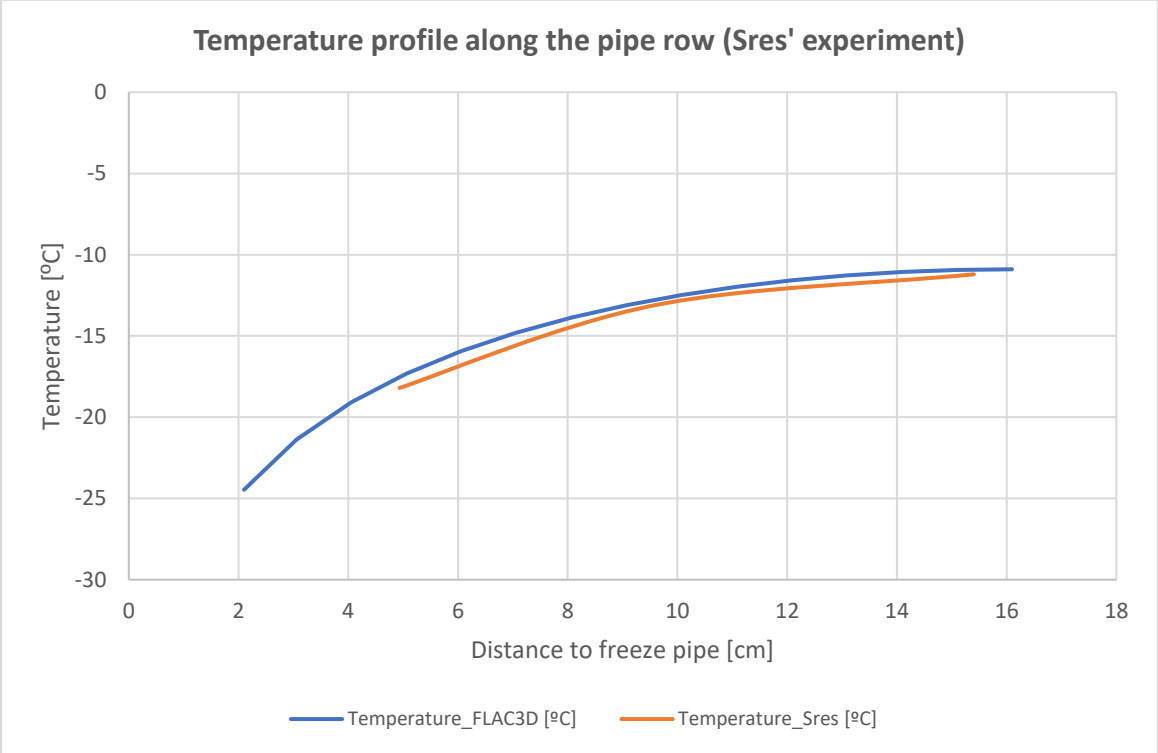

Figure 8.10: Temperature profile along the pipe row: experimental data and FLAC3D results

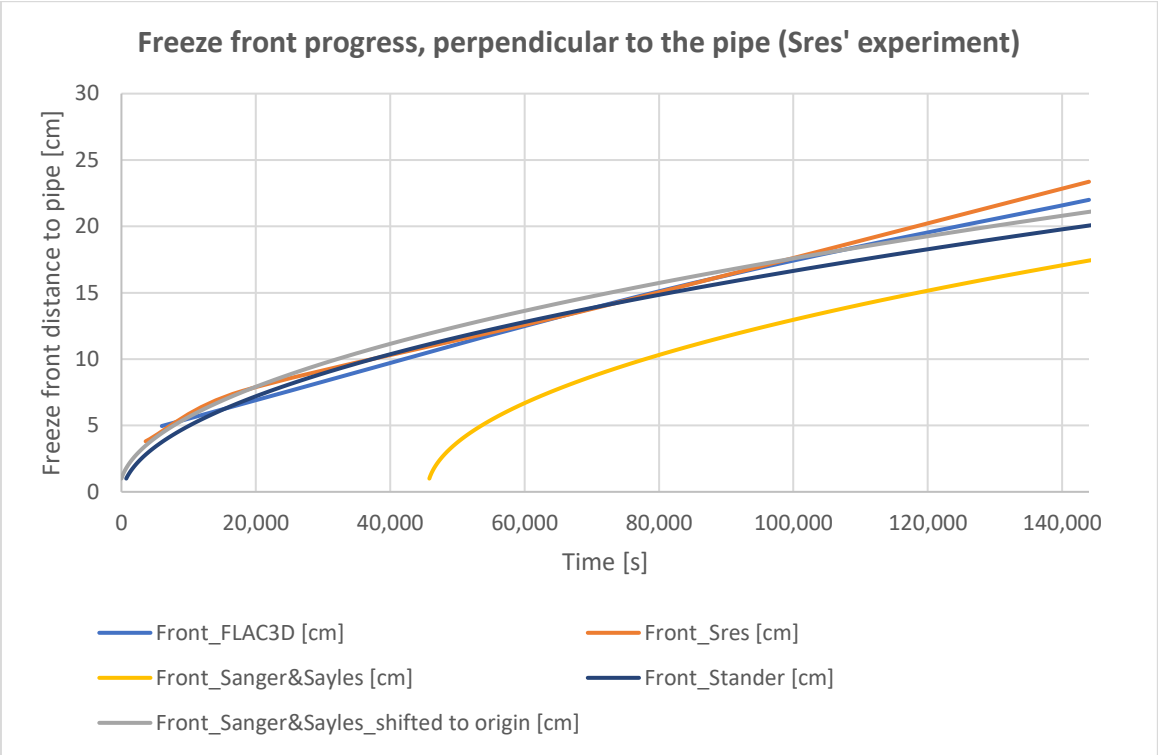

Figure 8.11: Freeze front progress, perpendicular to the pipe row: experimental data, FLAC3D results and analytical solutions

9. Application of the verified numerical model and approximate analytical solutions to artificial ground freezing projects

Real data from ground freezing engineering projects may be used to further validate the approach used in the numerical simulations and approximate analytical formulae from the previous chapters. Unfortunately, there is only a limited number of projects for which detailed, complete monitoring data is publicly available. In this chapter, two such projects were selected: the line 1 of Naples' subway and the Ust-Jaiwa mine freeze shafts. The numerical model verified in chapter 5 was applied to these construction projects. The results of the model are compared against the field measurements performed in the projects. The analytical solutions from Sanger & Sayles and Ständer were also applied to the projects.

9.1. The line 1 of Naples' subway

The section between the stations of Piazza Dante and Piazza Garibaldi of line 1 of Naples' (Italy) subway was excavated using the artificial ground freezing method (Colombo, 2010). The measurements performed to monitor the freezing progress are reported in Colombo (2010). An overview of the freeze pipe arrangement is shown in Figure 9.1.

Figure 9.1: Overview of freeze pipe arrangement (Colombo, 2010)

The results reported in Colombo (2010), from a numerical simulation for a single pipe (used to approximate the pre-closure phase of the wall) with the software ABAQUS, which applies the Finite Element Method, and from his calculation with Sanger & Sayles' solution, are shown in Figure 9.2.

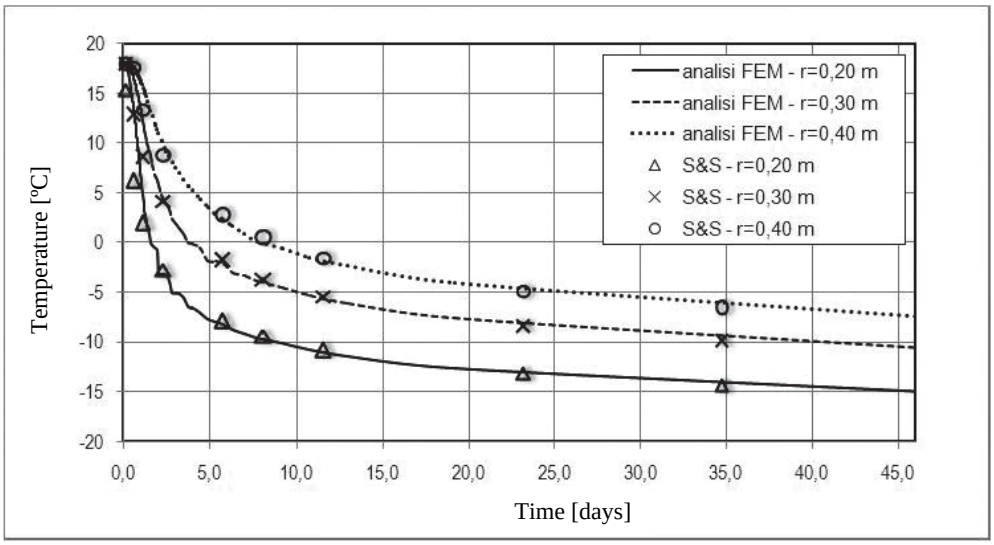

Figure 9.2: Results of thermal calculations with ABAQUS and Sanger & Sayles (single freeze pipe) (Colombo, 2010).

Note: r=0.20 m/0.30 m/0.40 m in the graph legend refer to the temperature at a distance of 0.20 m / 0.30 m / 0.40 m from the freeze pipe. S&S refers to the Sanger & Sayles' results and FEM refers to the results from ABAQUS.

This single-pipe problem was simulated in FLAC3D and with the analytical solutions presented in chapter 6. The boundary conditions and soil characteristics are relatively similar to those of Problem 7 (see chapter 6.2.2). Therefore, not surprisingly, Sanger & Sayles' solution forecasts for this case a faster freeze front progress than the one predicted by the numerical model, an analogous result to the one for Problem 7. Also in line with the results in chapter 6, Ständer's solution provides results which are very close to the ones of the numerical model. Figure 9.3 presents the results from the numerical model and the five analytical solutions evaluated for a time of up to 46.2 days.

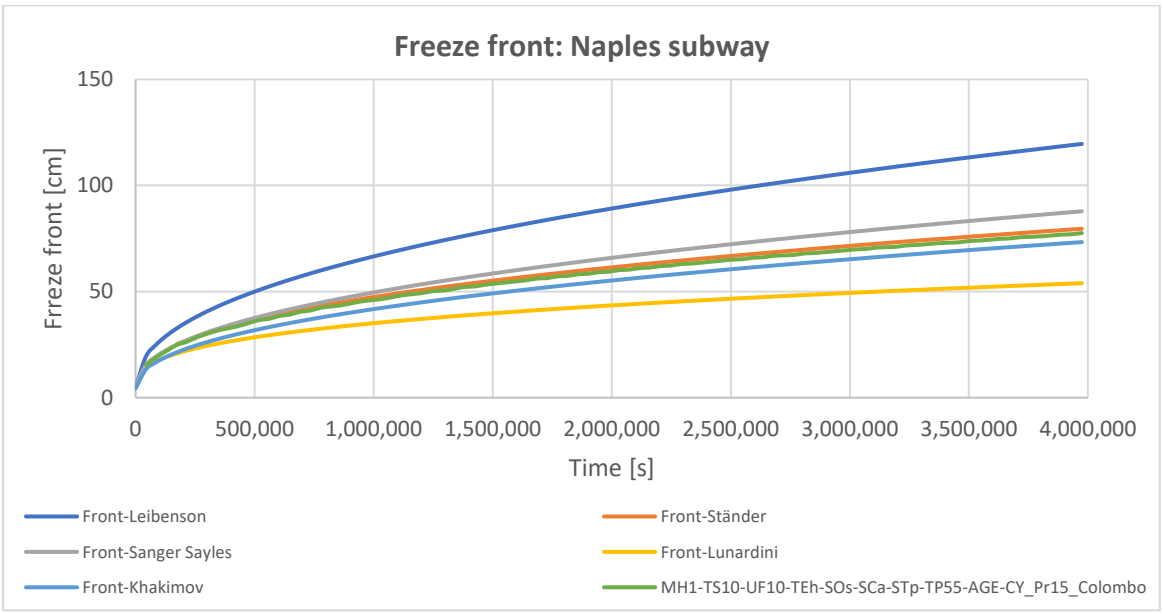

Figure 9.3: Calculation of the freeze front advance for the Naple's subway project with the numerical model and five analytical solutions

The results obtained from the FLAC3D simulation match the ABAQUS results from Colombo (2010) very well, and to a lesser extent, the results derived from the Sanger & Sayles' solution (see Figure 9.4).

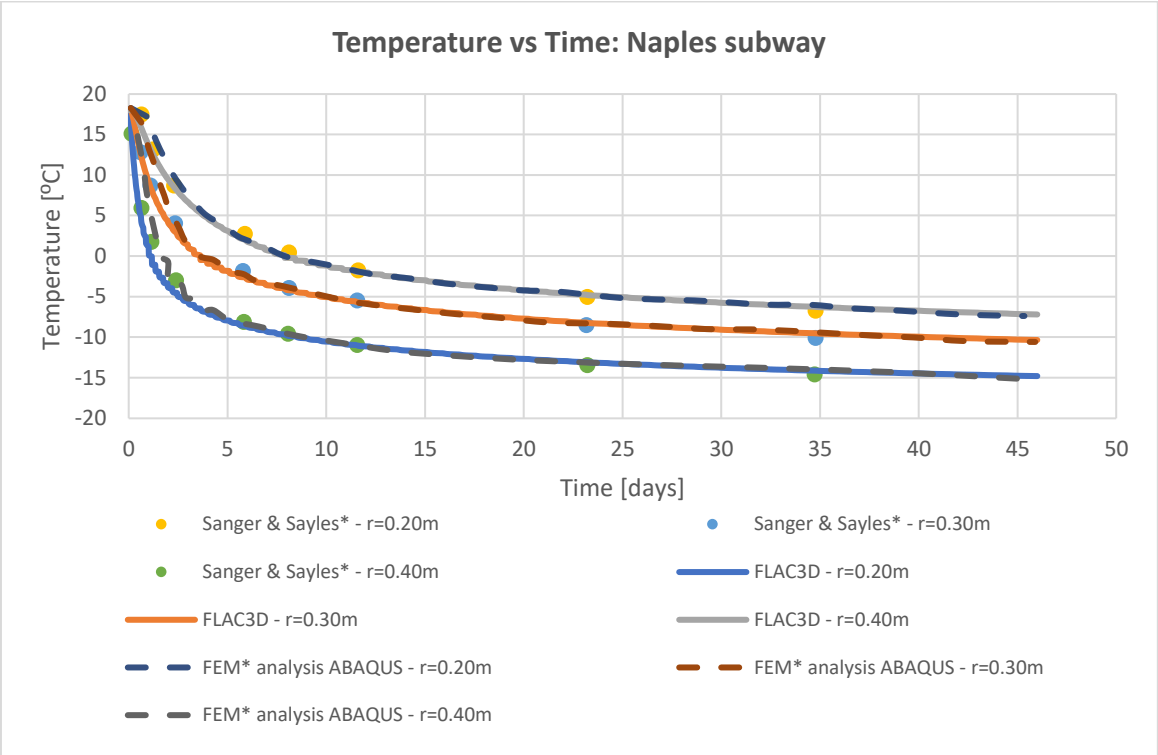

Figure 9.4: Results of simulations of the ground freezing process, Naples metro, single freeze pipe

Note: The results marked with "" are from Colombo (2010).*

For the case of an isolated pipe, no measurement data is available, because the pipes were installed in a row so that a freeze body could be closed in order to protect the tunnelling works. Furthermore, unfortunately, the measurement data available for the project is influenced by several practical factors for which insufficient data is available in Colombo (2010), such as the combination of nitrogen and brine freezing, time-variable freeze pipe temperature, possible groundwater movements and freeze pipe deviations, among others. As these factors are likely to have a high influence on the results, engineering assumptions were made in Colombo (2010) to be able to use the numerical model. However, these factors introduce too much uncertainty in the models, making them effectively unusable for the scientific purpose of verifying either the numerical models or the analytical solutions.

9.2. Ust-Jaiwa mine shafts

Artificial ground freezing was used to sink two freeze shafts for the Ust-Jaiwa potash mine in the Ural region in Russia. The project has been chosen to be analysed in this thesis because the thermal design and monitoring of its freeze circle are thoroughly documented in Hentrich and Franz (2015). In the context of this project, two new mine shafts were sunk with a diameter of 8 m and a depth of about 500 m. Several water-bearing strata were frozen for groundwater control and to achieve shaft wall stability during shaft sinking.

Based on the boundary conditions described in the paper from Hentrich and Franz (2015) and shown in Table 9.1, the single-pipe problem was evaluated with the Leibenson, Lunardini, Khakimov, Sanger & Sayles, adjusted Sanger & Sayles (see chapter 7) and Ständer solutions and simulated with the verified numerical FLAC3D model. Afterwards, the freeze wall and freeze circle geometries were evaluated using the same ground thermal properties.

Table 9.1: Boundary conditions and parameters, Ust-Jaiwa project, modified from Hentrich and Franz (2015)

Technical parameters	**Input**	**Unit**
Radius of freeze pipe	0.06985	m
Half distance between two freeze pipes	0.595	m
Planned thickness of the freeze wall	3.3	m
Radius of freeze circle	8.5	m
Number of freeze pipes	45	nº of pipes
Temperature at freeze pipe wall	−35	°C
Characteristics of the rock (Salt-marl strata)	**Input**	**Unit**
Initial rock temperature	+6	°C
Phase-change temperature	-21	°C
Thermal conductivity of the rock (frozen/unfrozen) – from geotechnical report	8.80/5.72	kJ/hmK
Specific heat capacity of the rock (frozen/unfrozen) – from geotechnical report	2.231/2.878	MJ/m³K
Water content – from geotechnical report	16.4	%
Thermal conductivity of the rock (frozen/unfrozen) – recalculated in Hentrich and Franz (2015)	10.04/6.83	kJ/hmK
Specific heat capacity of the rock (frozen/unfrozen) – recalculated in Hentrich and Franz (2015)	2.231/2.878	MJ/m³K
Water content – recalculated in Hentrich and Franz (2015)	10	%

9.2.1. Simulation of one freeze pipe

As a first step, a single freeze pipe was simulated, using the analytical solutions and a FLAC3D model. The results are shown in Figure 9.5. It is apparent that the adjusted Sanger & Sayles' solution (in this case with the adjusted parameter $a_r = 19.85$) matches the results of the numerical models very well (specially for the one-year timeframe, for which a_r was adjusted). Ständer's and Lunardini's solutions also match the numerical solution reasonably well. It is important to highlight that, even if the difference after one year of about 12 cm for the Ständer solution seems relatively small (implying an error of about 23%), the difference in the required time to achieve a certain radius may be very

large. For practical design purposes, it is often the estimation of the freezing time which is critical, because it determines the waiting time to start excavating and the period of use of the freezing station. As an example, a freeze radius of 53 cm is reached after about 1 year according to the numerical solution, but it would only take about 152 days following Ständer's solution, a difference which implies that this analytical solution should be used with caution in this practical case. No monitoring data is available for the single freeze pipe case because the pipes were located in a freeze circle.

Finally, the results obtained for the single freeze pipe differ widely from the closure time (time to reach the half-distance between pipes, in this case a freeze radius of 59.5 cm) for the freeze circle, which was the geometry in the project. Indeed, a model simulating the freeze circle with the numerical program Temp/W in Hentrich and Franz (2015), which was calibrated based on measurement data, predicted a closure time of 20 days (see Figure 9.6), while the FLAC3D model which considers only one freeze pipe takes longer than one year to reach the freeze radius of 59.5 cm (see Figure 9.5). In this particular case, where the phase-change temperature is low and close to the freeze pipe temperature, the effect of the neighbouring pipes is very accentuated, because the heat that needs to be extracted before the phase change occurs is high (Ständer, 1967).

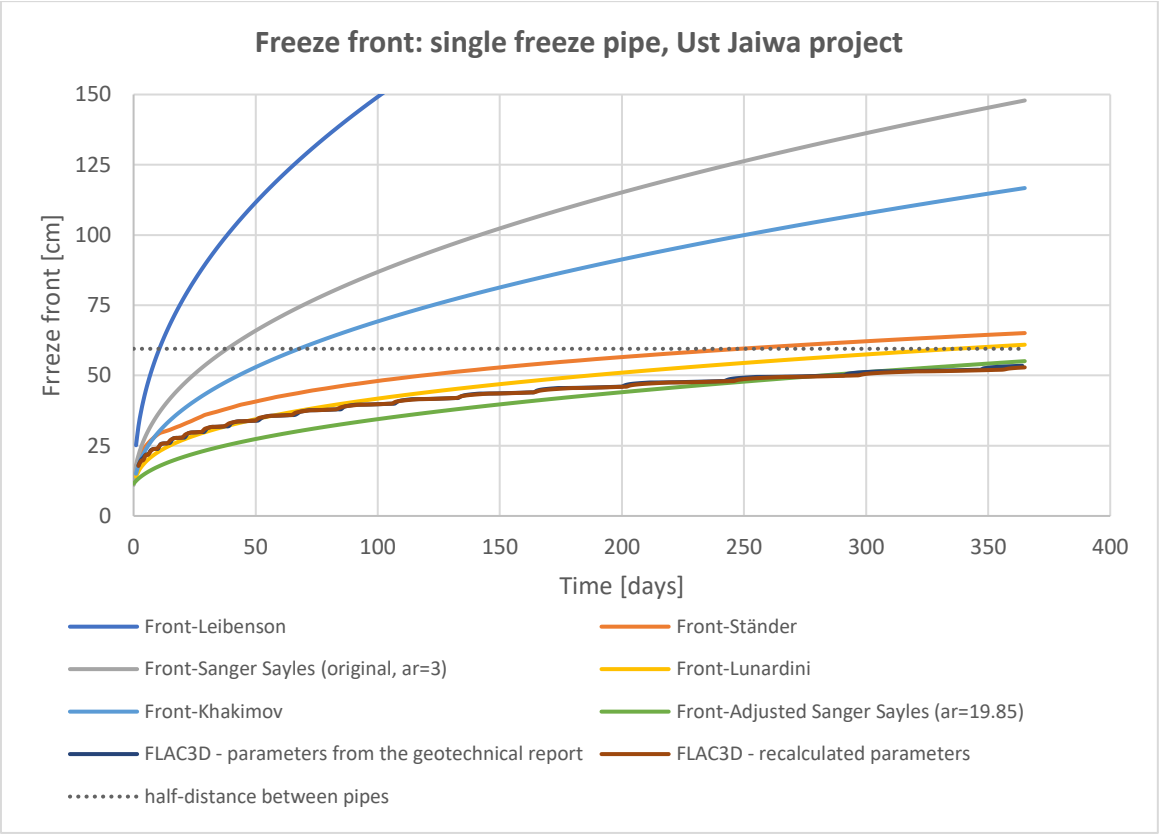

Figure 9.5: Freeze front, one freeze pipe, Ust-Jaiwa project

9.2.2. Simulation of two neighbouring pipes (freeze wall)

A model accounting for two neighbouring pipes (via symmetry) was simulated in FLAC3D as a first approximation to the freeze circle. This can be considered a reasonable approximation in the first period after closure, when the circle can be approximated by a flat freeze wall; afterwards the freeze circle geometry leads to notoriously different freeze radius advance velocities on the outside and inside of the freeze circle. The results of this model with two neighbouring pipes show, as expected, a much faster freeze radius advance than in the model in the previous chapter, which only considered one single pipe. The closure time of about 14 days, corresponding to a radius of 59.5 cm (the half-distance between the pipes), matches only moderately well the 20 days obtained with a numerical model for the ideal freeze circle geometry from Hentrich and Franz (2015), which was calibrated based on monitoring data. The significant difference may be accounted for by several practical effects, which are not considered in the FLAC3D model, but which may have been considered in Hentrich's calibrated TEMP/W model, such as the cooling of the system in the first days of freezing or the excavation of the shaft.

The freeze body grows much faster between the pipes (due to the influence of the neighbouring pipes) than perpendicular to them (see Figure 9.6). For instance, it takes about 33 days for the freeze body to reach a radius of 59.5 cm from the pipe centre in the perpendicular direction, in comparison to the closure time of 14 days. The progress of the freeze front in the directions parallel and perpendicular to the pipes is shown in Figure 9.6. The results for the single pipe are presented as well in Figure 9.6 for comparison. The solutions of Sanger & Sayles and Ständer for the freeze wall geometry have also been evaluated for the recalculated thermal parameters and are presented in the same figure. In accordance with the results in chapter 6.3, Ständer's solution provides a quite good approximation of the numerical results. Finally, the results from Hentrich and Franz (2015) for the freeze circle are also showed in Figure 9.6. Comparing them to the freeze wall simulation from FLAC3D, it can be observed that the progress of the freeze front for the freeze wall is approximately the average progress of the inner and outer freeze fronts for the freeze circle.

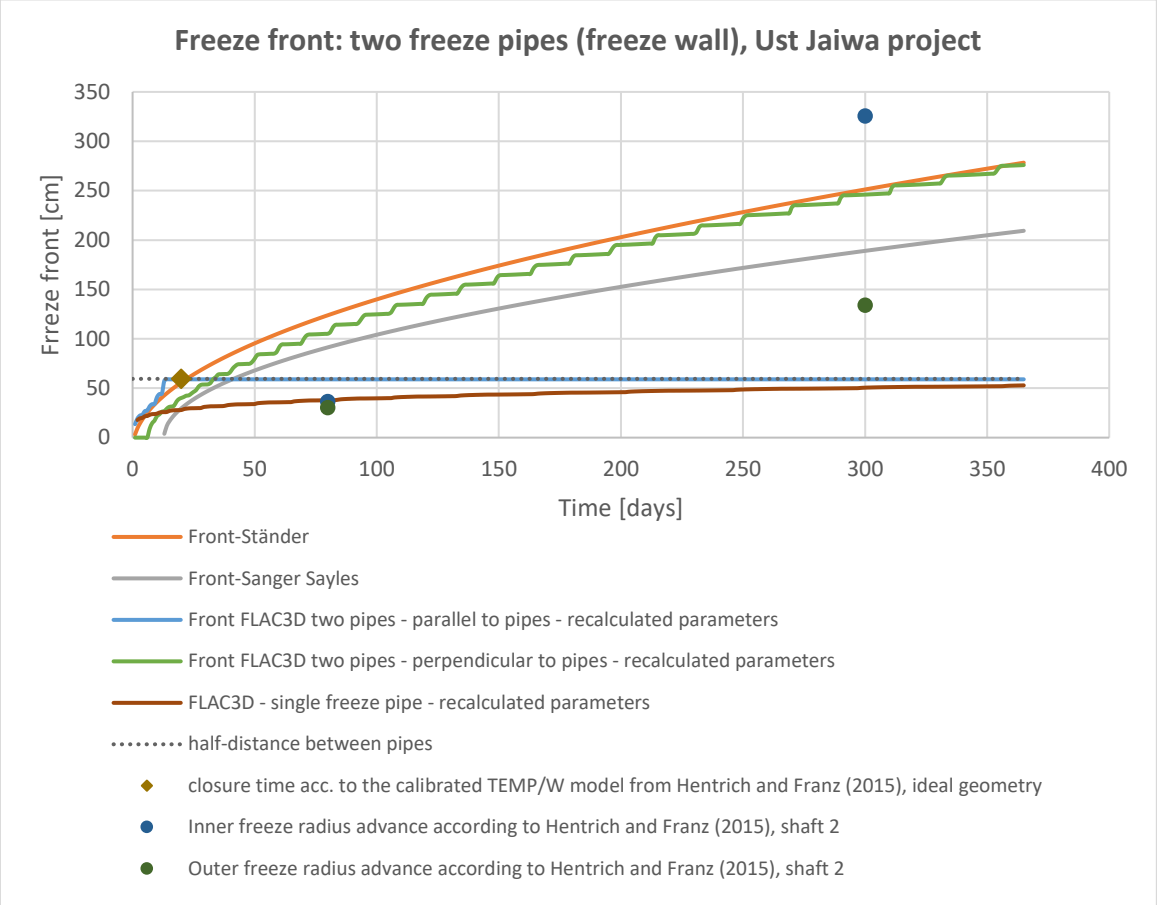

Figure 9.6: Freeze front, two freeze pipes simulated (freeze wall), Ust-Jaiwa project

9.2.3. **Simulation of the freeze circle**

The Ust-Jaiwa problem has been simulated in FLAC3D likewise for the freeze-circle geometry, using the same meshing approach of Figure 5.48. The analytical solutions from Sanger & Sayles and Ständer have also been evaluated for this geometry. The results are presented in Figure 9.7. The numerical results match the results from the simulations from Hentrich and Franz (2015) for the outer freeze front very accurately, but not for the inner freeze front. This may be due to Hentrich and Franz (2015) having considered the thermal influence of elements from inside the shaft related to the sinking process. Ständer's solution produces very poor results in this case, largely underestimating the freeze front progress. Interestingly, if computed for a higher water content of 21% instead of 10%, it produces more accurate results, yielding a faster freeze front progress (also shown in Figure 9.7). This issue of Ständer's solution for the freeze circle generating unplausible results for low water contents has already been identified in Problem 10_fc and described in chapter 6.4.2. Sanger & Sayles' solution overestimates the outer freeze radius and underestimates the inner freeze radius.

The analyses performed in this chapter give further confidence in the verified numerical model, whereas they also show that the specific boundary conditions of the project at hand, which may not be reported in publications, can have a major influence on the thermal field.

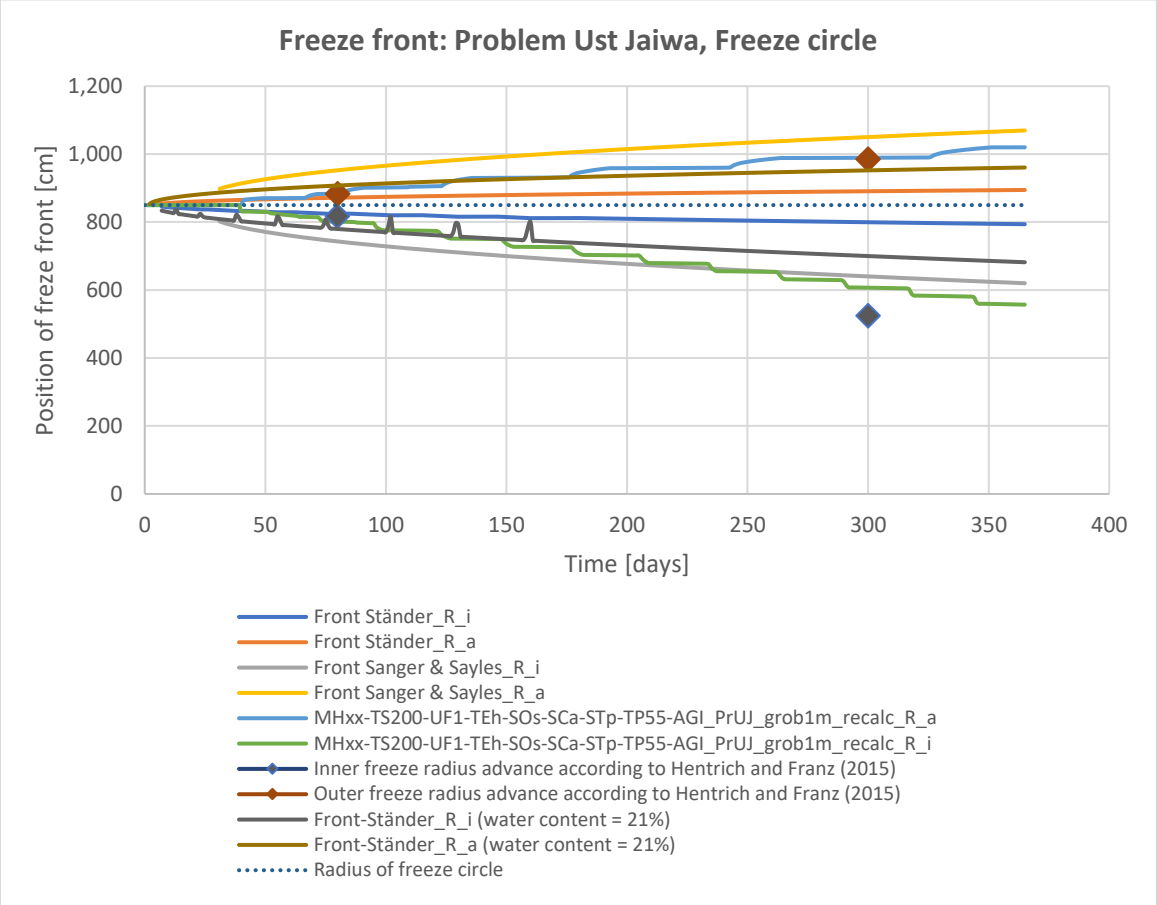

Figure 9.7: Freeze front, Ust-Jaiwa problem, freeze-circle geometry
Note: Graph origin is the centre of the freeze circle.

10. Discussion of the investigations on thermal calculations for ground freezing design

The results obtained in the previous chapters of this thesis are discussed here with the aim of reaching practical conclusions which can be of use in real-life engineering projects. First, the results of the numerical experiments from chapter 5 are analysed and conclusions drawn towards the creation of a code of good practice for numerical modelling of thermal problems with phase change. Afterwards, the results of the sensitivity analysis with analytical solutions from chapter 6 and the adjusted solution from chapter 7 are discussed, aiming to provide designers with sufficiently accurate and practical tools for design, along with a database of the accuracy of the different solutions for a variety of potential scenarios.

10.1. Effects of the numerical parameters on the accuracy and efficiency of numerical models for thermal calculations with phase change

This discussion is based on data gained from the evaluation of the numerical model performed in chapter 5, done primarily by means of sensitivity analyses. That study was mainly focused on the accuracy of both the temperature field and the position of the phase-change interface. The accuracy of the power consumption, which is also related to the accuracy of the temperature, as the thermal flux is directly proportional to the temperature gradient, was also shortly investigated in chapter 5.13. These results are discussed in the following sections.

The dependency of the error with the mesh size and frequency of update of the freeze status of the elements, for the explicit and implicit methods, is discussed in this chapter. The dependency with the time step is only evaluated for the implicit method because it has been shown in chapter 5.4 that the size of the time step does not have a significant influence on the accuracy of the results of the explicit method.

After investigating the effects of several numerical parameters on the accuracy and computing time of the numerical models in chapter 5, several clear conclusions can be drawn. For instance, the mesh size is the parameter with the most predominant effect according to the sensitivity analyses, largely influencing the size of the plateaux of the temperature which are typical of the enthalpy method. The plateaux in turn make the numerical results deviate from the exact, smooth solution. Although the results tend to converge for longer times, the inaccuracies appear mostly in the areas near the freeze front, where the phase change is occurring. The accuracy of the freeze front location is also affected by the mesh size. On the other hand, the time step, for the explicit solving method, does not have a major effect on the accuracy, as long as it is kept under the critical time step, which depends on the mesh size used (see chapter 5.4). For this reason, the effect of the time step on the accuracy of the explicit method is not studied in further detail in this chapter. Both the mesh size and time step are parameters which have a high, direct influence on the computing time. Consequently, a sufficiently small mesh size, depending on the

required accuracy, along with the corresponding critical time step should be used for modelling.

The frequency of updating the freezing status of the elements, i.e. the frequency of execution of the "freeze code", has a moderate effect on the accuracy and on the computing time. Nevertheless, the time between updates should be significantly smaller than the required time to freeze the elements (or the duration of the appearing plateaux in the graphs).

A way to smooth the plateaux and improve the accuracy of the enthalpy method is using a larger phase-change temperature range (see chapter 5.8). However, it has to be considered whether this represents the actual phase change process of the ground. Using this approach also increases the computing time.

The results of the explicit and implicit algorithms were compared in chapter 5.11. In general, for the critical time step, the explicit and implicit methods produced results of similar accuracy and required similar computing times. The implicit method is, however, more flexible in certain cases. For instance, it can be used with larger time steps than the critical one, sparing computing time and producing reasonably accurate results. Additionally, for complex models, with very variable mesh sizes including some very small elements, the explicit method requires very small time steps, the critical time step for the model being determined by the smallest elements, and may therefore require very long computing times. In those cases, the implicit method has the advantage that it can use larger time steps, requiring shorter computing times.

Regarding the type of thermal source, a surface source instead of a punctual source should be used, e.g. to model a freeze pipe (see chapter 5.16). First, a punctual source is infinitesimally small, so it tends to produce local issues in the numerical calculations. Besides, a surface source is a more realistic representation of the geometry of a freeze pipe.

Even under very extreme conditions of extremely high latent heat or very high initial temperature gradient, the numerical model proved to be stable and reasonably accurate, provided that appropriate numerical parameters (mesh size, time step, etc.) were chosen. Numerical results converged to the exact analytical solutions when the discretisation was refined (finer mesh, smaller time step, etc.).

A qualitative analysis of the existing errors in the numerical models may be attempted based on sensitivity analyses. In chapter 5, it was shown that the most decisive parameter of the numerical model, which usually dominates the accuracy of the model, is the mesh size. Additionally, as already reported by several authors (see chapter 4.3.2.1 and e.g. Furzeland (1980), Voller and Cross (1981), Basu and Date (1988), Mackenzie and Robertson (2000)), the numerical results of the enthalpy method, which is the most extended and practical phase-change method, oscillate around the exact solution. The oscillations result in the temperature-versus-time and freeze-front-versus time graphs presenting plateaux or "steps" (see e.g. chapter 5.3). The size of these "steps" is directly related to the mesh size, as

illustrated in Figure 10.1. Therefore, the question presents itself, whether it is possible to estimate the error of the results in the cases where no exact analytical solution is known.

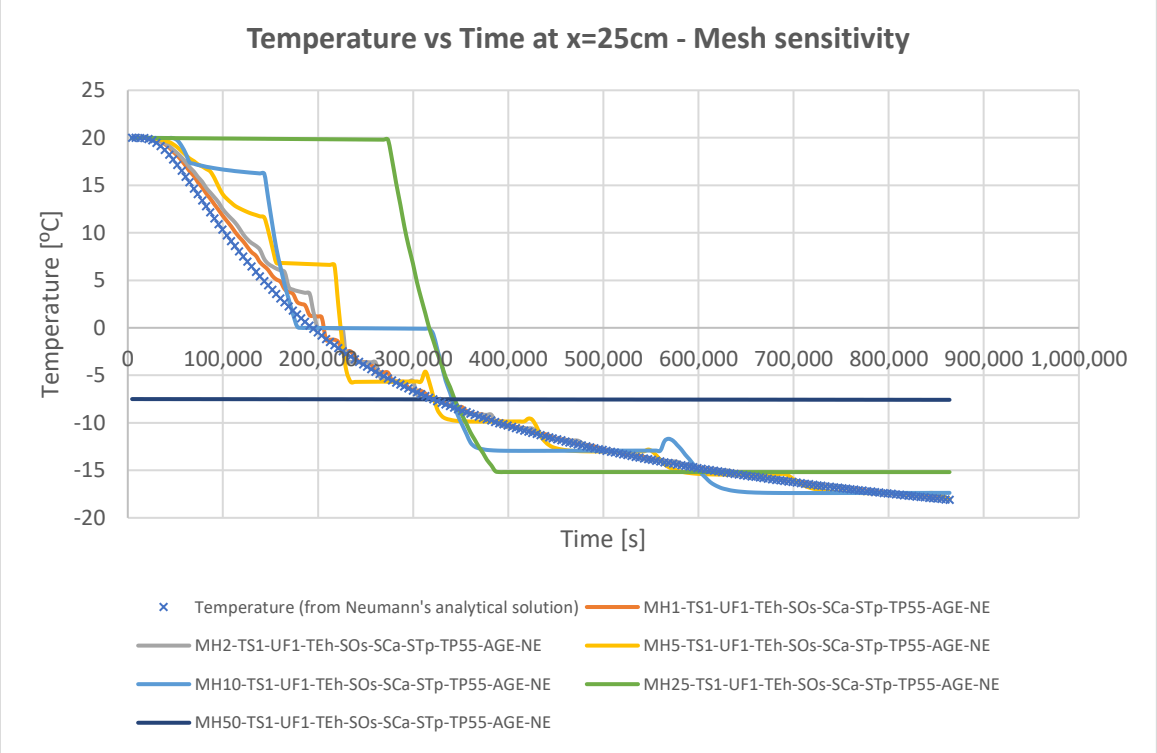

Figure 10.1: Temperature vs time at x=25cm, mesh sensitivity for Problem 1

When the mesh size is decreased, the results of the numerical model tend to match the exact solution with increasing accuracy (see e.g. Figure 10.1). This effect may be exploited in practical problems, where the exact solution is not known, in order to estimate the error of the numerical model. For example, a model with a small mesh may be run in order to compare it with the models with a larger mesh, which makes it possible to estimate their accuracy. Then, once the approximate accuracy of the models with larger mesh and lower computing time is known and thus confidence on their performance has been won, it is possible to calculate other models or design variants with those faster models, sparing time for the design engineer. As a rough assumption, the unknown exact solution could be approximated by a line which interpolates the plateaux (see e.g. Figure 10.1).

10.1.1. Mesh size

The relationship between the error of the freeze front position and the mesh size is presented in this chapter. The figures below provide an overview of the results of the models listed in Table 10.1 and Table 10.2, which simulated problems with the Neumann geometry. They are based on the results obtained in chapter 5 with the explicit solving algorithm. From this study, it is again confirmed that the mesh size is a dominant parameter affecting the error of the results of numerical simulations (see also e.g. Stout and Billings (2002)).

Table 10.1: Models considered in Figures 10.2, 10.3, 10.6 and 10.7

MH1-TS1-UF1-TEh-SOs-SCa-STp-TP55-AGE-NE
MH2-TS1-UF1-TEh-SOs-SCa-STp-TP55-AGE-NE
MH5-TS1-UF1-TEh-SOs-SCa-STp-TP55-AGE-NE
MH10-TS1-UF1-TEh-SOs-SCa-STp-TP55-AGE-NE
MH25-TS1-UF1-TEh-SOs-SCa-STp-TP55-AGE-NE
MH50-TS1-UF1-TEh-SOs-SCa-STp-TP55-AGE-NE
MH1-TS1-UF1-TEh-SOs-SCa-STp-TP250-AGE-NE
MH2-TS1-UF1-TEh-SOs-SCa-STp-TP250-AGE-NE
MH5-TS1-UF1-TEh-SOs-SCa-STp-TP250-AGE-NE
MH10-TS1-UF1-TEh-SOs-SCa-STp-TP250-AGE-NE
MH25-TS1-UF1-TEh-SOs-SCa-STp-TP250-AGE-NE
MH50-TS1-UF1-TEh-SOs-SCa-STp-TP250-AGE-NE
MH1-TS1-UF1-TEh-SOs-SCa-STp-TP10-AGE-NE
MH2-TS1-UF1-TEh-SOs-SCa-STp-TP10-AGE-NE
MH5-TS1-UF1-TEh-SOs-SCa-STp-TP10-AGE-NE
MH10-TS1-UF1-TEh-SOs-SCa-STp-TP10-AGE-NE
MH25-TS1-UF1-TEh-SOs-SCa-STp-TP10-AGE-NE
MH50-TS1-UF1-TEh-SOs-SCa-STp-TP10-AGE-NE
MH1-TS1-UF1-TEh-SOs-SCg-STp-TP10-AGE-NE
MH2-TS1-UF1-TEh-SOs-SCg-STp-TP10-AGE-NE
MH5-TS1-UF1-TEh-SOs-SCg-STp-TP10-AGE-NE
MH10-TS1-UF1-TEh-SOs-SCg-STp-TP10-AGE-NE
MH25-TS1-UF1-TEh-SOs-SCg-STp-TP10-AGE-NE
MH50-TS1-UF1-TEh-SOs-SCg-STp-TP10-AGE-NE
MH1-TS1-UF1-TEh-SOs-SCa-STp-TP250-AGE-NE_LHTx10
MH2-TS1-UF1-TEh-SOs-SCa-STp-TP250-AGE-NE_LHTx10
MH5-TS1-UF1-TEh-SOs-SCa-STp-TP250-AGE-NE_LHTx10
MH10-TS1-UF1-TEh-SOs-SCa-STp-TP250-AGE-NE_LHTx10
MH25-TS1-UF1-TEh-SOs-SCa-STp-TP250-AGE-NE_LHTx10
MH50-TS1-UF1-TEh-SOs-SCa-STp-TP250-AGE-NE_LHTx10

Table 10.2: Models considered in Figures 10.4 and 10.5

MH1-TS20-UF1-TEh-SOs-SCa-STp-TP250-AGE-NE
MH5-TS200-UF1-TEh-SOs-SCa-STp-TP250-AGE-NE
MH10-TS1-UF1-TEh-SOs-SCa-STp-TP250-AGE-NE
MH25-TS1-UF1-TEh-SOs-SCa-STp-TP250-AGE-NE
MH50-TS1-UF1-TEh-SOs-SCa-STp-TP250-AGE-NE

The root-mean-square error (RMSE), which is a commonly used measure of the error (see e.g. Ivanovic et al. (2017)) and the maximum error were calculated for the numerical results of the models listed above, taking as basis the exact solution from Neumann. Both errors have a linear correlation with the mesh size (see Figure 10.2, Figure 10.3, Figure 10.4 and Figure 10.5) and are also linearly correlated to one another (see Figure 10.6). As already noticed previously (see chapter 5.3), the error tends to decline with time: the RMSE considering the first 10 days of simulation (see Figure 10.2) is higher than the RMSE for the first 365 days (see Figure 10.4). Equation (10.1) shows the formula for the application of the RMSE.

$$RMSE = \sqrt{\frac{1}{n}\sum_{i=1}^{n}(x_i^{num} - x_i^{exact})^2} \tag{10.1}$$

where:

n: number of data points

x_i^{exact}: value of the variable x, from the exact analytical solution

x_i^{num}: value of the variable x, from the numerical method

The figures and correlations below show that the error of the freeze front (RMSE and maximum error) can be expressed as a fraction (or percentage) of the mesh size, which shows that the method is convergent and matches the widely accepted concept that a lower mesh size provides more accurate results (Recktenwald, 2004). The correlations explain most of the variability in the error ($R^2 > 0.95$) and all the obtained points fall into the bands of the 99.73% confidence interval ($\mu \pm 3\sigma$).

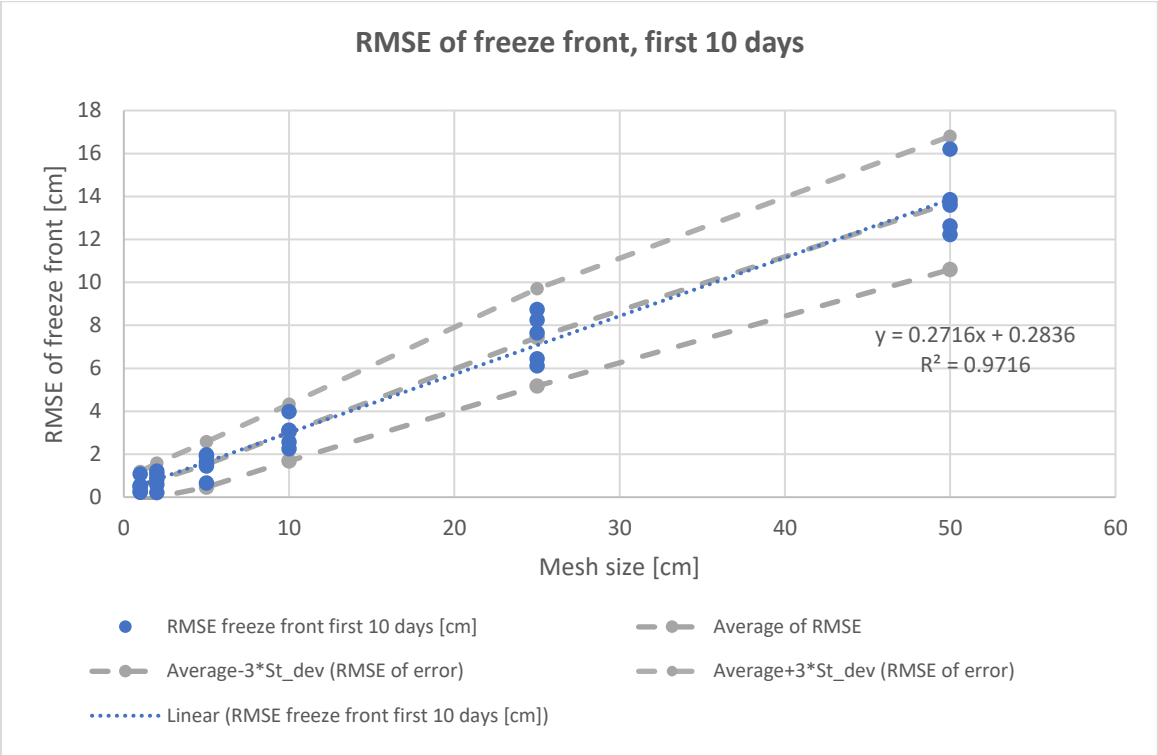

Figure 10.2: RMSE of freeze front, first 10 days (models from Table 10.1)

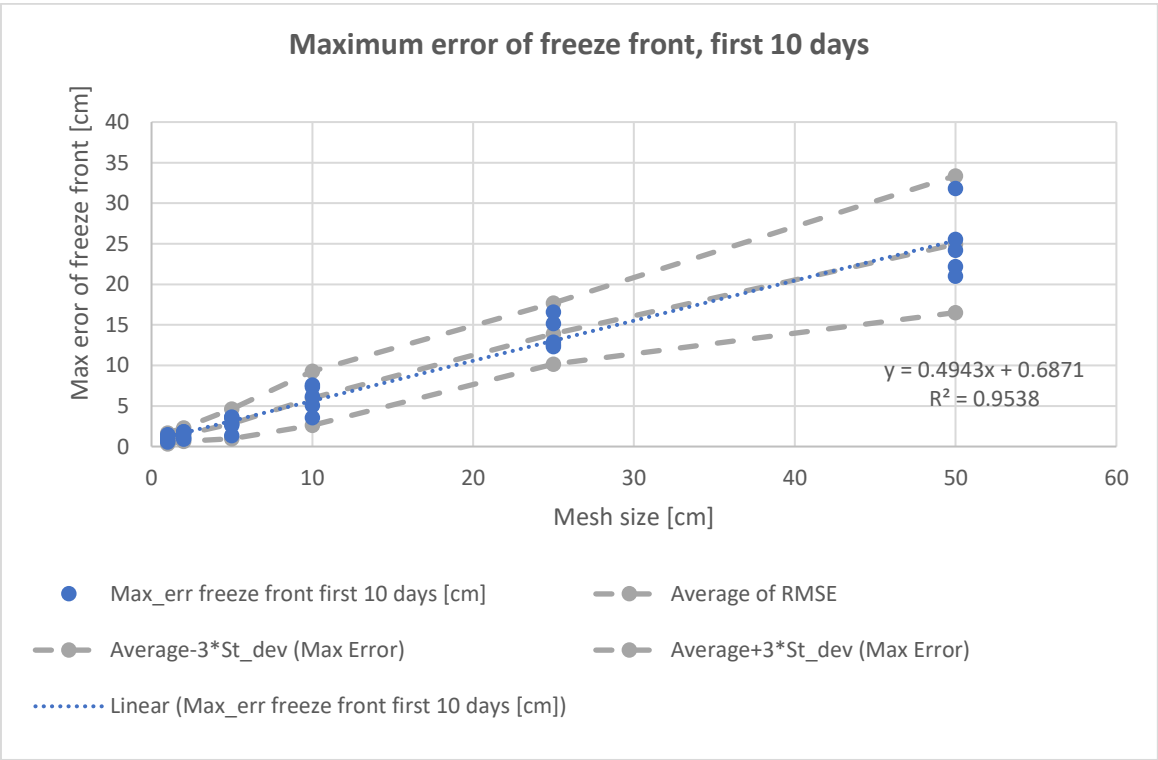

Figure 10.3: Maximum error of freeze front, first 10 days (models from Table 10.1)

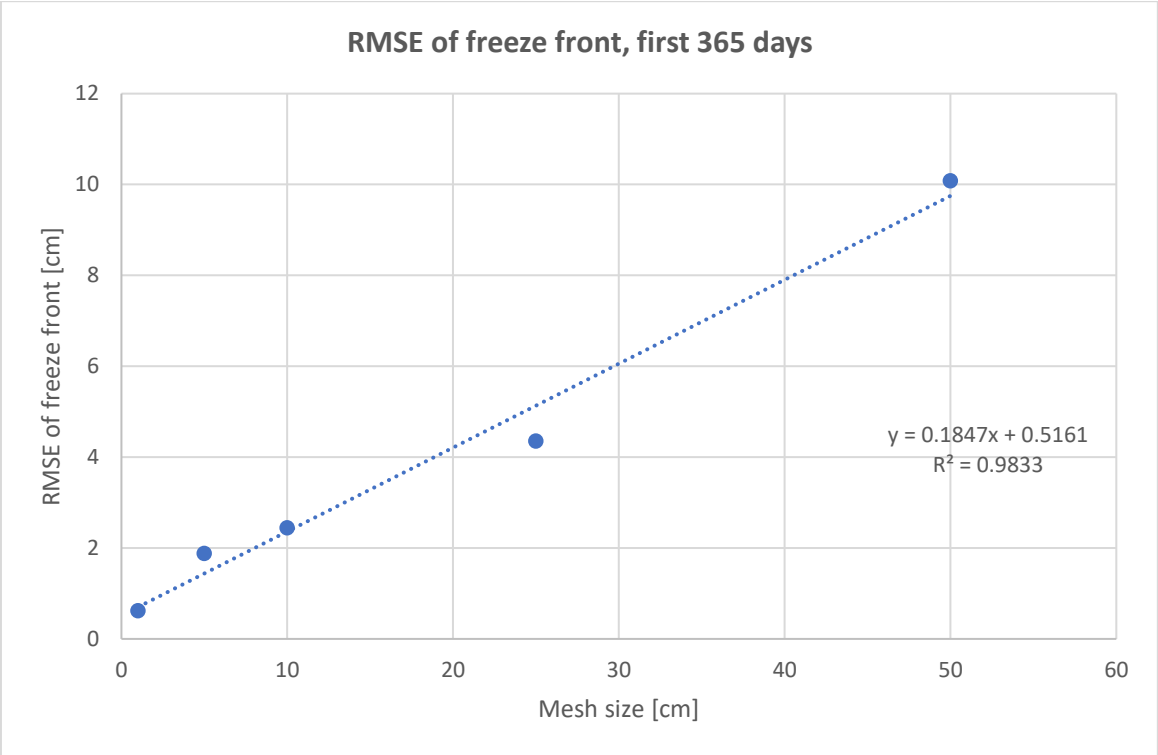

Figure 10.4: RMSE of freeze front, first 365 days (models from Table 10.2)

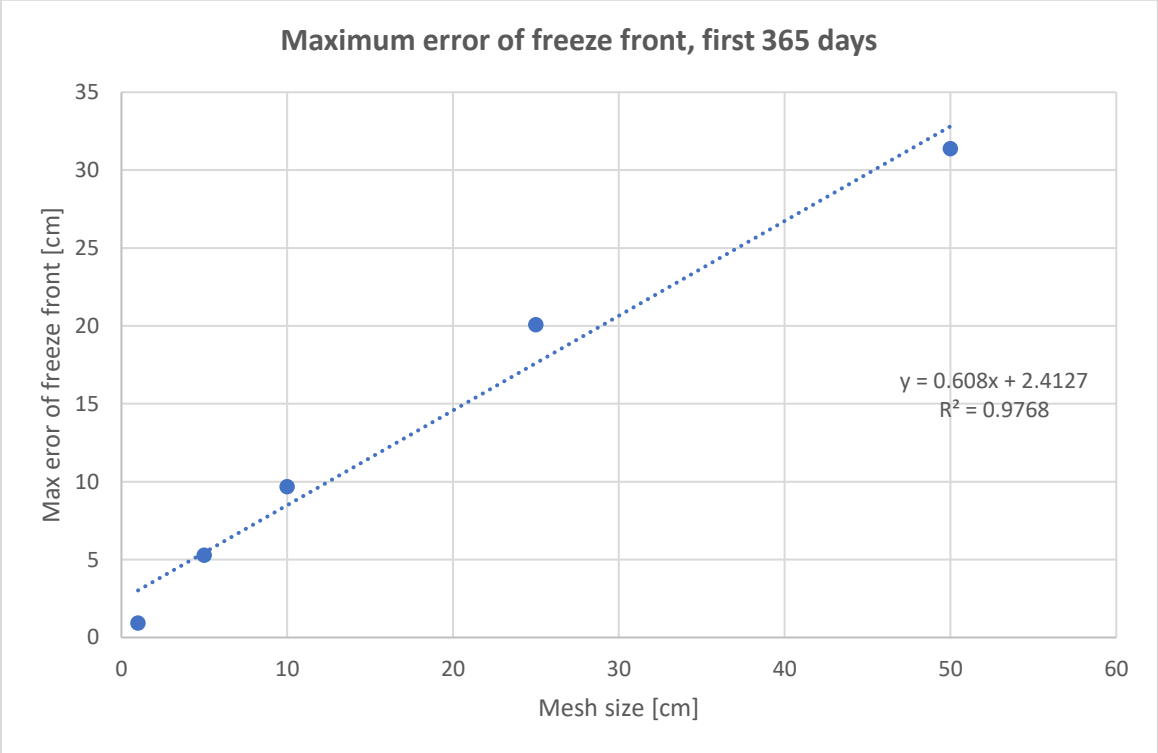

Figure 10.5: Maximum error of freeze front, first 365 days (models from Table 10.2)

In chapter 5, the evaluation of the accuracy of the models was mainly based on average and maximum errors. Figure 10.6 and Figure 10.7 show the very high correlation between the

RMSE and the maximum and average of the absolute value of the errors, respectively. Therefore, the approach used in chapter 5 can be considered valid.

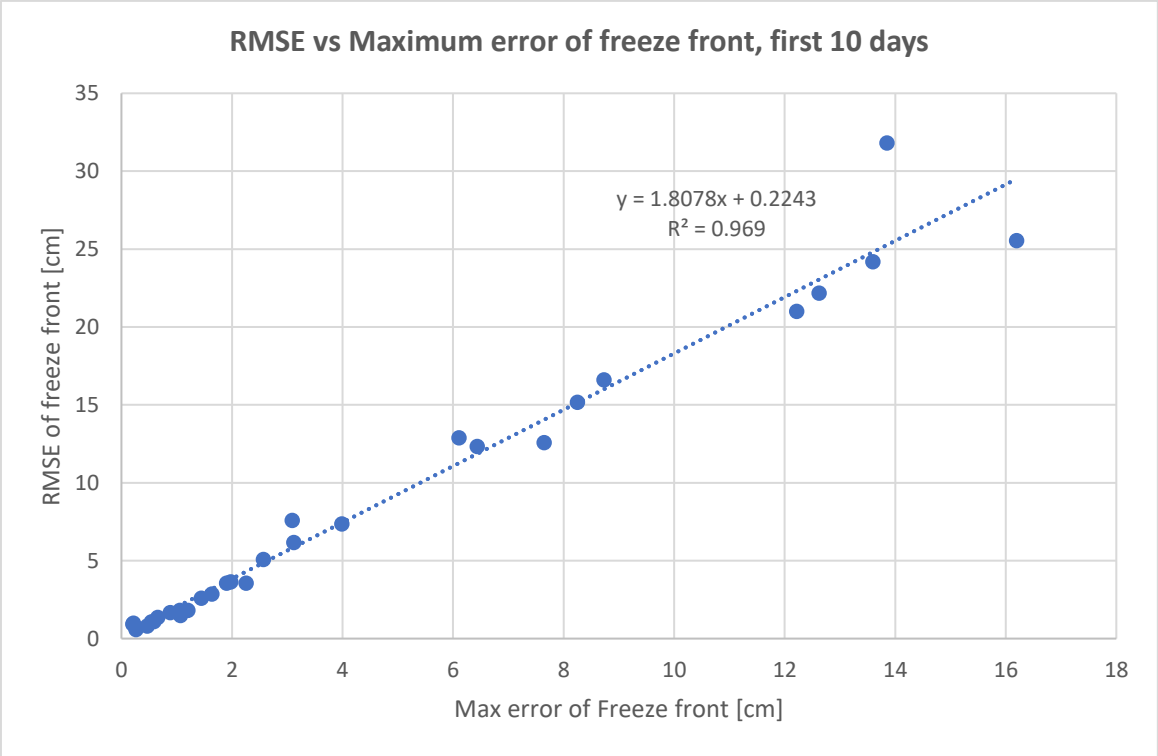

Figure 10.6: RMSE and maximum error of freeze front, first 10 days (models from Table 10.1)

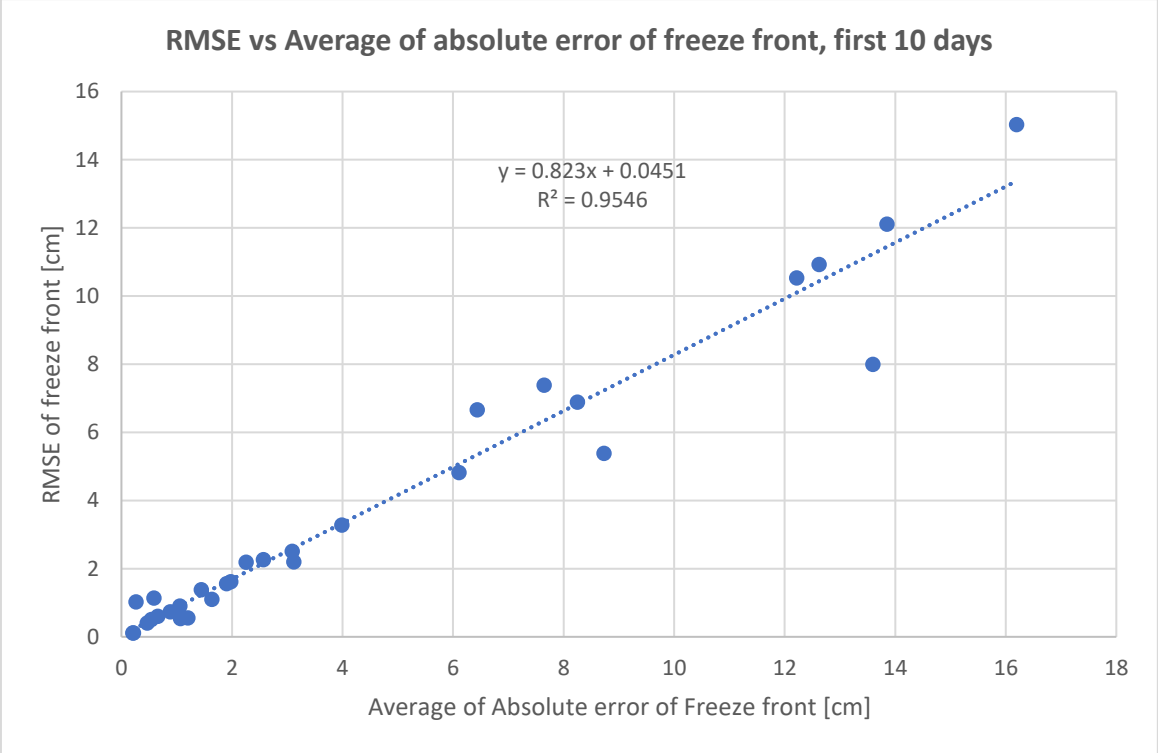

Figure 10.7: RMSE and average of absolute error of freeze front, first 10 days (models from Table 10.1)

10.1.2. **Computing time**

The subject of study of this chapter is the correlation of the computing time with the number of elements in the model, the number of time steps simulated and the update interval of the freeze status. The parameter used, which was adjusted so that it correlates linearly with the computing time, is defined in Equation (10.2). It was adjusted by modifying the values of the exponents g, h and i based on the data for a computed thermal time of 10 days from the models listed in Table 10.3.

$$q = {n_1}^g \cdot {m_1}^h \cdot u^i / 10^5 \tag{10.2}$$

where:

$g = 0.65$: exponent of the variable n_1, number of elements in the model

$h = 1.0$: exponent of the variable m_1, number of time steps simulated

$i = 0.6$: exponent of the variable u, number of time steps after which the freeze status is updated

m_1: number of time steps simulated

n_1: number of elements in the model

q: calibrated parameter

u: update period (the "freeze block" routine is executed every u time steps)

This analysis shows that the computing time depends on the number of elements, which obviously affects the duration of the calculation time for each time step, on the number of time steps (the total computing time is the sum of the computing time for each of the time steps) and on the update period at which the freeze block is executed (which adds some computing time to the time steps in which it is executed). It has to be highlighted here that the variable with the most marked effect on the computing time is the number of time steps simulated. That can also be observed from its exponent, which is the largest of the three in Equation (10.2). The three variables considered, along with the adjusted exponents, explain most of the variability in computing time in the different models ($R^2 > 0.93$). Figure 10.8 and Figure 10.9 represent the correlations of the defined parameter q with the computing time, for models with computed thermal times of 10 and 365 days, respectively.

Table 10.3: Models used for the correlation of the parameter q with the computing time and shown in Figure 10.8

Model name	Computing time	Parameter q
MH1-TS1-UF1-TEh-SOs-SCa-STp-TP250-AGE-NE_LHTx10	0:37:13	270.51
MH1-TS1-UF1-TEh-SOs-SCa-STp-TP250-AGE-NE	0:29:37	270.51
MH1-TS1-UF1-TEh-SOs-SCa-STp-TP55-AGE-NE	0:29:27	270.51
MH2-TS1-UF1-TEh-SOs-SCa-STp-TP250-AGE-NE	0:24:59	172.39
MH2-TS1-UF1-TEh-SOs-SCa-STp-TP250-AGE-NE_LHTx10	0:18:30	172.39
MH2-TS1-UF1-TEh-SOs-SCa-STp-TP55-AGE-NE	0:16:24	172.39

MH5-TS1-UF1-TEh-SOs-SCa-STp-TP250-AGE-NE	0:13:08	95.03
MH10-TS1-UF1-TEh-SOs-SCa-STp-TP250-AGE-NE_LHTx10	0:10:02	60.56
MH5-TS1-UF1-TEh-SOs-SCa-STp-TP250-AGE-NE_LHTx10	0:09:57	95.03
MH5-TS1-UF1-TEh-SOs-SCa-STp-TP55-AGE-NE	0:08:25	95.03
MH1-TS1-UF10-TEh-SOs-SCa-STp-TP250-AGE-NE_LHTx10	0:08:07	67.95
MH1-TS5-UF1-TEh-SOs-SCa-STp-TP250-AGE-NE_LHTx10	0:08:02	54.10
MH1-TS1-UF10-TEh-SOs-SCa-STp-TP55-AGE-NE	0:07:32	67.95
MH25-TS1-UF1-TEh-SOs-SCa-STp-TP250-AGE-NE_LHTx10	0:07:16	33.38
MH10-TS1-UF1-TEh-SOs-SCa-STp-TP250-AGE-NE	0:07:08	60.56
MH1-TS1-UF1000-TEh-SOs-SCa-STp-TP250-AGE-NE_LHTx10	0:06:51	4.29
MH1-TS5-UF1-TEh-SOs-SCa-STp-TP55-AGE-NE	0:06:49	54.10
MH50-TS1-UF1-TEh-SOs-SCa-STp-TP250-AGE-NE_LHTx10	0:06:02	21.27
MH25-TS1-UF1-TEh-SOs-SCa-STp-TP250-AGE-NE	0:06:00	33.38
MH1-TS5-UF1-TEh-SOs-SCa-STp-TP250-AGE-NE	0:05:57	54.10
MH1-TS1-UF10-TEh-SOs-SCa-STp-TP250-AGE-NE	0:05:32	67.95
MH10-TS1-UF1-TEh-SOs-SCa-STp-TP55-AGE-NE	0:05:27	60.56
MH1-TS10-UF1-TEh-SOs-SCa-STp-TP250-AGE-NE_LHTx10	0:05:26	27.05
MH1-TS1-UF1000-TEh-SOs-SCa-STp-TP250-AGE-NE	0:05:23	4.29
MH50-TS1-UF1-TEh-SOs-SCa-STp-TP250-AGE-NE	0:05:19	21.27
MH1-TS1-UF100-TEh-SOs-SCa-STp-TP55-AGE-NE	0:05:02	17.07
MH1-TS1-UF100-TEh-SOs-SCa-STp-TP250-AGE-NE_LHTx10	0:04:21	17.07
MH1-TS1-UF100-TEh-SOs-SCa-STp-TP250-AGE-NE	0:04:07	17.07
MH1-TS1-UF1000-TEh-SOs-SCa-STp-TP55-AGE-NE	0:04:01	4.29
MH25-TS1-UF1-TEh-SOs-SCa-STp-TP55-AGE-NE	0:03:43	33.38
MH1-TS10-UF1-TEh-SOs-SCa-STp-TP55-AGE-NE	0:03:38	27.05
MH50-TS1-UF1-TEh-SOs-SCa-STp-TP55-AGE-NE	0:03:16	21.27
MH1-TS20-UF1-TEh-SOs-SCa-STp-TP250-AGE-NE_LHTx10	0:03:08	13.53
MH1-TS10-UF1-TEh-SOs-SCa-STp-TP250-AGE-NE	0:02:12	27.05
MH1-TS20-UF1-TEh-SOs-SCa-STp-TP55-AGE-NE	0:01:48	13.53
MH1-TS40-UF100-TEh-SOs-SCa-STp-TP250-AGE-NE_LHTx10	0:01:14	6.76
MH1-TS20-UF1-TEh-SOs-SCa-STp-TP250-AGE-NE	0:01:13	13.53
MH1-TS40-UF1-TEh-SOs-SCa-STp-TP55-AGE-NE	0:01:01	6.76
MH1-TS40-UF100-TEh-SOs-SCa-STp-TP55-AGE-NE	0:00:47	0.43
MH1-TS40-UF1-TEh-SOs-SCa-STp-TP250-AGE-NE	0:00:38	6.76
MH5-TS200-UF1-TEh-SOs-SCa-STp-TP250-AGE-NE_LHTx10	0:00:18	0.48
MH1-TS40-UF100-TEh-SOs-SCa-STp-TP250-AGE-NE	0:00:17	0.43
MH1-TS40-UF100-TEh-SOs-SCa-STp-TP250-AGE-NE_LHTx10	0:00:16	0.43
MH10-TS400-UF1-TEh-SOs-SCa-STp-TP250-AGE-NE_LHTx10	0:00:14	0.15
MH20-TS800-UF1-TEh-SOs-SCa-STp-TP250-AGE-NE_LHTx10	0:00:13	0.05
MH5-TS200-UF1-TEh-SOs-SCa-STp-TP55-AGE-NE	0:00:11	0.48
MH5-TS200-UF1-TEh-SOs-SCa-STp-TP250-AGE-NE	0:00:09	0.48
MH10-TS400-UF1-TEh-SOs-SCa-STp-TP55-AGE-NE	0:00:07	0.15
MH10-TS400-UF1-TEh-SOs-SCa-STp-TP250-AGE-NE	0:00:07	0.15
MH20-TS800-UF1-TEh-SOs-SCa-STp-TP55-AGE-NE	0:00:07	0.05
MH20-TS800-UF1-TEh-SOs-SCa-STp-TP250-AGE-NE	0:00:07	0.05

Table 10.4: Models run for a thermal time of 365 days, presented in Figure 10.9

Model name	Computing time	Parameter *q*
MH10-TS1-UF1-TEh-SOs-SCa-STp-TP250-AGE-NE	45:44:46	17,911.71
MH25-TS1-UF1-TEh-SOs-SCa-STp-TP250-AGE-NE	30:03:54	11,115.88
MH1-TS1-UF10-TEh-SOs-SCa-STp-TP250-AGE-NE	29:41:44	8,785.97
MH50-TS1-UF1-TEh-SOs-SCa-STp-TP250-AGE-NE	11:08:45	6,292.26
MH1-TS20-UF1-TEh-SOs-SCa-STp-TP250-AGE-NE	5:18:54	1,748.88
MH1-TS1-UF100-TEh-SOs-SCa-STp-TP250-AGE-NE	4:20:37	1,996.52
MH1-TS40-UF100-TEh-SOs-SCa-STp-TP250-AGE-NE	0:27:19	55.17
MH5-TS200-UF1-TEh-SOs-SCa-STp-TP250-AGE-NE	0:26:16	100.83
MH10-TS400-UF1-TEh-SOs-SCa-STp-TP250-AGE-NE	0:15:06	44.78
MH20-TS800-UF1-TEh-SOs-SCa-STp-TP250-AGE-NE	0:10:58	14.27
MH50-TS1600-UF1-TEh-SOs-SCa-STp-TP250-AGE-NE	0:04:43	3.93

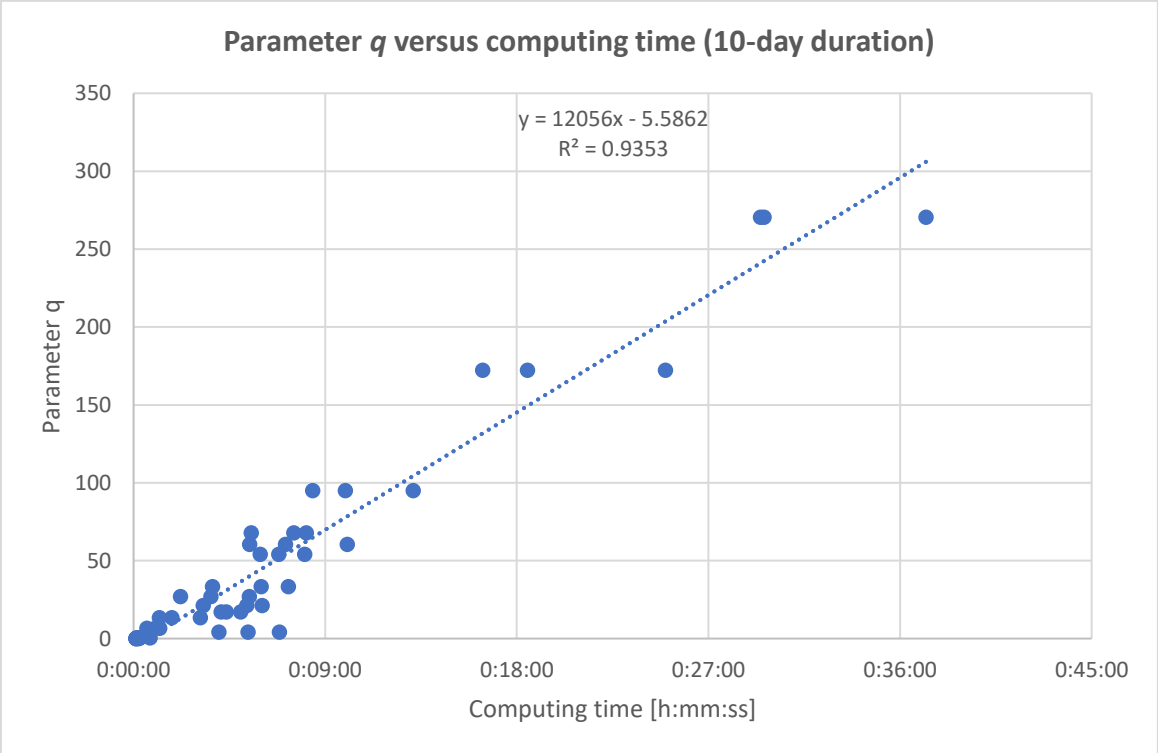

Figure 10.8: Computing time versus the defined parameter" q", total time of 10 days (models from Table 10.3)

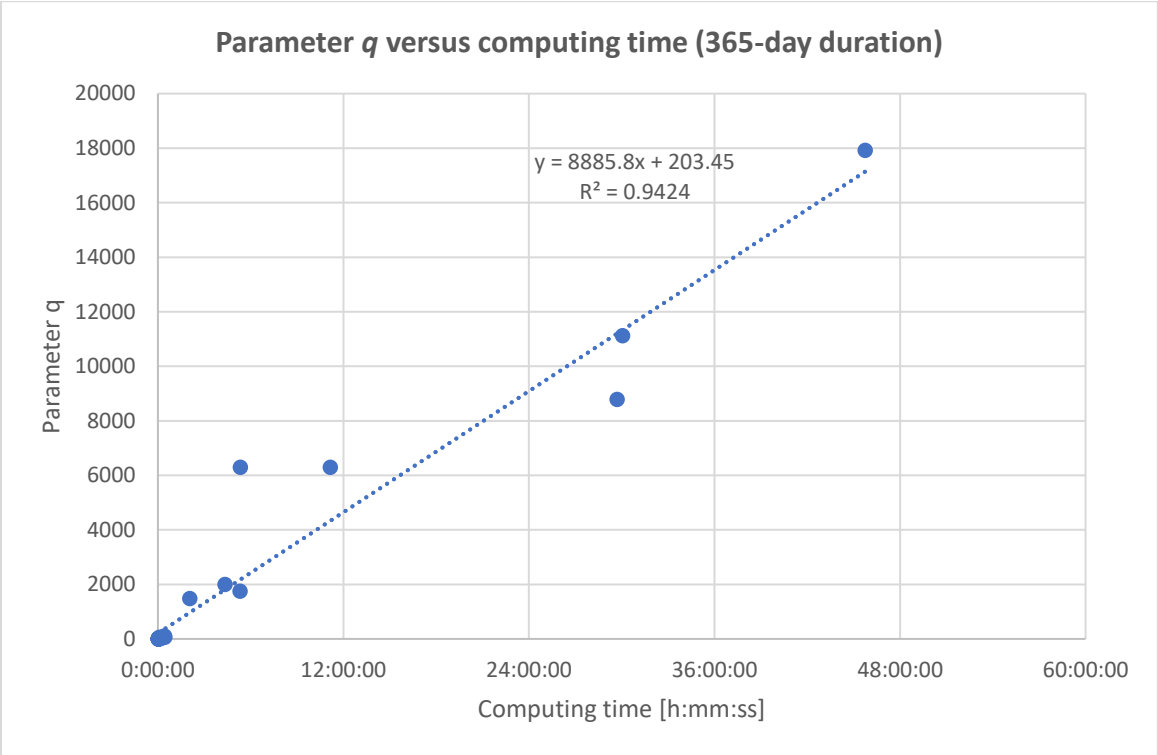

Figure 10.9: Computing time versus the defined parameter "q", total time of 365 days (models from Table 10.4)

10.1.3. Update of freeze status

The RMSE error was represented in Figure 10.10 against the update period of the freeze status for the models MH50-TS1600-UFxx-TEh-SOs-SCa-STp-TP55-AGE-NE, with update periods of 1 to 2,000 steps (i.e. 1,600 to 3,200,000 seconds). In this case, the error increases with the update period initially, up to an update period of approx. 500,000 seconds (about 5.8 days). Further increasing the update period does not appear to have a negative influence on the accuracy, as the errors stabilise. However, the error of the freeze front in this case is already quite large and in the order of magnitude of the size of one mesh element (50 cm). It has to be highlighted here that this may be different for other cases, e.g. with smaller mesh sizes, such as the model MH1-TS200-UF1000-TEh-SOs-SCa-STp-TP55-AGI-NE, which generates high errors due to zones of the model becoming "stuck" in the freezing status (see Figure 5.31). To avoid that issue, smaller time steps could be used at the beginning, when the freezing progress is quickly advancing.

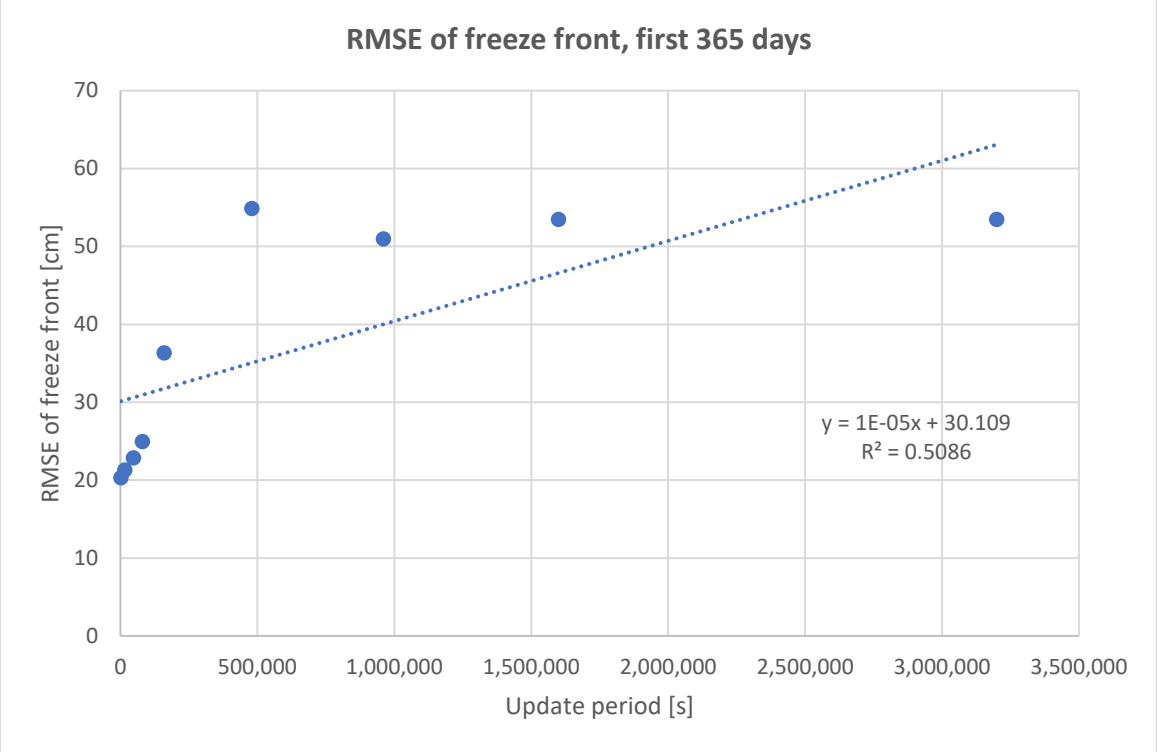

Figure 10.10: RMSE of freeze front vs update period of freeze status, first 365 days, models with mesh size 50 cm, time step 1600 s and 55ºC initial temperature difference

10.1.4. Implicit method

An overview of the accuracy of the results of the implicit method and their dependency with the mesh size, time step and update period of the freeze status is provided in this chapter, similarly to the one performed in the previous chapters for the explicit method. In this case, as shown in chapter 5.11, unlike for the explicit method, the time step does influence the accuracy of the results. The results, which are shown in Figures 10.11 to 10.14, demonstrate that the error is linearly correlated with the mesh size, the time step and the update interval of the freeze status. Regarding the mesh size sensitivity, it can be observed from Figure 10.11 that the maximum errors are roughly of the size of the mesh size (for the chosen time steps and update periods). The maximum errors are also linearly correlated with the RMSE for the implicit method. The models shown in the graphs are listed in Table 10.5 for reference.

Table 10.5: Models considered in Figures 10.11 to 10.14

Mesh sensitivity
MH1-TS200-UF1-TEh-SOs-SCa-STp-TP55-AGI-NE
MH2-TS400-UF1-TEh-SOs-SCa-STp-TP55-AGI-NE
MH5-TS1000-UF1-TEh-SOs-SCa-STp-TP55-AGI-NE
MH10-TS2000-UF1-TEh-SOs-SCa-STp-TP55-AGI-NE
Time step sensitivity
MH1-TS200-UF1-TEh-SOs-SCa-STp-TP55-AGI-NE
MH1-TS100-UF1-TEh-SOs-SCa-STp-TP55-AGI-NE
MH1-TS250-UF1-TEh-SOs-SCa-STp-TP55-AGI-NE
MH1-TS280-UF1-TEh-SOs-SCa-STp-TP55-AGI-NE
MH1-TS45.4-UF1-TEh-SOs-SCa-STp-TP55-AGI-NE
Update freeze status sensitivity
MH1-TS200-UF1-TEh-SOs-SCa-STp-TP55-AGI-NE
MH1-TS200-UF10-TEh-SOs-SCa-STp-TP55-AGI-NE
MH1-TS200-UF100-TEh-SOs-SCa-STp-TP55-AGI-NE

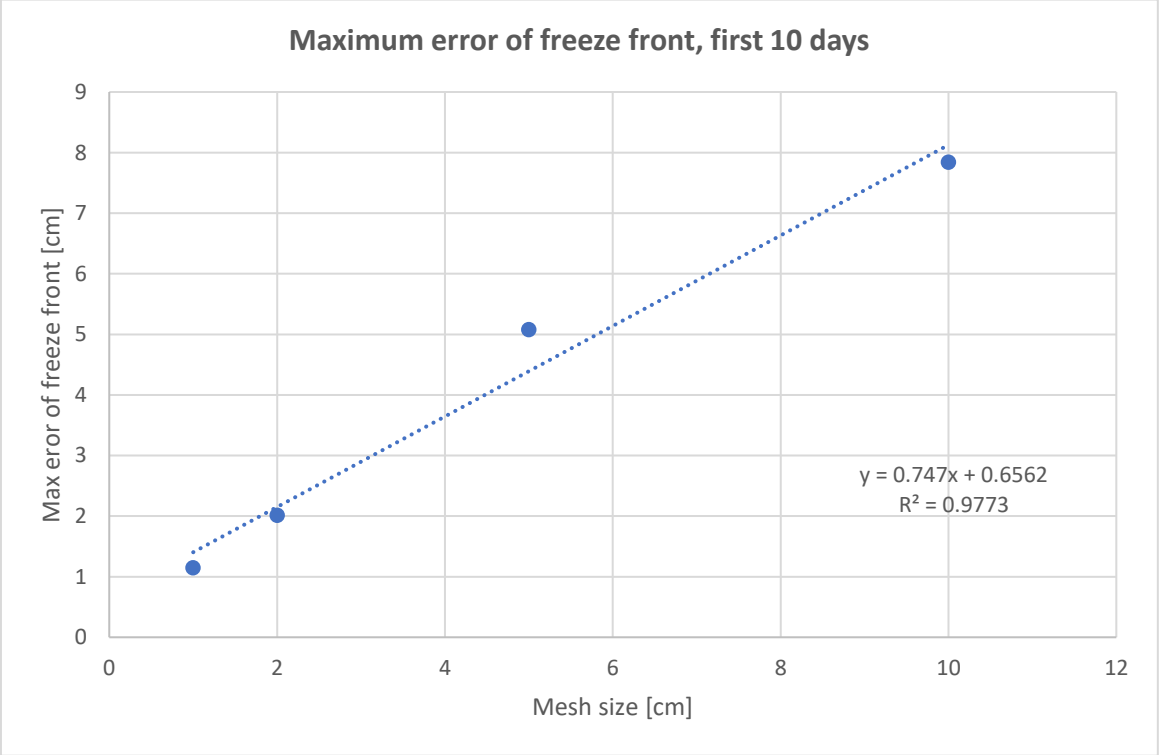

Figure 10.11: RMSE of freeze front vs mesh size, first 10 days, implicit method (models from Table 10.5)

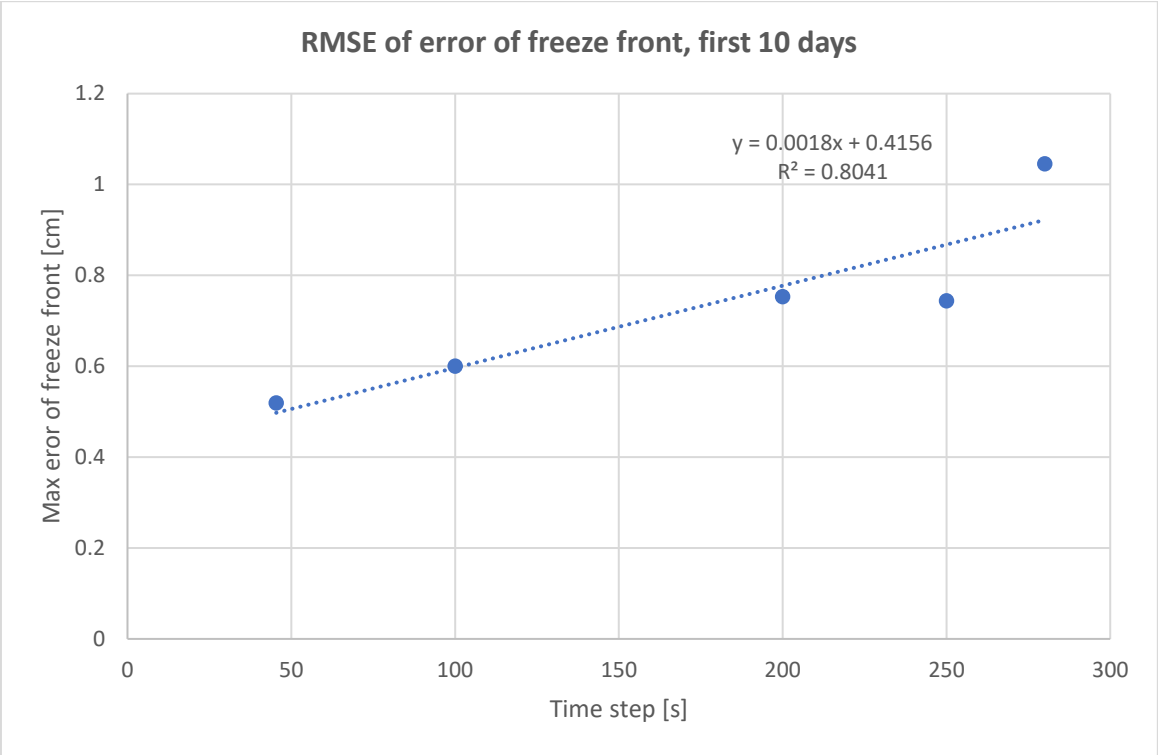

Figure 10.12: RMSE of freeze front vs time step, first 10 days, implicit method (models from Table 10.5)

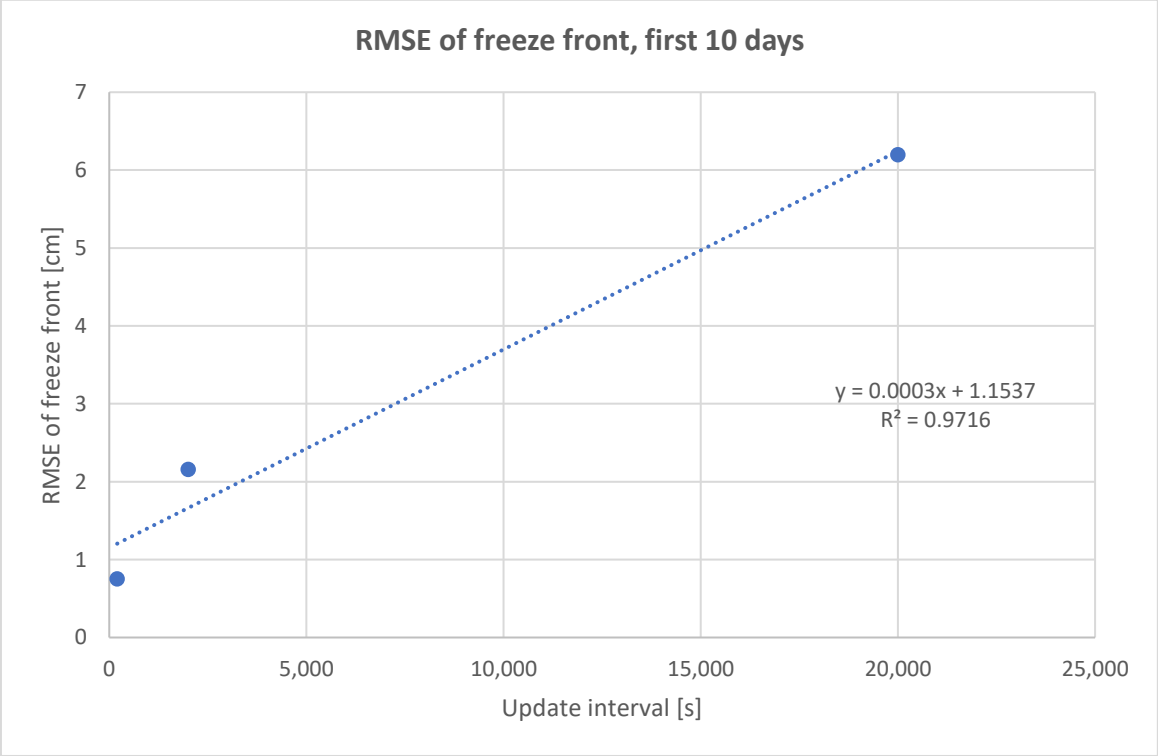

Figure 10.13: RMSE of freeze front vs update interval of freeze status, first 10 days, implicit method (models from Table 10.5)

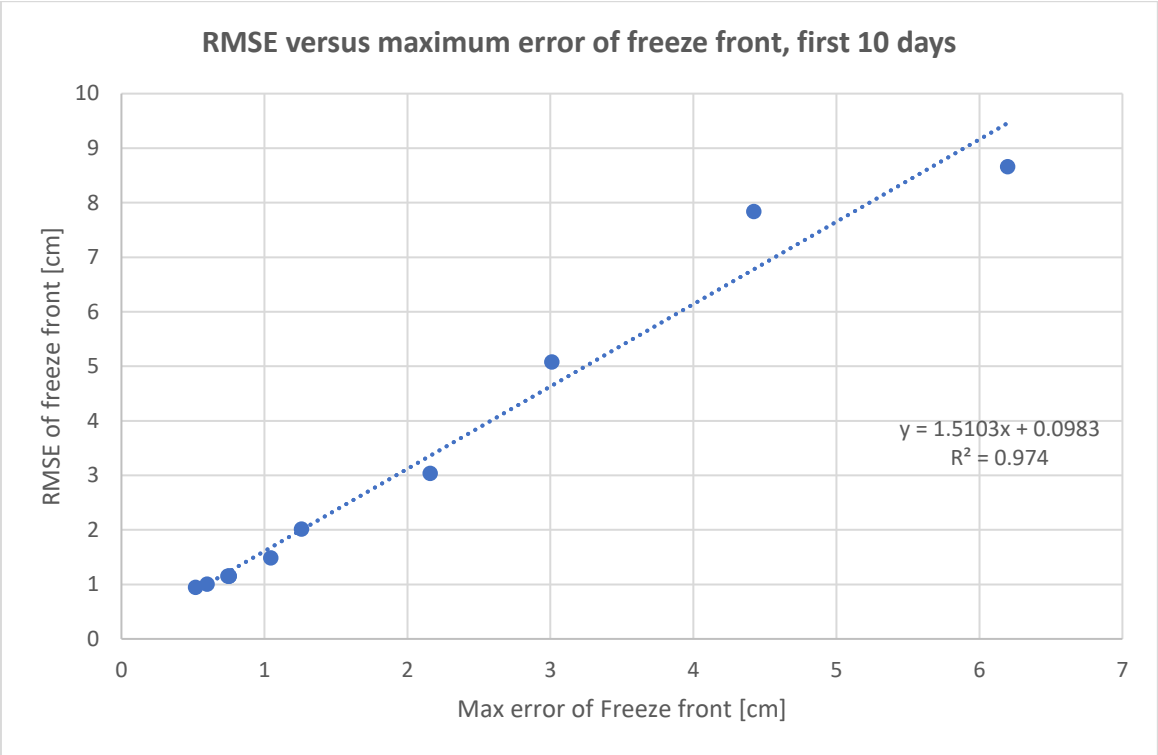

Figure 10.14: RMSE vs maximum error of freeze front, first 10 days, implicit method (models from Table 10.5)

10.1.5. Analysis of the error and its relationship with the plateaux of the enthalpy method

This chapter aims to perform a qualitative study of the error of the enthalpy method and its relationship with the mesh size and the plateaux characteristic of this method. The plateaux in the temperature-time graph corresponding to a certain point in space are caused by the discretisation of time and space. Indeed, they are due to the finite zones in the vicinity of the freeze front preventing the temperature from decreasing for the period of time in which they are in the freezing status, when they are assigned a very high apparent heat capacity. This effect can be observed in Figure 10.15.

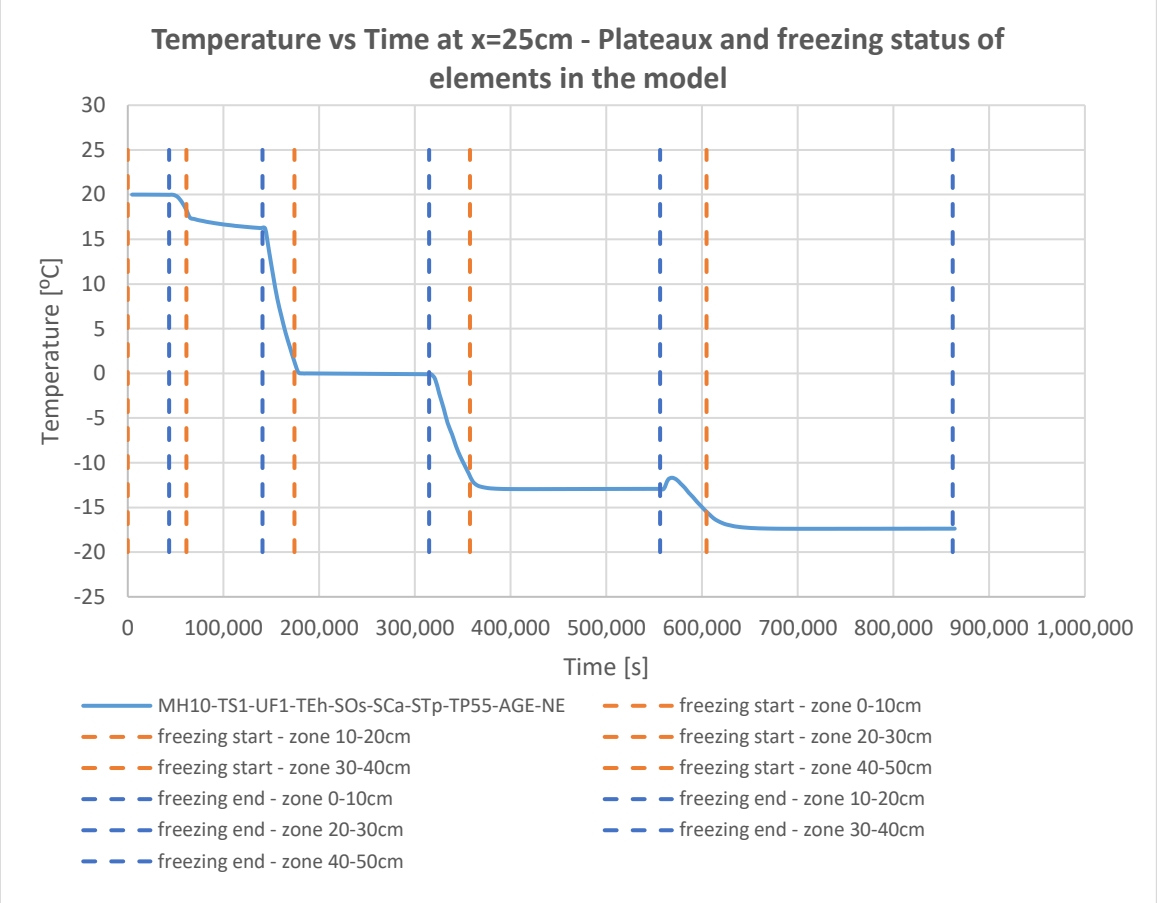

Figure 10.15: Relationship between the plateaux and the freezing status of the elements (zones) of the numerical model

Hence, it has been shown above that the duration of the plateaux is closely related to the duration of the freezing process in the elements (zones). This duration is in turn inversely proportional to the average rate at which energy is being absorbed from the zone which is freezing (E') and directly proportional to the amount of latent heat in the zone (L_{zone}) (considering the amount of sensible heat in the freeze range as negligible):

$$\Delta t = \frac{L_{zone}}{E'} \tag{10.3}$$

The total latent heat in the zone is proportional to the zone volume V, the water content per unit mass $\omega/(\omega + 1)$ and the volumetric latent heat of water l_{water}:

$$L_{zone} \propto V \cdot \frac{\omega}{\omega + 1} \cdot l_{water} \tag{10.4}$$

As not only the latent heat in the zone, L_{zone}, but also the rate of energy absorption, E', is proportional to the surface of the zone (mesh element) perpendicular to the direction of the energy transmission $S_{\perp}$, the duration of the plateaux is proportional to the length of the zones in the direction of the energy transmission, d_{zone}. The latent heat per unit volume of the zone is proportional to the water content (assuming the latent heat of water is constant). Thus, the duration of the plateaux is also proportional to the water content per unit mass. These conclusions are shown in Equations (10.5) to (10.7):

$$V = S_{\perp} \cdot d_{zone} \tag{10.5}$$

$$E' \propto S_{\perp} \tag{10.6}$$

$$\Delta t \propto \frac{V \cdot \frac{\omega}{\omega + 1} \cdot l_{water}}{S_{\perp}} = d_{zone} \cdot \frac{\omega}{\omega + 1} \cdot l_{water} \tag{10.7}$$

The dependency of the duration of the plateaux with the mesh size, which coincides with d_{zone} in the case of the Neumann model, can be appreciated in Figure 10.1. The relationship between these two magnitudes is explicitly apparent in Figure 10.16, Figure 10.17 and Table 10.6.

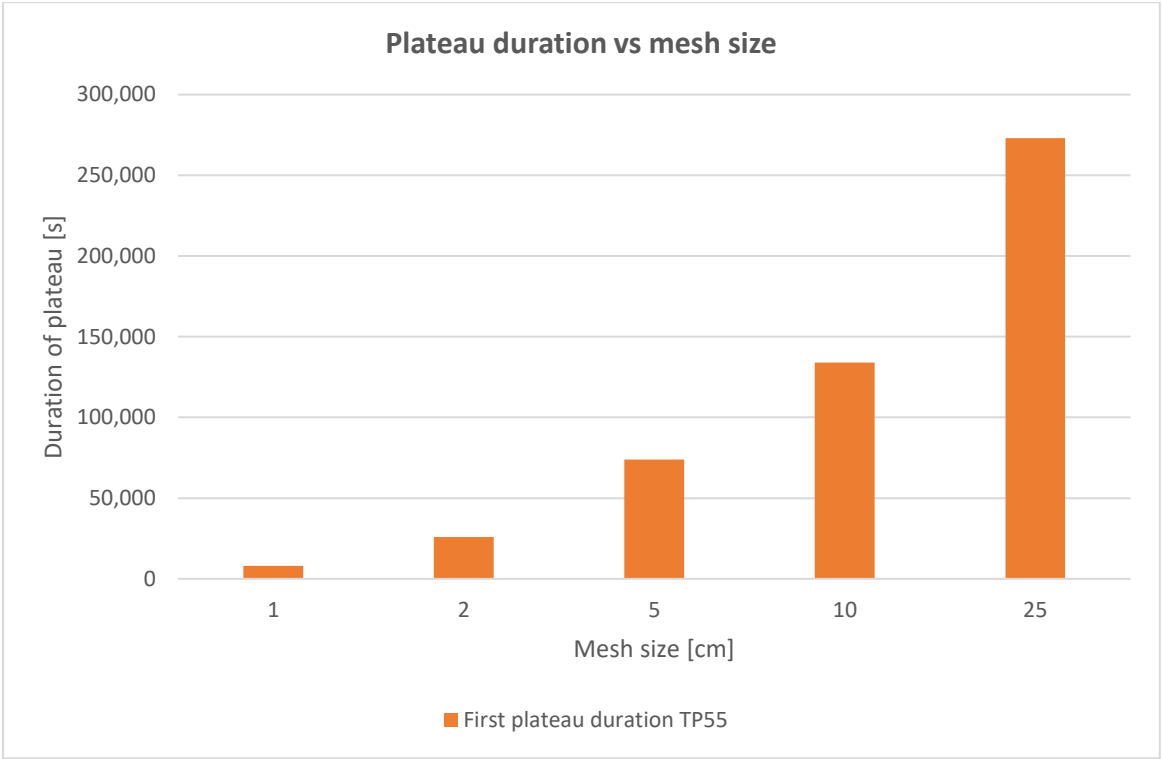

Figure 10.16: Duration of the first plateau and mesh size for models with 55ºC initial temperature difference

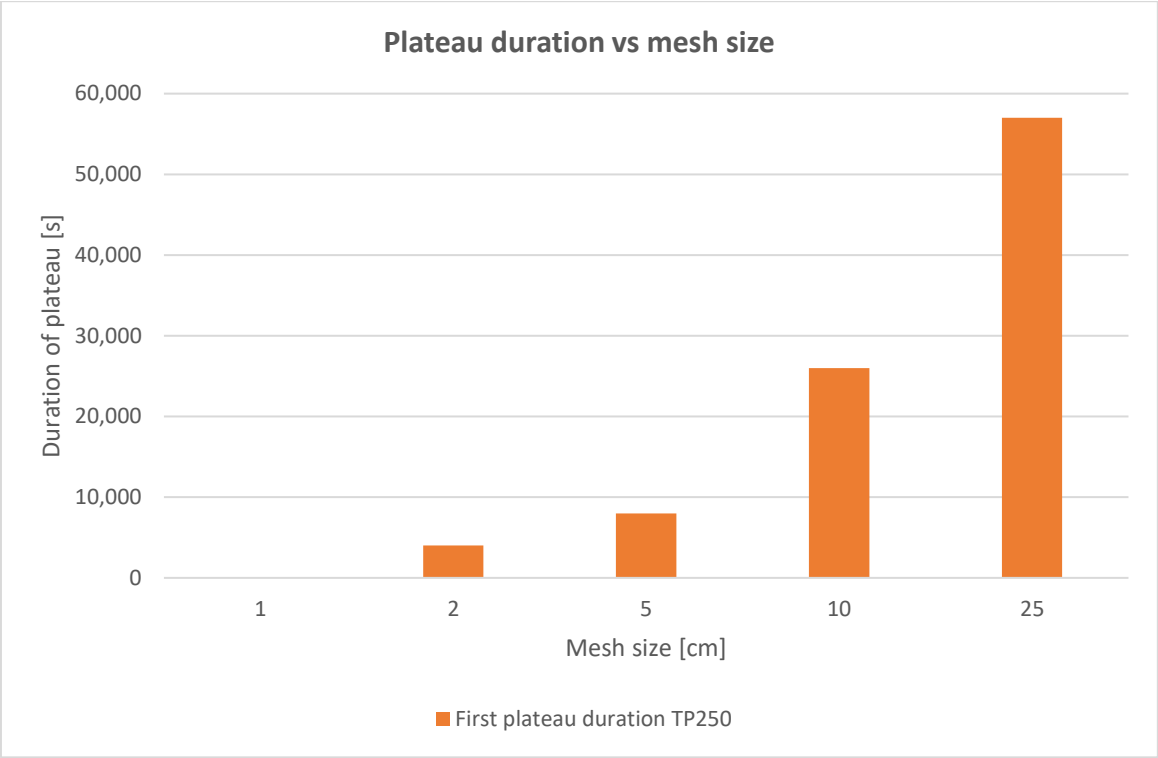

Figure 10.17: Duration of the first plateau and mesh size for models with 250ºC initial temperature difference

Table 10.6: Duration of the first plateau and mesh size

Model name	Duration of first plateau	Ratio of plateau duration to plateau duration with 2 cm mesh	Ratio of mesh to 2 cm mesh
MH25-TS1-UF1-Teh-SOs-SCa-STp-TP55-AGE-NE	273,000	10.50	12.5
MH10-TS1-UF1-Teh-SOs-SCa-STp-TP55-AGE-NE	134,000	5.15	5
MH5-TS1-UF1-Teh-SOs-SCa-STp-TP55-AGE-NE	74,000	2.85	2.5
MH2-TS1-UF1-Teh-SOs-SCa-STp-TP55-AGE-NE	26,000	1.00	1
MH1-TS1-UF1-Teh-SOs-SCa-STp-TP55-AGE-NE	8,000	0.31	0.5

The dependency of the duration of the plateaux with the energy extraction rate E' is presented in Table 10.7. This table gives an overview of the plateau duration of the models with initial (maximum) temperature differences of 55ºC and 250ºC. Indeed, the higher initial gradient implies a higher extraction rate, which decreases the size of the plateaux.

The dependency of the plateau duration with the latent heat is also shown in Table 10.7. It can be appreciated that the model with a latent heat 10 times higher (which could be caused,

ceteris paribus, by a water content per unit mass 10 times higher, if physically possible) also generates plateaux which are about 10 times longer than the ones from the other model. This results in higher errors compared to the model with the lower latent heat (see also chapter 5.7). Figure 10.18 provides an overview of the dependency of the duration of the first plateau with the mesh size for the three different types of models considered here. The plateau duration and the mesh size have a high linear correlation ($R^2 > 0.98$).

Table 10.7: Duration of the plateaux for different models

Model name	Mesh	Plateau duration TP55	Plateau duration TP250	Plateau duration TP250_LHTx10
MH25-TS1-UF1-Teh-SOs-SCa-STp-TPxx-AGE-NE(_LHTx10)	25	273,000	57,000	590,000
MH10-TS1-UF1-Teh-SOs-SCa-STp-TPxx-AGE-NE(_LHTx10)	10	134,000	26,000	186,000
MH5-TS1-UF1-Teh-SOs-SCa-STp-TPxx-AGE-NE(_LHTx10)	5	74,000	8,000	87,000
MH2-TS1-UF1-Teh-SOs-SCa-STp-TPxx-AGE-NE(_LHTx10)	2	26,000	4,000	34,000
MH1-TS1-UF1-Teh-SOs-SCa-STp-TPxx-AGE-NE(_LHTx10)	1	8,000	*non measurable plateau*	18,000

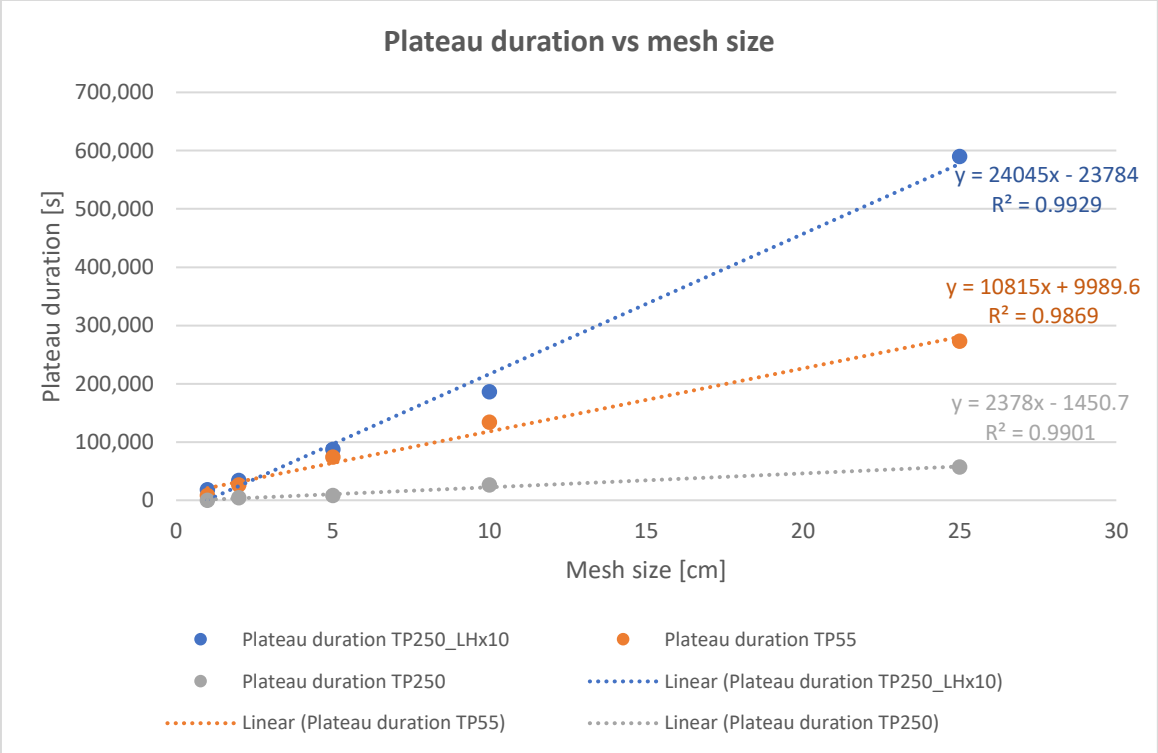

Figure 10.18: Duration of the plateaux versus the mesh size, models from Table 10.7

Finally, it is useful to notice that the average and maximum errors (which are usually unknown, except for the cases in which an exact analytical solution is available) are linearly correlated with the duration of the first "step" or plateau in the temperature versus time

graph, which is easily obtainable from the results of the numerical model. This correlation can be observed in Figure 10.19, as well as the dependency of the errors and plateau duration with the mesh size.

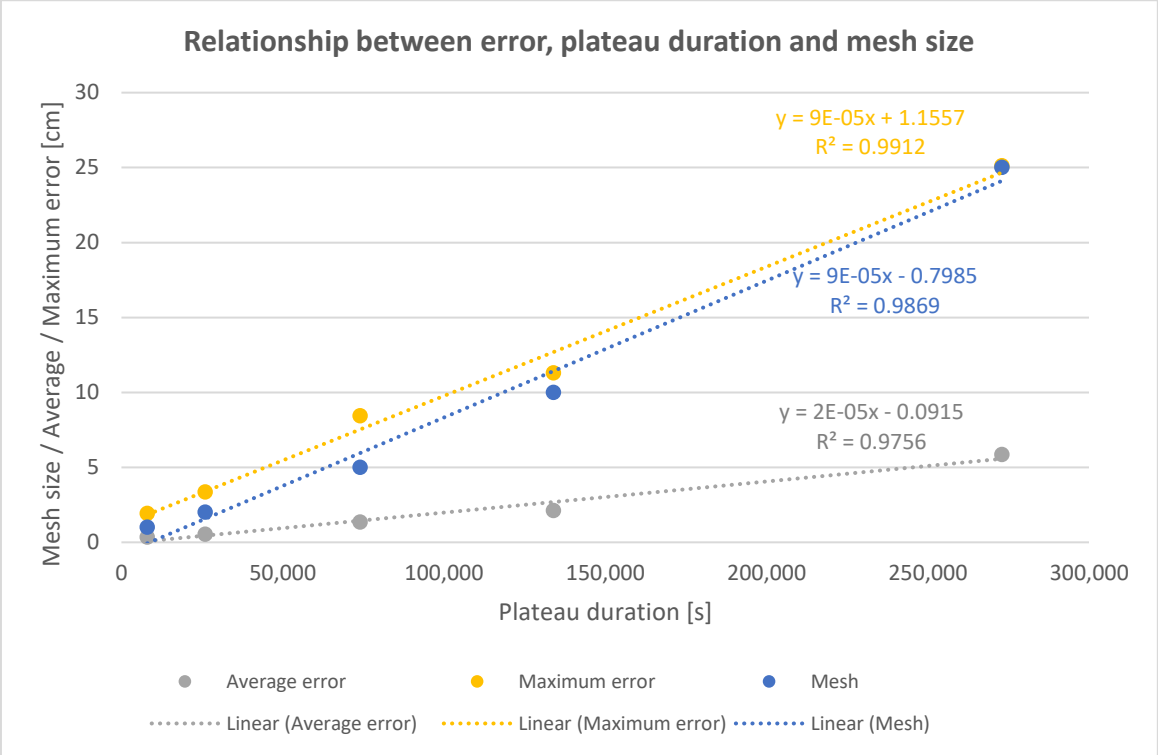

Figure 10.19: Correlation between average and maximum of absolute values of errors, mesh size and plateau duration (Neumann problem, models with thermal gradient of 55ºC)

Another relevant numerical parameter is the frequency of the update of the freeze status. If the status of the elements (zones) (frozen or unfrozen) is updated infrequently, it also affects the duration of the plateaux, because the zone remains in the "freezing status" (with a high specific heat capacity representing the latent heat) for a larger temperature range than it should be the case. Thus, if the update period is of significant duration, it may have a major negative influence on the accuracy of the model (see e.g. Table 5.9). In the extreme case that the time between updates is larger than the duration of the plateaux would have been, the plateaux would become of the same or more duration as the time between updates. These negative effects of infrequent "freezing status" updates can be appreciated for the model MH1-TS200-UF1000-TEh-SOs-SCa-STp-TP55-AGI-NE in Figure 5.31.

10.2. Code of good practice for thermal numerical modelling

This chapter attempts to provide guidance to designers of ground freezing projects for thermal numerical modelling, based on the data and discussions from the previous chapters. It should be noticed that it is extremely difficult to provide advice on the specific values of the numerical parameters to be used in engineering practice, as they are highly dependent on the specific problem at hand and the required accuracy. For instance, it has to be highlighted that the errors of the results from the sensitivity analyses in chapter 5 need to

be considered carefully when trying to extrapolate them to practical engineering models. The first reason for this is that in the models used with Neumann geometry with structured meshing, all the elements at the freeze front freeze at the same time (due to the symmetry of the problem and of the meshing), whereas in engineering models using unstructured meshes, the elements tend to freeze successively at different time steps. This has a beneficial effect on the accuracy of the model, because the typical plateaux of the enthalpy method appear progressively and are smaller (see chapter 5.12). Another point to be taken into consideration is that, as shown in chapter 5, the maximum errors usually appear in the phase-change area, while the rest of the model has lower errors (see chapter 5.3). Therefore, as long as the average errors and/or the errors in the area of interest are below the accuracy threshold set, relatively high maximum errors may be acceptable for practical purposes.

Notwithstanding the difficulty of providing specific quantitative rules for numerical modelling, the vast amount of results obtained in the performed evaluations and sensitivity analyses have been condensed here in order to deliver at least a qualitative guide for practitioners. Based on the simulations performed, which have been analysed in the previous chapters, qualitative recommendations for thermal numerical modelling are outlined in Table 10.8. The numerical models were also compared to real data, from experiments and real projects, in chapter 9. This confirmed that following the conclusions stated in Table 10.8 is a good basis to achieve results of good accuracy within a reasonable computing time.

Performing numerical experiments is often cited in the literature as a necessary way of evaluating the performance of numerical methods (see Causon and Mingham (2010) and GEO-SLOPE International Ltd. (2014)). In addition to the recommendations in Table 10.8, a reasonable approach may be to use models with fine discretisations (of time and space) and compare their results with models with coarser discretisations. As the numerical schemes converge, the results of finer models approximate the exact solution with increasing accuracy. Therefore, if results of coarser models differ to them only in an acceptable quantity, it can be inferred that the coarser models provide acceptable results and may be used, sparing computing time. Another possibility is to create graphs such as Figure 10.2, in which the deviations of the results of several models with coarser discretisations are graphically compared to a model considered “sufficiently fine” and are correlated with their corresponding numerical parameters (mesh size, time step, etc.). To finalise, it needs to be highlighted that numerical models for engineering design always need to be complemented with good engineering judgement and cautiousness during the construction phase (Sagaseta and Castro, 2021).

Table 10.8: Code of good practice for thermal numerical modelling based on the analyses performed in the present thesis

Numerical Parameter	Recommendation
Mesh Size	The mesh size is a determining factor for the accuracy and computing time of the model. The mesh size which should be chosen is a compromise between the desired accuracy and the available time for modelling. The error in the determination of the freeze front is linearly correlated with the mesh size. The mesh size can be increased in the areas where no phase change will happen, in order to spare computing time. The detailed evaluations on the mesh size sensitivity are presented in chapters 5.3, 5.9, 5.10 and 10.1.1.
Time step	For the explicit algorithm: a sub-critical time step (a time step slightly lower than the critical time step) should be used. The reason is that the accuracy does not improve significantly for any time step below the critical time step. For the implicit algorithm: a larger time step than the critical one for the explicit method may be used with good accuracy. The accuracy decreases with increasing time step. The detailed evaluations on the time-step sensitivity are presented in chapters 5.4, 5.9, 5.10 and 10.1.4.
Frequency of execution of "freeze block" routine	The "freeze block" should be executed with sufficient frequency. An excessively long thermal time between two executions may produce high errors in the model, e.g. by leaving zones “stuck” in the freezing status. The update period of the “freeze code” should be small compared to the duration of the freezing process for any element. The detailed evaluations on the time-step sensitivity are presented in chapters 5.5, 5.9, 5.10 and 10.1.3.
Abrupt / Gradual phase change modelling	A gradual phase change (e.g. using a phase range interval larger than 1ºC), is recommended because it smooths the results of the numerical model and thus provides a better accuracy (see chapter 5.8).
Structured / unstructured mesh	Unstructured meshes are recommended because they produce more accurate results. This is due to the fact that the elements of structured meshes may tend to freeze at the same time, as a result of the symmetry of the model. This effect accentuates the typical plateaux of the enthalpy method, which generate higher errors (see chapter 5.12).
Punctual / surface source	Surface sources are recommended to avoid instability problems and to better represent the real geometry of the sources. As an example, a punctual source representing a freeze pipe produces a much slower freeze front progress than simulating the pipe with its real radius (see chapter 5.16).
Explicit / Implicit algorithm	Both the explicit and implicit algorithms worked well. The implicit algorithm can be used for quicker calculations, as it allows larger time steps (see chapters 5.11 and 10.1.4). Furthermore, the time step is not limited to the critical time step, which is especially important for models with elements of very different sizes, for which the explicit algorithm may require very small time steps.
Model boundaries	The model should be sufficiently large so that the model boundaries do not influence the results. That is, the areas near the outer model boundaries should suffer only negligible temperature changes (see chapter 5.2).

Physical Property	Effect
Initial temperature gradient	Higher initial temperature gradients tend to produce higher errors (see chapters 5.6 and 5.8).
Stefan number (latent heat)	A significantly higher latent heat produces higher errors (see chapter 5.7). However, in the ranges of latent heat of natural soil, its influence on the error is probably not dominant compared to the effects of other parameters.

10.3. Discussion of the analytical solutions used in engineering practice

As already highlighted, the exact solutions presented in chapter 3.2 are constrained to very specific conditions and/or geometries, so their practical use is restricted. Furthermore, most of them are mathematically complex and consequently not easy to evaluate with simple calculations or spreadsheets, so they are of limited application in engineering design. Nevertheless, they can be used to verify numerical schemes or approximate analytical solutions. Intensive research has been and is still being performed in this area, but, even so, very few solutions with direct applicability to everyday engineering problems have been found.

With respect to the approximate solutions for thermal design in ground freezing projects, only a few analytical formulae exist. Five of the most significant solutions were presented in chapter 3.4. They are based on different key assumptions and simplifications. Accordingly, their results vary widely, as has been shown in chapter 6. Furthermore, some of the simplifications made, on which these formulae are based, do not completely match the reality of ground freezing projects, which limits their applicability and accuracy. A few of these simplifications, which are especially relevant in engineering design are listed below:

- constant freeze pipe temperature (no consideration of the initial cool-down period and other temperature changes, e.g. those due to break-downs, etc.)
- constant distance between freeze pipes (no consideration of drilling deviations)
- homogeneous ground (no consideration of layering or geological inhomogeneities)
- no consideration of additional sources of energy (warm air during excavation opening, hydration heat of cement when concreting against the freeze wall, etc.)

Despite these limitations, approximate analytical solutions are useful in engineering in the early stages of design (e.g. concept design, tender design, etc.), when the time and resources available may not be sufficient to set up a numerical model (Sancho-Calderón et al., 2021). Moreover, these solutions may also be used as a benchmark to compare numerical results against (Sancho-Calderón et al., 2021). Even at the detail design and execution stages, some of these solutions have been used, see e.g. Colombo (2010) and Franz (2015).

Therefore, these approximate analytical solutions are still practical and relevant. As their results differ widely between themselves and also in comparison to numerical solutions, the boundaries of their applicability and accuracy have to be determined. An attempt on this task has been performed in chapter 6, where the results of the five solutions considered

were evaluated, compared and analysed for seven problems with different initial and boundary conditions (including freeze pipe temperature, initial ground temperature, amount of latent heat, thermal characteristics of the ground and phase change temperature of the groundwater).

The results of the problems studied in chapter 6 were compared against a verified numerical model with parameters based on the conclusions of chapter 5, which can be considered a solid benchmark to analyse their accuracy against. Verified numerical simulations resulted very useful to check the analytical solutions.

Experimental data were also used to verify the analytical solutions. However, they were generally only available for comparatively short times (e.g. in Ständer (1967) for approx. 4 hours or in Sres (2009) for approx. 40 hours) with respect to the duration of ground freezing in projects, which is typically in the order of magnitude of weeks or several months. It was possible to use some data from an engineering project from Hentrich and Franz (2015). Nevertheless, further details than those published would have been required for a more reliable verification of the analytical solutions and numerical model. Indeed, the high complexity of a real engineering project requires an in-depth knowledge of the boundary conditions before an attempt can be made to verify a numerical model or analytical solutions against such data. Furthermore, even with detail knowledge of the ground parameters, construction sequence and construction events and detailed monitoring data, many unknowns stay, such as ground inhomogeneities, unknown groundwater flow, etc, which could only be potentially defined by a very extensive and untypical monitoring program. Therefore, it is extremely difficult to verify the accuracy of a numerical model or analytical solutions based on data from engineering projects, as the uncertainties from these sources may be much larger than the ones from the numerical parameters or analytical formulae.

In engineering projects, the solution most widely used for the three usual geometries (single freeze pipe, freeze wall and freeze circle) is the one published by Sanger and Sayles (1979) (see e.g. Chang and Lacy (2008), Colombo (2010), Hentrich and Franz (2015) and Filippo Mira-Cattò (2016)). The solution by Ständer (1967) has also been applied, but it seems to be somewhat constrained to German-speaking countries (see e.g. Hentrich and Franz (2015), Bosch (2017) and Schüller (2015)). Along with these two, the solutions from Khakimov, Lunardini and Leibenson were also studied in chapter 6. On the one hand, Ständer's solution proved to be very accurate, while being relatively complex to compute. On the other hand, Sanger & Sayles' solution is easy to compute, as it can be expressed as a closed formula, but it often does not provide the accuracy required for practical purposes, especially when a high amount of sensible heat from the unfrozen phase needs to be accounted for.

An example of the high errors which can render some of these solutions impracticable for practical purposes can be taken from Figure 10.20 (for Problem 7, cf. chapter 6.2.2). For instance, let us assume that in a ground freezing project a freeze radius of 120 cm is required for stability/geotechnical reasons. For that freeze radius, the solutions yield the results

shown in Table 10.9. In this case, only the errors from Ständer's and Khakimov's solutions would be moderate and usually acceptable for practical purposes. For instance, the widely used solution from Sanger & Sayles yields an error of about one month, which could have major consequences on the project schedule, budget and risk. Similar analyses can be done for the other problems (see chapter 6.2 and the overview of the RMSE errors in Figure 10.21), concluding that the only solution for the single freeze pipe problem which is consistently usable for practical purposes is Ständer's solution.

Table 10.9: Time estimate for a freeze front of 120 cm, Problem 7

	Time Leibenson	**Time Ständer**	**Time Sanger & Sayles**	**Time Lunardini**	**Time Khakimov**	**Time numerical**
Time estimate [days]	28.3	85.2	63.7	226.6	100.8	94.7
Error of time [days]	-66.4	-9.5	-31.0	131.9	6.1	-

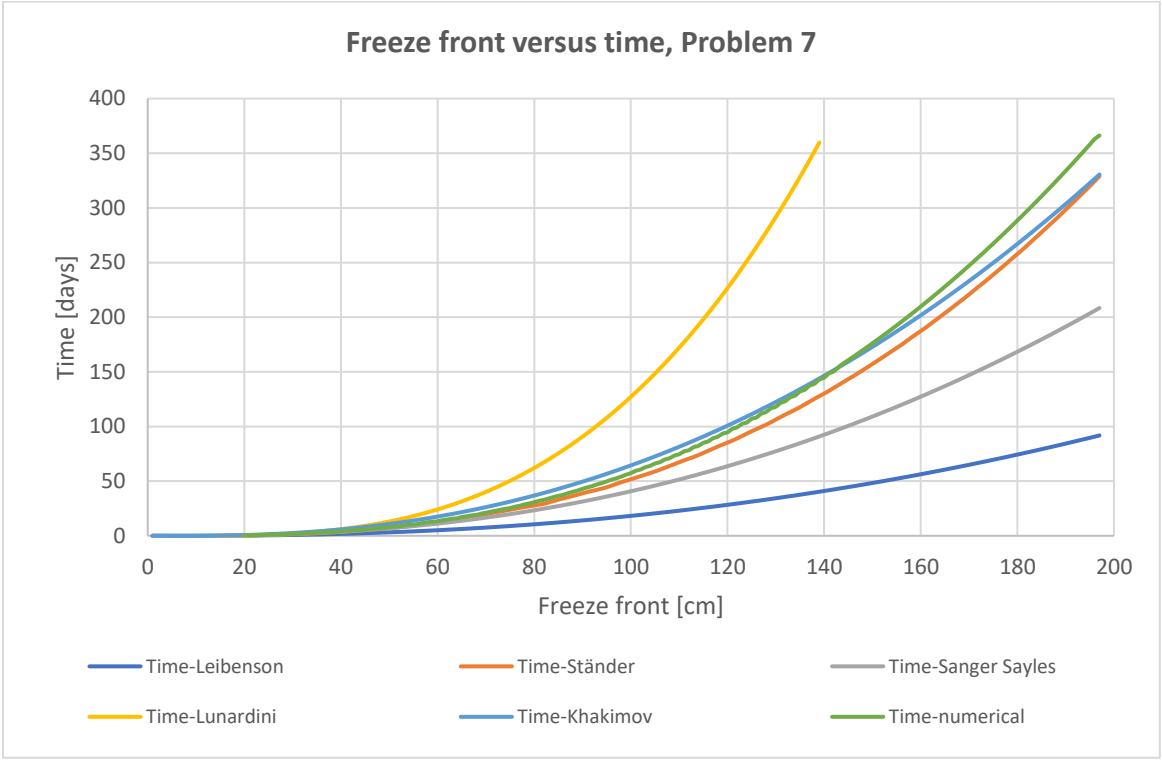

Figure 10.20: Time vs freeze front, Problem 7

From these analyses and from the literature research, the following can be concluded:

- The five analytical methods considered for the single freeze pipe problem pose high differences in accuracy.
- The accuracy of the analytical methods varies significantly when applied to different conditions, such as the thermal characteristics of the ground, initial

temperature, freeze-pipe temperature, phase-change temperature and the amount of latent heat present.

- The solution with the highest accuracy across the different problems studied for the single freeze pipe geometry is Ständer's solution (see Figure 10.21). This solution generates errors for the problems considered which are within the usual limits for practical application. No other solution generates such consistently low errors.
- Despite its dependably high accuracy, Ständer's solution is not widely used in engineering design, according to the number of published papers found during the research for this thesis. Ständer's solution may be suffering two burdens in this regard: its complexity, i.e. it is not based on a closed formula, and the fact that the original publication from Ständer is in German language (to the author's knowledge, this paper has not been translated into English).
- The analyses conducted for the freeze wall versions of Ständer's and Sanger & Sayles' formulae have led to similar conclusions: Ständer's formula appears to be reliable and usually sufficiently accurate (freeze front accuracy higher than 5% for all but one of the problems studied) for the early stages of engineering design, although it produces higher errors than the solution for a single freeze pipe.
- The evaluation of Ständer's and Sanger & Sayles solutions for the freeze circle geometry has produced results of highly variable accuracy, which call for an extremely cautious use of these formulae. An issue which was identified with Ständer's formula was that, for water contents lower than a certain value, it yields a slower freeze front progress for lower values of water content, which is physically incorrect. This issue should be present to the designer when using Ständer's solution for the freeze circle, especially for ground with low water content.

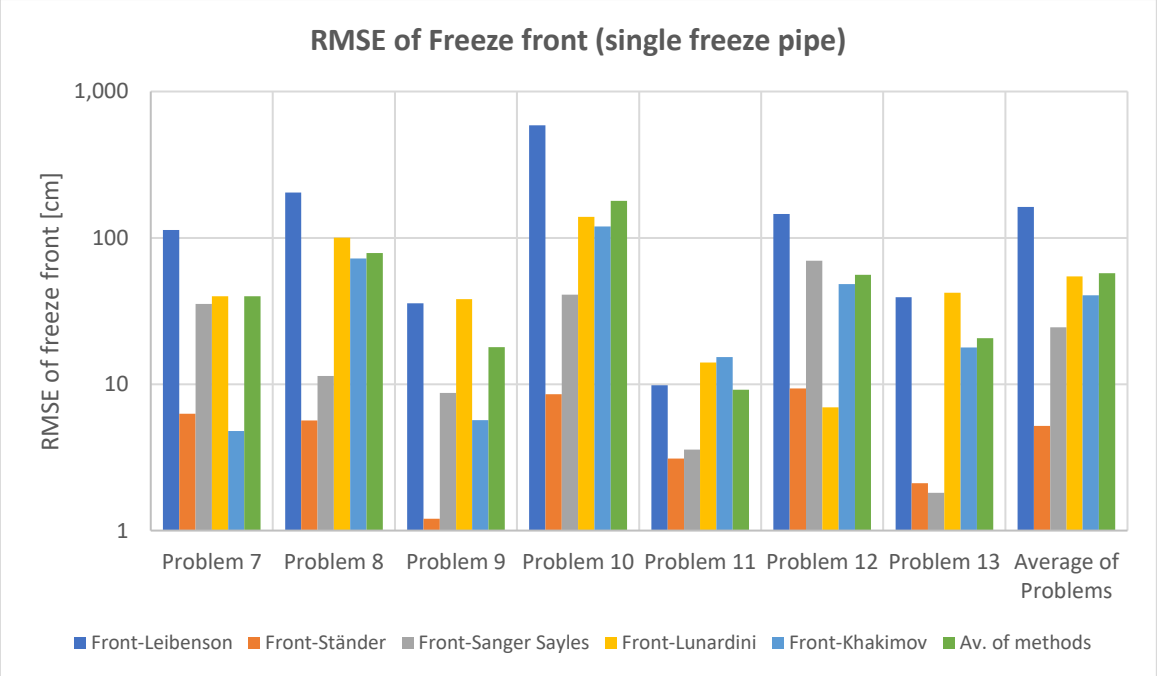

Figure 10.21: RMSE of the estimation of the freeze front by five approximate analytical solutions, single freeze pipe (logarithmic scale)

10.4. Adjustment of the Sanger & Sayles formula

In chapter 7, an attempt was made to improve the accuracy of the Sanger & Sayles' solution for the single freeze pipe, while maintaining its easiness of use for practical engineering. The formula (more precisely the ratio a_r, which is the ratio of the temperature penetration radius to the freeze radius) was adjusted for several different conditions against verified numerical models. Based on these studies, an expression to calculate a_r was proposed as a function of the problem's parameters, such as the initial, freeze-pipe and phase-change temperatures, the average thermal conductivity and average specific heat of the ground, the latent heat content and the freeze pipe radius. The effect of the time point for the adjustment of a_r was also studied in chapter 7.2 by comparing the adjustments for 10 and 365 days. It was concluded that the adjustment for 365 days provided a lower average error than the one for 10 days for times between 0 and 365 days after the start of freezing.

Although the adjustment of the Sanger & Sayles formula was based on an empirical correlation with numerical results, the values of a_r yielded by the adjustment correlate very well with the ratio $a_{r0.1}$ (ratio of the radius in which the temperature has changed by 0.1ºC to the freeze radius) extracted from the numerical models. This implies that a_r, as used in the formula, has indeed the physical meaning defined in Sanger and Sayles (1979).

The adjusted formula was applied to a practical case, the Ust-Jaiwa project, in chapter 9.2.1, obtaining significantly better results than with the original Sanger & Sayles' formula, in which a_r is assumed as constant: $a_r = 3$. Therefore, the adjusted formula is deemed to be useful for practical engineering design. The importance of this solution has to be considered also in the light that the single freeze pipe is the basic geometry for artificial ground freezing. For instance, this solution may also be used as a basis to calculate the closure time of the freeze body for other geometries. An overview of the accuracy improvement of the adjusted solution is presented in Figure 10.22, where it can be observed that its errors are under 10% for all the problems but for Problem 13.

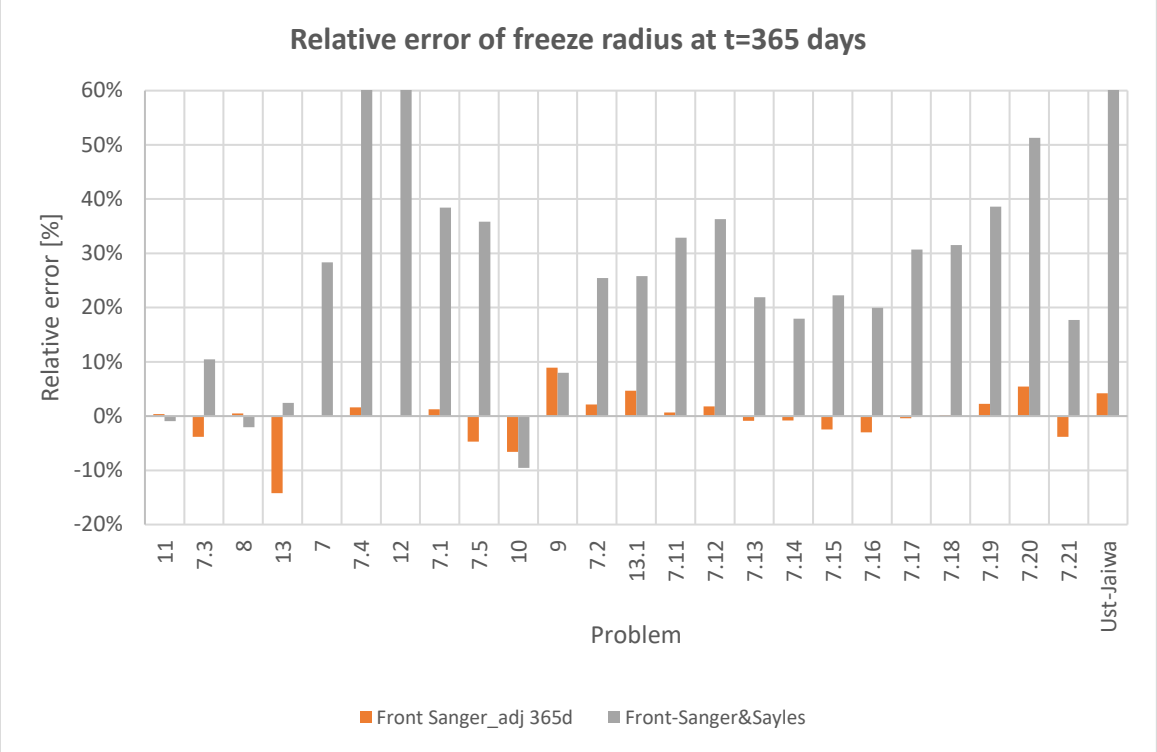

Figure 10.22: Relative error of freeze radius at t=365 days, for all problems studied for the adjusted Sanger & Sayles formula

10.5. On the applicability and practicality of numerical and analytical methods for thermal modelling

The numerical models have proven to be reliable and, assuming that the numerical parameters are reasonably well chosen, sufficiently accurate for their use in most engineering projects. Furthermore, the computing times and hardware requirements have been found to be acceptable for practical uses even for large models, as shown in the example in chapter 5.17. Contrarily, approximate analytical solutions have been shown to produce results of variable accuracy, in some cases generating too high an error to be of use in practical projects (see chapter 6).

In this regard, based on the experience gained from the investigations described in the previous chapters, the following recommendations, shown in Table 10.10 below, have been compiled. Naturally, the field of thermal calculations with phase change being large and complex, the recommendations will need to be critically adapted for the case in hand.

In a nutshell, analytical and numerical methods (and also laboratory tests and monitoring) have both pros and cons, so it is recommendable to use several methods in combination to increase the quality of the results (Yan et al., 2019). Nevertheless, analytical solutions are by their bare nature more limited than numerical methods, especially for practical applications. On the other side, the advances in computing capacity in the recent decades have reduced one of the main disadvantages of numerical modelling, which is the higher computational effort required in comparison to analytical solutions.

Table 10.10: Recommendations on the use of numerical and analytical methods for thermal simulation and design for ground freezing projects

Method	Accuracy of the method	Effort	Degree of detail of data required and factors considered	Results obtained	Recommended use
Numerical model (FDM)	Mainly depends on the selected mesh size, but also on other numerical parameters (see Table 10.8).	Typically longer or much longer engineering time required than with analytical methods.	Highly detailed data required and possible to be considered: • Freeze pipe deviations • Variable freeze pipe temperature • Inhomogeneous ground, ground layers • Additional sources of energy (concrete binding, air temperature at open freeze walls) • Accidental events (e.g. freeze pipe outage)	• T(x,t) Temperature field • X(t) Freeze front advance • P(t) Power consumption	Highly recommended for basic and detail engineering
Ständer	Quite accurate for the single freeze pipe and freeze wall problems, of variable accuracy for the freeze circle problem (see chapter 6).	Complex to use. Added difficulty of the paper being in German and not widely known.	Low detail of data required. Detailed conditions of practical engineering projects can only be considered through rough simplifications. The following can be taken into account: • Regular freeze pipe spacing • Variable freeze pipe temperature • Homogeneous ground • No additional sources of energy	• X(t) Freeze front advance	Convenient for preliminary design (tender phase, concept engineering). To be used very cautiously for the freeze circle geometry.
Sanger & Sayles	Of variable accuracy, probably insufficient.	Closed form, easy to use.	Low detail of data required. Detailed conditions of practical engineering projects can only be considered through rough simplifications. The following can be taken into account: • Regular freeze pipe spacing • Constant freeze pipe temperature • Homogeneous ground • No additional sources of energy	• X(t) Freeze front advance • P(t) Power consumption	Order-of-magnitude calculations only. It should be checked or compared with other approaches.
Sanger & Sayles modified with adjusted parameter a_r (for single freeze pipe)	Quite accurate, especially in the calibrated time of 1 year (see chapter 7).	Closed form, easy to use.	Low detail of data required. Detailed conditions of practical engineering projects can only be considered through rough simplifications. The following can be taken into account: • Regular freeze pipe spacing • Constant freeze pipe temperature • Homogeneous ground • No additional sources of energy	• X(t) Freeze front advance • P(t) Power consumption	Convenient for preliminary design (tender phase, concept engineering)

11. Future lines of investigation on thermal design of artificial ground freezing

The present thesis is focused on the improvement of engineering solutions for thermal design of AGF, specifically on the verification of the conditions under which numerical models and existing analytical solutions for thermal ground freezing design provide reasonably accurate results. The potential future lines of investigation derived from these studies are presented in this chapter.

11.1. Future lines of investigation on numerical modelling for AGF thermal design

In the light of the findings of the thesis, there are several future lines of investigation which seem of interest regarding numerical modelling for AGF. To start with, although extensive sensitivity analyses of thermal numerical models with phase change have been performed in chapter 5, further sensitivity analyses would be very useful. Additional parameters could be studied, along with other numerical schemes (for instance FEM instead of FDM), additional software packages (e.g. TEMP/W or ABAQUS) or methods for the simulation of the phase change process other than the enthalpy method. For instance, the effects on the model accuracy of the type of mesh generation, type of mesh elements (tetrahedra, pyramids or hexahedra) and mesh quality metrics could be evaluated further. Specific mesh quality metrics focused on thermal simulations with phase change may be developed. Structured and unstructured meshes may be studied in more detail, e.g. for the freeze wall and freeze circle geometries. Other ideas to improve the computing efficiency of the code should also be investigated, such as adaptive meshes which are modified during the computation of the problem, which could be finer at the start of the simulation or near the (moving) interface boundary. The accuracy and sensitivity of the simulations should also be studied for the thawing case. These analyses could provide further practical rules for numerical modelling to complement the code of good practice presented in chapter 10.2, such as the ones in Voller and Cross (1981) on the time step size.

In addition to further sensitivity analyses, basic investigation should also be performed on new, powerful, accurate methods to numerically solve thermal problems with phase change. In the opinion of the author, this needs to be tackled as a multidisciplinary, joint effort between engineers and scientists (e.g. physicists and mathematicians). Until now it appears to have been a slight disconnect between the theoretical and practical areas of research, as exemplified in chapter 4.4.1.2. The following insight from the renowned mathematical-physicist John Crank in 1987 remains up-to-date and is shared by the author, especially in the hope that this thesis also contributes to enhance a more multidisciplinary approach on these problems:

> "The broad spectrum of active research workers includes three groups: engineers and others with practical problems; numerical analysts producing suitable numerical algorithms; and pure mathematicians who decide that certain problems and their solutions exist, are properly posed, and may even be unique. They also examine the convergence and stability properties of numerical schemes. A few people fit into all three groups. It is hoped that this book will help to alleviate the usual difficulties of communication between the various interested parties." (Crank, 1987).

Comparing the results of numerical models against exact analytical solutions has been the approach used in this thesis to validate the numerical simulations. However, as only a few exact analytical solutions for thermal problems with phase change are known, this is only possible for very specific cases and geometries. Thus, experimental data are also very useful for the validation of the models. Unfortunately, the experimental data which could be found during the literature research were not optimal for model calibration. Indeed, too many unknowns remain in the published data from engineering projects, and in the case of experiments, they were typically performed during very short periods of time of several hours. Therefore, it would definitely be useful in order to validate numerical models (and approximate analytical solutions) if well-documented and accurately monitored large-scale experiments with longer durations (i.e. several weeks to months) would be performed. Reliable monitoring data from engineering projects may also serve as a suitable alternative or complement to experiments in some cases, although the controlled environment of the laboratory usually leads to a higher knowledge of the system and its variables and therefore tends to provide more accurate data.

11.2. Future lines of investigation on analytical solutions for AGF thermal design

There is certainly room for investigation and improvement on approximate analytical solutions for thermal engineering design of ground freezing projects. The accuracy of several analytical solutions has been evaluated in the present thesis for seven different problems, for three common geometries: single freeze pipe, freeze wall and freeze circle. This approach should be expanded by evaluating additional problems (for instance with other geometries, different boundary conditions, other values of the variables assessed here or by studying additional variables). This could be the basis for a more detailed guideline for practitioners on the use of the existing analytical solutions.

Another potential improvement is that the adjustment performed for Sanger & Sayles' solution for the single freeze pipe could be expanded to consider the dependency of the ratio a_r with further factors, such as the thermal properties of the ground in frozen and unfrozen status and the duration of the freezing process. The calibration of the formula could also be done using the RMSE over time instead of the error of the formula at a certain point in time. This adjustment approach could also be applied to the Sanger & Sayles' solutions for the freeze wall and freeze circle geometries, potentially providing designers

with practical solutions which at the same time yield accurate results. Additionally, these adjustments should also be checked against further laboratory tests and monitoring data from engineering projects.

Ständer's work, which was checked against short-term laboratory experiments, could be further built upon by validating or calibrating it against numerical solutions or experiments with longer thermal times. In particular, the accuracy of Ständer's solution for the freeze circle geometry should be reviewed and possibly improved. In addition, it would be useful to translate the paper from Ständer (1967) into English in order to increase its visibility in the engineering and mathematical communities.

Another idea for further investigations which could be potentially applied in engineering design is to expand Ständer's and/or Sanger & Sayles' solutions, which only provide the freeze front location, by combining them with steady-state temperature distributions such as the ones in Hu and Han (2013) and Hu and Zhang (2013). In this way, solutions would be created for time-dependent temperature distributions $T(r,t)$.

The present thesis has focused on the evaluation of the accuracy of the analytical solutions in terms of the temperature field and freeze front. Further analyses should be performed in order to verify the accuracy of the existing solutions available to estimate the power consumption, such as the one by Sanger and Sayles (1979).

11.3. Outlook on thermal design of artificial ground freezing

Thermal design of artificial ground freezing has evolved in the past from being done based on empirical and analytical methods to using advanced 2D and 3D numerical models, which is the current trend. Although there is extensive literature on these methods available to the design engineer, a standard or norm on ground freezing design seems to be missing. It would be very practical for design engineers if a standard for thermal and geotechnical design of artificial ground freezing projects (AGF) were drafted. This standard could be based on the wide available experience and research on this topic, and it would assist in spreading the best practices and minimising the risks in the design of AGF projects.

Another substantial complement to the evaluations performed in the thesis would be assessing the outcomes from an economic and project perspective. That is, the implications of the results could be further evaluated in detail in terms of the consequences to the project budget, time schedule and health and safety risks.

Finally, an essential part of the broad outlook in thermal design of ground freezing projects is, in the view of the author, the return to the larger picture in the scientific setting. Finding the solution to Stefan problems, which also arise in a number of other engineering and scientific disciplines (see chapter 3), stands in the core of thermal design of AGF. Namely, these academic fields face similar problems and may both profit from and contribute to the studies in thermal ground freezing design. Therefore, the analytical and numerical techniques for AGF design could potentially be extrapolated to Stefan problems in other

areas, such as biology, economics, metallurgy, etc., and vice versa, solutions originated from these disciplines may be applicable to ground freezing thermal design.

12. Conclusions and implications

Dependable and practical solutions for thermal problems with phase change are required for engineering design of artificial ground freezing projects. In this regard, the present thesis has investigated the applicability of numerical and analytical methods for this purpose.

Analytical solutions for Stefan problems, which describe thermal problems with phase change, were searched for in the literature in chapter 3. The literature research showed that, as a result of the complexity of the mathematical problem involved, only a few exact solutions are available for such problems. One of those solutions is the Neumann solution, which solves the problem of a semi-infinite material with a cooled plane at its boundary. This solution was used as the benchmark against which the numerical model was verified.

The research on various numerical methods to solve Stefan problems has advanced significantly in the past decades. However, when it comes to the design of the ground freezing measure for a specific project, the complexity of the model tends to limit the number of applicable methods for phase change simulation. Indeed, the enthalpy method (and variants of it, e.g. the apparent heat capacity method) is the most commonly used method in numerical calculations for ground freezing design, because the alternative methods (see chapter 4.3) are of limited application for irregular geometries or complex boundary conditions. This is also the reason why the present thesis has focused its study on the enthalpy method. Accordingly, a code based on the apparent heat capacity method was implemented in the numerical software FLAC3D.

The results of the enthalpy method deviate from the exact solutions (as any numerical method) to a variable extent. After performing extensive sensitivity analyses on these grounds in chapter 5, it was found that numerical solutions for thermal problems with phase change are typically practical and efficient and provide sufficiently accurate results, as long as certain good practices for modelling are followed. However, if they are disregarded, for instance, in the case that too coarse meshes are used, the results may contain considerable oscillating errors, jeopardizing the accuracy and usefulness of the numerical model. From all the numerical parameters studied, the mesh size was found to be the most determinant one for the accuracy of the results.

With regard to analytical methods, as no exact solutions for the usual problems in thermal design of artificial ground freezing exist, approximate solutions which were developed with the focus on solving practical engineering problems were investigated and were presented in chapter 3.4. Five of them were evaluated in detail in chapter 6 under different initial and boundary conditions by comparing them against numerical models which used analogue numerical parameters to the model previously verified against the exact Neumann solution. This was done for three usual geometries in engineering practice: single freeze pipe, freeze wall and freeze circle. It was concluded that the solution from Ständer (1967) typically yields the most accurate results for the single freeze pipe and freeze wall geometries,

whereas it is the most complex one to use, because it is not in the form of a simple closed formula.

For the freeze circle geometry, the solutions from both Sanger & Sayles and Ständer yield results of very variable accuracy. As a further result of these analyses, Sanger & Sayles' solution for the single freeze pipe (Sanger and Sayles, 1979) was adjusted in chapter 7 against the verified numerical model. This made it possible to create an adjusted formula with enhanced accuracy but maintaining its ease-of-use for engineering design and physical significance. This approach could also be potentially useful to improve the analytical solutions for other geometries, such as the freeze wall and freeze circle.

Data from experiments and engineering projects were used in chapters 8 and 9 to further contrast the results of the numerical and analytical models. This provided a qualitative comparison, which confirmed the usability of these models. Especially the numerical models proved to be of high and stable accuracy over the different cases. While the limitations of the applicability of the analytical models in view of the complexity of real problems were apparent, it was shown that the proposed adjustment to Sanger & Sayles' solution provided a major improvement in accuracy compared to their original solution. In any case, the available experimental data is limited by the short duration and small scale of such studies and the data from projects is typically bound with many unknowns which stem from the practical difficulties of measuring many required variables, such as the thermal properties of the ground, the deviations of the freeze pipes and external thermal influences, for instance, the ones from the excavation process itself. These limitations prevented an exhaustive quantitative verification of the models used against experimental or project data.

The main results of the undertaken investigations were condensed and discussed in chapter 10. Noteworthy conclusions were presented in terms of the effect of the numerical parameters on the accuracy of thermal calculations. In this regard, a very high linear correlation was found between the RMSE (root-mean-square error) of the freeze front and the mesh size. It was also shown that the computing time is very correlated with the number of time steps simulated and, less markedly, with the number of elements in the model and the update interval of the freeze status of the elements. Whereas the time step was found not to influence the accuracy of the results for the explicit method, it was found to be correlated with the error when using the implicit method. Finally, it was shown that the mesh size and the duration of the plateaux typical of the enthalpy method are highly linearly correlated.

Based on the sensitivity analyses performed, the errors of the numerical models were extensively studied in the present dissertation in order to determine its application boundaries in engineering design and to define a code of good practice for numerical modelling containing, for instance, advice on appropriate time steps, meshing and other numerical parameters (see chapter 10.2). This code of good practice should be used as a starting point, whereas numerical experiments have to be performed also in engineering design in order to achieve suitable accuracy within an acceptable computing time. In fact, a purely theoretical analysis of the accuracy may support the numerical experimentation,

but it cannot be used alone to determine the accuracy of the model (see also Causon and Mingham (2010)). These recommendations and the current limitations of numerical modelling should, however, be present in the mind of the designers.

Further works should be strived for in the area of thermal calculations with phase change and Stefan problems in general, given their applicability in wide-ranging science and engineering fields. In-depth analyses of the effect of further numerical parameters, such as the type of mesh, would be interesting in order to optimise the models used in engineering design of ground freezing projects. Additional studies of the accuracy of numerical models with different commercial software would also provide more confidence on their reliability under different conditions. The research should continue with the focus on multidisciplinary collaboration between mathematicians, who work on the development of new numerical and analytical solutions for Stefan problems, and practitioners, such as engineers, who require those methods for their designs.

The present thesis has confirmed that numerical modelling is useful for thermal engineering design of artificial ground freezing problems, as it is sufficiently accurate and computationally efficient. For instance, it has been shown in chapter 5 that numerical models can achieve adequate accuracy and reasonable computing times for large-scale models. The accuracy was found to be satisfactory under very different boundary and initial conditions. Moreover, numerical modelling is very flexible with respect to the geometry, material characteristics and initial and boundary conditions which can be simulated. For instance, it is possible to adjust the numerical model to simulate practical details such as a time-dependent freeze pipe temperature, freeze pipe deviations from their theoretical positions as a result of drilling effects, inhomogeneous ground, etc.

The evaluation of approximate analytical solutions has also proven their applicability for different usual geometries in ground freezing projects, although their limitations in terms of accuracy and consideration of specific project conditions make them more suitable for the early engineering phases, such as concept design.

Reference List

ABBASI, B., RUSSELL, D. & TAGHAVI, R. FLAC 3D mesh and zone quality. Proceedings of the 3rd International FLAC/DEM Symposium, 2013 Hangzhou, P.R. China.

AERNI, K. 1979. Das Gefrierverfahren aus der Sicht des projektierenden Ingenieurs. [The ground freezing method from the perspective of the engineering designer]. *Referate der Studientagung vom 30./31. März 1979.* ETH-Zürich: SIA, Schweizerischer Ingenieur- und Architekten-Verein.

AKIN, J. E. 2009. Concepts of Thermal Analysis.

ALEKSEEV, A., GRIBOVSKII, G. & VINOGRADOVA, S. 2018. Comparison of analytical solution of the semi-infinite problem of soil freezing with numerical solutions in various simulation software. *IOP Conf. Series: Materials Science and Engineering.*

ALEXIADES, V. 2017. *Mathematical modeling of melting and freezing processes*, Routledge.

ALTAIR UNIVERSITY n.d. Introduction to meshing

ALZOUBI, M. A., NIE-ROUQUETTE, A., GHOREISHI-MADISEH, S. A., HASSANI, F. P. & SASMITO, A. P. 2019. On the concept of the freezing-on-demand (FoD) in artificial ground freezing for long-term applications. *International Journal of Heat Mass Transfer,* 143**,** 118557.

ALZOUBI, M. A., XU, M., HASSANI, F. P., PONCET, S. & SASMITO, A. P. 2020. Artificial ground freezing: A review of thermal and hydraulic aspects. *Tunnelling and Underground Space Technology,* 104**,** 103534.

AN, R., ZHANG, X., KONG, L., GONG, J. & LEI, X. 2021. Artificial Ground Freezing Impact on Shear Strength and Microstructure of Granite Residual Soil Under an Extremely Low Temperature. *Frontiers in Earth Science***,** 935:772459.

ANDERSLAND, O. B. & LADANYI, B. 2004. *Frozen ground engineering*, John Wiley & Sons.

ANSYS. 2004. ANSYS Thermal Analysis Guide.

ARBEITSGEMEINSCHAFT SCHACHT RHEINBERG n.d. Gefrierschacht Rheinberg. *In:* ARBEITSGEMEINSCHAFT SCHACHT RHEINBERG (ed.).

ARROYO, E. M. 2017. Congelación del terreno para ejecución de túneles bajo "cut-and-cover" existente en el metro de Varsovia. [Ground freezing for existing cut-and-cover tunnels in the Warsaw Metro]. *Jornadas Técnicas SEMSIG-AETESS.*

AYASOUFI, A. 2004. *Numerical simulation of heat conduction with melting and/or freezing by space-time conservation element and solution element method.* Doctor of Philosophy in Engineering, University of Toledo.

BABAEI, M. 2016. *Finite element analysis of freezing effect on soil nail wall.* Master of Applied Science in Civil Engineering.

BAIER, C. 2008. *Thermisch-hydraulische Simulationen zur Optimierung von Vereisungsmaßnahmen im Tunnelbau unter Einfluss einer Grundwasserströmung. [Thermal-hydraulic simulations for the optimisation of ground freezing measures*

in tunnel construction under the influence of groundwater flow]. Doktor der Ingenieurwissenschaften, Rheinisch-Westfälischen Technischen Hochschule Aachen.

BAKHOLDIN 1963. Selection of optimized mode of ground freezing for construction purpose. *State Construction Press*.

BASU, B. & DATE, A. W. 1988. Numerical modelling of melting and solidification problems — A review. *Sadhana,* 13**,** 169-213.

BAUER SPEZIALTIEFBAU GMBH 2018. BAUER Soil Freezing.

BERGGREN, W. P. 1943. Prediction of temperature-distribution in frozen soils. *Hydrology and snow conference.* Corvallis.

BOCK, S. F., J.; HENTRICH, N. New tools for ground control in freeze shaft sinking. AusRock 2018: The Fourth Australasian Ground Control in Mining Conference, 2018 Sydney, NSW. 393-406.

BOLLATI, J. 2019. *Soluciones exactas y aproximadas a problemas de frontera libre de tipo Stefan con calor latente variable. [Exact and approximate solutions to Stefan-type free boundary problems with varying latent heat]*. Doctorado en Matemáticas, Universidad Nacional de Rosario.

BOLLATI, J., SEMITIEL, JOSÉ A., TARZIA, DOMINGO A. 2018. Heat balance integral methods applied to the one-phase Stefan problem with a convective boundary condition at the fixed face. *Applied Mathematics and Computation,* 331**,** 1-19.

BONACINA, C. & COMINI, G. 1973. On the solution of the nonlinear heat conduction equations by numerical methods. *International Journal of Heat Mass Transfer,* 16**,** 581-589.

BOSCH, T. V. D. 2017. Thermische Berechnungen als wesentlicher Bestandteil der Arbeitsvorbereitung. [Thermal calculations as an essential part of job site preparation]. *68. Deutsche Brunnenbauertage und BAW-Baugrundkolloquium.* Bau-ABC Rostrup / Bad Zwischenahn.

BOUCÍGUEZ, A., LOZANO, R. & LARA, M. 2007. About the exact solution in two phase-stefan problem. *Revista de Engenharia Térmica (Thermal Engineering),* 6**,** 70-75.

BRAUN, B., SHUSTER, J. & BURNHAM, E. 1979. Ground freezing for support of open excavations. *Engineering Geology,* 13**,** 429-453.

BRIOZZO, A. & NATALE, M. 2014. One-dimensional nonlinear Stefan problems in storm's materials. *Mathematics,* 2**,** 1-11.

CAI, H., XU, L., YANG, Y. & LI, L. 2018. Analytical solution and numerical simulation of the liquid nitrogen freezing-temperature field of a single pipe. *AIP Advances,* 8**,** 055119.

CALDWELL, J. & KWAN, Y. 2004. Numerical methods for one-dimensional Stefan problems. *Communications in numerical methods in engineering,* 20**,** 535-545.

CARSLAW, H. & JAEGER, J. 1959. *Conduction of heat in solids: Oxford Science Publications*, Oxford, England.

CASINI, F., GENS SOLÉ, A., OLIVELLA PASTALLÉ, S. & VIGGIANI, G. 2016. Artificial ground freezing of a volcanic ash: laboratory tests and modelling. *Environmental Geotechnics,* 3**,** 1-14.

CAUSON, D. & MINGHAM, C. 2010. *Introductory finite difference methods for PDEs*, Bookboon.

CHANG, D. K. & LACY, H. S. 2008. Artificial ground freezing in geotechnical engineering. *6th International Conference on Case Histories in Geotechnical Engineering.* Arlington, VA, USA.

CHEN, G.-Q., SHAHGHOLIAN, H. & VAZQUEZ, J.-L. 2015. Free boundary problems: the forefront of current and future developments.

CHEN, L., LI, K., SONG, G., ZHANG, D. & LIU, C. 2021. Effect of freeze–thaw cycle on physical and mechanical properties and damage characteristics of sandstone. *Scientific Reports,* 11**,** 1-10.

CHEN, Y., WU, P., YU, Q. & XU, G. 2017. Effects of freezing and thawing cycle on mechanical properties and stability of soft rock slope. *Advances in Materials Science Engineering Geology,* 2017**,** 3173659.

CHERNIHA, R. & KOVALENKO, S. 2009. Exact solutions of nonlinear boundary value problems of the Stefan type. *Journal of Physics A Mathematical and Theoretical,* 42**,** 355202.

CHO, S. H. & SUNDERLAND, J. E. 1974. Phase Change Problems With Temperature-Dependent Thermal Conductivity. *Journal of Heat Transfer,* 96**,** 214-217.

CHRIS K W LEUNG, R. K. Y. L., ANSON K CHEUNG, W L CHAN 2012. Application of artificial ground freezing method for tunnel construction in Hong Kong – a construction case in harbour area treatment scheme stage 2a. *HKIE Civil Division International Conference 2012.*

CLEASBY, J., PEARSE, G. & GRIEVES, M. Shaft sinking at Boulby mine, Cleveland Potash Ltd. International Journal of Rock Mechanics and Mining Sciences & Geomechanics Abstracts, 1975. Pergamon, 60.

COLOMBO, G. 2010. Il congelamento artificiale del terreno negli scavi della metropolitana di Napoli: valutazioni teoriche e risultati sperimentali. [Artificial ground freezing in the excavations of the Naples metro: theoretical assessments and experimental results]. *Rivista Italiana di Geotecnica,* 4**,** 42-62.

CRANK, J. 1987. *Free and moving boundary problems*, Oxford University Press.

CRANK, J. & GUPTA, R. S. 1975. Isotherm migration method in two dimensions. *International Journal of Heat Mass Transfer,* 18**,** 1101-1107.

CZAJA, P., KAMIŃSKI, P. & DYCZKO, A. 2020. Polish experiences in handling water hazards during mine shaft sinking. *Mining Techniques-Past, Present and Future.* IntechOpen.

DAGHER, E., SU, G. & NGUYEN, T. Verification of the Numerical Simulation of Permafrost Using COMSOL Multiphysics® Software. COMSOL Conference, 2014 Boston.

DALLA SANTA, G. 2022. Deformations and permeability variations in fine sediments induced by freezing-thawing cycles caused by borehole heat exchangers. *EGU (European Geosciences Union) General Assembly 2021*.

DOMPIERRE, J., LABBÉ, P., GUIBAULT, F. & CAMARERO, R. Proposal of benchmarks for 3D unstructured tetrahedral mesh optimization. Proceedings of the 7th International Meshing Roundtable'98, 1998. Citeseer.

EMERY, A. & MORTAZAVI, H. 1982. A comparison of the finite difference and finite element methods for heat transfer calculations.

ESEN, A. & KUTLUAY, S. 2004. A numerical solution of the Stefan problem with a Neumann-type boundary condition by enthalpy method. *Applied Mathematics and Computation* 148**,** 321-329.

EYRES, N. R., HARTREE, D. R., INGHAM, J., SARJANT, R. J., JACKSON, R. & WAGSTAFF, J. B. 1946. The calculation of variable heat flow in solids. *Philosophical Transactions of the Royal Society of London. Series A, Mathematical and Physical Sciences,* 240**,** 1-57.

FAROUKI, O. T. 1981. Thermal properties of soils. Cold regions research and engineering lab Hanover, New Hampshire, USA.

FILIPPO MIRA-CATTÒ, A. M. R. P., ELENA ROVETTO. Ground freezing combined method for urban tunnel excavation. Deep Foundations Institute, 2016 Calcutta (India).

FILIPPO MIRA-CATTO, P. R. 2018. Ground Freezing as Temporary Excavation Support: A Sustainable Geotechnical Technique. *TAC/NASTT-NW Tunnelling and Trenchless Conference.* Edmonton, Alberta.

FOSSA, M. & ROLANDO, D. Fully Analytical Finite Line Source Solution for Fast Calculation of Temperature Response Factors in Geothermal Heat Pump Borefield Design. 11th IEA Heat Pump Conference, 2014 Montréal.

FOURIER, J. 1955. Analytical Theory of Heat (Théorie analytique de la chaleur), translated from the French by A Freeman. 359.

FRANZ, J., HENTRICH, NIKOLAI 2014. Numerische Simulationen zur Prognose von Frostausbreitungsvorgängen am Beispiel des Gefrierschachtprojekts Ust-Jaiwa. [Numerical simulations for the prediction of frost propagation processes using the example of the Ust-Jaiwa freeze shaft project]. *1. Internationales Freiberger Schachtkolloquium.* Freiberg.

FRANZ, J. K., ALOYS; HENTRICH, NIKOLAI. An investigation of Shaft Wall Stability in Low-Strength Rock Mass Conditions at the Ust-Jaiwa Freeze Shaft Project. ISRM Regional Symposium-EUROCK 2015, 2015 Graz. International Society for Rock Mechanics and Rock Engineering.

FRIEDMAN, A. 2000. Free boundary problems in science and technology. *Notices of the AMS,* 47**,** 854-861.

FRIVIK, P. 1981. State-of-the-art report. Ground freezing: thermal properties, modelling of processes and thermal design. *Engineering Geology,* 18**,** 115-133.

FROST 3D. 2018. *Verification universal Frost 3D* [Online]. Available: http://frost3d.ru/verifikatsiya-programmy/ [Accessed 17/12/2018].

FURZELAND, R. 1980. A comparative study of numerical methods for moving boundary problems. *IMA Journal of Applied Mathematics,* 26**,** 411-429.

G. GIODA, L. L., FRANCESCO GALLAVRESI 1994. On the artificial freezing of sands. *Computer Methods and Advances in Geomechanics.*

GALLARDO, A. H. & MARUI, A. 2016. The aftermath of the Fukushima nuclear accident: Measures to contain groundwater contamination. *Science of The Total Environment,* 547**,** 261-268.

GEO-SLOPE INTERNATIONAL LTD. 2014. Thermal Modeling with TEMP/W.

GEO-SLOPE INTERNATIONAL LTD. n.d. 1D Verification Freezing and Thawing.

GERAILI MIKOLA, R. 2015. *F2F: Free Software to Create 3D Mesh for FLAC3D* [Online]. Available: http://www.roozbehgm.com/codes/f2f/f2f.html [Accessed 26/06/2022].

GOODMAN, T. R. 1958. The heat-balance integral and its application to problems involving a change of phase. *Trans. ASME,* 80**,** 335-42.

GOTTLIEB, H. P. W. 2002. Exact solution of a Stefan problem in a nonhomogeneous cylinder. *Journal Applied mathematics letters,* 15**,** 167-172.

GUSTAFSSON, B. 2011. *Fundamentals of Scientific Computing*, Springer Science & Business Media.

HARRIS, J. S. 1995. *Ground freezing in practice*, Thomas Telford.

HAß, H. & SCHÄFERS, P. Application of ground freezing for underground construction in soft ground. Proc. 5th Int. Symp. TC28, 2013. 405-412.

HENTRICH, N. & FRANZ, J. About the Application of Conventional and Advanced Freeze Circle Design Methods for the Ust-Jaiwa Freeze Shaft Project. Vertical and Decline Shaft Sinking: Good Practices in Technique and Technology, International Mining Forum 2015, 2015. CRC Press, 89.

HETMANIOK, E., SŁOTA, D. & ZIELONKA, A. 2014. Experimental verification of selected artificial intelligence algorithms used for solving the inverse Stefan problem. *Journal of Numerical Heat Transfer, Part B: Fundamentals,* 66**,** 343-359.

HIRAI, E. & KOMORI, T. 1971. A proposal to solve Neumann's problem approximately, taking account of bulk dilatation by phase change-a semi-infinite solid. *Journal of Chemical Engineering of Japan,* 4**,** 96-99.

HOFFMANN, D. 1962. *Acht Jahrzehnte Gefrierverfahren nach Poetsch; ein Beitrag zur Geschichte des Schachtabteufens in schwierigen Fällen. [Eight decades of Poetsch's freezing method; a contribution to the history of shaft sinking in difficult cases]*, Verlag Glückauf.

HOLDEN, J. T. 1997. Improved thermal computations for artificially frozen shaft excavations. *Journal of geotechnical and geoenvironmental engineering,* 123**,** 696-701.

HONG, Z. & HU, X. 2019. Application of analytical solution to steady-state temperature field by double-row-pipe freezing and verification with field measurement: a case study of connected aisle. *Advances in Civil Engineering,* 2019.

HRISTOV, J. 2010. The heat-balance integral method by a parabolic profile with unspecified exponent: Analysis and benchmark exercises. *Thermal Science,* 13**,** 27-48.

HU, J., LIU, Y., WEI, H., YAO, K. & ZHAO, L. 2016a. Numerical analysis of temperature field of horizontal ground freezing for large-diameter tunnelling. *1st International Conference on Transactions on Engineering Technology Research***,** 718-725.

HU, R., LIU, Q. & XING, Y. 2018a. Case Study of Heat Transfer during Artificial Ground Freezing with Groundwater Flow. *Water,* 10.

HU, X.-D., FANG, T. & HAN, Y.-G. 2018b. Mathematical solution of steady-state temperature field of circular frozen wall by single-circle-piped freezing. *Cold Regions Science and Technology,* 148**,** 96-103.

HU, X.-D., GUO, W., ZHANG, L.-Y., WANG, J.-T. & DONG, X. 2016b. Mathematical models of steady-state temperature fields produced by multi-piped freezing. *Journal of Zhejiang University-SCIENCE A (Applied Physics & Engineering),* 17**,** 702-723.

HU, X.-D. & ZHANG, L.-Y. 2013. Analytical solution to steady-state temperature field of two freezing pipes with different temperatures. *Journal of Shanghai Jiaotong University,* 18**,** 706-711.

HU, X., FANG, T., CHEN, J., REN, H. & GUO, W. 2018c. A large-scale physical model test on frozen status in freeze-sealing pipe roof method for tunnel construction. *Tunnelling and underground space technology,* 72**,** 55-63.

HU, X. & HAN, Y. Analytical solution to steady-state temperature field of asymmetric frozen soil wall by single-row-pipe freezing. 2013 International Conference on Materials, Architecture and Engineering Technology. Pennsylvania: Destech Publications Inc, 2013. 636-641.

HUANG, S., LIU, Q., CHENG, A., LIU, Y. & LIU, G. 2018. A fully coupled thermo-hydro-mechanical model including the determination of coupling parameters for freezing rock. *International Journal of Rock Mechanics and Mining Sciences,* 103**,** 205-214.

HWANG, C., MURRAY, D. & BROOKER, E. 1972. A thermal analysis for structures on permafrost. *Canadian Geotechnical Journal,* 9**,** 33-46.

ITASCA CONSULTING GROUP. 2018. *Meshing Tools and Solutions for Numerical Modeling* [Online]. Available: https://www.itascacg.com/software/products/meshing-solutions/mesh-generation [Accessed 17/12/2018].

ITASCA CONSULTING GROUP n.d.-a. FLAC3D 5.01 Manual: Thermal Analysis.

ITASCA CONSULTING GROUP n.d.-b. FLAC 6.0 Manual: Thermal analysis.

ITASCA CONSULTING GROUP n.d.-c. Online Manual FLAC3D Version 5.01.

ITASCA CONSULTING GROUP. n.d.-d. *Physics Extension* [Online]. Available: https://www.itascainternational.com/software/physics-extension [Accessed 16/10/2021].

IVANOVIC, M., SVICEVIC, M. & SAVOVIC, S. 2017. Numerical solution of Stefan problem with variable space grid method based on mixed finite element/finite

difference approach. *Journal International Journal of Numerical Methods for Heat Fluid Flow,* 27**,** 2682-2695.

JAME, Y. W. & NORUM, D. I. 1980. Heat and mass transfer in a freezing unsaturated porous medium. *Water Resources Research,* 16**,** 811-819.

JAVIERRE, E., VUIK, C., VERMOLEN, F. & VAN DER ZWAAG, S. 2006. A comparison of numerical models for one-dimensional Stefan problems. *Journal of Computational Applied Mathematics,* 192**,** 445-459.

JESSBERGER, H. Gefrierschächte Gorleben. Proceedings of a Symposium, Bochum, Germany, 1994. 21-22.

JESSBERGER, H. L. 1979a. Theorie und Anwendungsgrenzen des Gefrierverharens im Bauwesen. [Theory and application limits of ground freezing in the construction industry]. *Referate der Studientagung vom 30./31. März 1979.* ETH-Zürich: SIA, Schweizerischer Ingenieur- und Architekten-Verein.

JESSBERGER, H. L. 1990. Frost im Baugrund. *In:* SOHN, E. (ed.) *Grundbau Taschenbuch.* 4 ed. Berlin.

JESSBERGER, H. L., VYALOV, S.S. 1979b. General Report Session. III: Engineering. *Engineering Geology,* 13**,** 19-27.

JOHANSSON, T. 2009. *Artificial Ground Freezing in Clayey Soils.* Doctoral Thesis, Royal Institute of Technology.

JONES, J. S. & BROWN, R. E. 1979. Design of tunnel support systems using ground freezing. *Engineering Geology,* 13**,** 375-395.

JONSSON, T. 2013. *On the one dimensional Stefan problem.* Bachelor of Mathematics, Umeå University.

JUMIKIS, A. 1979. Some aspects of artificial thawing of frozen soils. *Engineering Geology,* 13**,** 287-297.

JUMIKIS, A. R. 1966. Thermal soil mechanics.

KAMIŃSKI, P. 2021. Optimization Directions for Monitoring of Ground Freezing Process for Grzegorz Shaft Sinking. *Computational Optimization Techniques and Applications.* IntechOpen.

KANG, Y., LIU, Q., CHENG, Y. & LIU, X. 2016. Combined freeze-sealing and New Tubular Roof construction methods for seaside urban tunnel in soft ground. *Tunnelling and underground space technology,* 58**,** 1-10.

KARABENLI, H., ESEN, A. & AKSAN, E. N. 2016. Numerical solutions for a Stefan problem. *Journal New Trends in Mathematical Sciences,* 4**,** 175-187.

KAZEMI, A., ROOSTAIE, M., EGOROV, I. & LEONENKO, Y. 2022. An analytical solution for heat extraction from shallow ground using a single phase closed thermosyphon: a model for artificial ground freezing. *Available at SSRN 4033757.*

KELLNER, C. 2007. *Frosthebungsverhalten von Böden infolge tief liegender Vereisungskörper. [Frost heave behaviour of soils due to deep freeze bodies].* Doktor-Ingenieur, Technische Universität München.

KHAKIMOV, K. R. 1966. *Artificial Freezing of Soils, Theory and Practice: (Voprosy Teorii i Praktiki Iskusstvennogo Zamorazhivaniya Gruntov)*, Israel Program for Scientific Translations.

KIM, C.-J. & KAVIANY, M. 1990. A numerical method for phase-change problems. *Journal International journal of heat mass transfer,* 33**,** 2721-2734.

KLÖSGES, S. & MÜLLER, M. 2021. Artificial ground freezing as a consolidation measure for tunnelling under Bern main station. *Geomechanics and Tunnelling,* 14**,** 441-447.

KNUPP, P. M. 2001. Algebraic mesh quality metrics. *SIAM journal on scientific computing,* 23**,** 193-218.

KNUPP, P. M., ERNST, C., THOMPSON, D. C., STIMPSON, C. & PEBAY, P. P. 2006. The verdict geometric quality library. Sandia National Laboratories.

KUMAR, A. & SINGH, A. K. 2020. A Stefan problem with temperature and time dependent thermal conductivity. *Journal of King Saud University – Science,* 32**,** 97-101.

KURYLYK, B. L., HAYASHI, M. 2016. Improved Stefan Equation Correction Factors to Accommodate Sensible Heat Storage during Soil Freezing or Thawing. *Permafrost and Periglacial Processes,* 27**,** 189-213.

LAM, T. & PANG, P. Geotechnical control for artificial ground freezing works in tunnel projects in Hong Kong. Proceedings of the 8th Int. Symposium on Geotechnical Aspects of Underground Construction in Soft Ground., 2014. 117-122.

LAMÉ, G. & CLAPEYRON, B. P. 1831. Mémoire sur la solidification par refroidissement d'un globe liquide. *[Memoir on solidification by cooling of a liquid globe]. Ann. Chem. Phys,* 47**,** 250-256.

LAYENI, O. & ADEGOKE, A. 2011. A novel revision of Goodman's profile and its application to a one-phase Stefan problem. *Mechanics Research Communications,* 38**,** 456-462.

LAYENI, O. & JOHNSON, J. 2016. Exact closed-form solutions of some Stefan problems in thermally heterogeneous cylinders. *Mechanics Research Communications,* 71**,** 32-37.

LEIBENSON, L. S. 1931. Mechanics Handbook for the Oil Industry, pt. 1. Hydraulics (in Russian), GONTI.

LEUNG, C. K., LEUNG, R. K., CHEUNG, A. K. & CHAN, W. 2012. Application of artificial ground freezing method for tunnel construction in Hong Kong–a construction case in Harbour Area Treatment Scheme stage 2A. *Innovation and Creativity of Infrastructure Developments for Quality Cities***,** 1-12.

LEVIN, L. Y., SEMIN, M. A., PARSHAKOV, O. S. & KOLESOV, E. V. 2017. Method for solving inverse Stefan problem to control ice wall state during shaft excavation. *Perm Journal of Petroleum and Mining Engineering,* 16**,** 255-267.

LI, S., LAI, Y., ZHANG, M. & ZHANG, S. 2006. Minimum ground pre-freezing time before excavation of Guangzhou subway tunnel. *Cold Regions Science and Technology,* 46**,** 181-191.

LI, T., ZHOU, Y., SHI, X.-Y., HU, X.-X. & ZHOU, G.-Q. 2018. Analytical solution for the soil freezing process induced by an infinite line sink. *International Journal of Thermal Sciences,* 127**,** 232-241.

LINDE PLC. 2021. *Ground freezing with liquid nitrogen* [Online]. Available: https://www.linde-gas.com/en/industries/construction_infrastructure/ground-freezing/ground-freezing.html [Accessed 02/10/2021].

LOVERIDGE, F. 2012. *The Thermal Performance of Foundation Piles used as Heat Exchangers in Ground Energy Systems.* Doctor of Philosophy, University of Southampton.

LUNARDINI, V. 1981. Cylindrical phase change approximation with effective thermal diffusivity. *Cold Regions Science and Technology,* 4**,** 147-154.

LUNARDINI, V. Freezing of soil with phase change occurring over a finite temperature difference. Proceedings of the 4th international offshore mechanics and arctic engineering symposium. ASM, 1985.

LUNARDINI, V. Some Analytical Methods for Conduction Heat Transfer with Freezing/Thawing. Proc. Conf. Int. Symp. on Cold Regions Heat Transfer, Edmonton, Canada, 1987.

LUNARDINI, V. J. 1986. Heat conduction with freezing or thawing. Cold Regions Research and Engineering Lab. Hanover, NH.

LUNARDINI, V. J. 1988. Freezing of soil with an unfrozen water content and variable thermal properties. Cold regions research and engineering lab Hanover, NH.

LUNARDINI, V. J. Effect of convective heat transfer on thawing of frozen soil. Proceedings of the seventh international conference on permafrost. Canada: Yellowknife, 1998. 689-95.

MACKENZIE, J. & ROBERTSON, M. 2000. The numerical solution of one-dimensional phase change problems using an adaptive moving mesh method. *Journal of Computational Physics,* 161**,** 537-557.

MACKENZIE, J. & ROBERTSON, M. 2002. A moving mesh method for the solution of the one-dimensional phase-field equations. *Journal of Computational Physics,* 181**,** 526-544.

MANASSERO, V., DI SALVO, G., GIANNELLI, F. & COLOMBO, G. 2008. A combination of artificial ground freezing and grouting for the excavation of a large size tunnel below groundwater. *International Conference on Case Histories in Geotechnical Engineering.*

MAX BÖGL n.d. Infrastructure Ground freezing technology.

MISRA, A., BECKER, B. R. & FRICKE, B. A. 1995. A theoretical model of the thermal conductivity of idealized soil. *HVAC R Research,* 1**,** 81-96.

MITCHELL, S. L. & VYNNYCKY, M. 2009. Finite-difference methods with increased accuracy and correct initialization for one-dimensional Stefan problems. *Journal of Applied Mathematics and Computation,* 215**,** 1609-1621.

MITCHELL, S. L. & VYNNYCKY, M. 2014. On the numerical solution of two-phase Stefan problems with heat-flux boundary conditions. *Journal of Computational and Applied Mathematics,* 264**,** 49-64.

MOSALLY, F., WOOD, A. S. & AL-FHAID, A. 2002. An exponential heat balance integral method. *Journal Applied Mathematics and Computation,* 130**,** 87-100.

MUELLER, D. M., SOPKO, J. A., STORRY, R. & CHAMBERLAND, R. Ground freezing for tunnel cross passages: First application in North America. Proc., Rapid Excavation and Tunneling Conf. Englewood, CO: Society for Mining, Metallurgy and Exploration Inc, 2015.

MÜLLER, B. 2014. Kriterien der Bodengefriertechnik. [Criteria of the soil freezing technique]. *65. Deutsche Brunnenbauertage und BAW-Baugrundkolloquium.* Rostrup / Bad Zwischenahn.

MUZÁS, F., MARTÍN, F 1989. Trabajos llevados a cabo en la estación de Giorgeta del suburbano de Valencia. [Works carried out at Giorgeta station of the Valencia metro]. *Simposio sobre El Agua y el Terreno en las Infraestructuras Viarias (page 292).*

MUZÁS, F., MORENO-BARBERÁ, F., URIEL, A. 1985. Cimentación para la rehabilitación de un edificio antiguo. [Foundations for the renovation of an old building]. *Boletín SEMSC. y Boletín LCG* [Online]. Available: http://fernandomuzaslabad.com/4_archivos/Doc003.pdf [Accessed 25/069/2022].

MYERS, T. 2010. Optimal exponent heat balance and refined integral methods applied to Stefan problems. *International Journal of Heat and Mass Transfer,* 53**,** 1119-1127.

NAKANO, Y. & BROWN, J. 1971. Effect of a freezing zone of finite width on the thermal regime of soils. *Journal Water Resources Research,* 7**,** 1226-1233.

NASIR, O., FALL, M., NGUYEN, S. T. & EVGIN, E. 2013. Modeling of the thermo-hydro-mechanical–chemical response of sedimentary rocks to past glaciations. *International Journal of Rock Mechanics and Mining Sciences,* 64**,** 160-174.

NEAUPANE, K., YAMABE, T. & YOSHINAKA, R. 1999. Simulation of a fully coupled thermo–hydro–mechanical system in freezing and thawing rock. *International Journal of Rock Mechanics and Mining Sciences,* 36**,** 563-580.

NEUMANN, F. c.1860. Lectures given in the 1860's. *Die partiellen Differentialgleichungen der mathematischen Physik. [The partial differential equations of mathematical physics].*

NEWMAN, G., NEWMAN, L., CHAPMAN, D. & HARBICHT, T. 2011. Artificial Ground Freezing: An Environmental Best Practice at Cameco's Uranium Mining Operations in Northern Saskatchewan, Canada. *Mine water - Managing the challenges: Proceedings of the International Mine Water Association Congress.*

NIKOLAEV, P. & SHUPLIK, M. Low-temperature ground freezing methods for underground construction in urban areas. MATEC Web of Conferences, 2019. EDP Sciences, 04020.

ORTH, W. & MÜLLER, B. 2013. Temporary watertight connection of excavations to existing buildings and temporary waterproofing of structures by ground freezing. *Geomechanics and Tunnelling,* 6**,** 246-260.

OSTERKAMP, T. E. 1987. Freezing and thawing of soils and permafrost containing unfrozen water or brine. *Water Resources Research,* 23**,** 2279-2285.

OWEN, S. 1998. A survey of unstructured mesh generation technology. *IMR,* 239**,** 267.

ÖZIŞIK, M. & UZZELL JR, J. 1979. Exact solution for freezing in cylindrical symmetry with extended freezing temperature range. *Journal of Heat Transfer,* 101**,** 331-334.

ÖZIŞIK, M. N. 1993. *Heat conduction*, John Wiley & Sons.

P.E.FRIVIK, E. T. Thermal design of artificial soil freezing systems. 1981. 189-201.

PAYNTER, H. M. & LIFE, M. A retrospective on early analysis and simulation of freeze and thaw dynamics. Proceedings of the 10th International Conference on Cold Regions Engineering. Lincoln, NH: American Society of Civil Engineering, 1999. 160-172.

PÉBAY, P. P. Planar quadrangle quality measures: Is there really a choice? IMR, 2002. Citeseer, 53-62.

PENTLAND, J. S. & FREDLUND, D. G. 2001. Use of a general partial differential equation solver for solution of mass and heat transfer problems in geotechnical engineering.

PHILLIPS, M., FADHEL, H., RAAFAT, I. & EL-KELESH, A. 2021. Use of artificial ground freezing in construction of cross passages under Suez Canal. *Geomechanics and Tunnelling,* 14**,** 298-307.

PIGORINI, A., SCIOTTI, A., ZOPPO, G. & CALABRESI, G. Prediction and performance of a ground freezing application to the rehabilitation works of an existing tunnel. Proceedings of the 7th International Symposium on Geotechnical Aspects of Underground Construction in Soft Ground, 2012. 165-172.

PIMENTEL, E., PAPAKONSTANTINOU, S. & ANAGNOSTOU, G. Case studies of artificial ground freezing simulations for urban tunnels. World Tunnel Congress, 2011 Helsinki, Finland.

PIMENTEL, E., PAPAKONSTANTINOU, SPYRIDON, ANAGNOSTOU, GEORG 2012. Numerical interpretation of temperature distributions from three ground freezing applications in urban tunnelling. *Tunnelling and underground space technology,* 28**,** 57-69.

POETSCH, H. F. 1883. *Verfahren zur Abteufung von Schächten in schwimmendem Gebirge. [Method for sinking shafts in buoyant rock]*.

POWERS, J. P., CORWIN, A. B., SCHMALL, P. C. & KAECK, W. E. 2007. *Construction dewatering and groundwater control: new methods and applications*, John Wiley & Sons.

QI, Y., ZHANG, J., YANG, H. & SONG, Y. 2020. Application of artificial ground freezing technology in modern urban underground engineering. *Advances in Materials Science and Engineering,* 2020.

RAMAECKERS, C., VAN COTTHEM, A. & DE BRUYN, D. 2000. Construction d'un second puits à Mol dans le cadre des études pour l'enfouissement géologique des déchets hautement radioactifs en Belgique. *Tunnels et ouvrages souterrains***,** 315-325.

RAMOS, M., AGUIRRE-PUENTE, J., POSADO CANO, R. 1996. Soil freezing problem: an exact solution. *Soil Technology,* 9**,** 29-38.

RECKTENWALD, G. W. J. M. E. 2004. Finite-difference approximations to the heat equation. *Mechanical Engineering,* 10**,** 1-27.

REES, S., ADJALI, M., ZHOU, Z., DAVIES, M. & THOMAS, H. 2000. Ground heat transfer effects on the thermal performance of earth-contact structures. *Renewable and Sustainable Energy Reviews,* 4**,** 213-265.

RITTER, C. 1962. Recent developments in liquefaction and transportation of natural gas. *Chemical Engineering Progress,* 58**,** 61-69.

RIZWAN-UDDIN 1998. An approximate-solution-based numerical scheme for Stefan problem with time-dependent boundary conditions. *Numerical Heat Transfer,* 33**,** 269-285.

ROACHE, P. 1993. Perspective: A method for uniform reporting of grid refinement studies. *J. Fluids Eng.,* 158**,** 109-109.

ROBERTI, P. 2012. La congelación del suelo, técnica, tecnología y obras recientes. [Ground freezing, technique, technology and recent works]. *Revista Digital del Cedex***,** 43-43.

ROBERTSON, E. C. 1988. Thermal properties of rocks. United States Department of the Interior - Geological Survey.

RODRIGUES, J. F. & URBANO, J. M. 1999. On a Darcy–Stefan problem arising in freezing and thawing of saturated porous media. *Continuum Mechanics Thermodynamics,* 11**,** 181-191.

ROSCANI, S. D. & TARZIA, D. A. 2018. Explicit solution for a two-phase fractional Stefan problem with a heat flux condition at the fixed face. *Computational Applied Mathematics,* 37**,** 4757–4771.

ROSE, M. E. 1960. A method for calculating solutions of parabolic equations with a free boundary. *Mathematics of Computation***,** 249-256.

ROWORTH, M. R. 2013. *Understanding the effect of freezing on rock mass behaviour as applied to the Cigar Lake mining method.* Master of Applied Sciences (Mining Engineering), University of British Columbia.

SAGASETA, C. & CASTRO, J. 2021. Tres décadas de evolución del análisis numérico de túneles. Una visión subjetiva a la luz de un caso real. [Three decades of evolution of numerical analysis of tunnels. A subjective view in the light of a real case study]. *Geotecnia***,** 251-272.

SALVA, N. N., TARZIA, DOMINGO ALBERTO 2011. Explicit solution for a Stefan problem with variable latent heat and constant heat flux boundary conditions. *Journal of Mathematical Analysis and Applications,* 379**,** 240-244.

SANCHO-CALDERÓN, D., IBÁÑEZ, S. J., ORTIZ-PALACIO, S. & BOCK, S. 2021. Revisión del estado del arte de cálculos térmicos para congelación de terreno en aplicaciones de ingeniería geotécnica. *In:* BURGOS, U. D. (ed.) *VII Jornadas de Doctorado de la Universidad de Burgos* Burgos, Spain.

SANGER, F. J. & SAYLES, F. H. 1979. Thermal and rheological computations for artificially frozen ground construction. *Engineering Geology,* 13**,** 311-337.

SAVOVIC, S. & CALDWELL, J. 2009. Numerical solution of Stefan problem with time-dependent boundary conditions by variable space grid method. *Journal Thermal Sciences,* 13**,** 165-174.

SCHEERLINCK, N., FIKIM, K., VERBOVEN, P., DE BAERDEMAEKER, J. & NICOLAÏ, B. 1997. Numerical solution of phase change heat transfer problems with moving boundaries using an improved finite element enthalpy method. *Journal Transactions on Modelling and Simulation,* 18.

SCHMALL, P. C. & BRAUN, B. 2006. Ground freezing—a viable and versatile construction technique. *13th; International Conference, Cold regions engineering; current practices in cold regions engineering.* Orono, ME: American Society of Civil Engineers.

SCHMALL, P. C. & MAISHMAN, D. 2007. Ground freezing a proven technology in mine shaft sinking. *Tunnelling & Underground Construction*, 59**,** 25-30.

SCHÜLLER, R. 2015. *Energetische Optimierung von Vereisungsmaßnahmen im Tunnelbau. [Energetic optimisation of ground freezing measures in tunnel construction]*. Doctoral Thesis, Universitätsbibliothek der RWTH Aachen.

SCHULTZ, M., GILBERT, M. & HASS, H. 2008. Ground freezing-principles, applications and practices. *Tunnels & Tunnelling International*.

SHAWN, P., JUAN, L. & MICHAEL, A. Ground freezing to repair leaks in a slurry wall shaft. Proceedings of world tunnel congress, 2016. 22-28.

SHUPLIK, M. & NIKOLAEV, P. Advanced ground freezing method and its applications in underground construction. MATEC Web of Conferences, 2019. EDP Sciences, 04021.

SONG, H., CAI, H., CHENG, H. & YAO, Z. J. A. A. 2018. Physical model testing and numerical simulation for temperature distribution of mass concrete freezing shaft lining in deep alluvium. 8**,** 075328.

SOPKO, J. & BRAUN, B. 2000. Investigative and remedial methods for breach in a frozen shaft. *Ground Freezing 2000-Frost Action in Soils.* CRC Press.

SOPKO, J. A. 2017a. Coupled heat transfer and groundwater flow models for ground freezing design and analysis in construction. *Geotechnical Frontiers 2017.*

SOPKO, J. A. 2017b. Forensics by Freezing. *Grouting 2017.*

SOPKO, J. A. 2017c. Ground Control. *Tunnels and Tunnelling,* October - November 20217**,** 34-37.

SOPKO, J. A., CURRY, ADAM, CHAMBERLAND, ROBERT R., KHORSHIDI, BEHZAD. n.d.-a. Southeast Collector (SeC) Gravity Trunk Sewer Ground Freezing. Available: https://groundfreezing.com/technical-papers/southeast-collector-sec-gravity-trunk-sewer-ground-freezing/

SOPKO, J. A., NORMAN, MICHELE R. n.d.-b. Ground Freezing for Tunnel Support No. 7 Line Subway Extension New York City.

SOPKO JR., J. A. 1990. *New design method for frozen earth structures with reinforcement.* Michigan State University.

SPIRIDONOV, D., STEPANOV, S. & VASILIY, V. 2022. An Online Generalized Multiscale finite element method for heat and mass transfer problem with artificial ground freezing. *arXiv preprint:01896*.

SRES, A. 2009. *Theoretische und experimentelle Untersuchungen zur künstlichen Bodenvereisung im strömenden Grundwasser. [Theoretical and experimental*

investigations on artificial soil freezing in flowing groundwater]. Doktor der Wissenschaften, ETH Zürich.

STÄNDER, W. 1967. Mathematische Ansätze zur Berechnung der Frostausbreitung in ruhendem Grundwasser im Vergleich zu Modelluntersuchungen für verschiedene Gefrierrohranordnungen im Schacht- und Grundbau. [Mathematical approaches for calculating frost propagation in still groundwater compared to model investigations for different freeze pipe arrangements in shaft and geotechnical engineering]. *Veröffentlichungen des Institutes für Bodemechanik und Felsmechanik der Technischen Hochschule Fridericiana in Karlsruhe,* 28.

STEFAN, J. 1891. Über die Theorie der Eisbildung, insbesondere über die Eisbildung im Polarmeere. [On the theory of ice formation, especially on ice formation in the polar oceans]. *Annalen der Physik,* 278**,** 269-286.

STOUT, R. & BILLINGS, D. Accuracy and time resolution in thermal transient finite element analysis. Proc. ANSYS Conference & Exhibition, 2002.

STUIZALEC, A. 1989. Groundwater Flow Effects in Processes of Soil Freezing. *Numerical Heat Transfer, Part A,* 15**,** 399-409.

STURK, R. & STILLE, B. 2008. Advanced Ground Freezing at the Hallandsås Project, Sweden. *Geomechanik und Tunnelbau,* 1**,** 512-517.

SUDISMAN, R. A., OSADA, M. & YAMABE, T. 2019. Experimental investigation on effects of water flow to freezing sand around vertically buried freezing pipe. *Journal of Cold Regions Engineering,* 33**,** 04019004.

TAKASHI, T., KIRIYAMA, S. & KATO, T. 1979. Jointing of two tunnel shields using artificial underground freezing. *Engineering Geology,* 13**,** 519-529.

TAO, Y. & ZHENG, M.-Y. 2009. An improvement to the simulation of phase-change heat-transfer during soil freezing and thawing. *Mining Science and Technology* 19**,** 262-268.

TARZIA, D. A. 2000. *A bibliography on moving-free boundary problems for the heat-diffusion equation. The Stefan and related problems.,* Rosario, Argentina., Universidad Austral. Facultad de Ciencias Empresariales.

TARZIA, D. A. 2011. Explicit and approximated solutions for heat and mass transfer problems with a moving interface. *Advanced topics in mass transfer.* InTech.

TARZIA, D. A. 2015. Determination of one unknown thermal coefficient through the one-phase fractional Lamé-Clapeyron-Stefan problem. *Applied Mathematics,* 6**,** 2182-2191.

TOUNSI, H., ROUABHI, A., TIJANI, M. & GUÉRIN, F. 2019. Thermo-hydro-mechanical modeling of artificial ground freezing: application in mining engineering. *Rock Mechanics and Rock Engineering,* 52**,** 3889-3907.

TRUPAK, N. G. 1954. Ground Freezing in Shaft Sinking.

UNKNOWN. n.d.-a. Brief overview of numerical methods for phase change problems Available: http://www.math.utk.edu/~vasili/475/Handouts/6.PhChgbk.4.2-4.3D.pdf [Accessed 30/08/2019].

UNKNOWN. n.d.-b. Heat Conduction in Cartesian Coordinates. Available: http://www.ewp.rpi.edu/hartford/~ernesto/S2006/CHT/Notes/ch02.pdf [Accessed 29/09/2016].

UNKNOWN. n.d.-c. Heat conduction in cylindrical and spherical coordinates. Available: https://kipdf.com/chapter-3-heat-conduction-in-cylindrical-and-spherical-coordinates_5ac98a7d1723dd30ced3acac.html [Accessed 08/06/2022].

UNKNOWN. n.d.-d. Stability of Finite Difference Methods. Available: http://web.mit.edu/16.90/BackUp/www/pdfs/Chapter14.pdf [Accessed 30/08/2019].

UNKNOWN. n.d.-e. Transient analysis. Available: https://www.scribd.com/document/429413971/Transient-Analysis [Accessed 08/06/2022].

VASILYEV, V., POPOV, VV 2009. Numerical solution of the soil freezing problem. *Mathematical Models and Computer Simulations,* 1**,** 419-427.

VASILYEVA, M., STEPANOV, S., SPIRIDONOV, D. & VASIL'EV, V. 2020. Multiscale Finite Element Method for heat transfer problem during artificial ground freezing. *Journal of Computational Applied Mathematics,* 371**,** 112605.

VIGGIANI, G. & DE SANCTIS, L. 2009. Geotechnical aspects of underground railway construction in the urban environment: the examples of Rome and Naples. *Journal Geological Society, London, Engineering Geology Special Publications,* 22**,** 215-240.

VITEL, M., ROUABHI, A., TIJANI, M. & GUÉRIN, F. 2015. Modeling heat transfer between a freeze pipe and the surrounding ground during artificial ground freezing activities. *Computers and Geotechnics,* 63**,** 99-111.

VITEL, M., ROUABHI, A., TIJANI, M. & GUÉRIN, F. 2016. Modeling heat and mass transfer during ground freezing subjected to high seepage velocities. *Computers and Geotechnics,* 73**,** 1-15.

VOLLER, V. & CROSS, M. 1981. Accurate solutions of moving boundary problems using the enthalpy method. *International Journal of Heat and Mass Transfer,* 24**,** 545-556.

VOLLER, V. R. 1996. An overview of numerical methods for solving phase change problems. *Advances in numerical heat transfer.*

VOLLER, V. R. 2014. Fractional Stefan problems. *International Journal of Heat and Mass Transfer,* 74**,** 69-277.

VOLLER, V. R., SWENSON, J. B. & PAOLA, C. 2004. An analytical solution for a Stefan problem with variable latent heat. *International Journal of Heat Mass Transfer,* 47**,** 5387-5390.

WANG, B., RONG, C.-X., LIN, J., CHENG, H. & CAI, H.-B. 2019. Study on the formation law of the freezing temperature field of freezing shaft sinking under the action of large-flow-rate groundwater. *Advances in Materials Science and Engineering,* 2019**,** 1670820.

WANG, B., RONG, C., CHENG, H., CAI, H., DONG, Y. & YANG, F. 2020. Temporal and spatial evolution of temperature field of single freezing pipe in large velocity infiltration configuration. *Cold Regions Science and Technology,* 175**,** 103080.

WANG, Z.-L., SHEN, L.-F. & XIE, J.-B. 2015. 3D Numerical Analyses of Temperature Field for Construction of Connecting Passage in Metro using Artificial Freezing Method. *13th ISRM International Congress of Rock Mechanics.* International Society for Rock Mechanics and Rock Engineering.

WANG, Z., XIN, L., XU, Z. & SHEN, L. 2017. Lattice Boltzmann simulation of heat transfer with phase change in saturated soil during freezing process. *Journal of Numerical Heat Transfer, Part B: Fundamentals*, 72**,** 361-376.

WEINER, J. H. 1955. Transient heat conduction in multiphase media. *British Journal of Applied Physics,* 6**,** 361.

WENKE, M. & WILLNER, M. 2008. Statentunnel in Rotterdam–Ausführungserfahrungen von Vereisungsbohrungen und der Vereisung von Querschlägen. [Statentunnel in Rotterdam–Experience from the execution of freeze boreholes and freezing of cross passages]. *Geomechanik und Tunnelbau,* 1**,** 504-511.

WILSON, D. 1978. Existence and uniqueness for similarity solutions of one dimensional multi-phase Stefan problems. *SIAM Journal on Applied Mathematics,* 35**,** 135-147.

WU, Z.-C. & WANG, Q.-C. J. T. S. 2012. Numerical approach to Stefan problem in a two-region and limited space. *Thermal Science,* 16.

XU, M., AKHTAR, S., ZUETER, A. F., AUGER, V., ALZOUBI, M. A. & SASMITO, A. P. 2020. Development of analytical solution for a two-phase stefan problem in artificial ground freezing using singular perturbation theory. *Journal of Heat Transfer,* 142**,** 122401.

YAN, Q., WU, W., ZHANG, C., MA, S. & LI, Y. 2019. Monitoring and evaluation of artificial ground freezing in metro tunnel construction-a case study. *KSCE Journal of Civil Engineering,* 23**,** 2359-2370.

YAN, Q., XU, Y., YANG, W. & GENG, P. 2017. Nonlinear transient analysis of temperature fields in an AGF project used for a cross-passage tunnel in the Suzhou Metro. *KSCE Journal of Civil Engineering,* 22**,** 1473-1483.

YIGIT, F. 2008. Approximate analytical and numerical solutions for a two-dimensional Stefan problem. *Journal Applied Mathematics and Computation,* 202**,** 857-869.

ZAVALETA CAMACHO, S. 2017. *Numerical methods in heat transfer and fluid dynamics.* MSc Energy Enginering, Escuela Técnica Superior de Ingeniería Industrial de Barcelona.

ZHANG, C., YANG, W.-H., QI, J.-G. & ZHANG, T. 2012. Analytic computation on the forcible thawing temperature field formed by a single heat transfer pipe with unsteady outer surface temperature. *Journal of Coal Science Engineering,* 18**,** 18-24.

ZHANG, S., YUE, Z., SUN, T., ZHANG, J. & HUANG, B. 2021. Analytical determination of the soil temperature distribution and freezing front position for linear arrangement of freezing pipes using the undetermined coefficient method. *Cold Regions Science Technology,* 185**,** 103253.

ZHANG, Y. 2014. *Thermal-Hydro-Mechanical Model for Freezing and Thawing of Soils.* Doctor of Philosophy (Civil Engineering), University of Michigan.

ZHANG, Y., CAREY, S. K. & QUINTON, W. L. 2008. Evaluation of the algorithms and parameterizations for ground thawing and freezing simulation in permafrost regions. *Journal of Geophysical Research,* 113.

ZHAO, Y. Influence of Frost Heave and Thaw Settlement of Connected Aisle on Tunnel Structure. Journal of Physics: Conference Series, 2019. IOP Publishing, 042027.

ZHELNIN, M., KOSTINA, A., PLEKHOV, O. & LEVIN, L. 2020. Numerical simulation of cement grouting of saturated soil during a mine shaft sinking using the artificial ground freezing. *Procedia Structural Integrity,* 28**,** 693-701.

ZHELNIN, M., KOSTINA, A., PLEKHOV, O. & LEVIN, L. Numerical simulation of vertical shaft sinking using artificial ground freezing. E3S Web of Conferences, 2021. EDP Sciences, 03008.

ZHOU, J., ZHAO, W. & TANG, Y. 2021. Practical prediction method on frost heave of soft clay in artificial ground freezing with field experiment. *Tunnelling and Underground Space Technology,* 107**,** 103647.

ZHOU, M. 2013. *Computational simulation of soil freezing: multiphase modeling and strength upscaling.* Doctor of Engineering, Ruhr University Bochum.

ZHOU, Y., SHI, X.-Y. & ZHOU, G.-Q. 2018. Exact solution for a two-phase Stefan problem with power-type latent heat. *Journal of Engineering Mathematics,* 110**,** 1-13.

ZHU, M. & MICHALOWSKI, R. L. Simulation of heat transfer in Freezing soils using Abaqus. Abaqus Users' Conference, 2005. 1-7.

ZIEGLER, M., AULBACH, B. & BAIER, C. 2010. *Erweiterung des Vereisungsverfahrens zur umweltverträglichen Herstellung komplizierter Untergeschosskonstruktionen bei strömendem Grundwasser. [Extension ground freezing method for the environmentally friendly construction of complicated basement works with flowing groundwater],* Fraunhofer-IRB-Verlag.

ZIEGLER, M., SCHULLER, R. & MOTTAGHY, D. Numerical simulation of energy consumption of artificial ground freezing applications subject to water seepage. Proc. 18th Int. Conf. on soil mechanics and geotechnical engineering, Paris, France, 2013. 2985-88.

ZUETER, A., NIE-ROUQUETTE, A., ALZOUBI, M. A. & SASMITO, A. P. 2020. Thermal and hydraulic analysis of selective artificial ground freezing using air insulation: Experiment and modeling. *Computers and Geotechnics,* 120**,** 103416.

ZUETER, A. F., XU, M., ALZOUBI, M. A. & SASMITO, A. P. 2021. Development of conjugate reduced-order models for selective artificial ground freezing: Thermal and computational analysis. *Applied Thermal Engineering,* 190**,** 116782.